

CHAPTER 1

Mass spectrometry and gas-phase ion chemistry of dienes and polyenes

DIETMAR KUCK

Fakultät für Chemie, Universität Bielefeld, Universitätsstraße 25, D-33615 Bielefeld, Germany and Fachbereich Chemie und Chemietechnik, Universität-Gesamthochschule Paderborn, Warburger Straße 100, D-33098 Paderborn, Germany
e-mail: dietmar.kuck@uni-bielefeld.de

and

MICHAEL MORMANN

Fachbereich Chemie und Chemietechnik, Universität-Gesamthochschule Paderborn, Warburger Straße 100, D-33098 Paderborn, Germany

I. INTRODUCTION	2
II. GASEOUS RADICAL CATIONS OF SOME DIENES AND POLYENES: THERMOCHEMISTRY OF SOME TYPICAL REACTIONS	3
III. UNIMOLECULAR ISOMERIZATION AND FRAGMENTATION	6
A. Selected Linear Dienes: Allylic Cleavage and Isomer Distinction	6
B. Linear Dienes that Cannot Undergo Allylic Cleavage: Allene and Butadienes	11
C. Linear Dienes and Polyenes: McLafferty Reactions	12
D. Butadiene and Cyclobutene	15
E. Cyclic Dienes and Polyenes: Retro-Diels–Alder and (Apparent) Diels–Alder Reactions	16
F. Selected Cycloalkadienes and Cycloalkapolyenes	19
IV. GASEOUS ANIONS GENERATED FROM DIENES AND POLYENES	24
A. Trimethylenemethane and Related Radical Anions	25
B. Deprotonation of 1,3,5-Cycloheptatriene: <i>cyclo-C₇H₇[−]</i> and the Benzyl Anion	27

C. Deprotonation of Bicyclo[3.2.1]alkadiene, Some Other Cycloalkadienes and Cyclooctatetraene: Bishomoaromaticity and Transannular Cyclization	27
V. BIMOLECULAR REACTIONS OF DIENES AND POLYENES	30
A. Ionized Dienes and Neutral Molecules	30
B. Neutral Dienes and Odd-electron Reagent Ions	34
C. Neutral Dienes and Even-electron Reagent Ions	35
D. Reactions of Diene-derived Anions	38
VI. LOCALIZATION OF THE C–C BOND UNSATURATION	39
A. Liquid-phase Derivatization Followed by Mass Spectrometry	39
B. Gas-phase Derivatization by Chemical Ionization	39
VII. MASS SPECTROMETRY OF MONO- AND OLIGOTERPENES, TERPENOIDS AND CAROTENOIDS	43
VIII. ACKNOWLEDGEMENTS	49
IX. REFERENCES	49

I. INTRODUCTION

As compared to other functional groups, mass spectrometry of olefins is special, and this holds for dienes and polyenes as well. The reason for this lies in the gas-phase ion chemistry of C–C double bonds. Unsaturated C–C bonds have medium ionization energies and are readily attacked by protons and other electrophiles and, in this sense, react similarly to other unsaturated functional groups. However, they are ‘symmetrical’ in that they connect, by definition, identical atoms, viz. carbons. Moreover, they are constituents of the carbon skeleton of organic molecules, not pending groups which are prone to be lost from the molecular framework by fragmentation. For these reasons, molecular ions, or ions in general, that contain C–C double (and triple) bonds easily undergo isomerization. Thus, removal of an electron from the π electron system of the $>C=C<$ unit or addition of an electrophile to it may cause much more perturbation to the gaseous ion than, for example, ionization or protonation of a carbonyl group. The well-known loss of stereospecificity of *cis*- or *trans*-configured double bonds under most mass spectrometric ionization conditions presents another problem in gaseous ions derived from dienes and polyenes.

On the other hand, unimolecular reactions of a molecular ion triggered by $>C^{+}-C<$ or $>C^{+}-CH<$ units are comparable to those triggered by other electron-deficient centres. For instance, formal abstraction of a hydrogen atom or a hydride, respectively, by these cationic groups and proton transfer from the allylic α -C–H bonds to other parts of the molecular ions can be understood similarly well as the corresponding reactions of related heteroatomic unsaturated groups. A lucid example is the McLafferty reaction, which occurs in the radical cations of olefins as it does in the radical cations of carbonyl groups. Also, allylic cleavage may be considered a well-behaved fragmentation reaction for olefins.

Yet, there is another complication with double (and triple) bonds. Things get more complicated because of the sp^2 (and sp) hybridization of the carbon atoms involved. Fragmentation of a bond attached directly to the unsaturated C–C unit (i.e. α -C–X) generates an sp^2 - (or even sp -) hybridized carbenium ion, the formation of which requires much more energy than, e.g., allylic cleavage. Therefore, highly unsaturated carbon frameworks of dienes and polyenes in which the double bonds are either cumulated, conjugated or homoconjugated require relatively high internal excitation to undergo skeletal fragmentation. For the same reason, in turn, mass spectrometry of aromatic ions is relatively straightforward.

All these features have rendered mass spectrometry of dienes and polyenes somewhat diverse. In view of analytical applicability of mass spectrometry for distinguishing between isomeric olefins, there has been pertinent interest in the interplay of fundamental and applied aspects of mass spectrometry. Thus, besides the traditional investigation of the unimolecular chemistry of gaseous ions generated from these compounds, there has been a considerable body of research on the bimolecular gas-phase ion chemistry of alkenes and their higher unsaturated analogues, aiming mostly at the localization of the double bond(s) within the compound under investigation. Much effort has been made to perform 'gas-phase derivatization' of olefins, that is, to generate ionic derivatives which undergo more structure-specific fragmentation than the original substrates do. As the liquid-phase variant, derivatization of the neutral olefins followed by mass spectrometric analysis has also been studied in greater detail.

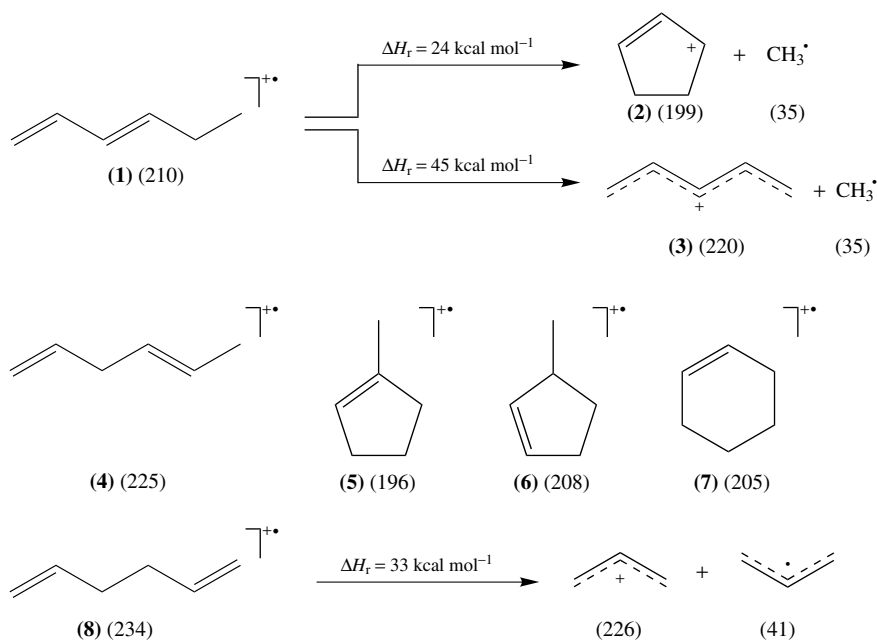
This review will first concentrate on the unimolecular gas-phase chemistry of diene and polyene ions, mainly cationic but also anionic species, including some of their alicyclic and triply unsaturated isomers, where appropriate. Well-established methodology, such as electron ionization (EI) and chemical ionization (CI), combined with MS/MS techniques in particular cases will be discussed, but also some special techniques which offer further potential to distinguish isomers will be mentioned. On this basis, selected examples on the bimolecular gas-phase ion chemistry of dienes and polyenes will be presented in order to illustrate the great potential of this field for further fundamental and applied research. A special section of this chapter will be devoted to shed some light on the present knowledge concerning the gas-phase derivatization of dienes and polyenes. A further section compiles some selected aspects of mass spectrometry of terpenoids and carotenoids.

Only a few reviews on mass spectrometry of monoolefins and cyclic isomers have appeared during the last two decades. Within this series, ionized alkenes and cyclopropanes have been discussed¹⁻³. With regard to dienes and polyenes, reviews by Dass⁴ on (formally) pericyclic reactions and by Tureček and Hanuš⁵ and by Mandelbaum⁶ on retro-Diels-Alder reactions in gaseous radical cations have to be noted. The gas-phase ion chemistry of ionized alkylbenzenes, a classical field of organic mass spectrometry ever since, was also reviewed in 1990 and overlaps in part with that of ionized cycloolefins such as cycloheptatriene, norbornadiene and cyclopentadiene⁷. Gaseous protonated alkylbenzenes, which can be considered positively charged olefinic species rather than aromatic ones, have been of particular interest and reviewed several times during the last decade⁸⁻¹⁰. It is noted here for curiosity that the EI mass spectra of terpenes and other highly unsaturated olefins show many prominent peaks that indicate the formation of both $[M - H]^+$ and $[M + H]^+$ ions of alkylbenzenes (cf Section VII)^{11,12}.

II. GASEOUS RADICAL CATIONS OF SOME DIENES AND POLYENES: THERMOCHEMISTRY OF SOME TYPICAL REACTIONS

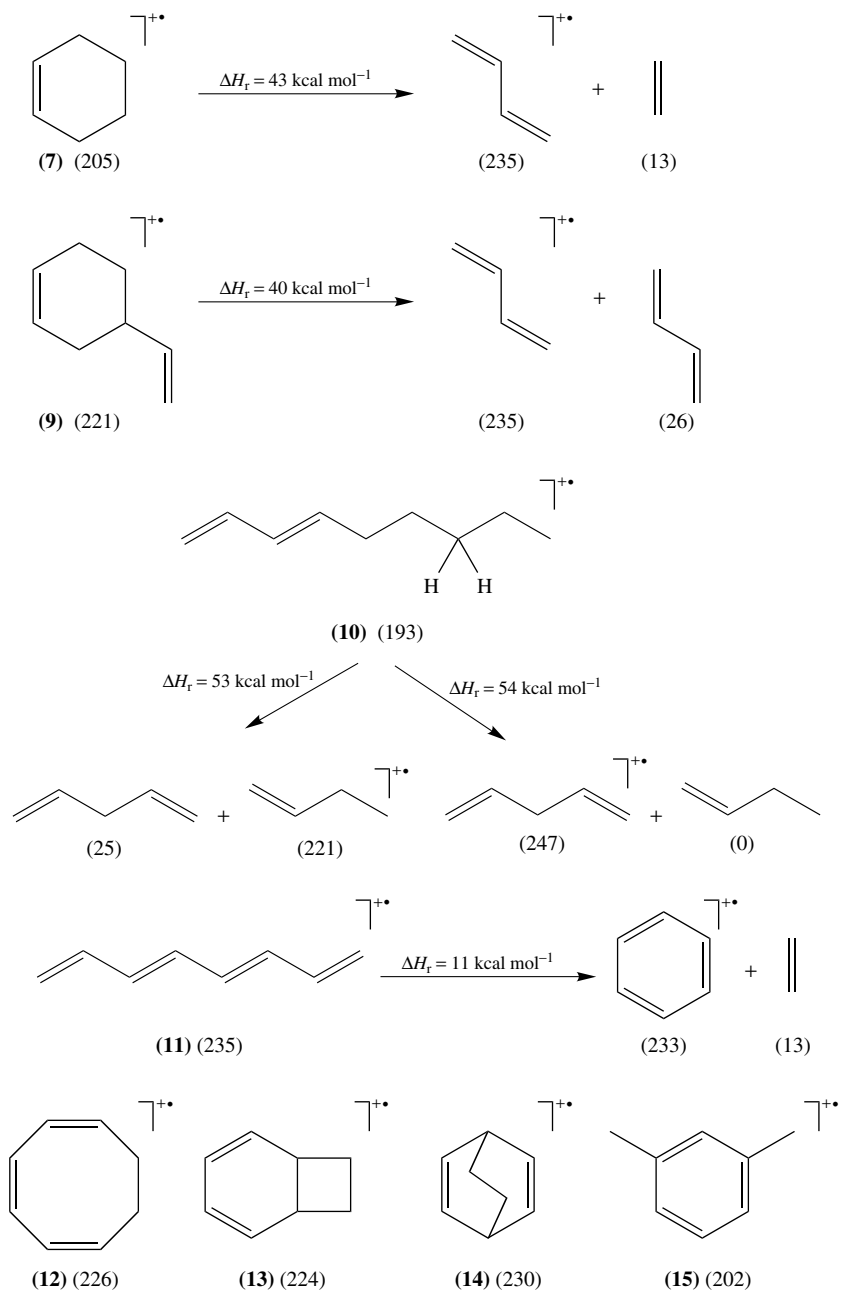
As mentioned in the Introduction, diene and polyene ions cannot undergo facile fragmentation reactions unless suitable saturated carbon centres are present at which C-C (or C-X) bond cleavage can occur to generate stable fragments. On the other hand, the availability of one or more unsaturated C-C bonds in the vicinity of a formally charged centre can easily give rise to bonding interaction, i.e. cyclization reactions. Moreover, 1,2-H shifts may lead to reorientation of the individual double bonds and open additional paths for C-C bonding between parts of the same or formally isolated π -electron systems. As a consequence, isomerization by cyclization is prevalent in the odd- and even-electron ions of dienes and polyenes, and negatively charged ions of these compounds also tend to undergo cyclization quite easily.

This section is mainly intended to demonstrate, by using some selected examples, the relative ease of cyclization reactions of organic cations containing two or several C–C double bonds. In fact, a multitude of such ring-forming isomerization processes take place prior to fragmentation but most of them remain obscured due to the reversibility of these processes. Only a few of them lead directly to energetically favourable exit channels, i.e. to specific fragmentation of the reactive intermediates. From the examples collected in Schemes 1 and 2, the reader may recognize some general trends on the energy requirements of the cyclization processes preceding the actual fragmentation reaction of ionized dienes and polyenes. The heats of formation of the reactant ions and their fragments are given in kcal mol⁻¹ below the structural formulae. The collection is restricted to the radical cations since the thermochemical data on these are better known than on the even-electron cations. It may be noted, however, that the wealth of thermochemical data on organic cations and anions is steadily growing¹³ and the reader is referred to recent compilations which are readily accessible nowadays¹⁴.



SCHEME 1

In Scheme 1, the radical cations of the linear hexadienes and some cyclic isomers are contrasted. The heats of formation, ΔH_f , as determined from the heats of formation of the species involved, as well as the heats of formation of the isomeric radical cations themselves clearly reveal the favourable stability of the cyclic isomers and/or fragment ions. Thus, instead of the linear pentadienyl cation (3), the cyclopenten-3-yl cation (2) is eventually formed during the loss of a methyl radical from ionized 1,3-hexadiene (1). Since 1,2-H⁺ shifts usually have low energy requirements (5–12 kcal mol⁻¹), interconversion of the linear isomers, e.g., 4, and subsequent formation of the cyclic isomers, in particular of the ionized methylcyclopentenes 5 and 6, can take place easily on the level of the



SCHEME 2

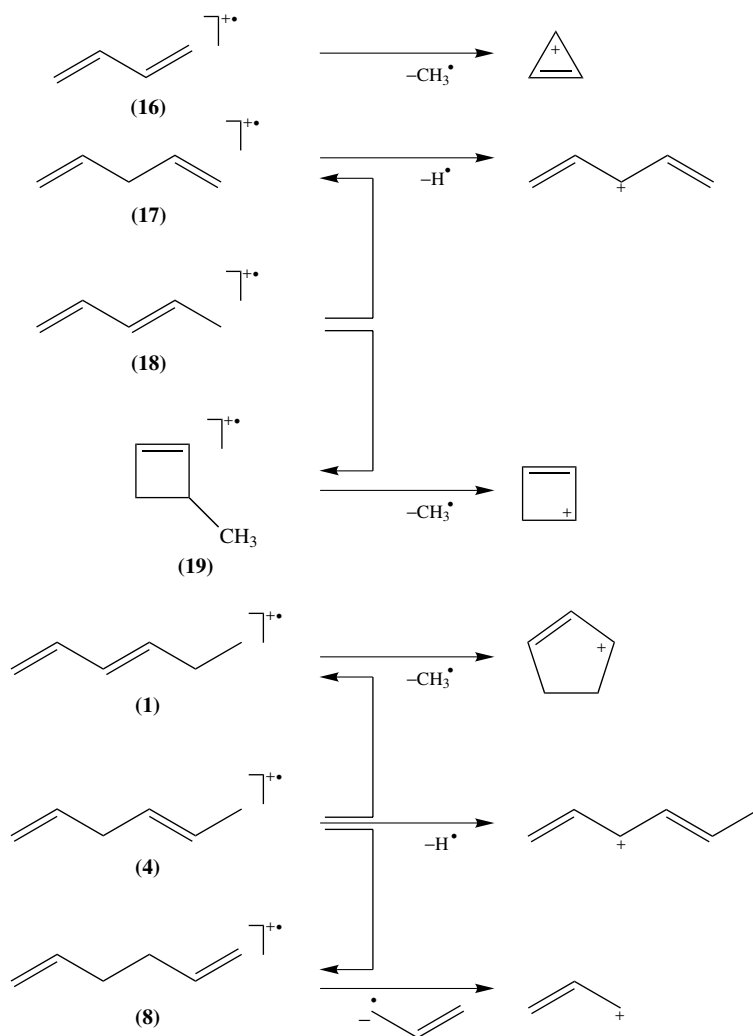
radical cations. It is also obvious that the direct bis-allylic C–C bond cleavage of ionized 1,5-hexadiene (**8**) is a kinetically fast process, but thermochemically it is still rather unfavourable as compared to isomerization to the methylcyclopentene radical cations followed by CH_3^\bullet loss. Details of the gas-phase chemistry of $\text{C}_6\text{H}_{10}^{+\bullet}$ ions are discussed in Section III.

In Scheme 2, three types of elimination reactions from ionized dienes and polyenes are contrasted, again merely as examples for more complex reactant systems. The retro-Diels–Alder (RDA) reaction of ionized cyclohexenes (cf **7**) often occurs also in suitable diene and polyene analogues, e.g. in vinylcyclohexene radical cations (cf **9**). As can be seen from Scheme 2, the thermochemical energy requirements of the RDA reaction are relatively high, and again higher than those for CH_3^\bullet loss. The McLafferty reaction of ionized 1,3-alkadienes, involving the rearrangement of a $\gamma\text{-H}^\bullet$ atom to the ionized double bond with subsequent cleavage of the allylic C–C bond, requires even more energy than the fragmentation processes discussed above, as shown for the case of 1,3-nonadiene (**10**). Part of the endothermicity originates from the deconjugation of the 1,3-diene system and, in fact, McLafferty reactions are relatively rare with ionized dienes and polyenes. Finally, the expulsion of an arene from the radical cations of conjugated polyenes represents a lucid example for the intermediacy of cyclized isomers during the fragmentation of polyene ions such as **11**. Scheme 2 also shows that cyclic $\text{C}_8\text{H}_{10}^{+\bullet}$ ions, in particular ionized 1,3,5,7-cyclooctatriene (**12**) but also the bicyclic isomers **13** and **14**, are again more stable than acyclic ones, and all of them are much less stable than the *o*-xylene radical cations such as **15**. However, an intramolecular metathetic reaction between two remote C–C double bonds, viz. $\Delta(1)$ and $\Delta(7)$ in the case of 1,3,5,7-octatetraene (**11**), leads to C(2)–C(7) and C(1)–C(8) bond formation. Thus, a stable arene unit is released, either as the ionic or the neutral fragment, leaving a neutral or ionized olefin, respectively. The reaction is believed to involve ionized bicyclo[4.2.0]octa-2,4-dienes (cf **13**) as intermediates, and charged fragments $[\text{M} - \text{arene}]^{+\bullet}$ (not shown in Scheme 2) prevail when the C–C double bond in the olefinic fragment is part of a larger conjugated π -electron system, as is the case in carotenoids (cf Section VII). The energy requirements of the arene elimination are intriguingly low for the parent case, but also for the higher analogues where a neutral arene is eliminated.

III. UNIMOLECULAR ISOMERIZATION AND FRAGMENTATION

A. Selected Linear Dienes: Allylic Cleavage and Isomer Distinction

As mentioned in the Introduction, isomerization is a common feature of the radical cations of dienes and polyenes. This holds unless allylic cleavage of one or two C–C bonds offers a both energetically and entropically favourable exit channel and the reacting ions are relatively highly excited. Thus, for 1,3-butadiene radical cations (**16**) a minimum of 57 kcal mol^{-1} is required to expel a CH_3^\bullet radical and form the cyclopropenyl cation, $c\text{-C}_3\text{H}_3^+$ (Scheme 3). Aromaticity of the latter ion helps to let the reaction run but propargyl ions, $\text{HC}\equiv\text{C}-\text{CH}_2^+$, may also be formed. The high barrier towards fragmentation enables profound rearrangement of these relatively small ions. In the case of the pentadiene ions **17** and **18**, the least energy-demanding direct cleavage would be the loss of an H $^\bullet$ atom, but preceding cyclization to **19** offers a means to expel a CH_3^\bullet radical as well. This is one of the simplest examples in which for highly unsaturated ions the number of sp^3 -hybridized atomic centres is increased, thus opening the way for an energetically relatively favourable (allylic) cleavage (Scheme 3). Similar mechanisms apply for most of the next higher homologues, but here 1,2-H shifts — well known to occur in neutral olefins and allyl radicals — give rise to formation of the 1,5-hexadiene radical cation, which undergoes the least energetically expensive double allylic C–C bond cleavage (cf



SCHEME 3

Section II). Thus, the C_3H_5^+ (m/z 41) fragment ion generates an intensive peak in all of the standard (70 eV) EI mass spectra of the isomeric hexadienes. However, the molecular ion peak ($\text{C}_6\text{H}_{10}^+$, m/z 82) also gives relatively strong signals for all isomers, except for 1,5-hexadiene (8), where it is completely absent¹⁵. Similar specificity has been observed for isomeric terpenes such as allo-ocimene, a triene containing a 1,4-diene substructure, and myrcene, bearing a 1,5-diene unit. In contrast, homosqualene presents an example of a 1,5-diene which undergoes both specific double allylic cleavage and single allylic cleavage after attaining conjugation by repeated H shift¹⁶. In general, allylic cleavage is a relatively specific process for higher branched alkenes and for alkadienes and -polyenes containing highly substituted double bonds and/or extended conjugated double bonds^{17,18}. Special

methods such as field ionization (FI) mass spectrometry helps to make highly structure-specific allylic C–C bond cleavage become dominant^{19,20}. EI-induced allylic cleavage has also been studied for a number of 1,2-alkadienes²¹.

A number of papers discuss the behaviour of small diene ions in terms of gas-phase ion chemistry. Holmes²² investigated the mass spectra of isomeric C₅H₈ hydrocarbons by deuterium labelling and found that the hydrogen atoms lose their identity prior to fragmentation. The standard EI spectra (obtained at 70 eV electron energy) of 1,3-pentadiene, isoprene and cyclopentene exhibit only minor differences. H[•] atom loss from the molecular ion (M^{+•}) produces the most abundant fragment ions, C₅H₇⁺, and it may be argued that the highest [(M – H)⁺]/[M^{+•}] ratio, found for cyclopentene, is due to the both energetically and entropically favourable formation of the allylic *c*-C₅H₇⁺ cation. Clearly, the C₅H₈^{+•} molecular ions attain a common structure or mixture of isomeric structures prior to fragmentation. The almost identical mass spectra of piperylene and isoprene suggest that, in fact, not only hydrogen but also carbon scrambling occurs in these ions. Interestingly, the mass spectrum of spiro-pentane is most structure-specific in that the C₄H₄^{+•} ion (*m/z* 40) is particularly abundant, reflecting the preformation of the strained C₂H₄ units eliminated as ethene. Nevertheless, complete scrambling occurs in the spirocyclic isomer as well, in particular in the long-lived, metastable ions.

Metastable ions are those which survive the acceleration region of a sector-field mass spectrometer but fragment somewhere during the flight. If mass selection has been effected before fragmentation, the mass-analysed ion kinetic energy (MIKE) spectrum of the particular ions, or mixtures of ions, of the selected *m/z* ratio are obtained, reflecting the isomerization of these relatively weakly excited ions. When stable ions (i.e. those which would not undergo spontaneous fragmentation) are excited during their flight, e.g. by collision or by laser irradiation, the mass-selected, originally non-excited and thus non-interconverting ions can be sampled through their more or less structure-specific, collision-induced dissociation (CID)²³. Much work has been devoted to the structure elucidation of organic ions, in particular to the classical problem of isomeric C₇H₈^{+•} and C₇H₇⁺ ions^{7,24}. Besides simply exciting the ions, they can be oxidized by stripping off another electron from a cation ('charge stripping', CS, or 'collisional ionization') or two electrons from an anion ('charge reversal', CR), or reduced by single electron transfer (in neutralization/reionization mass spectrometry, NRMS). Subsequent fragmentation, e.g. of the dications formed in the CS process, results in structure-specific mass spectra of doubly charged fragment ions. Maquestiau and coworkers²⁵ and Holmes and coworkers²⁶ have demonstrated this method to be useful for the identification of unsaturated radical cations including various C₅H₈^{+•} isomers.

Gross and coworkers²⁷ have generated the radical cations of fourteen acyclic and cyclic C₅H₈ isomers by using a soft ionization method, viz. 'charge exchange' (CE) with ionized carbon disulphide. This limits the excitation energy of the molecular ions, in this case C₅H₈^{+•}, to a well-defined amount and thus the extent of isomerization is low. By using the combination of charge exchange and charge stripping (CE/CS) mass spectrometry, piperylene, cyclopentene and isoprene were found to undergo individual, i.e. structure-specific fragmentation. In these cases, substantial energy barriers exist, preventing the ions from interconversion at low internal energies. In all other cases, barriers towards isomerization are much lower. Thus, the remaining linear radical cations, i.e. ionized 1,2-, 1,4- and 2,3-pentadienes and the linear ionized pentynes, as well as vinylcyclopropane and 3-methylcyclobutene, readily adopt the 1,3-pentadiene structure prior to charge stripping, whereas the branched acyclic radical ions and ionized 1-methylcyclobutene are converted to ionized isoprene. As a consequence of the differently high isomerization barriers, adjustment of the pressure of the CS₂ charge exchange gas in the CI source may be used to

affect the internal energy of the $C_5H_8^{+*}$ ion population which, in turn, is reflected by characteristic changes of the CS spectra.

Detailed measurements have been performed on the formation and fragmentation of radical cations of C_5H_8 hydrocarbons including the heats of formation of the $C_5H_7^+$ ions^{22,28}. The proton affinities (PA) of cyclopentadiene (as well as of its heteroaromatic derivatives) have been determined by Houriet and his associates²⁹ using ion cyclotron resonance (ICR) mass spectrometry. Similar to pyrrole, furan and thiophene, protonation at the terminal positions of the diene system (C_α) of cyclopentadiene is thermodynamically more favourable than at the C_β positions, with cyclopentadiene exhibiting the largest PA difference (*ca* 8 kcal mol⁻¹). Semi-empirical calculations suggested a non-classical, pyramidal structure for the product of C_β protonation. More recent computational work adds detailed information on the thermochemical stabilities of the individual $C_5H_7^+$ ions³⁰. In fact, the allylic *c*- $C_5H_7^+$ ion was both measured²⁹ and calculated³⁰ to be *ca* 21 kcal mol⁻¹ more stable than the homoallylic, non-classical cyclopenten-4-yl cation. Since the experimental work discussed above provides only semi-quantitative, if any, information on low-lying isomerization barriers, computational approaches to the energy hypersurface of gaseous ions have gained much importance.

The $C_5H_8^{+*}$ ion manifold has been used also by other groups as a test case to explore the possibilities of using special mass spectrometric techniques to distinguish the ionic isomers and, thereby, their neutral precursors. An interesting additional degree of freedom available in CID and CS measurements is to vary the collision energy and the number of collisions. Thus, energy-resolved mass spectrometry (ERMS) was studied with $C_5H_8^{+*}$ ions by Jennings, Cooks and coworkers³¹ and revealed the potential to identify isomers, viz. ionized 1,3- and 1,4-pentadiene, which were found to be indistinguishable otherwise. Beynon and coworkers³² compared energy-dependent collision-induced dissociation, high-energy CID and a refined charge stripping technique comprising electron capture of the doubly charged ions (CS/EC). Although this work reflects the sensitivity of structure elucidation of highly unsaturated radical cations, it confirms that distinction is possible, in particular with CS techniques, between the branched acyclic (isoprene-type) and cyclic (cyclopentene) isomers. Besides CS and CS/EC mass spectrometry of mass-selected stable singly charged ions, doubly charged ions already generated in the EI ion source can be mass-selected after acceleration and subsequently subjected to electron capture. Such doubly-charged-ion ($2E^+$) mass spectra have been examined by Moran and coworkers³³ for a large set of alkenes including acyclic and cyclic alkadienes. Double ionization energies of a particular C_5H_8 isomer, 1,1-dimethylallene, concerning the triplet state of $C_5H_8^{2+}$ were determined by Harris and coworkers³⁴.

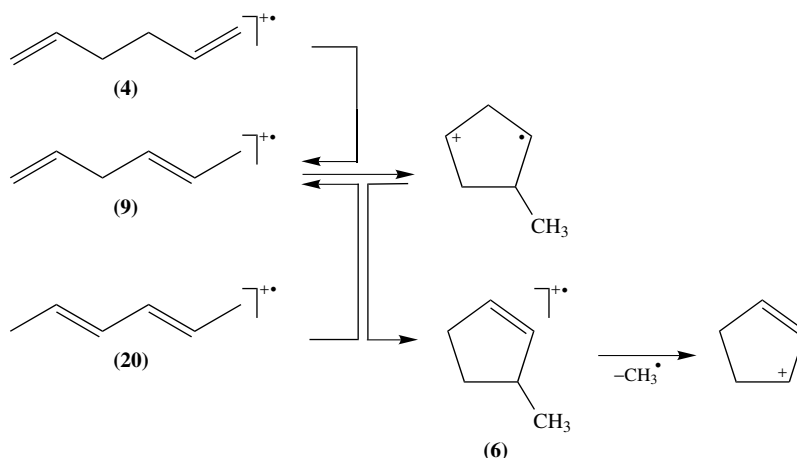
An alternative mass spectrometric technique to distinguish alkenes and more highly unsaturated radical cations is photodissociation mass spectrometry. In this method, laser light of variable wavelength is focused onto the beam of mass-selected ions and rapid, structure-specific dissociation may be achieved. By using this technique, $C_5H_8^{+*}$ ions were probed by Wagner-Redeker and Levens³⁵ and found to exhibit clearly distinct wavelength-dependent dissociation. For example, ionized 1,2- and 1,3-pentadiene not only exhibit extremely different cross sections in the wavelength range of $450 \leq \lambda \leq 535$ nm, but also clearly distinct mass spectra. Many related studies using light-induced excitation of gaseous olefinic ions have been reported. Dunbar and coworkers³⁶ investigated the photodissociation of six hexadiene radical cations. The spectra of the 1,3- and the 2,4-hexadienes were distinguishable and, by using laser light in the visible region ($478 \leq \lambda \leq 510$ nm), even all of the three stereoisomeric 2,4-hexadiene ions gave distinct spectra. Less long-lived stereoisomeric 2,4-hexadiene (and 1,3-pentadiene) radical cations studied by

Krailler and Russell³⁷ were found to give indistinguishable photodissociation mass spectra but different wavelength-dependence of the kinetic energy released upon fragmentation. Dunbar and coworkers³⁶ also showed that ionized 1,4-hexadiene is readily converted to the 2,4-isomer(s) whereas ionized 1,5-hexadiene is not. Thus, the radical cations of the conjugated dienes do not suffer H shift or rotation about the ionized double bonds under these conditions; likewise, H shifts do not take place in the isomer containing 'fully isolated' double bonds, but they do occur in the isomer containing the 1,4-diene unit. In the latter case, activation by two adjacent vinylic groups certainly drives the formal 1,3-H shift, whereas single allylic activation is not sufficient. Note that in the case of the ionized 1,5-isomer, competition due to the particularly favourable cleavage of the central C–C bond cannot occur (see below).

Photodissociation-photoionization mass spectrometry (PDPIMS) represents another technique involving photolysis of gaseous ions. In this approach, the neutral precursors are first photodissociated with ultraviolet laser light and the neutral fragments produced then softly ionized by coherent vacuum UV irradiation. A special feature of the method is that isomerization of the neutral precursor can be detected. Among the cases reported for dienes, Van Bramer and Johnston³⁸ recently described the identification of various alkene isomers by PDPIMS, including various C₆H₁₀⁺ isomers. By using 9.68 and 10.49 eV photons for ionization of the neutral fragments, the four conjugated hexadienes were found to exhibit highly individual PDPI mass spectra. Distinct from the other three isomers, 1,5-hexadiene gave intense allyl fragments, in line with the facile cleavage of the central, two-fold allylic C–C bond, followed by ionization to C₃H₅⁺ ions. This method is certainly interesting for direct analytical application.

In more early but very extensive and impressive work on C₆H₁₀⁺ ions, eight of the ten possible linear hexadienes and related unsaturated isomers have been investigated by Wolkoff, Holmes and Lossing³⁹. A total of thirty C₆H₁₀⁺ ions were studied. By again combining several experimental methods such as deuterium labelling, ionization and appearance energy measurements and metastable peak shape analysis, the authors conclude that the allylic *c*-C₅H₇⁺ ion is the only structure of the [M – CH₃]⁺ ions formed from all these precursors. Successive 1,2-H and 1,3-H shifts were postulated to interconvert alkyne, allene and diene isomers, with preferential intermediacy of the conjugated diene radical cations such as **20** and ionized 3-methylcyclopentene (**6**) as the key isomer undergoing the final CH₃[•] loss (Scheme 4). These results suggest that the C₅H₇⁺ ion with the cyclopenten-3-yl structure is the origin of the ubiquitous *m/z* 67 signal giving the base or second most prominent peak in the EI mass spectra of heptadienes, octadienes and some higher homologues. A related study was focused on the CH₃[•] loss from 1,5-hexadiene radical cations **8** generated both by field ionization (FI) and by EI and confirmed the isomerization of C₆H₁₀⁺ ions by formation of a five-membered rather than a six-membered ring⁴⁰.

Recently, another useful method for the distinction of easily isomerizing olefinic radical cations has been developed by Tureček and Gu⁴¹. The whole set of positive ions generated in the EI source from isomeric hexadienes and 3-methyl-1,3-pentadiene were accelerated and then neutralized by passing through a zone filled with Xe or NO gas. The fast neutrals are then reionized by collisions with O₂ in a cell floated at high negative electric potential to exclude all of the fragment ions which were generated during the neutralization and reionization processes from transmission. The cationic products that had survived the whole flight path were then mass analyzed. In the case of the C₆H₁₀⁺ ions, the 'survivor-ion' mass spectra yield better isomer differentiation than standard EI mass spectra, and the origin of this effect has been ascribed, *inter alia*⁴², to the enhanced survival chance of most highly unsaturated ions as compared to those containing saturated



SCHEME 4

carbon centres and thus being able to fragment relatively easily, e.g. by allylic cleavage (cf Section I).

B. Linear Dienes that Cannot Undergo Allylic Cleavage: Allene and Butadienes

A number of studies using the same or closely related methodology deal with lower homologues of the pentadienes and hexadienes. They will only be mentioned here briefly. For isomerization of ionized butadienes by electrocyclic reactions, see Section III.D.

Allene and the butadiene radical cations have been studied extensively with respect to isomerization and fragmentation. Very recently, Hayakawa and coworkers⁴³ published their investigation on the dissociation of electronically excited C_3H_4 isomers generated during charge reversal (CR, also called 'charge inversion') with metal vapours in the mass spectrometer. In previous work⁴⁴, these authors reported that unequivocal discrimination is possible between ionized allene and ionized propyne using this technique. This is in line with early experimental work by Stockbauer and Rosenstock⁴⁵, Levsen and coworkers⁴⁶ and also with *ab initio* calculations by Frenking and Schwarz⁴⁷. However, ionized propyne tends to isomerize to allene radical cation prior to fragmentation, as found by photoionization and photodissociation measurements by Parr and coworkers⁴⁸ and by van Velzen and van der Hart⁴⁹. The latter authors suggest that the energy barrier for interconversion of these $C_3H_4^{+\bullet}$ isomers by consecutive 1,2-H shifts is similarly high, as is that for the loss of H^\bullet yielding $c\text{-}C_3H_3^+$. A more recent work by van der Hart⁵⁰ offers a detailed computational analysis of the allyl radical and allyl cationic intermediates formed by the first 1,2-H shift. The CID and CS spectra of ionized cyclopropene have been compared with those of ionized allene and propyne⁵¹. A completely different approach by Cornaggia⁵² may be mentioned; he used Coulomb explosion mass spectrometry to determine the geometry of the carbon skeleton of $C_3H_4^{+\bullet}$ ions. Also, photoionization and photodissociation of allene clusters (dimers and trimers) has been studied⁵³ (cf Section V.A).

Early EI studies by King⁵⁴ suggested that 1,3-butadiene radical cations suffer isomerization and complete hydrogen scrambling prior to loss of H^\bullet and C_2H_2 . Later, Gross, Nibbering and coworkers⁵⁵ showed by field ionization kinetic (FIK) measurements that

hydrogen scrambling prior to loss of CH_3^\bullet , giving $c\text{-C}_3\text{H}_3^+$, is complete within $ca\ 10^{-11}$ s while carbon scrambling is relatively slow. It is only with metastable ions of lifetimes of 10^{-5} – 10^{-4} s that the carbon atoms lose their identity, too. Besides their unimolecular reactivity⁵⁶, in particular in pericyclic reactions (see Section III.D), gaseous $\text{C}_4\text{H}_6^{+\bullet}$ ions have also been investigated in detail by photodissociation techniques. Bunn and Baer⁵⁷ studied the isomerization of ionized 1,3-butadiene and 1- and 2-butyne by coincidence methods. Laser light (e.g. at $\lambda = 510$ nm) which photodissociates the butadiene radical ions does not affect the butyne ions. However, when the internal energy of the butyne ions was increased in a controlled manner, photodissociation set in at 10.6 eV, i.e. at some 1.8 eV (42 kcal mol⁻¹) above the ground state of the 1,3-butadiene ions. This value was interpreted to reflect the activation barrier towards hydrogen shift to form both of the isomeric butyne radical cations. In a more recent study, Baer and coworkers⁵⁸ investigated the details of the energetics and dynamics of the unimolecular isomerization of 1,3-butadiene radical cations, including the intermediacy of ionized 3-methylcyclopropene, prior to CH_3^\bullet loss. The isomerization barrier towards the skeletal rearrangement was determined to be $ca\ 46$ kcal mol⁻¹ and only 8 kcal mol⁻¹ below the threshold of dissociation giving pure $c\text{-C}_3\text{H}_3^+$ ions⁵⁹. Two-colour laser multiphoton ionization (MPI) and dissociation of 1,3-butadiene was measured by Chupka and coworkers⁶⁰. The geometry of ionized 1,3-butadiene as determined by matrix infrared and resonance Raman spectroscopy by Bally and coworkers^{61,62} may be mentioned here.

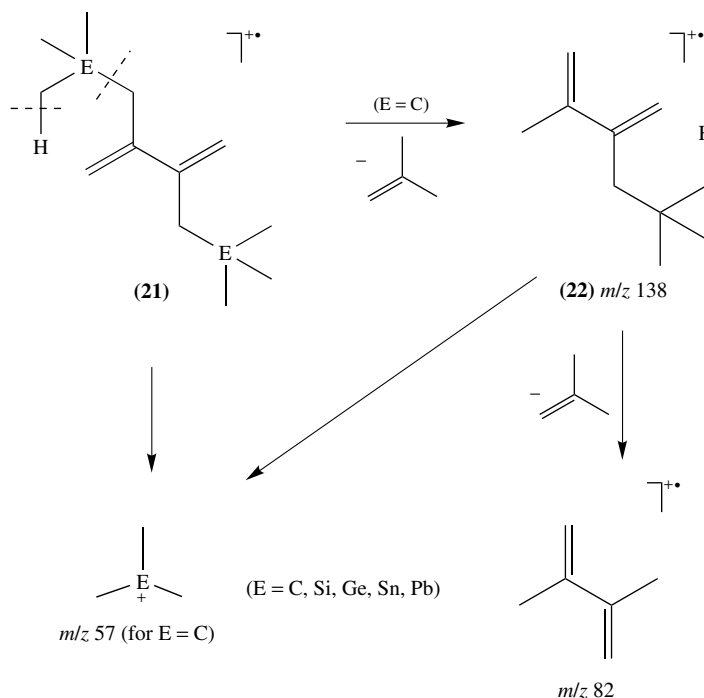
Not surprisingly, the presence of a hydroxy group in ionized 1,3-butadiene strongly affects the overall mechanism of the CH_3^\bullet loss. Tureček, Gäumann and coworkers⁶³ generated the highly stable dienol ion radical cation of 2-hydroxybutadiene radical cations by a retro-Diels–Alder reaction (see Section III.E) and showed, by extensive deuterium and ¹³C labelling, that the highly stable acryloyl cations, $\text{H}_2\text{C}=\text{CH}-\text{CO}^+$, are formed, rather than hydroxycyclopropenyl cations. The EI mass spectra of several fluoro- and fluorochloro-substituted 1,3-butadienes have also been reported⁶⁴.

C. Linear Dienes and Polyenes: McLafferty Reactions

As mentioned in the Introduction, the ionized C–C double bond can trigger a characteristic hydrogen rearrangement reaction which, in turn, leads to allylic cleavage of the intermediate. Whereas the McLafferty reaction of ionized heteroatomic double bonds and aromatic nuclei is highly characteristic for the structure of the precursor molecule, the analytical value for this process with olefins decisively depends on the site stability of the unsaturation. Therefore, alkene ions which tend to undergo facile hydrogen shifts or even scrambling may give McLafferty rearrangement reactions which do not reflect the original structure. Of course, the presence of suitable saturated carbon centres is necessary to allow the γ -hydrogen migration to occur at all. In suitable cases, the relatively low energy requirements for the McLafferty reaction may help to compete with isomerization by H shifts. In the case of monoolefins, the McLafferty reaction was found to be rather unspecific for 1,2-alkyl-substituted dienes but quite specific for 1,1-dialkyl- and all more highly alkyl-substituted congeners⁶⁵. For dienes and polyenes, however, fragmentation by McLafferty reactions is extremely rare, much in contrast to the fragmentation behaviour of alkylbenzene radical cations⁷. It is quite obvious that isomerization by C–C bond formation between the unsaturated sites predominates in ionized alkadienes and alkapolyenes, provided such cyclization reactions are sterically possible. Interestingly, in their comprehensive review published in 1974 on the McLafferty reaction, Bursley and coworkers⁶⁶ have commented on the suppression of the γ -H rearrangement to C–C double bonds when arene or/and carbonyl functions are also available in the radical cation⁶⁷. Thus, in

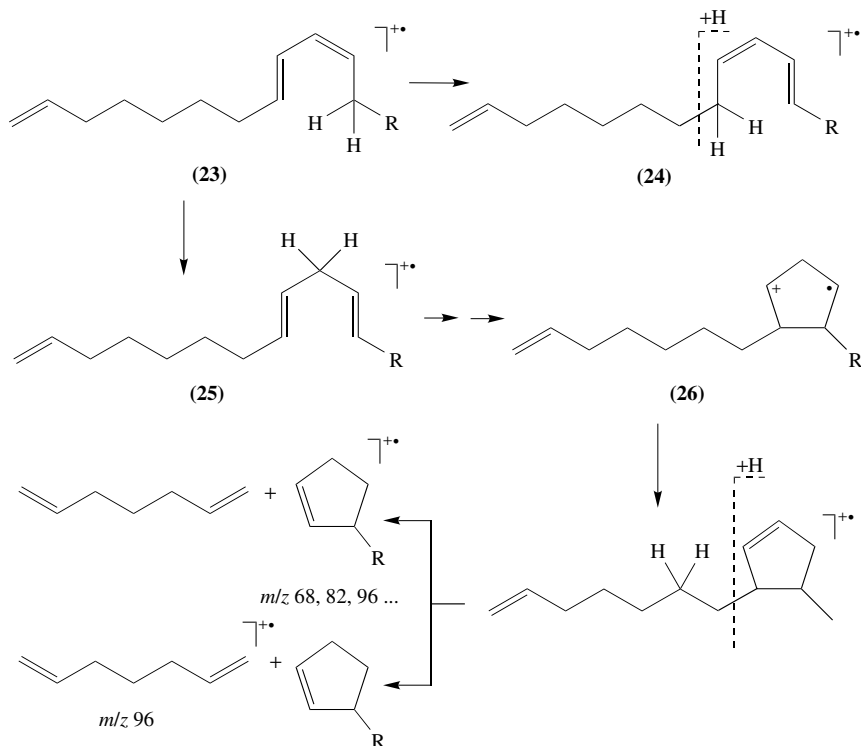
a case where the γ -H rearrangement to a C–C double bond was found to compete with that to a C–O double bond, the former is shifted to an internal position of the aliphatic chain prior to the actual McLafferty process⁶⁸.

Since C–C double bond shifts are even more frequent in ionized dienes and polyenes, clear-cut McLafferty reactions are extremely rare for these compounds. 2,3-Alkyl-substituted 1,3-butadienes may present an exception if 1,2-H shifts are also suppressed. An interesting example was reported by Bates and coworkers⁶⁹ for 2,3-neopentyl-1,3-butadiene (**21**, E = C) (Scheme 5). Despite the high tendency to undergo allylic cleavage yielding $C_4H_9^+$ ions (m/z 57), a peak of considerable relative intensity was observed at m/z 138 for the loss of C_4H_8 (isobutene). The $[M - C_4H_8]^{+\bullet}$ ions (**22**), in which an ionized 1,3-diene unit has been preserved, suffers another McLafferty reaction to give $[M - 2 C_4H_8]^{+\bullet}$ ions with m/z 82, of likewise moderate intensity. Without any doubt, ionized 2,3-dimethyl-1,3-butadiene is formed in this sequence of elimination reactions. The analogues containing Si, Ge, Sn and Pb, instead of carbon, at the neopentane centres did not give the corresponding element-organic alkadiene ions owing to the more facile allylic cleavage and the low stability of the corresponding element-organic isobutenes.



SCHEME 5

Another, and quite telling, example concerns the structure-specific elimination of olefins from acyclic trienes (Scheme 6). Bestmann and coworkers⁷⁰ found that the EI spectra of (8*E*,10*Z*)-1,8,10-dodecatriene (**23**, R = H), (11*E*,13*Z*)-1,11,13-pentadecatriene and some of their homologues display characteristic peaks at m/z 68, 82, 96 etc., corresponding to the formation of ionized alkadienes $C_{5+n}H_{8+2n}^{+\bullet}$, along with a neutral diene. The peaks



SCHEME 6

corresponding to the complementary charge distribution were also observed. Measurements at low ionization energy clearly favoured these rearrangement reactions, a typical behaviour for slow reorganization processes requiring only low activation energies but long ion lifetimes. Although no clear-cut mechanism has been forwarded, it is obvious that the (ionized) 1,3-butadiene unit triggers hydrogen rearrangements such as specific ones, e.g. 1,5-H shifts leading to **24** and subsequent allylic C–C bond cleavage, but also unspecific ones, i.e. by repeated 1,2-H shifts. In the present case, the latter process would convert the 1,3-diene (**23**), to the 1,4-diene (**25**) which is prone to cyclization. The alkylalkenyl-substituted cyclopentene (**26**) thus formed can undergo a 1,2-H shift followed by the McLafferty reaction to yield even-mass fragments which are characteristic for the initial 1,3-butadiene unit.

However, things may become even more difficult. In a recent communication, Miyashi and coworkers⁷¹ discussed the possibility of the Cope rearrangement in the radical cations of five dimethyldiphenyl-substituted 1,5-hexadienes and three isomeric dimethyldiphenyl-substituted bicyclo[2.2.0]hexanes. The 70 eV EI spectra of these compounds exhibit slight differences and the cleavage of the bis-allylic C–C bond is a minor fragmentation channel only. Unexpectedly, the base peak (m/z 158) corresponds to the elimination of 104 mass units. The authors attribute this to a McLafferty reaction as major exit from the putative equilibrium of the isomers produced by the Cope rearrangement. However, in view of the general tendency of highly unsaturated alkylbenzene radical cations to undergo cyclization⁷, various other isomerization paths seem likely to intervene.

In concluding this section, the EI mass spectra of some 'true' polyolefins may be discussed. Remarkably, the normal 1, 5, 9, ... sequence of double bonds in oligoterpenes does not permit elimination processes such as the McLafferty reaction. Several double bond shifts would enable this type of reaction to occur. Although structure-specific allylic or bis-allylic cleavage occurs in large isoprenoids, random H migrations may compete and suppress structure-specific analytical information. Bhalerao and Rapoport⁷² performed a systematic study of several isoprenyl ketones bearing three to five isoprene units, one of which is saturated, as model cases for higher isoprenoids. Extensive hydrogen migration was observed, and the major primary fragmentations were found to be alkyl loss ($C_nH_{2n+1}^+$, $1 \leq n \leq 6$). Only in one case do the spectra contain an abundant even-mass fragment ion (m/z 136) corresponding to the mass of a monoterpene unit, $C_{10}H_{16}$. However, formation of this radical cation requires double 1,2-H shift along the chain and is thus non-diagnostic for analytical purposes. As the authors stated, this shows the 'limitations of [conventional EI] mass spectrometry for detection of the position of a saturated isoprene unit in polyisoprenoids'. Likewise, some olefin eliminations have been reported⁷³ for the EI spectra of carotenoids, but the details of the mechanism appear doubtful in view of nowadays general insights into the complexity of ionic rearrangements.

D. Butadiene and Cyclobutene

The interconversion of butadiene radical cations and ionized cyclobutene represents a model case for a formal pericyclic process. Much work has been invested to study not only the distinguishability of these isomers and their derivatives by mass spectrometry, but also to check the role of orbital symmetry in the ionic species. Dass⁴ has addressed the latter problem in depth in a review on pericyclic reactions in radical cations in both the gas and condensed phases and no further survey on the papers mentioned there will be given here. The topic pertains also to the ring-opening of ionized benzocyclobutene to ionized *ortho*-quinodimethane (cf Section V) and various other phenyl-, methyl- and carboxy-substituted derivatives. In this context, we restrict ourselves here mentioning that an upper limit of 7 kcal mol⁻¹ only has been determined by CE mass spectrometry for the activation barrier of the cycloreversion of the parent cyclobutene radical cations⁷⁴. The energy requirement for the cycloreversion of ionized 1- and 3-substituted cyclobutenes were found, by experiment, to be markedly different. Obviously, dissociation of the (in a sense bis-allylic) strained C–C bond is much more facile when the substituent is at C-3, i.e. at the α position to the bond to be cleaved⁷⁵. Also, it may be pointed out that the agglomeration of several double bonds in olefins containing aromatic nuclei gives rise to various cyclization paths. For example, 1-phenylcyclobutene and 2-phenyl-1,3-butadiene radical cations were shown to isomerize to ionized 1-methylindene⁷⁶. This behaviour holds also for other alkylbenzenes containing unsaturated bonds in the side chain⁷.

Mandelbaum and coworkers⁷⁷ reported on the partial retention of the stereochemical identity of the 1,3-butadiene skeleton prior to fragmentation in the EI mass spectra of the isomeric dimethyl 3,4-diethylmuconates. Whereas the radical cations of the *trans,trans*-isomer exhibits loss of methanol, those of the *cis,cis*- and the *cis,trans*-isomers both expel a methoxy radical during cyclization to the respective pyrylium cations. In a subsequent work⁷⁸, the EI mass spectra of the dimethyl esters of the stereoisomeric dimethyl muconates and some 3,4-disubstituted derivatives have also been studied with respect to electrocyclic ring closure to the corresponding dimethyl cyclobut-3-ene-1,2-dicarboxylates. To a great extent, both the stereoisomers and constitutional isomers were found to behave in a distinct way and it was concluded that electrocyclization is largely suppressed by specific neighbouring group interactions involving the carboxylate and the 3,4-alkyl groups.

The proton affinities of 1,2- and 1,3-butadiene and of 2-butyne have been determined by Lias and Ausloos⁷⁹ using equilibrium measurements in an Fourier transform ion cyclotron resonance (FT-ICR) mass spectrometer. Surprisingly, they were found to be almost identical. The bimolecular reactivity of the $C_4H_7^+$ cations formed from the three isomers was also reported.

E. Cyclic Dienes and Polyenes: Retro-Diels–Alder and (Apparent) Diels–Alder Reactions

One of the most characteristic fragmentation reactions of ionized cycloalkenes is the expulsion of a C_2 unit from the ring as an olefin. In the simplest case, cyclohexene radical cations undergo dissociation of the allylic C–C bonds to produce neutral ethene and ionized 1,3-butadiene. Substituents on the cyclohexene ring may favour the allylic cleavage but also invert the distribution of the positive charge, to generate ionized ethene and neutral butadiene pair of fragments. Further, H shifts may precede fission of the C–C bond(s) and lead to RDA products of non-specific masses. Fortunately, the highly excited molecular ions produced in the standard 70 eV EI mass spectra are sufficiently short-lived to favour the allylic cleavage reactions over competing rearrangement processes. In contrast, long-lived cyclohexene radical cations, i.e. metastable ions, are known to undergo extensive H shifts^{80,81}.

Mass spectrometric retro-Diels–Alder reactions are particularly interesting for the characterization of complex alicyclic molecular frameworks. Just as Diels–Alder reactions in synthetic organic chemistry allow one to construct complex structures by a single preparative step, the retro-Diels–Alder reaction yields literally ‘clear-cut’ analytical information although more than one bond has to be broken. Moreover, the formal analogy between the retro-Diels–Alder reaction of neutral reactants and the cycloreversion of radical cations in the mass spectrometer offers the potential to use this fragmentation as a probe for the stereochemistry of the cyclic or polycyclic compounds under investigation. An important question directly associated with this problem refers to the concertedness or non-concertedness of pericyclic reactions in (open-shell) radical cations. Therefore, extensive work has been done on the applicability of the RDA-type fragmentation in mass spectrometry. Since a number of comprehensive reviews have appeared during the past decades, the following discussion will be restricted to a few selected examples on dienes and polyenes and in particular to more recent work on this class of alkenes.

An interesting prototype case which has been under intense study concerns the RDA reaction of the radical cations of 4-vinylcyclohexene. By using appropriate deuterium labelling, Smith and Thornton⁸² studied the distribution of the positive charge between the two formally identical 1,3-butadiene fragments, one involving an original intra-ring C_4 subunit and the other a C_4 subunit including the original vinyl group. A considerable preference for charge retention in the latter fragment was observed. Since this is at odds with the Stevenson–Audier rule⁸³, which would predict strictly equal probability for ionization of the two butadiene fragments, the degree of concertedness of the C–C bond cleavage and the conservation of orbital symmetry was invoked to explain the experimental results^{84,85}. Tureček and Hanuš⁸⁶ investigated the parent 4-vinylcyclohexene and four higher congeners generating two identical diene fragments. For 4-vinylcyclohexene and the 1,4-dimethyl derivative, these authors found only a slight preference for the charged butadiene and isoprene fragments, respectively, whereas the $1,\Delta^1$ -dimethyl isomer (limonene), dicyclopentadiene and dicyclohexadiene all exhibited symmetrical charge distribution. As a tentative rationalization, unsymmetrical retention of charge in the fragments was attributed to unsymmetrical charge distribution in the molecular ions.

Notably, the labelling studies with the ionized vinylcyclohexenes enabled the distinction of the two moieties in the molecular ions that eventually yield the diene fragments. In fact, H atom shifts were found to be relatively slow in the ions undergoing the RDA processes, in contrast to ionized cyclohexene which is known to suffer fast and extensive hydrogen scrambling after field ionization (FI) even at very short ion lifetimes⁸⁰. Obviously, once again, dissociation of the particularly weak bis-allylic C–C bond present in the 4-vinylcyclohexene-type radical cations is sufficiently fast to largely suppress isomerization by 1,2- or 1,3-H shifts.

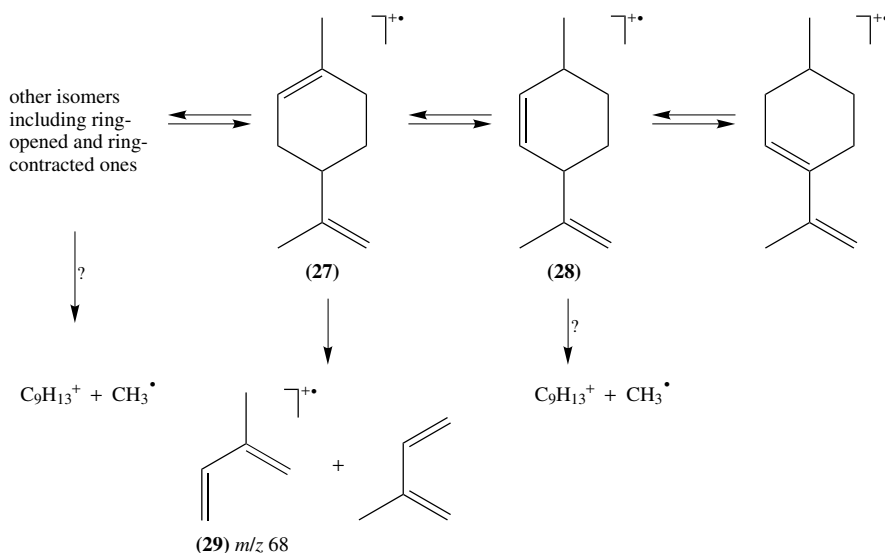
In this context, the striking difference of the standard 70 eV EI mass spectra of the isomeric cyclooctadienes may be mentioned here (see below)⁸⁷. Whereas the radical cations of the stereoisomeric 1,5-cyclooctadienes, containing two bis-allylic C–C bonds, give the products of the two-fold allyl cleavage as the base peak ($[C_8H_{12}]^{+\bullet}/[M]^{+\bullet} \approx 10 : 1$), the *cis,cis*-1,4- and *cis,cis*-1,3-cyclooctadiene ions are reluctant to do so ($[C_8H_{12}]^{+\bullet}/[M]^{+\bullet} \approx 1 : 3$). Clearly again, 1,2- and 1,3-H shifts cannot efficiently compete with dissociation of the bis-allylic C–C bond.

The EI-induced fragmentation of gaseous [4 + 2]- and [2 + 2]dicyclopentadiene radical cations has been studied by Roth and coworkers⁸⁸ using Fourier transform ion cyclotron resonance mass spectrometry, and compared to the cleavage of these ions in solution using chemically induced dynamic nuclear polarization (CIDNP). Both in the gas and in the liquid phase, the isomers of the molecular ions formed by single C–C bond cleavage were observed. It is noteworthy that these distonic ions were termed ‘non-vertical radical’ cations.

In the case of the parent $C_8H_{12}^{+\bullet}$ system, the reverse process of the RDA reaction, i.e. the formal Diels–Alder addition of a 1,3-butadiene radical cation to neutral 1,3-butadiene, has been studied in great detail. Groenewold and Gross generated the adduct ions in a usual CI source of a sector-field mass spectrometer. Characterization of the adduct ions by CID revealed the presence of a mixture of isomers, the composition of which strongly depends on the internal energy imposed on the adducts. 4-Vinylcyclohexene ions and an acyclic $C_8H_{12}^{+\bullet}$ isomer, probably with distonic structure, were identified as the major components and a stepwise mechanism, rather than a concerted one, was invoked⁸⁹. In contrast, Bauld and coworkers⁹⁰ had suggested a concerted, albeit non-synchronous path for the formal ‘cation-radical Diels–Alder’ reaction on the basis of semiempirical and *ab initio* molecular orbital (MO) calculations. Later, the complexity of the $C_8H_{12}^{+\bullet}$ ion hypersurface was clearly demonstrated by Chen and Williams⁹¹ using electron-spin resonance (ESR) spectroscopy of the bicyclo[3.2.1]oct-2-ene radical cations generated by skeletal rearrangement of 4-vinylcyclohexene upon radiolytic oxidation in freon matrix at 77 K.

Gross and coworkers⁹² demonstrated that both $C_8H_{12}^{+\bullet}$ isomers reside in distinct potential wells and can be characterized by CID in both sector-field and FT-ICR mass spectrometers. The mass spectrometric experiments were in line with calculation in that the ionized bicyclic isomer appears to be more stable than 4-vinylcyclohexene ions, and with the radiolytic results in that a closely related bicyclic isomer, viz. ionized bicyclo[2.2.2]octene, is not easily formed upon ionization of the other C_8H_{12} hydrocarbons. The retro-Diels–Alder reaction of ionized bicyclo[2.2.2]octa-2,5-dienes leading to expulsion of the initially saturated bridge as an alkene gives rise to the base peak in the EI spectra⁹³.

Limonene, one of the most prominent natural monoterpenes (cf Section VII), represents a particular derivative of 4-vinylcyclohexene since it has been studied with respect to the pronounced energy dependence of its fragmentation behaviour (Scheme 7). Counter-intuitively, and in contrast to 4-vinylcyclohexene, the radical cations of limonene (**27**) do not undergo the retro-Diels–Alder reaction if the internal energy of the ions is low. As



SCHEME 7

pointed out by Boyd and coworkers⁹⁴, ionization at 70 and even at 20 eV leads to abundant ionized and neutral isoprene expected for the RDA process, the $\text{C}_5\text{H}_8^{+\bullet}$ ions (*m/z* 68) giving rise to the base peak in the spectra, but neither the metastable ion (B/E linked scan) spectra nor CID spectra of stable ions exhibit a peak at *m/z* 68. Rather, loss of CH_3^\bullet prevails as the primary fragmentation process. The origin of the *m/z* 68 peak from the singly charged molecular ion of limonene, $\text{C}_{10}\text{H}_{16}^{+\bullet}$ (*m/z* 136), is beyond any doubt since occurrence of a thermal RDA reaction or doubly charged $\text{C}_{10}\text{H}_{16}^{2+\bullet}$ ions were excluded. Moreover, the structure of the $\text{C}_5\text{H}_8^{+\bullet}$ ions formed from the high-energy molecular ions was confirmed to resemble that of ionized isoprene (29). Deuterium labelling revealed extensive hydrogen scrambling prior to fragmentation, including the splitting into the moieties formed by the RDA path. As a consequence, low-energy molecular ions, e.g., 27, obviously undergo even more extensive isomerization generating isomers such as 28 from which less energetically demanding C–C bond cleavages can occur, in particular loss of CH_3^\bullet . Later, the pronounced energy dependence of the fragmentation of ionized limonene was used by Cooks and coworkers as a probe to study the effects of energy deposition by surface-induced dissociation (SID) and energy- and angle-resolved mass spectrometry⁹⁵ and also under various conditions of tandem mass spectrometry present in triple quadrupole and FT-ICR instruments⁹⁶. More recent work addressed the same problem using electron-induced dissociation (EID), by which electrons are collided with the ions of interest⁹⁷.

Many other ion–molecule reactions involving highly unsaturated hydrocarbon ions and neutral olefins or the equivalent strained cycloalkanes have been studied by mass spectrometry⁹⁸. For example, we may mention here the addition of ionized cyclopropane and cyclobutane to benzene radical cations giving the respective *n*-alkylbenzene ions but also isomeric cyclodiene ions such as ionized 8,9-dihydroindane and 9,10-dihydrotetralin, respectively. Extensive studies have been performed on the ‘dimerization’ product of charged and neutral styrene⁴.

In their recent landmark femtosecond-resolved mass spectrometry studies, Zewail and coworkers⁹⁹ have used mass spectrometry for monitoring the time-resolved unimolecular fragmentation of neutral norbornene and norbornadiene. In both cases, the RDA reactions occurred, but only in the norbornadiene case was the well-known H[•] loss giving rise to C₇H₇⁺ ions found to compete. Still, non-concertedness and biradicaloid character of the intermediates is being addressed by femtosecond dynamic studies. In this context, Kompa and coworkers¹⁰⁰ have compared the expulsion of H⁺ from femtosecond-laser-irradiated 1,3-cyclohexadiene and 1,3,5-hexatriene. The closed-shell cation analogy of the RDA reaction of norbornene is the cycloreversion of bicyclo[3.2.1]oct-6-en-3-yl cations, which have been studied very recently by the present authors¹⁰¹ in the context of the isomerization of protonated cycloheptatrienes¹¹. The reverse reaction type, viz. cycloaddition of the allyl cation to 1,3-butadiene, has been recently studied by Pascual-Teresa and Houk¹⁰² using *ab initio* calculations. In all cases mentioned, the results point to stepwise paths of cycloreversion or cycloaddition, respectively.

F. Selected Cycloalkadienes and Cycloalkapolyenes

Mass spectrometry of certain cyclic dienes and polyenes deserves special discussion owing to their prototypical isomerization and fragmentation behaviour. Among them, C₅H₆⁺ ions from 1,3-cyclopentadiene, C₆H₈⁺ ions from the cyclohexadienes, C₇H₈⁺ and C₇H₉⁺ ions from 1,3,5-cycloheptatriene and its isomers, as well as ions derived from 1,3,5,7-cyclooctatriene and its less unsaturated analogues will be treated here briefly.

Methylenecyclopropene and Cyclobutadiene. The radical cations of these smallest cycloalkadienes have been of high interest owing to their fundamental importance in physical organic chemistry¹⁰³. Lifshitz and coworkers¹⁰⁴ were the first to find indications for the formation of isomeric C₄H₄⁺ ions upon EI of benzene¹⁰⁵. Using their distinct bimolecular reactivity in an ICR mass spectrometer, Ausloos¹⁰⁶ detected the presence of both a linear and a second, non-linear C₄H₄⁺ isomer in the [M – C₂H₂]⁺ ions generated by EI of benzene and suggested them to be ionized methylenecyclopropene. Bowers and coworkers¹⁰⁷ confirmed these results by CID spectrometry and elucidated the quantitative composition of the C₄H₄⁺ ion mixture. Further experimental data on the C₄H₄⁺ manifold were contributed by McLafferty and coworkers^{108,109} by using CID mass spectrometry and neutralization–reionization mass spectrometry of the C₄H₄⁺ ions generated, e.g. from Nenitzescu's hydrocarbon, tricyclo[4.2.2.0^{2,5}]deca-3,7,9-triene, as well as CID spectrometry of the C₄H₇N⁺ adducts formed from C₄H₄⁺ with ammonia¹¹⁰. Besides these C₄H₄⁺ isomers, ionized vinylacetylene and butatriene were also distinguished by this method. Quantitation of the four isomers in mixtures of C₄H₄⁺ ions generated from a large variety of neutral precursors was also performed¹¹¹. For example, benzene radical cations were found to give 70% of ionized methylenecyclopropene and 30% of vinylacetylene, whereas ionized cyclobutadiene is the main product generated from CO loss of the radical cations of the benzoquinones, besides other suitable sources. The presence of minor amounts of butatriene radical cations (10%), besides a major fraction of ionized vinylacetylene (60%) and cyclic isomer(s) (30%, probably ionized methylenecyclopropene) was also determined by van der Hart¹¹² using photodissociation of benzene and 1,5-hexadiyne as precursors. Later, Cooks and coworkers¹¹³ generated these C₄H₄⁺ isomers in a directed way. Pure *c*-C₄H₄⁺ ions were also generated by Jacobsen and coworkers¹¹⁴ starting from *cis*-3,4-dichlorobutene and performing a well controlled ion/molecule reaction with bare Fe⁺ ions in the cell of an FT-ICR mass spectrometer. The identity of these ions was probed by characteristic ion/molecule reactions (see Section V).

Schwarz and coworkers¹¹⁵ used 1,2,3-butatriene, along with 1,3-butadiyne, as a precursor for the generation of neutral 1,2,3-butatrienylidene in a neutralization/reionization mass spectrometric sequence ($C_4H_4 \rightarrow C_4H_2^{-\bullet} \rightarrow C_4H_2 \rightarrow C_4H_2^{+\bullet}$).

Cyclopentadienes. Maquestiau, Beynon and coworkers¹¹⁶ have studied the charge-stripping and collision-induced dissociation spectra of ionized cyclopentadiene and of the $C_5H_6^{+\bullet}$ ions generated from various precursors including dicyclopentadiene. Evidence for the presence of both cyclic and acyclic isomers was obtained. Cooks and coworkers¹¹⁷ confirmed these results by applying surface-induced dissociation spectrometry, an alternative method using the excitation of mass-selected ions by bombarding them onto a surface and measuring the ionic fragments being 'reflected', to a similar set of $C_5H_6^{+\bullet}$ ions generated, *inter alia*, from norbornadiene, dicyclopentadiene and 2-methylenenorbornane.

The EI mass spectra of methyl-substituted cyclopentadienes were studied by Harrison and coworkers¹¹⁸ and their fragmentation behaviour was found to be very similar to that of the isomeric cyclohexadienes. Major fragmentation paths were suggested to lead to protonated alkylbenzenes such as benzenium ($C_6H_7^+$) and toluenium ($C_7H_9^+$) ions. Obviously, formation of antiaromatic cyclopentadienyl cations is circumvented; however, other isomers may also be formed along with the (most stable) arenium-type fragment ions (see below). Open-chain 1,3,5-hexatriene isomers were also found to give similar EI mass spectra.

Cyclohexadienes and 1,3,5-Hexatrienes. Not only the standard EI mass spectra but also the CID spectra of the isomeric cyclohexadienes are indistinguishable, as shown by McLafferty and coworkers¹¹⁹. Owing to the conjugated π electron system, the 1,3-isomer has a significantly lower ionization energy than the 1,4-isomer ($\Delta IE = 13 \text{ kcal mol}^{-1}$)¹⁴ but fragmentation to, e.g., $C_6H_7^+$ ions, whose structure has been a matter of debate in several aspects (see below)¹²⁰⁻¹²², is preceded by fast hydrogen scrambling. Among other sources, fragmentation of ionized 4-vinylcyclohexene and 1,5-cyclooctadiene generates cyclohexadiene radical cations as the major product^{85,119}. Among other isomers, 1,3,5-hexatriene radical cations do not convert completely to the cyclohexadiene ions, as also shown by CID spectrometry¹¹⁹. Photodissociation of stereoisomeric 1,3,5-hexatrienes was stated to be identical¹²³. The interconversion of 1,3-cyclohexadiene and its open-chain isomer has been reviewed together with related formally electrocyclic reactions in lower and higher analogues⁴. Schweikert and coworkers¹²⁴ recently demonstrated that plasma desorption (PD) mass spectra of the two isomeric cyclohexadienes are distinct, in contrast to their EI and CID spectra. It has to be noted that PD spectrometry not only yields the radical cations $M^{+\bullet}$ but also the protonated molecules $[M + H]^+$, along with their fragments, and the abundance ratio of these ions was found to be quite distinct. A comparative resonant two-photon ionization (R2PI) time-of-flight (TOF) mass spectrometry study on jet-cooled 1,3-cyclohexadiene and 1,3,5-hexatriene was performed by Share and Kompa¹²⁵. The photodissociation study of Baumgärtel and coworkers⁵³ on allene clusters, which essentially produce ionized dimers and trimers, $(C_3H_4)_2^{+\bullet}$ and $(C_3H_4)_3^{+\bullet}$, reveal that the latter aggregates behave very similarly to those of the covalently bound radical cations. For example, the ionized allene dimer reacts similarly to the cyclohexadiene radical cations forming abundant $C_6H_7^+$ ions by loss of H^\bullet .

Various substituted 1,3-cyclohexadienes and their open-chain isomers, the respective 1,3,5-hexatrienes, have been studied by EI mass spectrometry with special regard to the stereospecificity of the mutual pericyclic interconversion. A brief discussion including the parent systems, ionized 1,3-cyclohexadiene and 1,3,5-hexatriene has been provided by Dass in his review on pericyclic reactions of radical cations⁴. McLafferty and coworkers¹¹⁹ have shown that the two parent isomers are (almost) indistinguishable

by CID spectrometry. Thus, the barrier towards interconversion is very low as compared to those of fragmentation and the occurrence of the pericyclic process, in analogy to the neutral counterparts, appears to be rapid. Interestingly, *cis*- and *trans*-5,6-dimethyl-1,3-cyclohexadiene and the three corresponding acyclic $C_8H_{12}^{+\bullet}$ isomers, viz. *cis,cis,cis*-, *cis,cis,trans*- and *trans,cis,trans*-2,4,6-octatriene, also exhibit very similar EI mass spectra, as demonstrated by Rennekamp and Hoffman¹²⁶. Loss of CH_3^\bullet is the most prominent fragmentation in all cases, with a slight preference for the cyclic isomers, in which a direct exit path exists by dissociation of the allylic C–C bonds. Furthermore, CH_3^\bullet loss and the other fragmentation channels (expulsion of H^\bullet , H_2 and the ensemble of both) were found to be associated with identical kinetic energy release (T_{kin}) values. No clear evidence for the role of orbital-symmetry control is deducible from these studies. From a general view, it appears rather likely that other isomerization paths such as five-membered ring formation and extensive hydrogen shifts make up a highly complex hypersurface in these highly unsaturated radical cations.

Fulvene Radical Cations, Protonated Fulvene, and Isomeric $C_6H_6^{+\bullet}$ and $C_6H_7^+$ Ions. The radical cations of fulvene are isomeric to those of benzene and the open-chain $C_6H_6^{+\bullet}$ ions which have been studied in great detail with regard to the skeletal rearrangement of the prototype aromatic species prior to fragmentation. This topic has been reviewed earlier⁷. The chemistry of ionized fulvene and its derivatives has also been studied in various ways but is less understood than that of the linear $C_6H_6^{+\bullet}$ ions. An early work of Hanus and Dolejšek¹²⁷ showed that the EI-induced unimolecular fragmentation of 6-methylfulvene is very similar to that of toluene, 1,3,5-cycloheptatriene and some other C_7H_8 isomers. Rosenstock and coworkers¹²⁸ early indicated that the fulvene radical cation is the next stable $C_6H_6^{+\bullet}$ isomer beyond the benzene ion, which is only some 10 kcal mol⁻¹ more stable¹²⁹. Photoelectron spectroscopy had suggested an even smaller energy difference¹³⁰. In recent years, more quantitative data have become available by combining techniques such as ion/molecule reactions, photodissociation mass spectrometry and computational approaches. Owing to distinct ion/molecule reactivity as compared to ionized benzene, fulvene ions reside in a relatively deep energy well¹³¹. The critical energy for $C_6H_6^{+\bullet}$ ion interconversion still lies some 58 kcal mol⁻¹ above the heat of formation of the fulvene ion, as determined in computational work by van der Hart¹³². Yet, isomerization is possible since fragmentation is even more energy demanding.

Protonated fulvene (fulvenium) ions have been studied to a much lesser extent, although they represent isomers of benzenium ions, the prototype species for the major intermediates formed during electrophilic aromatic substitution. Based on ICR mass spectrometry, Lias and Ausloos¹³³ pointed out that loss of H^\bullet from the ionized cyclohexadienes, *trans*-1,3,5-hexatriene and the methylcyclopentenes leads to a mixture of two isomeric $C_6H_7^+$ ions, one being the benzenium ion and the other a less acidic species. Similar mixtures were obtained by ion/molecule reactions of ionized and neutral allene and propyne. The ‘non-benzenium’ ion was assigned the structure of protonated fulvene, and the C(1)-protonated form was suggested to be the most stable $C_6H_7^+$ isomer next to protonated benzene. Zhu and Gäumann¹³⁴ drew similar conclusions from infrared multiphoton dissociation of 1,4-cyclohexadiene radical cations formed under ICR conditions. Fulvenium ions were also identified as the product of ion/molecule reactions involving allyl bromide¹³⁵, vinyl chloride¹³⁶ and 1,3-butadiene¹³⁷. In analogy to the isomeric $C_6H_6^{+\bullet}$ ions derived from fulvene and benzene, the difference in stability was found to be rather small, and a recent theoretical study by Bouchoux and coworkers¹³⁸ suggested C(1)-protonated fulvene to be by only 10 kcal mol⁻¹ less stable than the benzenium ion. The details of the hypersurface were also calculated and, in further analogy

to the case of the radical cations, substantial energy barriers towards the skeletal rearrangement were calculated for the $C_6H_7^+$ ions. In the context of the ring contraction of protonated 1,3,5-cycloheptatriene and its 7-methyl derivative, $C_7H_9^+$ and $C_8H_{11}^+$, we have recently determined the thermochemical properties of protonated 6-methyl- and 6,6-dimethylfulvene¹³⁹.

For mass spectrometry and gas-phase chemistry of negative ions derived from fulvene, see Section IV.A.

Cycloheptatriene, Norbornadiene, Methylenecyclohexadienes (Isotoluenes) and Bicyclo[3.2.0]heptadienes. The gas-phase ion chemistry of ionized 1,3,5-cycloheptatriene is closely related to that of ionized toluene, in particular, and to that of norbornadiene and other 'non-aromatic' $C_7H_8^{+\bullet}$ isomers. This extensive body of work will not be discussed here since a detailed review on this topic has been published by one of these authors in the context of the gas-phase chemistry of the alkylbenzene radical cations^{7,140}. This chemistry pertains also to the well-known isomerization of the even-electron $C_7H_7^+$ ions and to their formation from the respective parents, e.g. $C_7H_8^{+\bullet}$. A related, albeit chemically different field concerns protonated cycloheptatriene, i.e. the even-electron $C_7H_9^+$ ions¹⁴¹, and alkylcycloheptatrienes, which are closely related to protonated toluene and higher alkylbenzenium ions. A parallel review by one of these authors⁸ on protonated alkylbenzenes has been published, and recent investigations on protonated alkylcycloheptatrienes have highlighted the complexity of this gas-phase ion chemistry^{11,142}. To a minor extent, ionized¹³⁵ and protonated¹³⁸ fulvenes have also been investigated with respect to their interconversion to their (mainly arene-derived) isomers.

More recent work on the chemistry of gaseous 1,3,5-cycloheptatriene radical cations concerns the energetics and dynamics of the interconversion with ionized toluene and the competing losses of H^\bullet from both isomers. Lifshitz and coworkers^{22,143} have reported on the details of the energy surface of the $C_7H_8^{+\bullet}$ ions. Most importantly, the critical energies for interconversion was determined to be only *ca* 4 and 5 kcal mol⁻¹ below that of H^\bullet loss from *c*- $C_7H_8^{+\bullet}$ and *c*- $C_6H_5CH_3^{+\bullet}$, respectively, and the potential wells for both isomers are very deep (28 and 45 kcal mol⁻¹ below the isomerization barrier). This is in line with the previous findings that the radical cations of cycloheptatriene and toluene exhibit distinct CID spectra and time-resolved photodissociation⁷. As a consequence, energy-dependent interconversion of isomeric ions can occur to a significant extent in mass spectrometers in which the ions survive several collisions. This problem was recently addressed by Yost and coworkers¹⁴⁴, who reported on the marked dependence of the ion breakdown behaviour of toluene and cycloheptatriene radical cations on the resonant excitation time in a quadrupole ion-trap mass spectrometer. The doubly charged ion ($2E$) mass spectra of cycloheptatriene and toluene were reported by Moran and coworkers¹⁴⁵ to be remarkably different. Distinct from the spectrum of toluene, $[M - 6 H]^+$ ions, generated from the corresponding doubly charged cations of cycloheptatriene, give rise to the predominant peak in the spectrum.

Gross and coworkers¹⁴⁶ recently published the CID spectra of ionized 7-methyl-1,3,5-cycloheptatriene generated by charge exchange with carbon disulphide $[CE(CS_2)]$. The spectra were found to be similar but not identical to those of ionized ethylbenzene and showed only minor dependence on the CE gas pressure (i.e. on the ions internal energy). Thus, partial interconversion was invoked. This result is in line with the previous finding by Grottemeyer and Grützmacher¹⁴⁷ that metastable 7-methylcycloheptatriene radical cations are kinetically trapped as stable ethylbenzene or xylene ions. Furthermore, the results are reminiscent of even earlier work by Kuck and Grützmacher¹⁴⁸ who found that metastable 7-(β -phenylethyl)-1,3,5-cycloheptatriene radical cations partially retain their

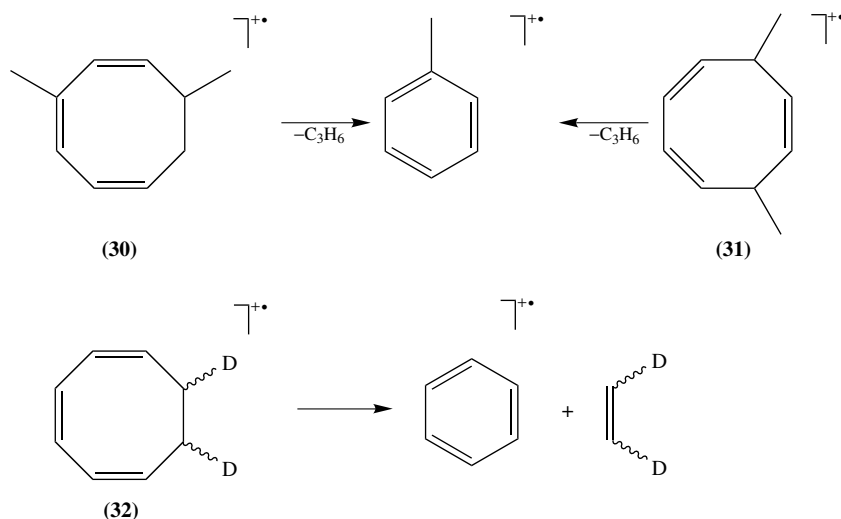
structure and partially rearrange into ionized 1,3-diphenylpropane and the isomeric 1-phenyl-2-tolyethane radical cations. The EI and FI mass spectra of cycloheptatriene and of 7,7'-ditropylyl have been reported, and only the latter were found to exhibit a molecular ion peak¹⁴⁹.

The intermediacy of the radical cations of isotoluenes (methylenecyclohexadienes) and their derivatives is a common feature in organic mass spectrometry; however, it is widely ignored because of the rather difficult experimental access to neutral isotoluenes. Again, the reader is referred to the discussion on methylenecyclohexadienes in the 1990 review on ionized alkylbenzenes⁷. An early paper by Lifshitz and Bauer¹⁵⁰ on mass spectrometry of bicyclo[3.2.0]hepta-2,6-diene, another C₇H₈ isomer, as well as of bicyclo[3.2.0]hept-6-ene and one of its isomers, cyclohepta-1,3-diene, may also be mentioned in this context.

Cyclooctadienes, Cyclooctatrienes and Cyclooctatetraene. As mentioned in Section III.E, the 70 eV EI mass spectra of the isomeric cyclooctadienes are strikingly different⁸⁷. Not surprisingly, the three possible stereoisomeric 1,5-cyclooctadienes give similar spectra, the product ions C₄H₆⁺ of the apparent [4 + 4] cycloreversion, i.e. loss of 1,3-butadiene, generating the base peak at *m/z* 54. A significant difference is recognized for the most highly strained *trans,trans*-isomer whose spectrum lacks the otherwise abundant C₃H₅⁺ ions (*m/z* 41). Contrary to the 1,5-isomers, the EI mass spectra of 1,3- and 1,4-cyclooctadiene both exhibit significantly more abundant molecular ions (C₈H₁₂⁺), reflecting the higher stability or, respectively, more facile accessibility of the conjugated π electron system. Also, loss of C₂H₅[•] gives rise to the base peak at *m/z* 79 with these isomers. This process and the analogous loss of CH₃[•] certainly generate protonated benzene (C₆H₇⁺) and toluene (C₇H₉⁺, *m/z* 93), again reflecting the interaction of the unsaturated C–C bonds in these C₈H₁₂⁺ isomers prior to fragmentation. In contrast to the PDMS spectra of the cyclohexadienes (see above), the PD mass spectra of 1,3- and 1,5-cyclooctadienes were found to be different and showed the same trend as the EI spectra. C₅H₇⁺ and C₆H₇⁺ ions represent the major fragment ions under PD conditions¹²⁴. The latter ions were again interpreted as benzenium ions, whose formation is particularly efficient for the conjugated diene in competition with allylic C–C bond cleavage.

The EI-induced fragmentation of various cyclooctadienes and cyclooctatrienes and of the respective bicyclo[3.3.0]octene and octadiene isomers was investigated by Pentz in a thesis of 1975¹⁵¹. The high-energy (70 eV) EI spectra of 3,8-dimethylcycloocta-1,3,5-triene (**30**) and of 5,8-dimethylcycloocta-1,3,6-triene (**31**) were found to be quite distinct and the low-energy (12 eV) spectra exhibit the elimination of propene as the exclusive fragmentation path. Interestingly, the ionized [7,8-D₂]-labelled isotopomer **32** of the parent 1,3,5-cyclooctatriene **12** (Scheme 2) was found to expel C₂H₂D₂ with relatively low selectivity (*ca* 60%) at 70 eV electron energy but with higher selectivity (*ca* 90%) at low internal energies (Scheme 8). This indicates that hydrogen scrambling is largely suppressed in the molecular ions from which the ionized arene is expelled and that this reaction is energetically highly favourable (cf Scheme 2). In contrast, loss of CH₃[•] is preceded by much more extensive hydrogen scrambling.

Later, gaseous 1,3,5-cyclooctatriene radical cations **12** were also studied by CID mass spectrometry, together with the ions generated from the acyclic isomer, 1,3,5,7-octatetraene (**11**), and some bicyclic isomers, viz. bicyclo[2.2.2]octa-2,5-diene (dihydrobarrelene) (**14**) and bicyclo[4.2.0]octa-2,4-diene (**13**) (Scheme 2)¹⁴⁸. The ions were formed by CE with CS₂⁺ and strong dependence of the spectra on the CE gas pressure, i.e. on the internal energy contents, was observed, indicating facile interconversion of the isomers. It is noteworthy that elimination of ethene from these C₈H₁₀⁺ ions is less pronounced for dihydrobarrelene ions⁸⁹, from which this path would formally correspond to a retro-Diels–Alder process, than for 1,3,5-cyclooctatriene ions. Interestingly, the spectra were



SCHEME 8

clearly distinct from those of ionized 7-methyl-1,3,5-cycloheptatriene and ionized styrene. Calculations suggested ionized cyclooctatriene to be the most stable isomer, in contrast to experimental data.

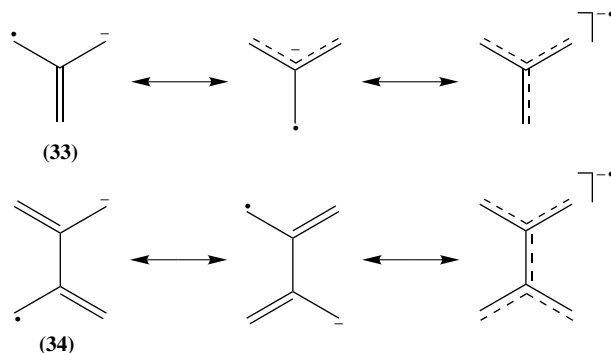
There appears to be not much knowledge available on the fragmentation of gaseous cations formed from 1,3,5,7-cyclooctatetraene besides the standard EI mass spectra. These are known to be quite similar to those of styrene^{14c}. In an attempt to elucidate the potential of combining field ionization and collision-induced dissociation (FI/CID) to differentiate isomeric cations, Levsen and Beckey¹⁵² compared the fragmentation of $C_8H_8^{+\bullet}$ radical cations generated from cyclooctatetraene and styrene. Again, the spectra were found to be rather similar, with the exception of the $[M - C_2H_3]^+$ ions (m/z 77), which were significantly more abundant in the CID spectrum of styrene, suggesting partial retention of structural specificity in these isomers. In contrast to the gas phase, the structural reorganization of $C_8H_{10}^{+\bullet}$ ions has been investigated in condensed media in much detail¹⁵³.

IV. GASEOUS ANIONS GENERATED FROM DIENES AND POLYENES

Knowledge about mass spectrometry and gas-phase chemistry of carbanions of dienes and polyenes is increasing although it still falls short of that on the respective carbocations. The relatively facile access to allyl anions from alkenes in the plasma of a negative chemical ionization (NCI) source and of flowing afterglow tubes has enabled investigations on unusual highly unsaturated, even- and odd-electron anions of fundamental interest. A lucid example is the recent comprehensive investigation of the thermochemistry of allene, methylacetylene, the propargyl radical and of related carbanions by DePuy and his associates¹⁵⁴, who have extensively used the flowing afterglow (FA) methodology, and in particular the selected ion flow tube (SIFT) technique. Also, negative ion mass spectrometry of dienes and polyenes has brought about relevant analytical applications. A brief overview will be given in the following paragraphs.

A. Trimethylenemethane and Related Radical Anions

Among the ‘small’ ions, the trimethylenemethane radical anion, $(\text{CH}_2)_3\text{C}^{\bullet-}$ (**33**)¹⁵⁵, and the tetramethyleneethane radical anion, $(\text{CH}_2)_2\text{C}=\text{C}(\text{CH}_2)_2^{\bullet-}$ (**34**)¹⁵⁶ (Scheme 9), have been of particular interest and several of their derivatives have been prepared in the gas phase. Recent work has been reviewed by Lee and Grabowski¹⁵⁷. These species and carbanions in general can be generated either by the reaction of either $\text{O}^{\bullet-}$ ions in the NCI source or in the flowing afterglow flow tube using $\text{N}_2\text{O}/\text{CH}_4$ mixtures, or by the sequential reaction of F^- ions, generated from NF_3 and neutral F_2 .

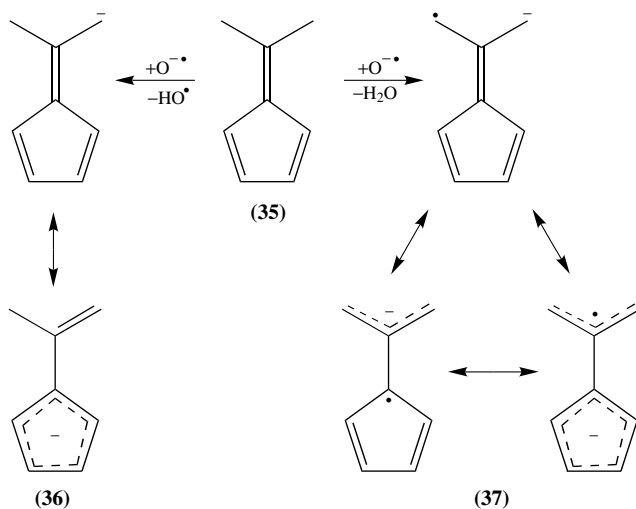


SCHEME 9

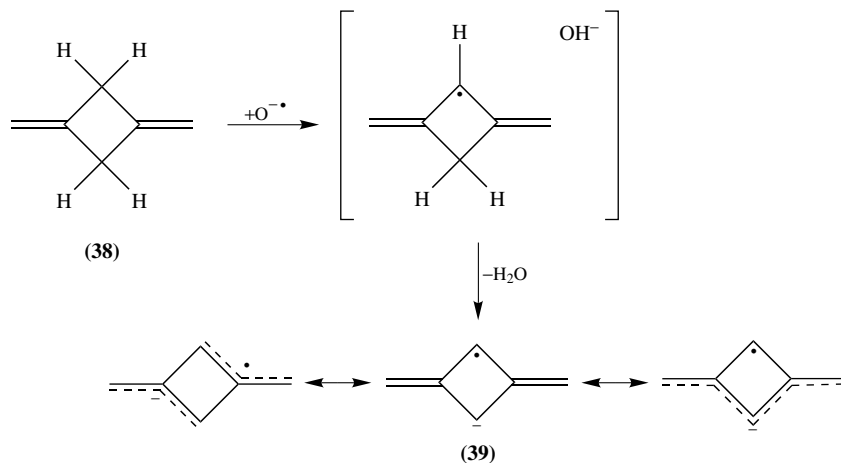
An impressive demonstration for the potential to generate ‘larger’ trimethylenemethane-type radical anions has been given in a more recent work using 6,6-dimethylfulvene (**35**) as the neutral precursor¹⁵⁸. As shown in Scheme 10, reaction of $\text{O}^{\bullet-}$ ions with this cross-conjugated polyene in a flowing afterglow apparatus generates the radical anion of (cyclopentadienylidene)di(methylene)methane (**37**) by subsequent highly regioselective proton and hydrogen atom abstraction. Deuterium labelling of the methyl groups revealed that a fraction of at least 94% of H^+ and H^{\bullet} transferred originate from the methyl groups. The distonic radical carbanion was demonstrated to be a better nucleophile than the related even-electron carbanion of 6,6-dimethylfulvene (**36**), studied earlier¹⁵⁹, and to display both radical and carbanionic reactivity towards various partners. Higher analogues of 6,6-dimethylfulvene were also studied. Negative-ion mass spectra of several 6,6-di-substituted fulvenes were reported by Tolstikov and coworkers¹⁶⁰.

The sequential removal of H^{\bullet} and H^+ from isobutene-type structural units (so-called ‘ $\text{H}_2^{\bullet+}$ abstraction’) was also used to generate the radical anion of ‘non-Kékulé benzene’, i.e. 1,3-dimethylenecyclobutane-1,3-diyl (**39**) (Scheme 11). As shown by Hill and Squires¹⁶¹, this highly unusual, distonic $\text{C}_6\text{H}_6^{\bullet-}$ isomer can be produced in pure form by reaction of $\text{O}^{\bullet-}$ with 1,3-dimethylenecyclobutane (**38**). Working in a flowing afterglow mass spectrometer, subsequent reactions were again used to characterize this radical anion and differentiate it from other $\text{C}_6\text{H}_6^{\bullet-}$ isomers.

The radical anion of the parent trimethylenemethane (**33**) has been generated and characterized by photoelectron spectroscopy by Squires, Lineberger and coworkers¹⁶², making use of the high affinity of fluoride ions towards the trimethylsilyl (TMS) group¹⁶³. Starting from the α -bis(trimethylsilyl)isobutene (**40**), sequential TMS^+ abstraction by F^- and dissociative electron transfer to an F_2 molecule generates an F^{\bullet} atom and an ion/neutral complex consisting of an F^- ion and the 2-(TMS-methyl)allyl radical (Scheme 12).



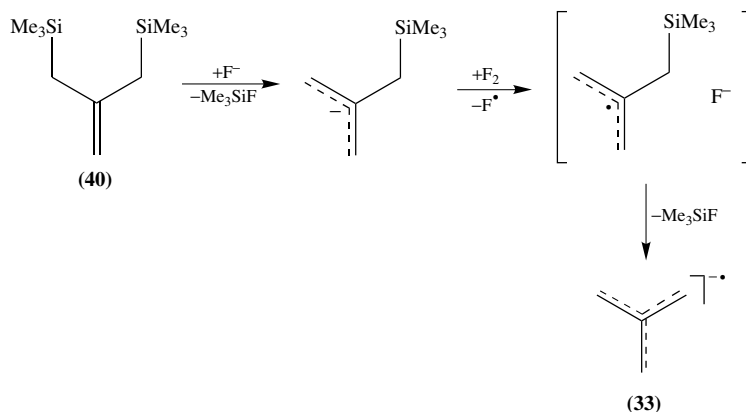
SCHEME 10



SCHEME 11

Intra-complex TMS^+ abstraction by F^- yields the trimethylenemethane radical anion **33**. Similarly, a number of other (mostly aromatic) distonic radical anions have been generated. Using the same approach, several other highly unsaturated distonic negative ions, such as the benzyne radical anions, were also studied¹⁶⁴.

It is obvious that the isobutene unit provides a good starting point for the generation of trimethylenemethane radical anions. However, even isobutane units can be used to produce these more highly unsaturated species. In a preliminary work aimed at two- and three-fold deprotonation processes in solution, Kuck, de Meijere and coworkers¹⁶⁵ have subjected triquinacene (**41**) and the tribenzotriquinacenes **44** to NCI conditions with



SCHEME 12

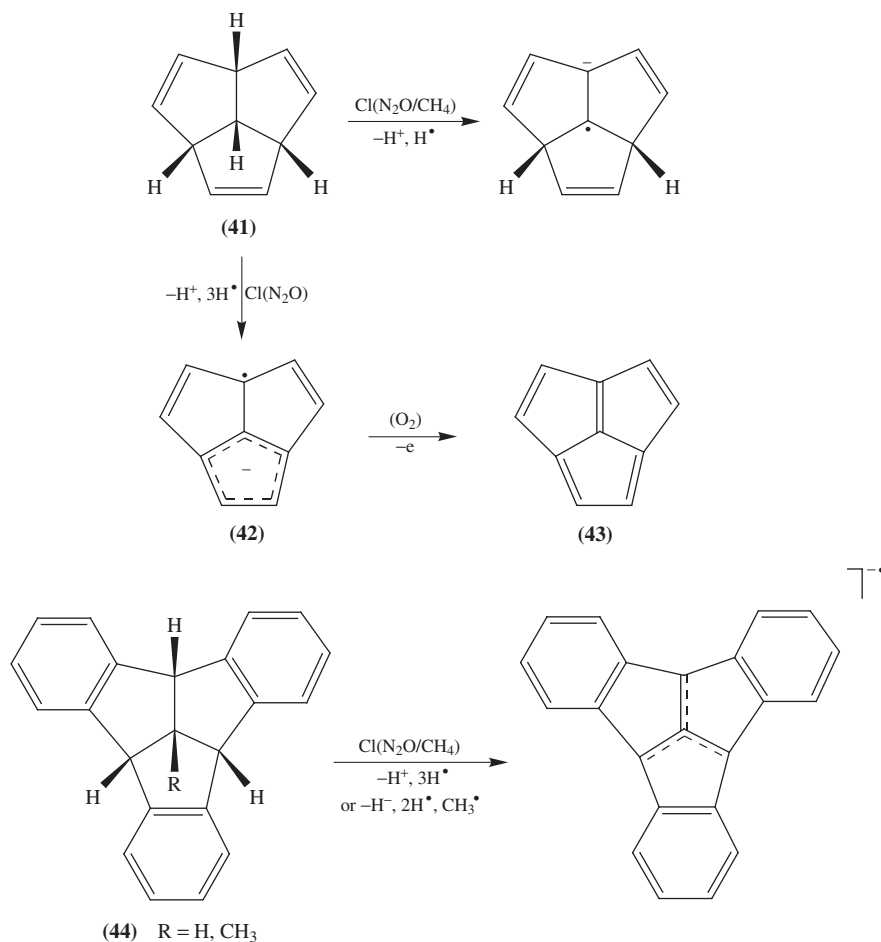
CH_4/O_2 and CF_4 as the reactant gases and observed the formation of $[\text{M} - 4 \text{H}]^-$ ions in the CI plasma (Scheme 13)¹⁶⁶. Thus, repeated deprotonation and electron transfer processes appear to offer an efficient access to more highly unsaturated and/or ring condensed trimethylenemethane radical anions. The $[\text{M} - 4 \text{H}]^-$ ion is considered identical to the molecular radical anion (42) of acetalene (43), which was generated as a short-lived species from the former by neutralization-reionization mass spectrometry¹⁶⁷. Efforts to apply Squires' methodology to triquinacene 41 and the tribenzotriquinacenes 44 have been made¹⁶⁸.

B. Deprotonation of 1,3,5-Cycloheptatriene: *cyclo*- C_7H_7^- and the Benzyl Anion

In contrast to the tropylium cation, the cycloheptatrienyl anion should be antiaromatic in the planar geometry. Although the *c*- C_7H_7^- anion is considerably less stable (*ca* 27 kcal mol⁻¹)¹⁶⁹ than the benzyl anion, it appears to be kinetically stabilized by a substantial energy barrier, and evidence for its existence in the gas phase has been reported^{170,171}. Wilkins, Staley and coworkers¹⁷² demonstrated by FT-ICR spectrometry that gas-phase deprotonation of cycloheptatriene (45) with OD^- and ND_2^- gives rise to isomerization to the benzyl anion because H/D exchange with D_2O and ND_3 , respectively, leads exclusively to the D_1 - and D_2 -isotopomers involving neutral toluene 46, (Scheme 14). In contrast, ring contraction of cycloheptatriene does not occur with the less basic anion CD_3O^- although slow but progressive H/D exchange is observed with CD_3OD ¹⁵⁴. Formation of an ion molecule complex $[\text{c-C}_7\text{H}_7^- \cdot \text{H}_2\text{O}]$ has been invoked to explain the relatively fast rearrangement of cycloheptatriene in the presence of $\text{OD}^-/\text{D}_2\text{O}$. The anion CID spectrum of deprotonated 7-methyl-1,3,5-cycloheptatriene has been reported by Nibbering and coworkers¹⁷³ and compared to those of the C_8H_9^- anions generated from other olefinic isomers such as 1,3,5-cyclooctatriene and spiro[2.5]octa-4,6-diene as well as from ethylbenzene.

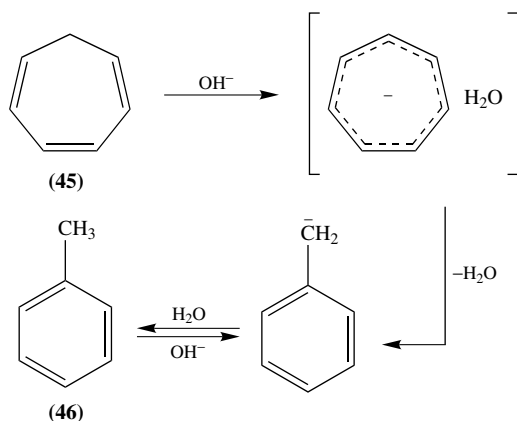
C. Deprotonation of Bicyclo[3.2.1]alkadiene, Some Other Cycloalkadienes and Cyclooctatetraene: Bishomoaromaticity and Transannular Cyclization

Another interesting bicyclic C_8H_9^- anion has been investigated by Lee and Squires¹⁷⁴, again by using the flowing afterglow methodology (Scheme 15). Gas-phase deprotonation

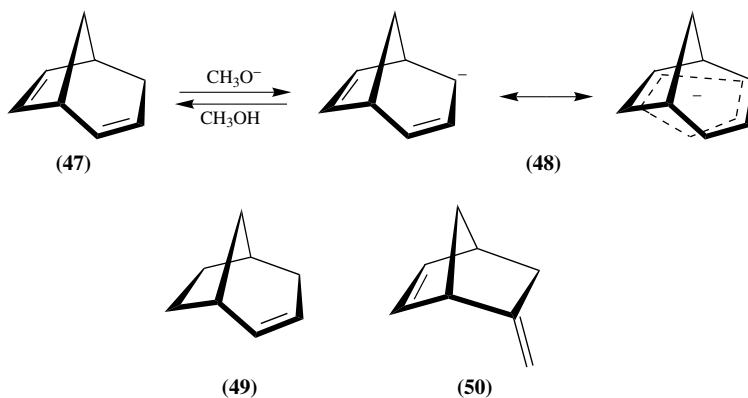


SCHEME 13

of bicyclo[3.2.1]octa-2,6-diene (**47**) by OH^- and OMe^- yields the bicyclo[3.2.1]octa-2,6-dien-3-yl anion (**48**) which, as a characteristic feature for its structural identity, incorporates two deuterium atoms in the respective reaction with D_2O . Most strikingly, the gas-phase acidity of the diene was found to be much higher (ΔK_a ca -10 kcal mol $^{-1}$) than that of an isomer, 5-methylene-2-norbornene (**50**), and the less unsaturated bicyclo[3.2.1]oct-2-ene (**49**). The major part of the increase in acidity (ΔK_a ca -6.4 kcal mol $^{-1}$) has been attributed to strong bis-homoconjugative stabilization of the bicyclo[3.2.1]octa-2,6-dien-3-yl anion. Slightly increased gas-phase acidities have been measured for 1,3-cyclohexadiene, 1,3-cyclooctadiene and 1,5-cyclooctadiene and the role of homoaromaticity in the conjugate anions considered there as well. In contrast to the above-mentioned dienes, 2,5-norbornadiene, known to be a relatively weak C–H acid¹⁷¹, turned out to undergo gas-phase deprotonation and slow H/D exchange exclusively at the olefinic C–H bonds. It is also noteworthy that the acidifying effect of homoaromaticity falls by far short of ‘regular’



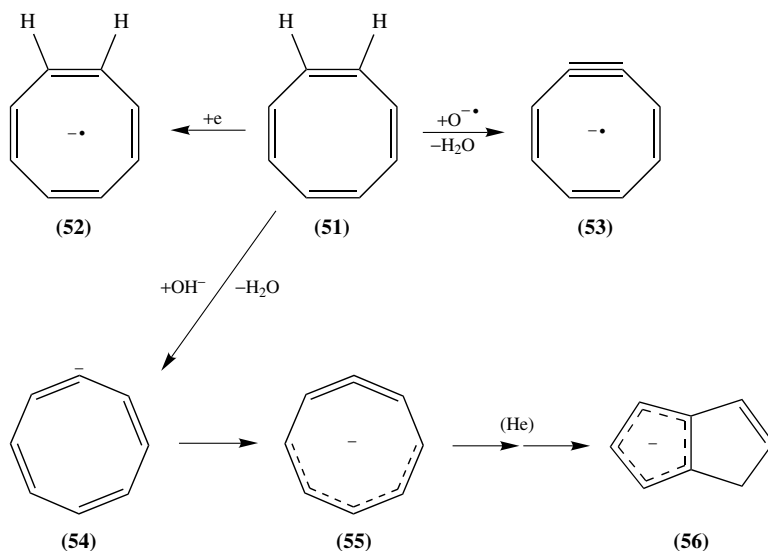
SCHEME 14



SCHEME 15

aromaticity: The gas-phase acidity of cyclopentadiene is by *ca* 24 kcal mol⁻¹ higher than that of bicyclo[3.2.1]octa-2,6-diene (**47**) and by 16 kcal mol⁻¹ higher than that of 1,3-cyclohexadiene.

The particular acidity of cyclopentadienes has become evident in a recent extended work by Bierbaum and coworkers¹⁷⁵ on the gas-phase properties of various anions derived from cyclooctatetraene (**51**). The molecular radical anion C₈H₈^{-•} (**52**) as well as the [M - H]⁻ and [M - 2 H]^{-•} ions, i.e. C₈H₇⁻ (**54**) and C₈H₆^{-•} (**53**), respectively, were generated in a flowing afterglow mass spectrometer and the gas-phase basicities, H/D exchange and other bimolecular reactions of these species were determined. The initial structure of the C₈H₇⁻ ions was characterized as a monocyclic species bearing both an allene and a pentadienyl anion unit, i.e. **55** rather than **54**. Upon collision with the helium atoms downstream the reaction tube, isomerization to a less-strained diquinane anion, the bicyclo[3.3.0]octa-1,3,6-trien-5-yl anion (**56**), takes place (Scheme 16). The relatively high stability of this C₈H₇⁻ isomer became evident from its generally low reactivity. Moreover, the proton affinity of the bicyclic C₈H₇⁻ ion **56** was determined to be very



SCHEME 16

close to that of the cyclopentadienide anion, about 24 kcal mol^{-1} higher than that of the initial monocyclic isomer. Thus, the conjugated hydrocarbon, bicyclo[3.3.0]octa-1,3,6-triene is by 24 kcal mol^{-1} less acidic than cyclooctatetraene. Note that the bicyclic anion can be regarded as the addition product of hydride ion to pentalene.

Recently, Cooks and coworkers¹⁷⁶ determined the electron affinity (EA) of 1,3,5,7-cyclooctatetraene by using the kinetic method, that is, by performing CID of the cluster anions of the cycloolefin with a number of reference molecules of known EA. The value obtained ($EA = 0.58 \pm 0.10 \text{ eV}$) was found to be in excellent accordance with that reported previously by Wentworth and Ristau¹⁷⁷.

V. BIMOLECULAR REACTIONS OF DIENES AND POLYENES

Bimolecular ion/molecule reactions of dienes and polyenes have been extensively studied for several reasons. Some of them have been mentioned implicitly in the previous sections, that is, in order to structurally characterize the gaseous cations derived from these compounds. In this section, bimolecular reactivity of cationic dienes, in particular, with various neutral partners will be discussed, and some anion/molecule reactions will be mentioned also (cf Section IV). In addition, the reactions of neutral dienes with several ionic partners will also be discussed. Of this latter category, however, the vast chemistry of reactions of neutral dienes with metal cations and metal-centred cations will not be treated here. Several reviews on this topic have been published in the last decade¹⁷⁸.

A. Ionized Dienes and Neutral Molecules

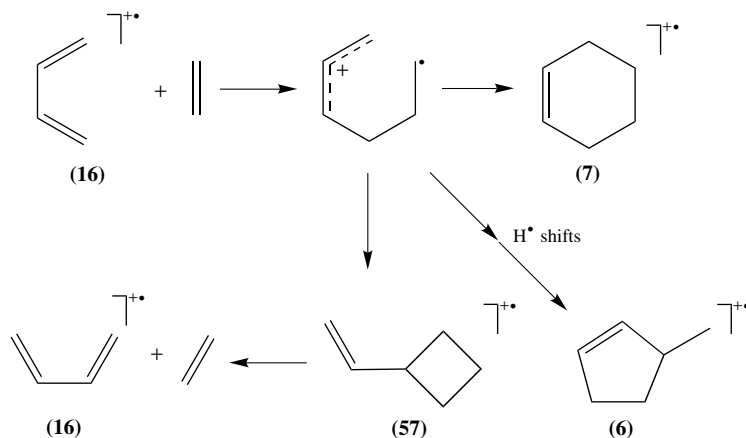
Allene Radical Cations. The bimolecular reactivity of the radical reactions of allene and propyne has been a longstanding matter of interest. Myher and Harrison¹⁷⁹ studied the ion/molecule reactions of ionized C_3H_4 with the respective neutral precursor in a medium-pressure chemical ionization source. $C_6H_7^+$ ions were found to be amongst

the most prominent charged adducts. Subsequently, Bowers, Jennings and coworkers¹⁸⁰ investigated this system by ICR mass spectrometry and found that the $C_6H_7^+$ ions result from a direct condensation reaction between $C_3H_5^+$ and C_3H_4 . Later, a photoionization mass spectrometric study by Tanaka and coworkers¹⁸¹ revealed that the yield of the $C_6H_7^+$ ions is much larger with allene and propyne as compared to cyclopropene, another isomer. Obviously, the reactivity of the ion/molecule complexes formed in the course of the exothermic reaction depends strongly on the internal energy contents. Lifshitz and coworkers^{182,183} studied the energy-dependent photoionization of allene in detail and considered the allene dimer to be formed by covalent coupling of the central carbon atoms, thus leading to the non-Kékulé structure of tetramethyleneethane, $*(CH_2)_2C-C(CH_2)_2^+$ (cf Scheme 9 for the radical anion). The different energy dependences of allene and propyne were explained by RRKM model calculations¹⁸⁴. Photoelectron-secondary ion coincidence mass spectrometry was applied by Niehaus and coworkers¹⁸⁵ to tackle the energy dependence problem. ICR studies by Anicich and coworkers¹⁸⁶ on allene, vinylacetylene and diacetylene, amongst other olefins, revealed that by far the largest fraction of ion/molecule reactions (>90%) leads to condensation reactions, i.e. to hydrocarbon ions larger than those of the starting system. Several groups assumed that the $C_6H_7^+$ product ions have the structure of protonated benzene (benzenium ions)¹⁸⁷. Subsequently, Lias and Ausloos¹³³ devoted a detailed ICR investigation to this structural problem and concluded that the $C_6H_7^+$ ions formed from the ion/molecule reactions of allene and propyne, as well as by unimolecular fragmentation of various cyclic and acyclic olefins (cf Section III), consist of at least two isomers, viz. the benzenium ion and, most probably, protonated fulvene (fulvenium ions).

Cyclobutadiene Radical Cations. Ionized cyclobutadiene represents a stable species in the gas phase. This prototype species has been studied, amongst other $C_4H_4^{+*}$ isomers, by its ion/molecule reactions under various conditions. Collision-induced dissociation (CID) of the adducts of $c-C_4H_4^{+*}$ with ammonia was found to be distinctive from those of the $C_4H_7N^{+*}$ adduct ions obtained with ionized methylenecyclopropene and vinylacetylene¹¹⁰. The CID behaviour as well as the association reactions of $c-C_4H_4^{+*}$ ions with e.g. 1,3-butadiene, furan and thiophene were studied by Cooks and coworkers¹¹³ in a pentaquadrupole mass spectrometer and revealed dramatic differences from the corresponding reactions of ionized methylenecyclopropene and the acyclic $C_4H_4^{+*}$ ions. The gas-phase reaction between $c-C_4H_4^{+*}$ ions and acetylene has also been measured¹⁸⁸.

Butadiene Radical Cations. Cycloaddition reactions between the radical cations of 1,3-butadiene and its derivatives with various neutral olefins have been a subject of intense research over the past decades because of the fundamental importance of this type of pericyclic reactions in organic chemistry. Reviews concerning Diels–Alder reactions involving radical cationic species in the gas phase and in general organic chemistry are mentioned here^{4,90c,189}. Cycloaddition reactions of ionized 1,3-butadiene (**16**) with ethene and of ionized furan with neutral 1,3-butadiene were discussed by Gross and coworkers¹⁹⁰. Very recently, Bouchoux and Salpin¹³⁷ presented convincing FT-ICR evidence on the prototypical addition of ionized **16** to ethene (Scheme 17). The reaction was shown to occur via an intermediate acyclic distonic ion which subsequently cyclizes to ionized vinylcyclobutane (**57**) which then undergoes [2 + 2] cycloreversion to generate the starting components with mutually interchanged methylene groups. In competition, cyclization also gives ionized cyclohexene (**7**), whereas various H shifts lead to acyclic diene and methylcyclopentene radical cations (**6**).

In an early ICR study, Gross and coworkers¹⁹¹ reacted ionized 1,3-butadiene (**16**) with several C_5 alkenes and found characteristically different fragmentation of the ionic



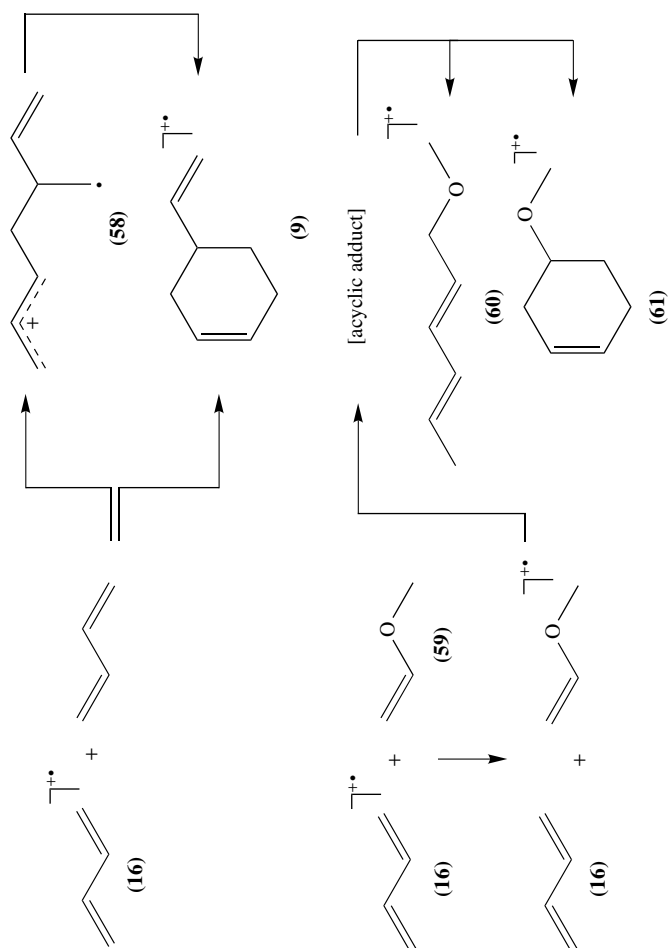
SCHEME 17

adducts, which themselves were not detectable due to the lack of collisional cooling at the time of the experiment. The distinct reactivities of the six C_5H_{10} isomers pointed to a potential means to identify these neutral isomers by ICR mass spectrometry. Interestingly, the highest substituted alkene, i.e. 2-methylbut-2-ene, reacted by charge exchange only. In a later work, the ionic adduct was stabilized by collisions with neutral gas in the ICR cell prior to collision-induced decomposition. Energy-dependent formation of two dimeric adducts was identified, one being the [2 + 4] cycloadduct **9** and the other a branched, acyclic isomer, to which the structure of a distonic ion (**58**) was assigned (Scheme 18)⁸⁹.

Nibbering, Jennings and coworkers¹⁹² reported on the [2 + 4] cycloaddition of ionized 1,3-butadiene **16** with methyl and ethyl vinyl ether (**59**) and identified the (again short-lived) adduct to be the 4-methoxycyclohexene radical cation **61**, from which methanol or ethanol, respectively, are eliminated regioselectively. Later, FT-ICR mass spectrometry work by Groenewold and Gross¹⁹³, using collisional cooling as well as CID spectrometric studies in a sector-field instrument, revealed that the cycloaddition process occurs stepwise and that both the acyclic adduct (**60**) and the [4 + 2] cycloadduct (**61**) can be identified (Scheme 18). The reaction starting with ionized 1,3-butadiene involves charge exchange prior to the formation of the covalent adduct. In contrast to the aforementioned cases, ionized 1,3-butadiene reacts with acrolein and methyl vinyl ketone as the ene component, and α,β -unsaturated ketones react as dienes to yield 2-vinyl-2,3-dihydropyrans¹⁹⁴.

The gas-phase reactions of the fulvene radical cation with neutral 1,3-butadiene, alkenes and 2-propyl iodide have been investigated by Russell and Gross^{131a} using ICR mass spectrometry. Unlike ionized benzene, ionized fulvene undergoes no C–C coupling with 2-propyl iodide. On the basis of deuterium and ^{13}C labelling, the reaction of ionized fulvene with 1,3-butadiene was suggested to occur by [6 + 4] cycloaddition to yield tetrahydroazulene radical cations. Cycloadditions of neutral fulvene were also studied in this work.

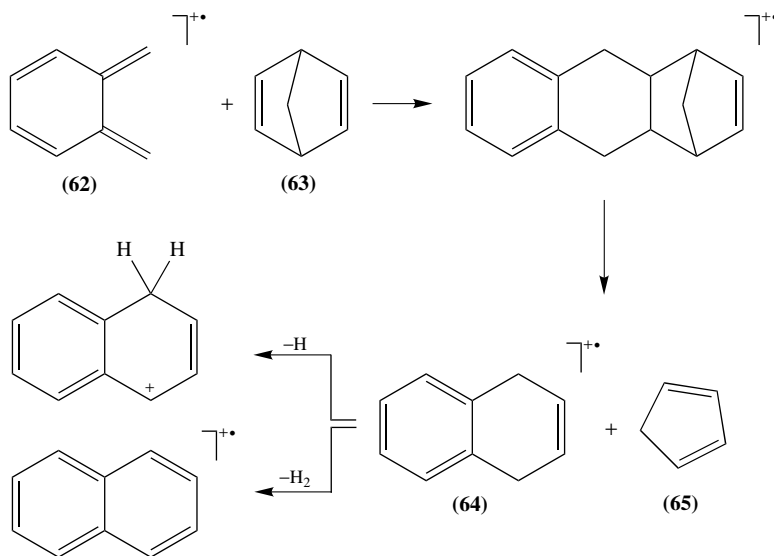
The radical cations of the quinodimethanes (xylylenes) represent particularly interesting members of the family of $\text{C}_8\text{H}_8^{+\bullet}$ isomers. Ionized *ortho*-quinodimethane is formed from a variety of neutral precursors such as benzocyclobutene (by ring opening), *ortho*-methylbenzyl alcohol and its esters and ethers (by 1,4-elimination) and from 1,4-dihydrobenzo[*c*]thiophene *S,S*-dioxide (by 1,1-elimination of SO_2). Gross and coworkers¹⁹⁵ generated the $\text{C}_8\text{H}_8^{+\bullet}$ species in a high-pressure ion source and characterized them by



SCHEME 18

the reaction with neutral styrene. The *ortho*-quinodimethane structure was deduced from labelling evidence and 2-phenyltetralin was suggested to be the product of a [4 + 2] cycloaddition. CID spectrometry of the cycloaddition product formed from ionized benzocyclobutene and from [β,β -D₂]-styrene and [3,3-D₂]-2-phenyltetralin confirmed the identity of these ions and thus the intermediacy of the *ortho*-quinodimethane radical cations¹⁹⁶.

In a very recent FT-ICR study employing an external ion source, Grützmaier and Barkow¹⁹⁷ compared the bimolecular reactivity of ionized *ortho*-quinodimethane (**62**) formed by water loss from 2-methylbenzyl alcohol under EI conditions with the benzocyclobutene radical cations formed from the neutral hydrocarbon by charge exchange and styrene radical cations formed by EI. Ionized benzocyclobutene was found to be distinguishable from the *ortho*-quinodimethane ions by its inertness towards neutral alkenes. A highly diagnostic probe reaction for ionized *ortho*-quinodimethane **62** has also been found in this work (Scheme 19): These ions undergo a [4 + 2] cycloaddition with neutral norbornadiene (**63**) followed by [4 + 2] cycloreversion of the Diels–Alder adduct to give ionized 1,4-dialin (1,4-dihydronaphthalene, **64**) and neutral cyclopentadiene (**65**), as well as the products of subsequent H[•] and H₂ loss. The possible formation of ionized quinodimethanes during the loss of benzene from long-lived radical cations of 1,2-diphenylethane, and of SO₂ and benzene from ionized dibenzyl sulphone, was also discussed recently¹⁹⁸. However, the probe reaction with norbornadiene turned out to be negative¹⁹⁹.



SCHEME 19

B. Neutral Dienes and Odd-electron Reagent Ions

Neutral dienes have been reacted with a large variety of ions in the gas phase. Besides the cases concerning the same reactants discussed above but with reversed charge distribution, e.g. those of neutral 1,3-butadiene with ionized alkenes, there are interesting studies of reactions of 1,3-dienes with even-electron cations and studies on ion/molecule

reactions of anions derived from dienes. Again, the reader is also referred to Section III describing the unimolecular gas-phase ion chemistry of dienes.

The reactions of neutral allene and other unsaturated hydrocarbons with carbon ions ($C^{+\bullet}$) have been studied by Bohme and coworkers²⁰⁰ using the flowing afterglow (selected ion flow tube, SIFT) technique, in order to gain insight into the fundamentals of the build-up mechanisms of carbon skeletons. Parent²⁰¹ reacted $C^{+\bullet}$, $Si^{+\bullet}$ and $Si_2C_2^{+\bullet}$ with allene and propyne in an FT-ICR mass spectrometer and found distinct reactivity towards insertion into single bonds. Isoprene has been amongst the various olefins which Španěl and Smith²⁰² recently subjected to reactions with $H_3O^{+\bullet}$, NO^+ and $O_2^{+\bullet}$. The ion/molecule reactions occurring between 3-methylbuta-1,2-diene and *ortho*-hydroxythiophenol under CI conditions were reported by Traldi and coworkers²⁰³.

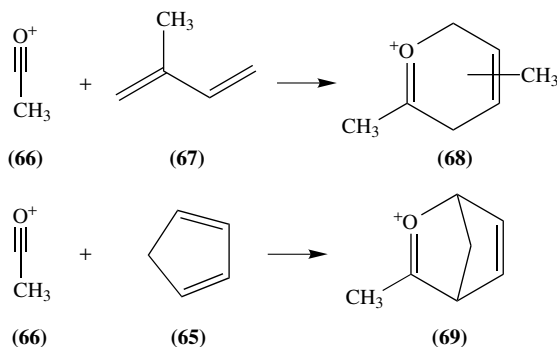
Various organic radical cations have been reacted with neutral dienes. The investigations by Groenewold and Gross¹⁹³ mentioned above also included the reactions of neutral 1,3-butadiene and ionized methyl vinyl ether (cf Scheme 18). Two distinct addition products were identified when benzene radical cations were reacted with neutral 1,3-butadiene, viz. ionized 2-phenylbut-2-ene and ionized 1-methylindane, depending on the internal energy of reactants²⁰⁴. Cooks and coworkers²⁰⁵ studied the reactions of ionized pyrene and the corresponding $[M - H]^+$ and $[M - H_2]^{+\bullet}$ ions with neutral isoprene using a quadrupole ion-trap mass spectrometer. Dass²⁰⁶ observed significantly different CID behaviour of the adduct ions formed from neutral 1,3- and 1,4-pentadienes with ionized ketene. Similarly, Bouchoux and Penaud-Berruyer²⁰⁷ found that ion/molecule reactions between ionized vinylamine and twelve neutral C_4 , C_5 and C_6 dienes lead to characteristically different products depending on whether the diene is conjugated or non-conjugated. Again, step-wise [4 + 2] cycloaddition was inferred to occur in the case of the 1,3-dienes whereas metathetic [2 + 2] cycloaddition appeared to be the key step with 1,4- and 1,5-dienes. The latter behaviour strictly parallels the regiospecific reactivity of ionized vinylamine with simple alkenes²⁰⁸ and leads to one of the useful methods for double bond localization in unsaturated hydrocarbon chains (cf Section VI).

Some special cases for reactions of radical cations with neutral dienes deserve mention here as well. Nibbering and coworkers²⁰⁹ demonstrated that the distonic dimethylmethyl-enesulphonium ion, $(CH_3)_2S^+CH_2^\bullet$, reacts with 1,4-cyclohexadiene predominantly by H^\bullet abstraction and competing radical addition to one of the double bonds. The adduct undergoes several structure-specific fragmentation reactions, such as CH_3^\bullet loss and elimination of $(CH_3)_2S$. Another special case is the investigation of the reactivity of fullerene $C_{60}^{+\bullet}$ ions with several neutral acyclic and cyclic dienes in the SIFT mass spectrometer²¹⁰. In contrast to the acyclic 1,3-dienes, 1,3-cyclopentadiene and 1,3-cyclohexadiene formed $C_{65}H_6^{+\bullet}$ and $C_{66}H_8^{+\bullet}$ adducts in which the diene unit is assumed to be added across a [6.6] bond of the fullerene skeleton. The same authors also reacted neutral 1,3-butadiene with C_{60}^{2+} and C_{70}^{2+} dications and observed the doubly charged adduct ions along with the products of charge exchange^{211,212}. A study on the adducts of $C_5H_5^+$ ions and C_{60} is also mentioned²¹³.

C. Neutral Dienes and Even-electron Reagent Ions

Unsaturated even-electron cations have been used in the gas phase to react with olefins, including dienes, in a way that characterizes their structure. In most cases, these ion/molecule reactions take place by [4 + 2] cycloadditions followed by specific elimination of even-electron neutrals. A most suitable instrumental setup for these studies are triple-quadrupole and pentaquadrupole mass spectrometers in which the ion/molecule addition reactions take place subsequent to the selection of the reagent ion. In most

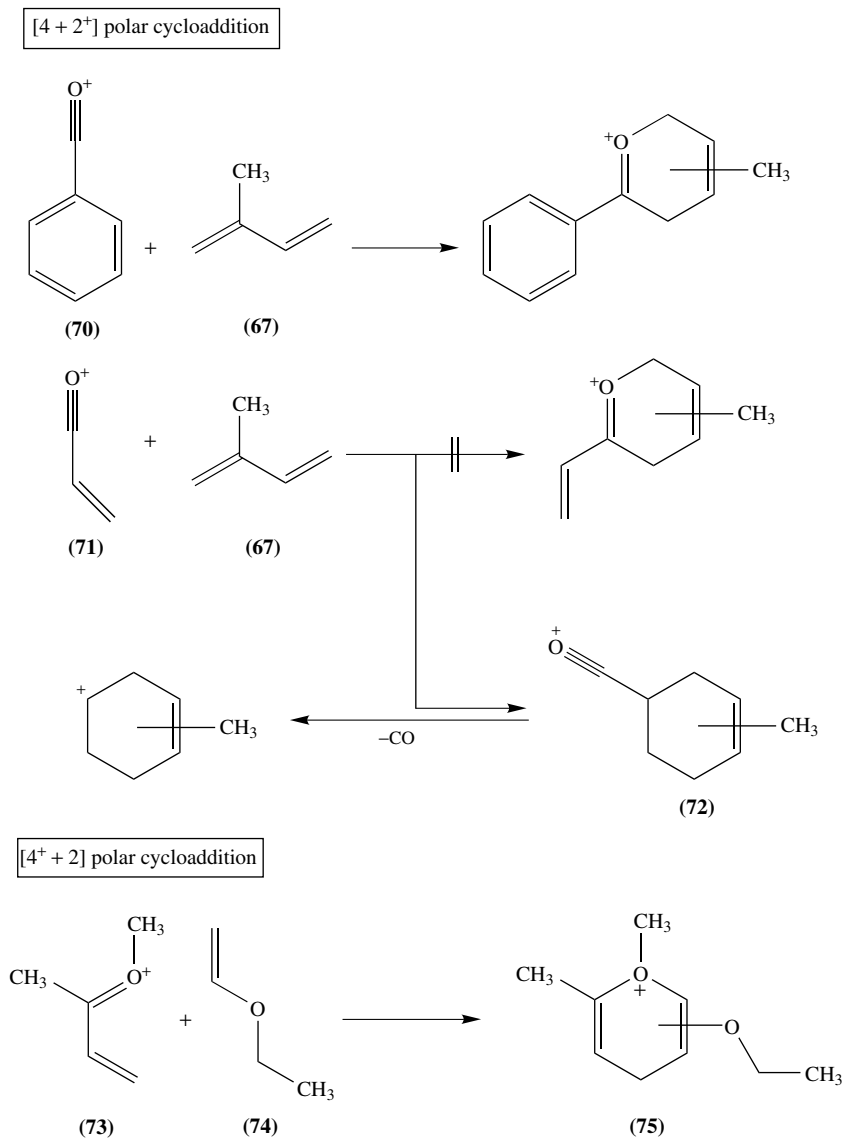
cases, the adduct is stabilized by collision cooling and can be re-excited by collision in the next quadrupole. Triple-stage pentaquadrupole (so-called 'QqQqQ') mass spectrometers even allow one to identify the ionic adduct by performing structure-specific CID. Eberlin²¹⁴ has recently reviewed this method and its applications. A prototype [4 + 2⁺] cycloaddition concerning dienes is the reaction of acetyl cations **66** with isoprene **67** and cyclopentadiene **65** to give the corresponding oxonium ions **68** and **69** as shown by Cooks and coworkers²¹⁵ (Scheme 20). Note that the charged 'ene' is the 2⁺ component in these 'polar' cycloaddition reactions. Collision-induced dissociation reverts this addition generating the initial reactants. Several analogous reactions have been studied, such as the cycloaddition of thioacetyl cations with isoprene. Unlike the product formed with acetyl cations, this cycloadduct was found to expel C₂H₄ and H₂S. A large variety of other acyl cations has been reacted in the same way with 1,3-butadiene, isoprene and 1,3-cyclopentadiene (Scheme 20)²¹⁶.



SCHEME 20

Many variants of the [4 + 2⁺] polar cycloaddition are possible including the reactions of unsaturated acyl cations. Cooks, Eberlin and coworkers also investigated the reactions of various nitrilium and immonium cations with isoprene. Again, cycloaddition is a common reaction path; however, protonated nitriles tend to undergo proton transfer to the relatively highly basic neutral diene²¹⁷. Protonated quinones and the *O*-Me⁺ adducts of quinones, α,β -unsaturated aldehydes and ketones and also protonated saturated ketones have been cycloadded to 1,3-butadiene. Peculiar combinations of reactants are possible, e.g. the reaction of the *O*-Me⁺ adduct of cyclohexen-3-one with 2,3-dimethoxybutadiene, the cycloadduct of which was found to undergo mainly the retro-Diels–Alder process upon CID. In the same work, Cooks and coworkers²¹⁸ also demonstrated a cycloaddition occurring with inverse electron demand (Scheme 21): The *O*-Me⁺ adduct of 2-butenone **73** adds to ethyl vinyl ether **74** by [4⁺ + 2] ion/molecule reaction since the cycloadduct **75** fragments differently as compared to the putative [4 + 2⁺] isomer. Whereas benzoyl cations **70** react with isoprene **67** in the expected [4 + 2⁺] orientation, cycloaddition of acryloyl cations (**71**) was suggested to take place at the α,β -unsaturated double bond, thus generating isocyclic [4 + 2⁺] cycloadducts **72** instead of a heterocyclic (dihydropyrylium-type) ion²¹⁹.

The reaction of thioacetyl cations with 2,5-dimethyl-1,5-hexadiene under low-pressure conditions in an FT-ICR mass spectrometer leads to elimination of propene. At variance from the [4 + 2⁺] polar cycloadditions observed under high-pressure conditions in the QqQqQ instrument, Caserio and coworkers²²⁰ invoked electrophilic attack of the CH₃CS⁺



SCHEME 21

cation at an inner position of the diene unit leading to a five-membered cycloadduct, from which a thiophenium cation is formed upon C_3H_6 elimination. It appears possible that the corresponding [4 + 2⁺] cycloadduct is formed initially and that ring contraction is a subsequent isomerization step, which becomes evident only in cases where a stable olefin can be expelled. Another interesting case was reported by Morizur and coworkers²²¹ who reacted the dimethoxyphosphenium ion, $(CH_3O)_2P^+$, with 2,3-dimethylbutadiene in

a quadrupole ion trap mass spectrometer. A chelotropic $[4 + 2^+]$ cycloaddition generates a 1,1-dimethoxyphosphoniocyclopent-3-ene ion which, under CID conditions, undergoes the retro-chelotropic reaction and competitive loss of methanol, to yield a phosphacyclopentenyl cation. Finally, a classical ICR paper by Ausloos and coworkers²²² may be mentioned which describes the reaction of benzyl cations with 1,3-butadiene, besides various monoalkenes. The primary $C_{11}H_{13}^+$ adduct, presumably the linear 5-phenylpent-1-en-3-yl cation rather than a formal $[4 + 2^+]$ cycloadduct bearing a seven-membered ring, expels ethene as the predominant reaction, suggesting the formation of the 1-indanyl cation as the final product.

D. Reactions of Diene-derived Anions

Some ion/molecule reactions of several even- and odd-electron carbanions derived from dienes and polyenes have already been mentioned (Section IV) in the context of their unimolecular gas-phase chemistry. Some additional aspects will be presented here concerning their bimolecular reactions. Using the flowing afterglow technique, the number of acidic C–H bonds and hidden isomerization reactions can be determined in the carbanions by H^+/D^+ exchange with D_2O . This was shown by Shapiro, DePuy and coworkers²²³ for a large set of $[M - H]^-$ ions including those of the butadienes and butynes. Only two hydrogens are exchanged in the anions generated from 1,2-butadiene, 1-butyne and 2-butyne whereas the 1,3-butadiene carbanion undergoes mainly D^+ abstraction from D_2O . Thus, 1,3-butadiene is deprotonated at one of the inner C–H bonds. When Lewis acids are allowed to react with carbanions, the formation of diagnostic addition products may be observed. In line with this, the same authors demonstrated²²⁴ that the $[M - H]^-$ ion of 1,3-butadiene reacts with N_2O by attack of one of the inner carbons at the terminal nitrogen atom of the neutral reagent since the adduct expels CH_2O . Information on the site of deprotonation of allene was gained by reacting its carbanion with CS_2 , as shown in a very recent work by DePuy and coworkers²²⁵. A complex isomerization was discovered in the primary adduct, $CH_2CCHCS_2^-$, by which the C(1) and C(3) atoms of the allenyl anion and the CS_2 carbon atom become equivalent. The reaction with COS and CO_2 were also studied.

DePuy and coworkers²²⁶ also reported on the rate constants of H^+/D^+ exchange of OH^- with several weakly acidic olefins, including 1,3-butadiene and norbornadiene, under flowing afterglow conditions. Another interesting FA investigation²²⁷ dealt with the proton transfer processes that occur in long-lived ion/molecule complexes formed from D_2O and allylic carbanions, including the carbanion of isoprene. In all cases, the H^+/D^+ exchange does not reach the statistical limit within the lifetime of the complexes.

A series of papers have appeared describing the bimolecular chemistry of gaseous anions derived from 1,3-cyclopentadiene. McDonald and coworkers²²⁸ reacted the $c-C_5H_5^-$ anion with several alcohols in a flowing afterglow apparatus and observed, surprisingly, that ion/molecule adducts such as $[c-C_5H_5^- CF_3CH_2OH]$ react with further alcohol molecules by anion switching, leaving neutral cyclopentadiene and the corresponding alcohol dimer anion, as well as higher clusters anions. The cyclopentadienyl anion and the cyclopentadienylidene radical anion, $c-C_5H_4^{\bullet-}$, were found to undergo nucleophilic 1,4-addition with α,β -unsaturated compounds, viz. acrylonitrile and methyl acrylate^{229,230}. A detailed study²³¹ was focused on the gas-phase chemistry of the $c-C_5H_4^{\bullet-}$ radical anion, generated from diazocyclopentadiene by electron attachment, followed by N_2 loss, or by sequential H^+/H^{\bullet} abstraction (cf Section IV). This unusual species also reacts by Michael addition with acrylonitrile, methyl acrylate and vinyl chloride, but also with a variety of other electrophiles.

VI. LOCALIZATION OF THE C—C BOND UNSATURATION

The determination of the sites of the C—C double bonds in unsaturated fatty acid derivatives and other lipids plays an outstanding role in the analytical application of mass spectrometry. Much work has been published on the localization of double bonds in monoolefins, and a number of extensive reviews has appeared on the topic^{232–235}. Two major methodologies have been employed. In the first one, unsaturated C—C bonds are converted to appropriate derivatives by synthesis in the liquid phase, which are then subjected to mass spectrometric analysis mostly by using standard EI techniques. These methods will be mentioned only briefly in the next section, including some recent work which has not yet been mentioned in the reviews. The second methodology takes advantage of the bimolecular reactivity of *neutral* olefins with ionic reagents in the gas phase, i.e. in the chemical ionization source of a mass spectrometer, or in the cell of an ion trap or ICR mass spectrometer. A diversity of reagent ions has been investigated during the past decades, and much of this chemistry has also been treated in the reviews.

Double bond localization in dienes and polyenes has also attracted much attention but the examples are less widespread than with simple olefins. However, the specific reactivity of 1,3-dienes deserves special notice and recent work will be presented in detail to some extent in the following sections.

A. Liquid-phase Derivatization Followed by Mass Spectrometry

Classical methods of derivatization of double bonds in dienes and polyenes comprise the oxidation of the olefin with osmium tetroxide or with permanganate, followed by methylation of the 1,2-diols^{236,237}. Alternatively, bromination of the double bonds in the presence of methanol gives the corresponding multiple α -bromo- β -methoxy adducts²³⁸. Also, the oligohydroxy derivative obtained from the diene or polyene can be converted to the multiple bis-trimethylsilyl derivatives^{239,240}. In all cases, structure-specific cleavage of the C—C single bond generated by derivatization occurs readily, owing to activation by the electron-rich groups added to the original double bond. Cleavage of the multiple α,β -bis(trimethylsilyloxy)ethylene units proved to be particularly prominent.

Still another related method consists in reacting dienes with dimethyl disulphide in the presence of iodine, to produce the corresponding bis(α,β -dimethylmercapto) derivative^{241–243}. Again, characteristic fragmentation is obtained in the standard EI spectra. However, this method involves complications if the double bonds are separated by less than four methylene groups due to the formation of cyclic thioethers.

A special method developed by Vouros and coworkers²⁴⁴ for 1,3-dienes makes use of the facile Diels–Alder reaction with 4-phenyl-1,2,4-triazolin-3,5-dione. Cycloaddition converts the original 1,3-butadiene unit of the olefin into a 1,2,3,6-tetrahydropyridazine unit, from which the pending alkyl groups are lost by diagnostic C—C bond cleavage. Hogge and coworkers²⁴⁵ performed combined epoxidation/hydrogenation for double-bond localization of polyunsaturated compounds. Vetter and coworkers²⁴⁶ recently reported on further methods for the double-bond localization in polyunsaturated fatty acids making use of charge-remote fragmentation²⁴⁷.

B. Gas-phase Derivatization by Chemical Ionization

When a neutral olefin forms covalent adducts with ionic reactants at one of its C—C double bonds, a new single C—C bond is formed which, owing to the influence of the substituents added during the ion/molecule reaction, may undergo facile dissociation. The

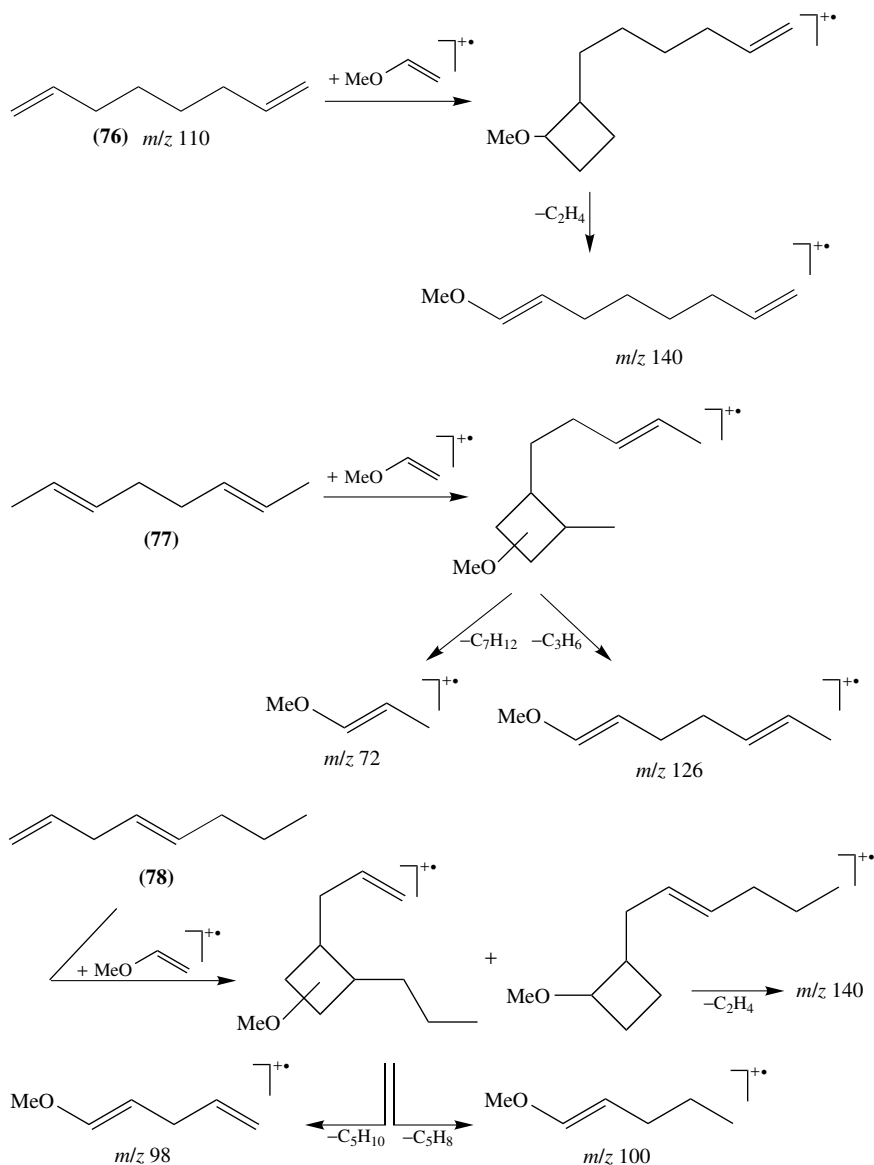
fragment ions formed are then characteristic indicators for the position of the unsaturation in the olefin under investigation. Due to the fact that double bonds are easily shifted in cationic (and even sometimes anionic) olefins, ion/molecule reactions between ionic olefins and neutral reagents are much less specific than are those involving neutral olefins and ionic reagents. During the last three decades, much work has been invested to develop methods for the localization of double and triple bonds in olefins, in particular in long-chain unsaturated aliphatic chains such as in fatty acids, by performing ion/molecule reactions in the dilute gas phase of a mass spectrometer. To this end, gas-phase derivatization of the olefin within the CI ion source is a most suitable approach. However, double-bond localization can also be carried out by selecting suitable ions within ion traps, FT-ICR cells and quadrupole mass spectrometers and allowing them to react subsequently with the olefin under investigation. Of course, this approach is more limited than the first one since the sample olefin has to be sufficiently volatile.

Jennings and coworkers²⁴⁸ were the first to report on a mass spectrometric method of locating double bonds by use of gas-phase ion/molecule reactions. Ionized alkyl vinyl ethers proved to be highly suitable reagent ions, and the principle of this gas-phase method for double-bond localization is illustrated for prototype dienes **76–78** in Scheme 22. At the same time, Hunt and coworkers^{249,250} introduced nitric oxide (NO) as a reagent gas in CI mass spectrometry and studied the reactions of the NO^+ and $[\text{NONO}]^+$ ions with alkenes and also with several acyclic dienes and 1,3,5-cycloheptatriene. Thereafter, several groups have contributed to the development and only some classical work concerning simple alkenes may be mentioned here.

Extended reviews on double bond localization have been published by Budzikiewicz²⁵¹ and Harrison²⁵². Besides the [2 + 2] cycloaddition, addition of gaseous alkyl cations, metal cations, ionized amines and of NO^+ offers a wide variety of reagents to locate double bonds. In an overview that appeared in 1990, Vairamani and coworkers^{253,254} have collected various, in part rather special, reagent gases used for this purpose in chemical ionization mass spectrometry. Some of these reactions occurring with 1,3-dienes under CI conditions have employed dimethyl ether as the reactant gas. Double-bond localization has been performed not only in conventional sector-field instruments but also in ion traps, in which ionized alkenes such as cyclooctene radical cations may be used as reagent ions²⁵⁵, and in FT-ICR mass spectrometers using Fe^+ as the reagent ion²⁵⁶.

In the remainder of this section, some cases concerning dienes and polyenes will be treated, and we restrict ourselves mainly to the more recent literature. Using standard chemical ionization techniques with isobutane as the reactant gas, Doolittle and coworkers²⁵⁷ demonstrated that conjugated dienes which may contain terminal functionalities such as aldehyde, alcohol and formate groups react with the major reagent ion, $t\text{-C}_4\text{H}_9^+$, to give structure-specific fragmentation. Limitations were encountered with dienes bearing the functional group proximal to the unsaturation and identification of stereoisomeric dienes proved also to be difficult. In closely related work and at the same time, Einhorn and coworkers^{258,259} used isomeric butyl chlorides, instead of isobutane, as the reactant gases and found that the reactions of conjugated dienes, $\text{R}^1(\text{CH}=\text{CH})_2\text{R}^2$, with $t\text{-C}_4\text{H}_9^+$ cations yield highly diagnostic fragment ions of the composition $\text{C}_4\text{H}_8(\text{R}^1)^+$ and $\text{C}_4\text{H}_8(\text{R}^2)^+$.

As mentioned above, gas-phase coordination of unsaturated C–C bonds to metal cations constitutes another means for double-bond localization. Peake and Gross²⁶⁰ determined the fragmentation of Fe^+ /olefin complexes by CID spectrometry and reported highly characteristic differences for several constitutional octadiene isomers. High-resolution mass spectrometry proved to be necessary in certain cases due to the isobaric masses of Fe and even two units of C_2H_4 and/or CO ²⁶¹. Although not based on gas-phase ion/molecule

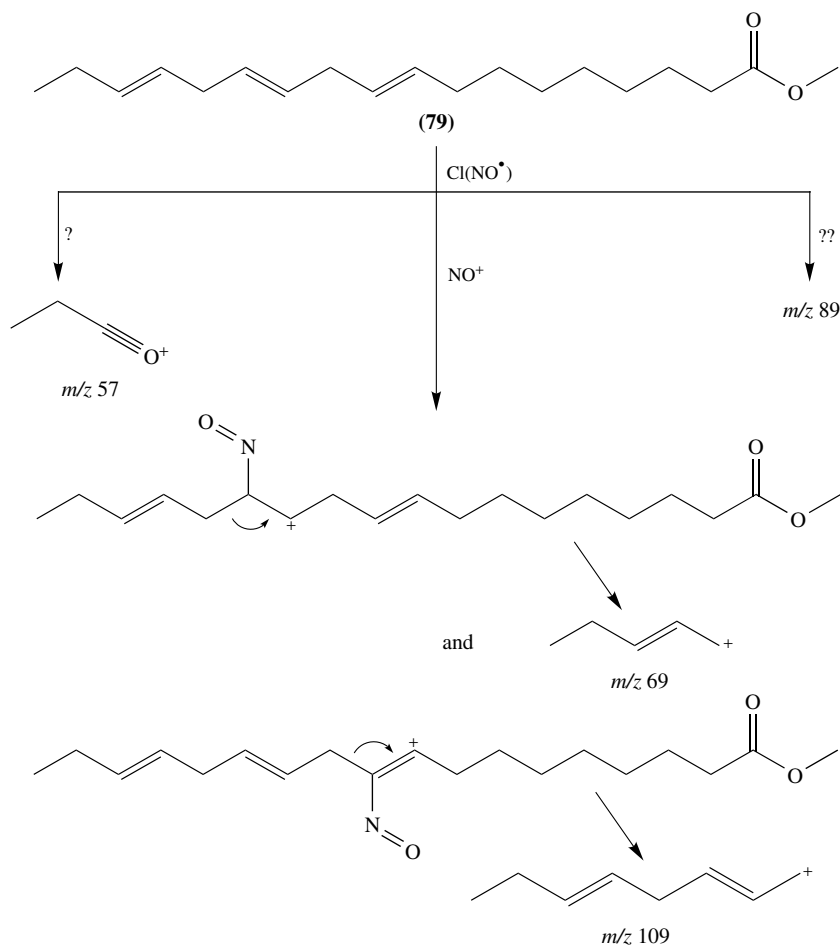


SCHEME 22

reactions, a study by Canty and Colton reporting electrospray ionization (ESI) mass spectrometry of several cyclic dienes and polyenes may be mentioned here²⁶².

Concerning special reactant gases used in CI mass spectrometry of dienes and polyenes, some more recent results are also of interest. It is noted that the distinction of isomers bearing C–C double bonds using CI mass spectrometry relies, in appropriate cases, on

the $[4 + 2^+]$ cycloaddition processes discussed in the previous section, as suggested by Keough²⁶³. Along the same line, Lange²⁶⁴ reported the use of oxirane as the reactant gas for CI mass spectrometry. Several olefins including 1,3-alkadienes and doubly and triply unsaturated fatty acids were examined and the $[M + 43]^+$ ion was found to be characteristic for 1,3-dienes. It appears reasonable that $C_2H_3O^+$ ions, formed in the CI(oxirane) plasma, presumably as acetyl cations, are able to undergo cycloaddition with 1,3-dienes. Distinction of stereoisomeric dienes was also reported. Furthermore, acetone has been tested as a reactant gas for CI mass spectrometry of olefins. The spectra of a few alkadienes have been reported in this context²⁶⁵.



SCHEME 23

Finally, a recent study on the localization of the double bonds in dienes will be exemplified. As an extension of the data presented in his reviews²⁵¹, Budzikiewicz and

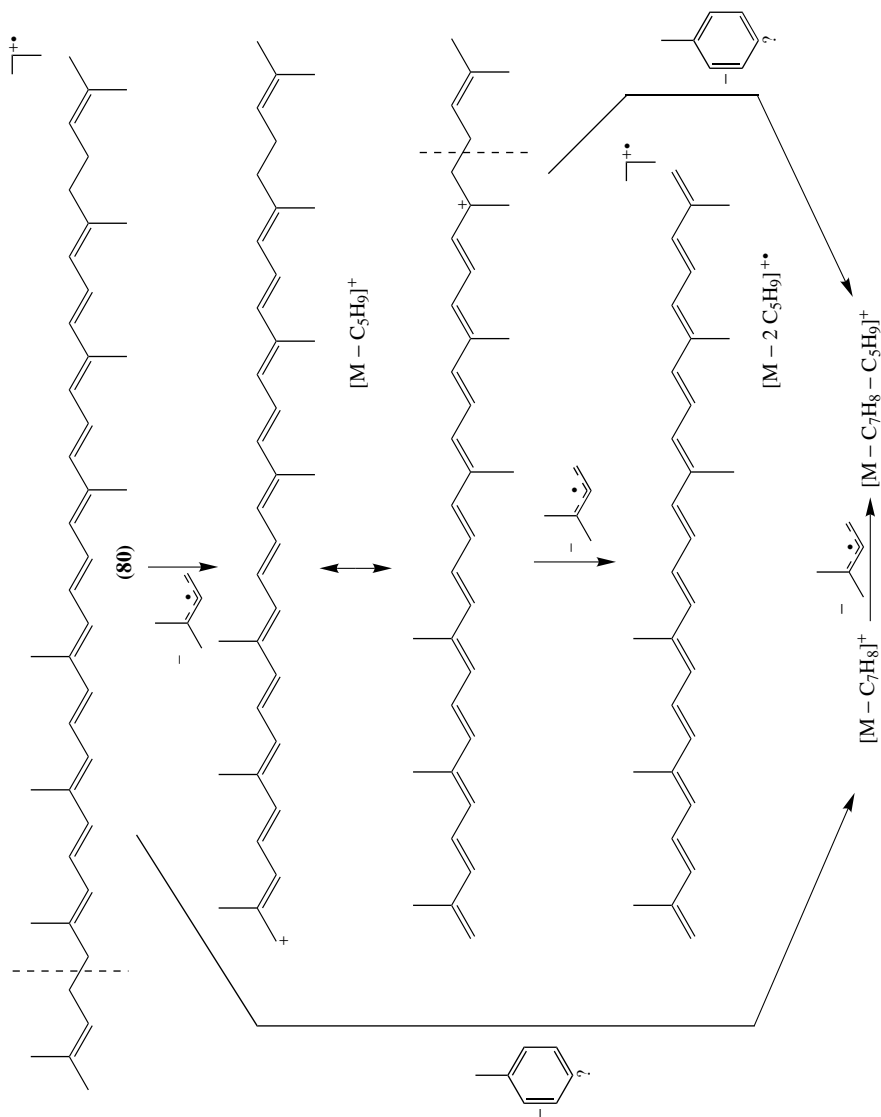
coworkers²⁶⁶ have reported on the fragmentation of several non-conjugated alkadiene hydrocarbons and of methyl linolenate, a two-fold homoconjugated alkatriene carboxylic ester, using nitric oxide, which is one of the most widely studied reagent gases used for this purpose. Complex rearrangement processes have been identified. However, as stated by the authors, the details of the parameters that influence the CI(NO) mass spectra have remained unclear, in spite of the tremendous work invested in this topic. Most importantly, the temperature of the ion source and possibly other parameters of the experimental setup strongly affect the diagnostically valuable analytical information, as demonstrated for the linolenate. Under suitable conditions, however, structure-specific acyl cations can be recognized in all cases, originating from (possibly surface-catalysed) oxidative cleavage of the C–C double bonds. Also, diagnostic allylic cations are formed, probably resulting from the direct gas-phase electrophilic attack of NO^+ on the double bonds of unsaturated fatty acids such as **79** (Scheme 23). Both of these types of fragment ions, amongst others, help to determine the position of the double bond close to the end of the hydrocarbon chain, whereas localization of double bonds close to the functionalized terminus of **79** was found to be difficult. Still, it is noteworthy that the recurring formation of quite abundant fragment ions (m/z 89) of obvious specificity, being formed from dienes bearing a terminal 1-buten-1-yl group, is not yet understood. There is no doubt that ‘unexpected’ peaks will keep mass spectrometry a field of both mystery and fascination²⁶⁷.

VII. MASS SPECTROMETRY OF MONO- AND OLIGOTERPENES, TERPENOIDS AND CAROTENOIDS

Owing to the vast occurrence of oligoterpenes in biological systems, instrumental analytical methods concerning these compounds have gained enormous interest during the past decades. Mass spectrometry of terpenoids and isoprenoids has become particularly important because of the extremely low detection limit as compared to other spectrometric techniques. From the mechanistically rather complicated isomerization reaction taking place in highly unsaturated radical cations, in particular, a detailed understanding of the gas-phase ion chemistry, as the origin of fragmentation behaviour, is difficult for terpenoid and carotenoid ions, too. Nevertheless, major fragmentation paths of these species have been found to correspond to the principles discussed in the previous sections for smaller diene and polyene ions. Thus, allylic and bis-allylic C–C bond cleavage, retro-Diels–Alder reactions and, most importantly, cyclization processes by C–C bond formation between the double bonds give rise to the most characteristic peaks in the positive-ion mass spectra of terpenoid and isoprenoid compounds.

Before returning to the deluge of literature that has built up on mass spectrometry of natural polyenes, the most impressive and highly diagnostic fragmentation reactions of carotenoid radical cations will be presented since this reflects the ‘well-behaved’, i.e. rational, gas-phase ion chemistry of these compounds. The major routes are collected in Scheme 24 for the case of lycopene (**80**)²⁶⁸. Bis-allylic cleavage leads to the $[\text{M} - \text{C}_5\text{H}_9]^+$ ions which lose another prenyl radical, as a notable exception of the even-electron rule. The other fragmentation path which is highly characteristic for carotenoids and other polyconjugated polyenes is the expulsion of neutral arenes, such as toluene and *meta*-xylene, from inner-chain units. Combinations of both fragmentation reactions provide also useful analytical information, although the sequence of the consecutive fragmentation is not unequivocal.

The expulsion of arenes from the inner sections of the polyene chain is very important for the determination of the positions of the side groups. Depending on the mutual distance of the methyl groups, either neutral toluene (92 u) and/or xylene (106 u) [u corresponds to Da = atomic mass unit, a symbol recommended by IUPAC] are eliminated from the



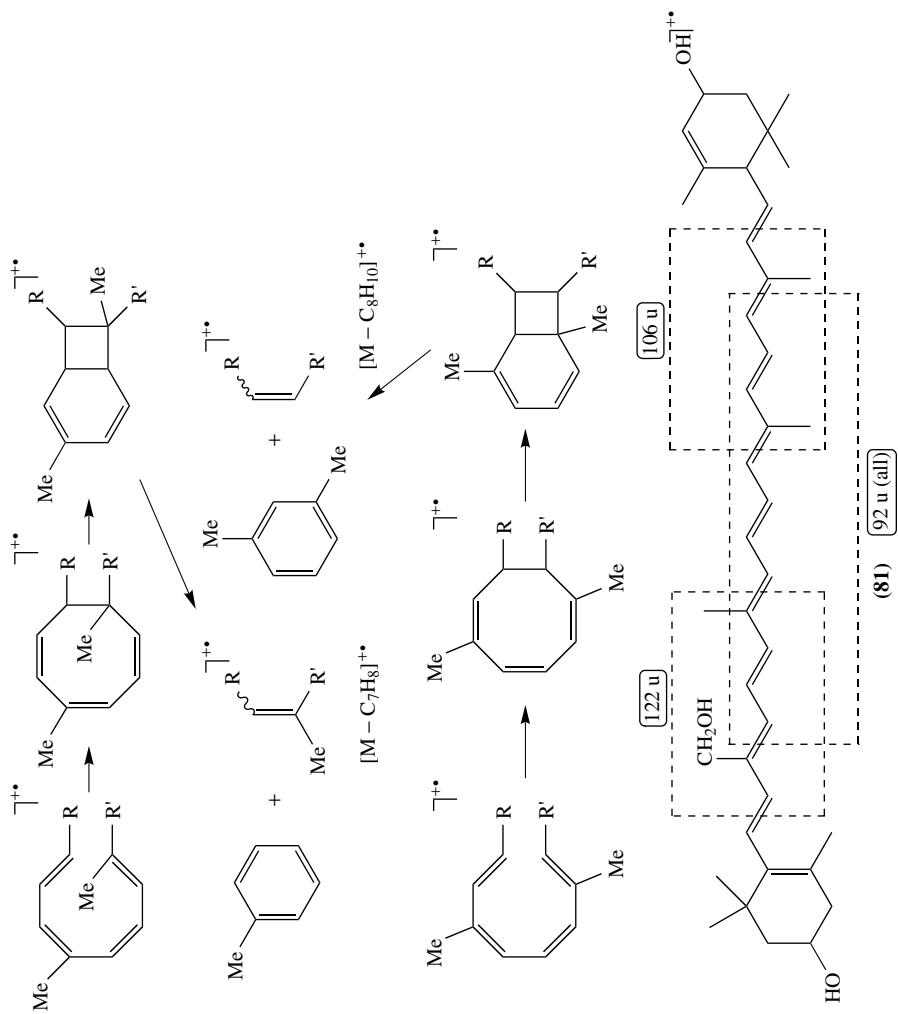
radical cations. In contrast to simple 1,3,5,7-octatetraene radical cations such as (**11**) (Scheme 2), the positive charge remains on the non-aromatic polyene fragment formed, owing to the lower ionization energy of the latter as compared with the arene. In the specific example of linoxanthin (**81**) shown in Scheme 25, the loss of 122 u indicates the presence of a hydroxymethyl group²⁶⁹.

The elimination of arenes is not limited to the radical cations of the carotenoids. Just as the neutral compounds themselves also tend to undergo (thermal) cyclization followed by arene loss, the protonated analogues, e.g. ion **82** generated by CI or fast atom bombardment (FAB) mass spectrometry are prone to eliminate one or even two arene molecules as well (Scheme 26)²⁷⁰.

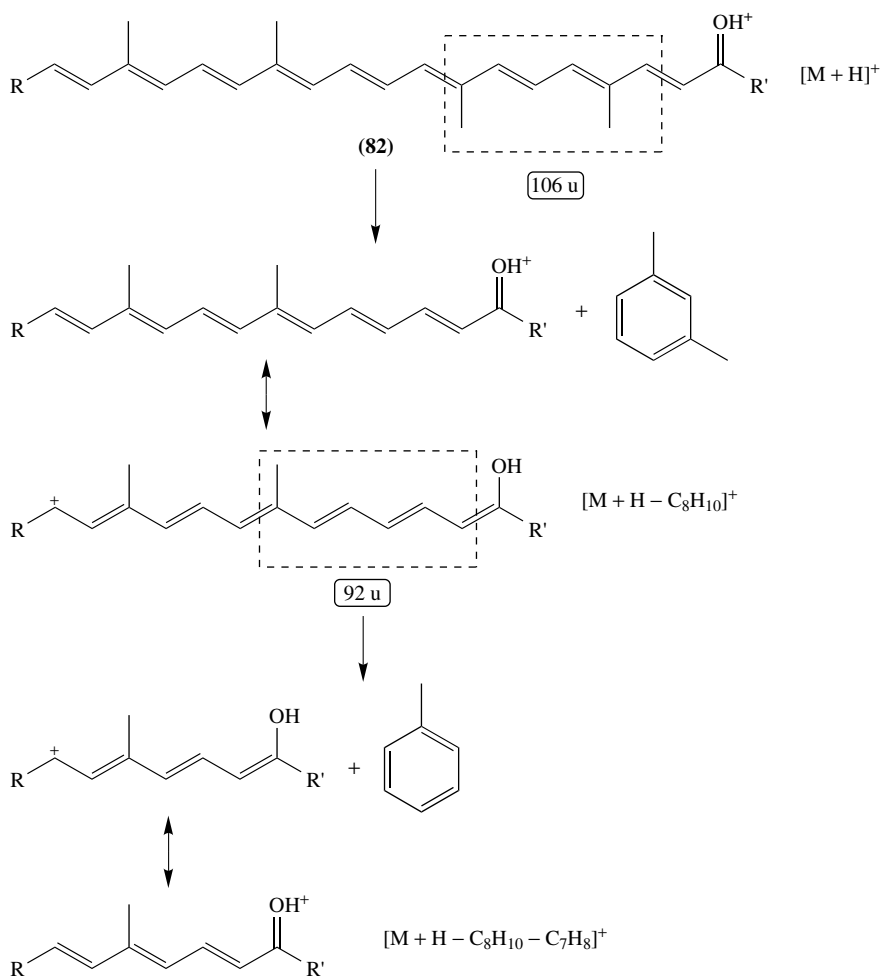
Mass spectrometry and gas-phase ion chemistry of monoterpenes have been reviewed several times during the last four decades¹². In recent years, more attention has been drawn to the gas-phase ion chemistry taking place upon ionization of terpenes. Fernandez and coworkers²⁷¹ determined the gas-phase basicity and proton affinity of limonene by proton transfer equilibrium measurements in an FT-ICR mass spectrometer. Theoretical calculations suggest that protonation at the external C–C double bond occurs with concomitant 1,2-H shift of the proton at C(1) to C(7), yielding a tertiary, endocyclic carbocation instead of a secondary, exocyclic one. Basic and Harrison²⁷² have compared the standard 70 eV EI mass spectra of ten monoterpenes as well as the MIKE and CID spectra of the molecular radical cations. The isomers were found to be distinguishable, although long-lived (metastable) ions apparently undergo enhanced interconversion. Thus, double-bond migration appears to be limited in these cases but pairs of isomers give very similar MIKE spectra. The fragmentation of the ubiquitous $[M - CH_3]^+$ ions (m/z 121), $[M - C_2H_5]^+$ ions (m/z 107) and $[M - C_3H_7]^+$ ions ($C_7H_9^+$, m/z 93) was also studied by MIKE spectrometry. The MIKE spectra exhibit very similar fragmentation, and two paths for the formation of the $C_7H_9^+$ ions from the molecular ions were elucidated. Most intriguingly, comparison of charge stripping (CS) spectra of the $C_7H_9^+$ ions with those of protonated toluene and 1,3,5-cycloheptatriene led to the conclusion that the $C_7H_9^+$ ions from the monoterpenes have the dihydrotropylium rather than the toluenium structure. The structural specificity of the EI mass spectra can be enhanced by working at low electron energies, as shown by Brophy and Maccoll²⁷³ in their study comprising nineteen monoterpenes. In almost all cases, the $[m/z$ 93] / $[m/z$ 121] intensity ratio provides a characteristic feature of the isomers. Previous investigations by Schwarz and coworkers²⁷⁴ had also shown that the molecular ions of the monoterpenes are rather reluctant to isomerization whereas the $C_7H_9^+$ ions undergo extensive interconversion to a common structure or mixture of structures. Interestingly, the structural ambiguity of $C_7H_9^+$ ions has been known as long as the much better recognized problem of the six- and seven-ring isomers of the $C_7H_7^+$ ions (i.e. benzyl vs tropylium) and $C_7H_8^{+\bullet}$ ions (i.e. ionized toluene vs ionized cycloheptatriene). With regard to the monoterpenes, Friedman and Wolf²⁷⁵ had already suggested in 1957 a monocyclic structure for the ion at m/z 93 in the EI spectrum of camphene.

Formation of dihydrotropylium ions is a key feature of the $C_7H_9^+$ hypersurface. Currently, efforts in our laboratory²⁷⁶ have concentrated on the presence of different $C_7H_9^+$ isomers by probing their bimolecular reactivity. Thus, gas-phase titration in the FT-ICR mass spectrometer has revealed that mixtures of $C_7H_9^+$ ions are formed by protonation of 1,3,5-cycloheptatriene, 6-methylfulvene and norbornadiene as the neutral precursors but that, in contrast to the results obtained by CS mass spectrometry, fragmentation of the radical cations of limonene yields almost exclusively toluenium ions²⁷⁵.

An impressive number of comprehensive reviews have appeared since the first overview on the structure elucidation of carotenoids by spectroscopic methods by Weedon appeared



SCHEME 25



SCHEME 26

in 1969²⁷⁷. This early review already collected the major fragmentation routes reflected by the EI spectra of the terpenoids containing 1,5-hexadiene units, viz. bis-allylic C–C bond cleavage, and the carotenes, viz. cyclization of the unsaturated chain leading to the elimination of toluene and xylene from inner positions of the chain (see above). The mechanisms of these and other important fragmentation reactions have been discussed in the 1971 review on carotenoids by Vetter and coworkers²⁷⁸. Only one year later, two further review articles appeared, one by Enzell and coworkers²⁷⁹ concerning mass spectrometry of terpenes and terpenoids, and another by Elliott and Waller²⁸⁰ on mass spectrometry of vitamins and cofactors. In the former article, the standard EI mass spectra of monoterpenes, sesquiterpenes and many higher terpenoids, including the carotenes, are presented and discussed with many mechanistic suggestions for the major fragmentation paths. The latter review is focused on the EI mass spectra of vitamins A and D and their

derivatives. Subsequently, Budzikiewicz²⁸¹ gave an exemplary view on the potential of EI mass spectrometry, concentrating in detail on the expulsion of arene molecules from the inner-chain positions of the radical cations of several carotenoids. In 1980, a supplemental volume of the series on biochemical applications of mass spectrometry appeared to which Enzell and Wahlberg contributed extensive overviews on the mass spectrometric fragmentation of terpenoids²⁸² and carotenoids²⁸³. Degraded isoprenoids, as present in substantial amounts in tobacco, contribute to the diversity of these polyene compounds, and another extensive review dealing with the mass spectra of tobacco isoprenoids appeared in 1984²⁸⁴. Stereochemical aspects reflected in the mass spectra of terpenes and terpenoids have been discussed in a separate survey²⁸⁵. A collection of spectral data of more than 300 sesquiterpene hydrocarbons, including the EI mass spectra, has appeared recently²⁸⁶. In their latest overview on mass spectrometry of carotenoids, Enzell and Back²⁸⁷ gave an exhaustive presentation and discussion on the topic, including various ionization techniques such as EI, FAB and CI, and examples on the application of tandem mass spectrometry such as MIKE spectrometry and the B/E linked scan techniques. Moreover, state-of-the-art combination of chromatographic techniques with mass spectrometry was discussed for carotenoids. While the major part of the discussion is again devoted to the mechanism of the elimination of in-chain units from the polyene skeleton in the radical cations formed upon EI (see above), even the mass spectra of carotenoid conjugates such as fatty and retinoic acid esters, sulphates and glycosides are included.

Several original papers must be mentioned that deal with mass spectrometric techniques which the numerous reviews do not comprise. Kaufmann and coworkers^{268,288} studied the mass spectrometric analysis of carotenoids and some of their fatty acid esters using matrix-assisted laser desorption/ionization (MALDI) mass spectrometry and its post-source-decay (PSD) variant. Some advantages concerning the thermal instability and limited solubility were discussed, but the fragmentation paths of the carotenoid cations were found to be essentially the same as those observed with conventional techniques.

Different from many other classes of organic compounds, the carotenoids have relatively high electron affinities. Capture of thermal electrons in the NCI plasma by a low-lying π^* orbital of the extended system of conjugated double bonds is facile and therefore electron capture negative chemical ionization (ECNCI) mass spectrometry is particular useful with carotenes and carotenoids. McClure and Liebler²⁸⁹ have recently demonstrated the characterization of β -carotene and three of its oxidation products by ECNCI tandem mass spectrometry, i.e. by performing collision-induced dissociation (CID) of the molecular radical anions and recording the fragment anions by B/E linked scanning. It is noteworthy that, in contrast to the positively charged molecular ions formed under EI, CI, FAB and MALDI conditions, the negative charge molecular ions do not undergo expulsion of arenes from the inner segments of the polyene chain. Instead of those rearrangement processes, the fragment anions formed originate from (apparently) simple cleavages of both single and double C—C bonds in a highly characteristic manner. Mechanistic explanations have not yet been provided. It may be suspected, however, that cyclization by C—C bond formation between unsaturated centers intervenes also in the radical anions as well. Also, owing to the particularly high electron affinity, the detection limits in carotenoid analysis by ECNCI mass spectrometry are considerably lower than under positive-ion conditions. The conversion of β -carotene to retinol under in-vivo conditions has been studied recently by ECNCI and atmospheric pressure chemical ionization (APCI) mass spectrometry²⁹⁰. Very recent work utilizing coupling of the ECNCI techniques with gas chromatography²⁹¹ and liquid chromatography²⁹² for monitoring of retinol and carotenoids, respectively, is also mentioned here. Analytical studies on carotenoids using other ionization techniques

such as fast-atom bombardment (FAB)²⁹³, electrospray ionization (ESI)²⁹⁴ and atmospheric pressure chemical ionization²⁹⁵, field desorption (FD)²⁹⁶ and plasma desorption mass spectrometry have been published²⁹⁷.

Selva and coworkers^{298–302} reported on their experiences to apply various mass spectrometric techniques to the analysis of β -carotene and carotenoids and their adducts formed in aqueous solution. EI mass spectrometry and field desorption (FD) mass spectrometry were applied to aqueous mixtures of β -carotene and β -cyclodextrin, and the polyene was found to be detectable²⁹⁸. Tandem mass spectrometry can be applied to identify β -carotenone as a minor component in complex carotenoid mixtures. EI/MIKE spectrometry of the molecular ion (m/z 600) was used in this case²⁹⁹. A previous study was focused on the characterization of *seco*-carotenoids using EI/MIKE and CID spectrometry³⁰⁰. The more recent ionization methods, viz. MALDI and its variant working without a matrix, laser desorption/ionization (LDI), as well as electrospray ionization (ESI) mass spectrometry, have also been applied to this topic. MALDI and LDI mass spectrometry were used to analyse mixtures of β -carotene and γ -cyclodextrin in aqueous solution. Adduct ions were not observed using these methods³⁰¹.

Also, a brief note has appeared concerning electrospray ionization mass spectrometry of mixtures of β -carotene with β - and with γ -cyclodextrin in aqueous methanol solutions. Whereas negative ion ESI produced 1:1 adduct ions of β -carotene with both of the cyclodextrin isomers, positive ESI gave these adducts only in the case of β -cyclodextrin³⁰².

VIII. ACKNOWLEDGEMENTS

We feel very much indebted to the Editor, Professor Zvi Rappoport, for kindly having invited us to write this review and for generously having kept his patience during our work on the manuscript. M. M. is also grateful to the Graduiertenförderung des Landes Nordrhein-Westfalen for a grant.

IX. REFERENCES

1. A. G. Loudon and A. Maccoll, in *The Chemistry of Alkenes*, Vol. 2 (Ed. J. Zabicky), Chap. 7, Wiley-Interscience, London, 1970, pp. 327–358.
2. M. N. Mruzek, in *The Chemistry of Double-bonded Functional Groups*, Vol. 2, Part 2 (Ed. S. Patai), Chap. 2, Wiley, Chichester, 1989, pp. 53–79.
3. H. Schwarz, in *The Chemistry of the Cyclopropyl Group*, Part 1 (Ed. Z. Rappoport), Chap. 4, Wiley, Chichester, 1987, pp. 173–211.
4. C. Dass, *Mass Spectrom. Rev.*, **9**, 1 (1990).
5. F. Tureček and V. Hanuš, *Mass Spectrom. Rev.*, **3**, 85 (1984).
6. A. Mandelbaum, in *Applications of Mass Spectrometry to Organic Stereochemistry* (Ed. J. S. Splitter), VCH, New York, 1994, pp. 299–324.
7. D. Kuck, *Mass Spectrom. Rev.*, **9**, 181 (1990).
8. D. Kuck, *Mass Spectrom. Rev.*, **9**, 583 (1990).
9. S. Fornarini, *Mass Spectrom. Rev.*, **15**, 365 (1996).
10. S. Fornarini and M. E. Crestoni, *Acc. Chem. Res.*, **31**, 827 (1998).
11. M. Mormann and D. Kuck, *J. Mass Spectrom.*, **34**, 384 (1999).
12. For early reviews, see:
 - (a) H. Budzikiewicz, C. Djerassi and D. H. Williams, *Structure Elucidation of Natural Products by Mass Spectrometry*, Vol II: Steroids, Terpenoids, Sugars and Miscellaneous Classes, Chap. 24, Holden-Day, San Francisco, 1964, pp. 141–164.
 - (b) J. H. Beynon, R. A. Saunders and A. E. Williams, *The Mass Spectra of Organic Molecules*, Chap. 3.2, Elsevier, Amsterdam, 1968, pp. 112–122.

13. See, for example: D. Kuck, *Angew. Chem.*, **112**, 129 (2000); *Angew. Chem., Int. Ed. Engl.*, **39**, 125 (2000).
14. (a) S. G. Lias, J. E. Bartmess, J. F. Liebman, J. L. Holmes, R. D. Levin and W. G. Mallard, *J. Phys. Chem. Ref. Data*, **17**, Suppl. 1 (1988).
(b) E. P. L. Hunter and S. G. Lias, *J. Phys. Chem. Ref. Data*, **27**, 413 (1998).
(c) W. G. Mallard and P. J. Linstrom (Eds.), *NIST Chemistry Webbook*, NIST Standard Reference Database No. 69; March 1998; National Institute of Standards and Technology: Gaithersburg, MD 20899 (<http://webbook.nist.gov>).
15. F. W. McLafferty and D. B. Stauffer, *The Wiley/NBS Registry of Mass Spectral Data*, Vol. 1, Wiley, New York, 1989, p. 16.
16. F. W. McLafferty and F. Tureček, *Interpretation of Mass Spectra*, 4th edn., University Science Books, Mill Valley, 1993, p. 230–231.
17. K. Levsen and E. Hilt, *Justus Liebigs Ann. Chem.*, 257 (1976).
18. J. C. A. Marques, A. Falick, A. Heusler, D. Stahl, P. Tecon and T. Gäumann, *Helv. Chim. Acta*, **67**, 425 (1984).
19. (a) K. Levsen, R. Weber, F. Borchers, H. Heimbach and H. D. Beckey, *Anal. Chem.*, **50**, 1655 (1978).
(b) K. Levsen, *Fundamental Aspects of Organic Mass Spectrometry*, Verlag Chemie, Weinheim, 1978, pp. 186–196 and 273–279.
20. S. A. Rang, A.-M. A. Mütirisepp, M. M. Liitma and O. G. Eisen, *Org. Mass Spectrom.*, **13**, 181 (1978).
21. A. A. Polyakova, K. I. Zimina, A. A. Petrov and R. A. Kheml'nitskii, *J. Gen. Chem. USSR (Engl. Transl.)*, **30**, 2949 (1960).
22. J. L. Holmes, *Org. Mass Spectrom.*, **8**, 247 (1974).
23. Synonymous terms used: Collisional activation (CA) and collision-activated dissociation (CAD).
24. C. Lifshitz, *Acc. Chem. Res.*, **27**, 138 (1994).
25. A. Maquestiau, Y. Van Haverbeke, R. Flammang, C. de Meyer and A. Menu, *Org. Mass Spectrom.*, **12**, 706 (1977).
26. J. L. Holmes, J. K. Terlouw, P. C. Burgers and R. T. B. Rye, *Org. Mass Spectrom.*, **15**, 149 (1980).
27. C. Dass, D. A. Peake and M. L. Gross, *Org. Mass Spectrom.*, **21**, 741 (1986).
28. F. P. Lossing and J. C. Traeger, *Int. J. Mass Spectrom. Ion Phys.*, **19**, 9 (1976).
29. R. Houriet, H. Schwarz, W. Zummack, J. G. Andrade and P. v. R. Schleyer, *Nouv. J. Chim.*, **5**, 505 (1981).
30. P. v. R. Schleyer, T. W. Bentley, W. Koch, A. J. Kos and H. Schwarz, *J. Am. Chem. Soc.*, **109**, 6953 (1987).
31. R. S. Mason, K. R. Jennings, S. Verma and R. G. Cooks, *Org. Mass Spectrom.*, **20**, 727 (1985).
32. J. M. Curtis, A. G. Brenton, J. H. Beynon and R. K. Boyd, *Org. Mass Spectrom.*, **22**, 779 (1987).
33. J. R. Appling, K. M. Musier and T. F. Moran, *Org. Mass Spectrom.*, **19**, 412 (1984).
34. S. R. Andrews, D. E. Parry and F. M. Harris, *Rapid Commun. Mass Spectrom.*, **8**, 913 (1994).
35. W. Wagner-Redeker and K. Levsen, *Org. Mass Spectrom.*, **16**, 538 (1981).
36. R. C. Benz, R. C. Dunbar and P. C. Claspy, *J. Am. Chem. Soc.*, **103**, 1799 (1981).
37. R. E. Krailler and D. H. Russell, *Anal. Chem.*, **57**, 1211 (1985).
38. S. E. Van Bramer and M. V. Johnston, *Org. Mass Spectrom.*, **27**, 949 (1992).
39. P. Wolkoff, J. L. Holmes and F. P. Lossing, *Can. J. Chem.*, **58**, 251 (1980).
40. P. Wolkoff and J. L. Holmes, *J. Org. Chem.*, **47**, 3342 (1982).
41. (a) F. Tureček and M. Gu, *Org. Mass Spectrom.*, **27**, 1335 (1992).
(b) F. Tureček and M. Gu, *J. Mass Spectrom.*, **30**, 144 (1995).
42. M. Gu and F. Tureček, *Org. Mass Spectrom.*, **29**, 85 (1994).
43. S. Hayakawa, H. Endoh, K. Arakawa and N. Morishita, *Int. J. Mass Spectrom. Ion Processes*, **171**, 209 (1997).
44. S. Hayakawa, H. Endoh, K. Arakawa, N. Morishita and T. Sugiura, *Int. J. Mass Spectrom. Ion Processes*, **151**, 89 (1995).
45. R. Stockbauer and H. Rosenstock, *Int. J. Mass Spectrom. Ion Phys.*, **27**, 185 (1978).
46. W. Wagner, K. Levsen and C. Lifshitz, *Org. Mass Spectrom.*, **15**, 271 (1980).

47. G. Frenking and H. Schwarz, *Int. J. Mass Spectrom. Ion Phys.*, **52**, 131 (1983).
48. A. C. Parr, A. J. Jason, R. Stockbauer and K. E. McCulloh, *Int. J. Mass Spectrom. Ion Phys.*, **30**, 319 (1979).
49. P. N. T. van Velzen and W. J. van der Hart, *Org. Mass Spectrom.*, **16**, 237 (1981).
50. W. J. van der Hart, *Int. J. Mass Spectrom. Ion Processes*, **151**, 27 (1995).
51. A. A. Mommers, P. C. Burgers, J. L. Holmes and J. K. Terlouw, *Org. Mass Spectrom.*, **19**, 7 (1984).
52. C. Cornaggia, *Phys. Rev. A*, **52**, R4328 (1995).
53. E. Rühl, B. Brutschy, P. Bisling and H. Baumgärtel, *Ber. Bunsenges. Phys. Chem.*, **92**, 194 (1988).
54. A. B. King, *J. Phys. Chem.*, **68**, 1409 (1964).
55. D. H. Russell, M. L. Gross, J. van der Greef and N. M. M. Nibbering, *J. Am. Chem. Soc.*, **101**, 2086 (1979).
56. J. L. Franklin and A. Mogenis, *J. Phys. Chem.*, **71**, 2820 (1967).
57. T. L. Bunn and T. Baer, *J. Chem. Phys.*, **85**, 6361 (1986).
58. J. W. Keister, T. Baer, M. Evans, C. Y. Ng and C.-W. Hsu, *J. Phys. Chem. A*, **101**, 1866 (1997).
59. P. C. Burgers, J. L. Holmes, A. A. Mommers and J. E. Szulejko, *J. Am. Chem. Soc.*, **106**, 521 (1984).
60. A. M. Woodward, W. A. Chupka and S. D. Colson, *J. Phys. Chem.*, **88**, 4567 (1984).
61. W. Tang, X.-L. Zhang and T. Bally, *J. Phys. Chem.*, **97**, 4373 (1993).
62. T. Keszthelyi, R. Wilbrandt and T. Bally, *J. Mol. Struct.*, **410–411**, 339 (1997).
63. F. Tureček, F. Maquin, N. Hill, D. Stahl and T. Gäumann, *Org. Mass Spectrom.*, **23**, 91 (1988).
64. B. G. Syrvatka, M. M. Gil'burd and A. L. Bel'ferman, *J. Org. Chem. USSR (Engl. Transl.)*, **9**, 1144 (1973).
65. M. Kraft and G. Spiteller, *Org. Mass Spectrom.*, **2**, 865 (1969).
66. D. G. I. Kingston, J. T. Bursey and M. M. Bursey, *Chem. Rev.*, **74**, 215 (1974).
67. H. Budzikiewicz, C. Fenseleau and C. Djerassi, *Tetrahedron*, **22**, 1391 (1966).
68. J. R. Dias, Y. M. Sheikh and C. Djerassi, *J. Am. Chem. Soc.*, **94**, 473 (1972).
69. R. B. Bates, J. J. White and K. H. Schramm, *Org. Mass Spectrom.*, **22**, 295 (1987).
70. O. Vostrowsky, K. Michaelis and H. J. Bestmann, *Justus Liebigs Ann. Chem.*, 1001 (1982).
71. H. Ikeda, T. Takasaki, Y. Takahashi and T. Miyashi, *J. Chem. Soc., Chem. Commun.*, 367 (1993).
72. U. T. Bhalerao and H. Rapoport, *J. Am. Chem. Soc.*, **93**, 105 (1971).
73. K. Schmidt, G. W. Francis and S. Liaaen-Jensen, *Acta Chem. Scand.*, **25**, 2476 (1971).
74. M. L. Gross and D. H. Russell, *J. Am. Chem. Soc.*, **101**, 2082 (1979).
75. C. Dass, T. M. Sack and M. L. Gross, *J. Am. Chem. Soc.*, **106**, 5780 (1984).
76. C. Dass and M. L. Gross, *J. Am. Chem. Soc.*, **105**, 5724 (1983).
77. E. Gil-Av, J. H. Leftin, A. Mandelbaum and S. Weinstein, *Org. Mass Spectrom.*, **4**, 475 (1970).
78. A. Mandelbaum, S. Weinstein, E. Gil-Av and J. H. Leftin, *Org. Mass Spectrom.*, **10**, 842 (1975).
79. S. G. Lias and P. Ausloos, *Int. J. Mass Spectrom. Ion Processes*, **81**, 165 (1987).
80. (a) P. J. Derrick, A. M. Falick and A. L. Burlingame, *J. Am. Chem. Soc.*, **94**, 6794 (1972).
(b) P. J. Derrick, A. M. Falick and A. L. Burlingame, *J. Am. Chem. Soc.*, **96**, 615 (1974).
81. P. Wolkoff and J. L. Holmes, *Can. J. Chem.*, **57**, 348 (1979).
82. E. P. Smith and E. R. Thornton, *J. Am. Chem. Soc.*, **89**, 5079 (1967).
83. (a) D. P. Stevenson, *Disc. Faraday Soc.*, **10**, 35 (1951).
(b) H. E. Audier, *Org. Mass Spectrom.*, **2**, 283 (1969).
84. R. C. Dougherty, *J. Am. Chem. Soc.*, **90**, 5788 (1968).
85. E. F. Brittain, C. H. J. Wells and H. M. Paisley, *J. Chem. Soc. B*, 503 (1969).
86. F. Tureček and V. Hanuš, *Org. Mass Spectrom.*, **15**, 4 (1980).
87. (a) G. M. Whitesides, G. L. Goe and A. C. Cope, *J. Am. Chem. Soc.*, **89**, 7136 (1967).
(b) G. M. Whitesides, G. L. Goe and A. C. Cope, *J. Am. Chem. Soc.*, **91**, 2608 (1969).
88. W. D. Reets, Jr, H. D. Roth, M. L. Schilling and C. J. Abelt, *Int. J. Mass Spectrom. Ion Processes*, **72**, 155 (1986).
89. G. S. Groenewold and M. L. Gross, *J. Am. Chem. Soc.*, **106**, 6569 (1984).

90. (a) N. L. Bauld, D. J. Bellville, R. Pabon, R. Chelsky and G. Green, *J. Am. Chem. Soc.*, **105**, 2378 (1983).
(b) D. J. Bellville and N. L. Bauld, *Tetrahedron*, **42**, 6167 (1986).
(c) N. L. Bauld, *Tetrahedron*, **45**, 5307 (1989).
91. G.-F. Chen and F. Williams, *J. Am. Chem. Soc.*, **113**, 7792 (1991).
92. D. Vollmer, D. L. Rempel and M. L. Gross, *J. Am. Chem. Soc.*, **117**, 1669 (1995).
93. D. A. Lightner, J. K. Gawroński and T. D. Bouman, *J. Am. Chem. Soc.*, **102**, 5749 (1980).
94. D. Harris, S. McKinnon and R. K. Boyd, *Org. Mass Spectrom.*, **14**, 265 (1979).
95. M. Vincenti, S. R. Horning and R. G. Cooks, *Org. Mass Spectrom.*, **23**, 585 (1988).
96. S. R. Horning, J. M. Wood, R. R. Gord, B. S. Freiser and R. G. Cooks, *Int. J. Mass Spectrom. Ion Processes*, **101**, 219 (1990).
97. J. R. Gord, S. R. Horning, J. M. Wood, R. G. Cooks and B. S. Freiser, *J. Am. Soc. Mass Spectrom.*, **4**, 145 (1993).
98. R. W. Holman, C. D. Warner, R. N. Hayes and M. L. Gross, *J. Am. Chem. Soc.*, **112**, 3362 (1990).
99. B. A. Horn, J. L. Herek and A. H. Zewail, *J. Am. Chem. Soc.*, **118**, 8755 (1996).
100. S. A. Trushin, W. Fuss, T. Schikarski, W. E. Schmid and K. L. Kompa, *J. Phys. Chem.*, **106**, 9386 (1997).
101. M. Mormann and D. Kuck, unpublished results.
102. B. de Pascual-Teresa and K. N. Houk, *Tetrahedron Lett.*, **37**, 1759 (1996).
103. See, for example:
 - (a) W. T. Borden, E. R. Davidson and D. Feller, *J. Am. Chem. Soc.*, **103**, 5725 (1981).
 - (b) D. W. Kohn and P. Chen, *J. Am. Chem. Soc.*, **115**, 2844 (1993).
104. (a) C. Lifshitz and M. Weiss, *Int. J. Mass Spectrom. Ion Phys.*, **34**, 311 (1980).
(b) C. Lifshitz, D. Gibson, K. Levsen and I. Dotan, *Int. J. Mass Spectrom. Ion Phys.*, **40**, 157 (1981).
105. T. Baer, G. D. Willett, D. Smith and J. S. Phillips, *J. Chem. Phys.*, **70**, 4076 (1979).
106. P. Ausloos, *J. Am. Chem. Soc.*, **103**, 3931 (1981).
107. W. Wagner-Redeker, A. J. Illies, P. R. Kemper and M. T. Bowers, *J. Am. Chem. Soc.*, **105**, 5719 (1983).
108. J. C. Ray, Jr., P. O. Danis, F. W. McLafferty and B. K. Carpenter, *J. Am. Chem. Soc.*, **109**, 4408 (1987).
109. M.-Y. Zhang, C. Wesdemiotis, M. Marchetti, P. O. Danis, J. C. Ray, Jr., B. K. Carpenter and F. W. McLafferty, *J. Am. Chem. Soc.*, **111**, 8341 (1989).
110. C. Wesdemiotis, M.-Y. Zhang and F. W. McLafferty, *Org. Mass Spectrom.*, **26**, 671 (1991).
111. M.-Y. Zhang, B. K. Carpenter and F. W. McLafferty, *J. Am. Chem. Soc.*, **113**, 9499 (1991).
112. W. J. van der Hart, *Org. Mass Spectrom.*, **23**, 187 (1988).
113. B. J. Shay, M. N. Eberlin, R. G. Cooks and C. Wesdemiotis, *J. Am. Soc. Mass Spectrom.*, **3**, 518 (1992).
114. R. Bakhtiar, J. J. Drader and D. B. Jacobsen, *Org. Mass Spectrom.*, **28**, 797 (1993).
115. N. Goldberg, D. Sülzle and H. Schwarz, *Chem. Phys. Lett.*, **213**, 593 (1993).
116. (a) R. Flammang, P. Meyrant, A. Maquestiau, E. E. Kingston and J. H. Beynon, *Org. Mass Spectrom.*, **20**, 253 (1985).
(b) E. E. Kingston, J. H. Beynon, T. Ast, R. Flammang and A. Maquestiau, *Org. Mass Spectrom.*, **20**, 546 (1985).
117. M. A. Mabud, T. Ast and R. G. Cooks, *Org. Mass Spectrom.*, **22**, 418 (1987).
118. A. G. Harrison, P. Haynes, S. McLean and F. Meyer, *J. Am. Chem. Soc.*, **87**, 5099 (1965).
119. T. E. Smith, S. R. Smith and F. W. McLafferty, *Org. Mass Spectrom.*, **13**, 254 (1978).
120. J. L. Franklin and S. R. Carroll, *J. Am. Chem. Soc.*, **91**, 6564 (1969).
121. (a) M. I. Gorfinkel, T. P. Sosedkina and V. A. Koptyug, *J. Gen. Chem. USSR (Engl. Transl.)*, **37**, 1373 (1967).
(b) M. I. Gorfinkel, I. S. Isaev, I. A. Shleider and V. A. Koptyug, *J. Gen. Chem. USSR (Engl. Transl.)*, **39**, 1333 (1969).
122. M. N. Glukhovtsev, A. Pross, A. Nicolaidis and L. Radom, *J. Chem. Soc., Chem. Commun.*, 2347 (1995).
123. R. C. Dunbar and H. H. I. Teng, *J. Am. Chem. Soc.*, **100**, 2279 (1978).
124. R. L. Betts, M. A. Park and E. A. Schweikert, *J. Mass Spectrom.*, **30**, 305 (1995).
125. P. E. Share and K. L. Kompa, *Chem. Phys.*, **134**, 429 (1989).

126. M. E. Rennekamp and M. K. Hoffman, *Org. Mass Spectrom.*, **10**, 1075 (1975).
127. V. Hanuš and Z. Dolejšek, *Collect. Czech. Chem. Commun.*, **28**, 6562 (1963).
128. H. M. Rosenstock, K. E. McCulloh and F. P. Lossing, *Int. J. Mass Spectrom. Ion Phys.*, **25**, 327 (1977).
129. See also: W. Roth, cited as personal communication in Reference 14a.
130. E. Heilbronner, R. Gleiter, H. Hopf, V. Hornung and A. de Meijere, *Helv. Chim. Acta*, **54**, 783 (1971).
131. (a) D. H. Russell and M. L. Gross, *J. Am. Chem. Soc.*, **102**, 6279 (1980).
(b) W. J. van der Hart, L. J. de Koning, N. M. M. Nibbering and M. L. Gross, *Int. J. Mass Spectrom. Ion Processes*, **72**, 99 (1986).
132. (a) W. J. van der Hart, *Int. J. Mass Spectrom. Ion Processes*, **130**, 173 (1994).
(b) W. J. van der Hart, *J. Am. Soc. Mass Spectrom.*, **6**, 513 (1995).
133. S. G. Lias and P. Ausloos, *J. Chem. Phys.*, **82**, 3613 (1985).
134. Z. Zhu and T. Gäumann, *Org. Mass Spectrom.*, **28**, 1111 (1993).
135. T. Gäumann, G. Zhao and Z. Zhu, *Rapid Commun. Mass Spectrom.*, **8**, 1 (1994).
136. J. A. Herman, K. Herman and T. B. McMahon, *Can. J. Chem.*, **69**, 2038 (1991).
137. (a) G. Bouchoux and J.-Y. Salpin, *Rapid Commun. Mass Spectrom.*, **8**, 325 (1994).
(b) G. Bouchoux, J.-Y. Salpin and M. T. Nguyen, to be published.
138. G. Bouchoux, M. Yáñez and O. Mó, *Int. J. Mass Spectrom.*, **185/186/187**, 241 (1999).
139. M. Mormann, J.-Y. Salpin and D. Kuck, *Eur. Mass Spectrom.*, in press.
140. For an early review, see: M. K. Hoffman, *Z. Naturforsch.*, **29a**, 1077 (1974).
141. (a) D. H. Williams and G. Hvistendahl, *J. Am. Chem. Soc.*, **96**, 6755 (1974).
(b) G. Hvistendahl and D. H. Williams, *J. Chem. Soc., Perkin Trans. 2*, 881 (1975).
142. J.-Y. Salpin, M. Mormann, M. T. Nguyen and D. Kuck, to be published.
143. C. Lifshitz, Y. Gotkis, A. Ioffe, J. Laskin and S. Shaik, *Int. J. Mass Spectrom. Ion Processes*, **125**, R7 (1993).
144. C. Basic, J. E. Eyler and R. A. Yost, *Org. Mass Spectrom.*, **29**, 329 (1994).
145. B. P. Mathur, E. M. Burgess, D. E. Bostwick and T. F. Moran, *Org. Mass Spectrom.*, **16**, 92 (1981).
146. K. N. Wiegel, R. W. Holman and M. L. Gross, *Int. J. Mass Spectrom. Ion Processes*, **146/147**, 239 (1995).
147. (a) J. Grotmeyer and H.-F. Grützmacher, *Org. Mass Spectrom.*, **17**, 353 (1982).
(b) J. Grotmeyer and H.-F. Grützmacher, in *Current Topics in Mass Spectrometry and Chemical Kinetics* (Eds. J. H. Beynon and M. L. McGlashan), Heyden, London, 1982, pp. 29–59.
148. D. Kuck and H.-F. Grützmacher, *Org. Mass Spectrom.*, **14**, 86 (1979).
149. J. Möller, C. Th. Pedersen, E. Egsgaard and E. Larsen, *Org. Mass Spectrom.*, **15**, 456 (1980).
150. C. Lifshitz and S. H. Bauer, *J. Phys. Chem.*, **67**, 1629 (1963).
151. (a) R. Pentz, *Massenspektrometrische Untersuchungen von C₈-Cycloalkenen: Zerfallsmechanismen von Cyclooctadi- und -trienen und von [3.3.0]-Bicyclooctenen und octadienen*, Doctoral Thesis. Universität Hamburg, Germany, 1975.
(b) R. Pentz and H.-F. Grützmacher, unpublished results.
152. K. Levsen and H. D. Beckey, *Org. Mass Spectrom.*, **9**, 570 (1974).
153. See, for example: T. Bally, L. Truttman and F. Williams, *J. Mol. Struct. (Theochem.)*, **398–399**, 255 (1997).
154. M. S. Robinson, M. L. Polak, V. M. Bierbaum, C. H. DePuy and W. C. Lineberger, *J. Am. Chem. Soc.*, **117**, 6766 (1995).
155. P. G. Wenthold, J. Hu and R. R. Squires, *J. Am. Chem. Soc.*, **116**, 6961 (1994).
156. J. Lee, P. K. Chou, P. Dowd and J. J. Grabowski, *J. Am. Chem. Soc.*, **115**, 7902 (1993).
157. J. Lee and J. J. Grabowski, *Chem. Rev.*, **92**, 1611 (1992).
158. J. Zhao, P. Dowd and J. J. Grabowski, *J. Am. Chem. Soc.*, **118**, 8871 (1996).
159. M. D. Brickhouse and R. R. Squires, *J. Am. Chem. Soc.*, **110**, 2706 (1988).
160. I. I. Furlei, E. A. Burmistrov, F. Z. Galin, V. N. Iskandarova, V. K. Mavrodiev and G. A. Tolstikov, *J. Acad. Sci. USSR, Ser. Chem. (Engl. Transl.)*, **8**, 1618 (1986).
161. B. T. Hill and R. R. Squires, *J. Chem. Soc., Perkin Trans. 2*, 1027 (1998).
162. P. G. Wenthold, J. Hu, R. R. Squires and W. C. Lineberger, *J. Am. Chem. Soc.*, **118**, 475 (1996).
163. P. G. Wenthold, J. Hu, B. T. Hill and R. R. Squires, *Int. J. Mass Spectrom.*, **179/180**, 173 (1998).

164. P. G. Wenthold, J. Hu and R. R. Squires, *J. Am. Chem. Soc.*, **118**, 11865 (1996).
165. D. Kuck, A. Schuster, B. Ohlhorst, V. Sinnwell and A. de Meijere, *Angew. Chem.*, **101**, 626 (1989); *Angew. Chem., Int. Ed. Engl.*, **28**, 595 (1989).
166. For a review, see: D. Kuck, *Top. Curr. Chem.*, **196**, 167 (1998).
167. R. Haag, D. Schröder, T. Zywiets, H. Jiao, H. Schwarz, P. v. R. Schleyer and A. de Meijere, *Angew. Chem., Int. Ed. Engl.*, **35**, 1317 (1996).
168. D. Kuck, A. de Meijere and R. R. Squires, unpublished results. See also Reference 13.
169. J. E. Bartmess and R. T. McIver, Jr., in *Gas Phase Ion Chemistry*, Vol. 2 (Ed. M. T. Bowers), Chap. 11, Academic Press, New York, 1979, pp. 87–121.
170. C. H. DePuy and V. M. Bierbaum, *Acc. Chem. Res.*, **14**, 146 (1981).
171. C. A. Wight and J. L. Beauchamp, *J. Am. Chem. Soc.*, **103**, 6499 (1981).
172. R. L. White, C. L. Wilkins, J. H. Heitkamp and S. W. Staley, *J. Am. Chem. Soc.*, **105**, 4868 (1983).
173. W. P. M. Maas, P. A. van Veelen and N. M. M. Nibbering, *Org. Mass Spectrom.*, **24**, 546 (1989).
174. R. E. Lee and R. R. Squires, *J. Am. Chem. Soc.*, **108**, 5078 (1986).
175. S. Kato, R. Gareyev, C. H. DePuy and V. M. Bierbaum, *J. Am. Chem. Soc.*, **120**, 5033 (1998).
176. J. W. Denault, G. Chen and R. G. Cooks, *J. Am. Soc. Mass Spectrom.*, **9**, 1141 (1998).
177. W. E. Wentworth and W. J. Ristau, *J. Phys. Chem.*, **73**, 2126 (1969).
178. (a) B. S. Freiser (Ed.), *Organometallic Chemistry*, Kluwer Academic Publ., Dordrecht, 1996.
(b) A. Fontijn (Ed.), *Gas Phase Metal Reactions*, North-Holland, Amsterdam, 1992.
(c) K. Eller and H. Schwarz, *Chem. Rev.*, **91**, 1121 (1991).
(d) D. H. Russell (Ed.), *Gas Phase Inorganic Chemistry*, Plenum, New York, 1989.
(e) S. W. Buckner and B. S. Freiser, *Polyhedron*, **7**, 1583 (1988).
(f) J. Allison, *Prog. Inorg. Chem.*, **34**, 627 (1986).
179. J. J. Myher and A. G. Harrison, *J. Phys. Chem.*, **72**, 1905 (1968).
180. M. T. Bowers, D. D. Elleman, R. M. O'Malley and K. J. Jennings, *J. Chem. Phys.*, **74**, 2583 (1970).
181. A. Nato, M. Niwa, K. Honma, I. Tanaka and I. Koyano, *Int. J. Mass Spectrom. Ion Phys.*, **34**, 287 (1980).
182. C. Lifshitz, Y. Gleitman, S. Gefen, U. Shainok and I. Dotan, *Int. J. Mass Spectrom. Ion Phys.*, **40**, 1 (1981).
183. C. Lifshitz and Y. Gleitman, *Int. J. Mass Spectrom. Ion Phys.*, **40**, 17 (1981).
184. C. Lifshitz and Y. Gleitman, *J. Chem. Phys.*, **77**, 2383 (1982).
185. D. van Pijkeren, J. van Eck and A. Niehaus, *Chem. Phys.*, **103**, 383 (1986).
186. V. G. Anicich, G. A. Blake, J. K. Kim, M. J. McEwan and W. T. Huntress, Jr., *J. Phys. Chem.*, **88**, 4608 (1984).
187. R. Wolfschütz, H. Schwarz and K. Levsen, unpublished work quoted in References 183 and 184.
188. M. F. Jarrold, W. Wagner-Redeker, A. J. Illies, N. J. Kichner and M. T. Bowers, *Int. J. Mass Spectrom. Ion Processes*, **58**, 63 (1984).
189. J. Mattay, *Nachr. Chem. Tech. Lab.*, **36**, 376 (1988).
190. M. L. Gross, D. H. Russell, R. Phongbetchara and P.-H. Lin, *Adv. Mass Spectrom.*, **7A**, 129 (1978).
191. M. L. Gross, P.-H. Lin and S. J. Franklin, *Anal. Chem.*, **44**, 974 (1972).
192. R. van Doorn, N. M. M. Nibbering, A. J. V. Ferrer-Correia and K. R. Jennings, *Org. Mass Spectrom.*, **13**, 729 (1978).
193. G. S. Groenewold and M. L. Gross, *J. Am. Chem. Soc.*, **106**, 6575 (1984).
194. L. W. Castle and M. L. Gross, *Org. Mass Spectrom.*, **24**, 637 (1989).
195. E. K. Chess, P.-H. Lin and M. L. Gross, *J. Org. Chem.*, **48**, 1522 (1983).
196. G. S. Groenewold, E. K. Chess and M. L. Gross, *Org. Mass Spectrom.*, **19**, 519 (1984).
197. H.-F. Grützmacher and A. Barkow, *Acta Chem. Scand.*, **51**, 619 (1997).
198. D. Kuck, A. Bruder, D. V. Ramana, *Int. J. Mass Spectrom. Ion Processes*, **167/168**, 55 (1997).
199. A. Barkow, Doctoral Thesis, Bielefeld, 1997.
200. D. K. Bohme, A. B. Rakshit and H. I. Schiff, *Chem. Phys. Lett.*, **93**, 592 (1982).
201. D. C. Parent, *Int. J. Mass Spectrom. Ion Processes*, **138**, 307 (1994).
202. P. Španěl and D. Smith, *Int. J. Mass Spectrom.*, **181**, 1 (1998).
203. G. Podda, A. Sturaro and P. Traldi, *Org. Mass Spectrom.*, **21**, 723 (1986).

204. R. W. Holman, M. D. Rozeboom, M. L. Gross and C. D. Warner, *Tetrahedron*, **42**, 6235 (1986).
205. B. D. Nourse, K. A. Cox and R. G. Cooks, *Org. Mass Spectrom.*, **27**, 453 (1992).
206. C. Dass, *Org. Mass Spectrom.*, **28**, 940 (1993).
207. G. Bouchoux and F. Penaud-Berruyer, *Org. Mass Spectrom.*, **29**, 366 (1994).
208. G. Bouchoux and J.-Y. Salpin, *Rapid Commun. Mass Spectrom.*, **11**, 1001 (1997).
209. M. W. van Amsterdam, P. O. Staneke, S. Ingemann and N. M. M. Nibbering, *Org. Mass Spectrom.*, **28**, 919 (1993).
210. H. Becker, G. Javahery, S. Petrie and D. K. Bohme, *J. Phys. Chem.*, **98**, 5591 (1994).
211. S. Petrie, G. Javahery, J. Wang and D. K. Bohme, *J. Am. Chem. Soc.*, **114**, 9177 (1992).
212. S. Petrie, G. Javahery, J. Wang and D. K. Bohme, *J. Phys. Chem.*, **96**, 6121 (1992).
213. X. Guo, Z. Liu and S. Liu, *J. Mol. Struct. (Theochem)*, **340**, 169 (1995).
214. M. N. Eberlin, *Mass Spectrom. Rev.*, **16**, 113 (1997).
215. M. N. Eberlin, T. K. Majumdar and R. G. Cooks, *J. Am. Chem. Soc.*, **114**, 2884 (1992).
216. M. N. Eberlin and R. G. Cooks, *J. Am. Chem. Soc.*, **115**, 9226 (1993).
217. M. N. Eberlin, N. H. Morgan, S. S. Yang, B. J. Shay and R. G. Cooks, *J. Am. Soc. Mass Spectrom.*, **6**, 1 (1995).
218. L. Lu, S. S. Yang, Z. Wang, R. G. Cooks and M. N. Eberlin, *J. Mass Spectrom.*, **30**, 581 (1995).
219. M. Soni, J. Amy, V. Frankevich, R. G. Cooks, D. Taylor, A. Mckewan and J. C. Schwartz, *Rapid Commun. Mass Spectrom.*, **9**, 911 (1995).
220. C. Paradisi, H. Kenttämä, Q. T. Le and M. C. Caserio, *Org. Mass Spectrom.*, **23**, 521 (1988).
221. S. Gevrey, M.-H. Taghanel and J.-P. Morizur, *J. Mass Spectrom.*, **33**, 399 (1998).
222. P. Ausloos, J.-A. J. Jackson and S. G. Lias, *Int. J. Mass Spectrom. Ion Phys.*, **33**, 269 (1980).
223. J. H. Stewart, R. H. Shapiro, C. H. DePuy and V. M. Bierbaum, *J. Am. Chem. Soc.*, **99**, 7650 (1977).
224. V. M. Bierbaum, C. H. DePuy and R. H. Shapiro, *J. Am. Chem. Soc.*, **99**, 5800 (1977).
225. C. H. DePuy, V. M. Bierbaum, M. S. Robinson, G. E. Davico and R. Gareyev, *Tetrahedron*, **53**, 9847 (1997).
226. J. J. Grabowski, C. H. DePuy and V. M. Bierbaum, *J. Am. Chem. Soc.*, **105**, 2565 (1983).
227. R. R. Squires, V. M. Bierbaum, J. J. Grabowski and C. H. DePuy, *J. Am. Chem. Soc.*, **105**, 5185 (1983).
228. R. N. McDonald, A. K. Chowdbury and D. W. Setser, *J. Am. Chem. Soc.*, **102**, 4836 (1980).
229. R. N. McDonald and A. K. Chowdbury, *J. Am. Chem. Soc.*, **102**, 6146 (1980).
230. R. N. McDonald, A. K. Chowdbury and D. W. Setser, *J. Am. Chem. Soc.*, **103**, 7586 (1981).
231. R. N. McDonald, A. K. Chowdbury and D. W. Setser, *J. Am. Chem. Soc.*, **102**, 6491 (1980).
232. P. Vouros, in *Mass Spectrometry*, Part B (Eds. C. Merritt, Jr. and C. N. McEwen), Chap. 2, Marcel Dekker, New York, 1980, pp. 129–251.
233. B. Schmitz and R. A. Klein, *Chem. Phys. Lipids*, **39**, 285 (1986).
234. N. J. Jensen and M. L. Gross, *Mass Spectrom. Rev.*, **6**, 497 (1987).
235. R. J. Anderegg, *Mass Spectrom. Rev.*, **7**, 395 (1988).
236. W. G. Niehaus and R. Ryhage, *Anal. Chem.*, **40**, 1840 (1968).
237. For further examples, see:
(a) J. H. Tumlinson, R. R. Heath and R. E. Doolittle, *Anal. Chem.*, **46**, 1309 (1974).
(b) N. J. Jensen and M. L. Gross, *Mass Spectrom. Rev.*, **6**, 497 (1987).
238. N. C. Shantha and T. N. B. Kaimal, *Lipids*, **19**, 871 (1984).
239. G. Janssen and G. Parmentier, *Biomed. Mass Spectrom.*, **5**, 439 (1978).
240. B. Schmitz and H. Egge, *Chem. Phys. Lipids*, **25**, 287 (1979).
241. M. Vincenti, G. Guglielmetti, G. Cassani and C. Tonini, *Anal. Chem.*, **59**, 694 (1987).
242. D. A. Carlson, C.-S. Roan, R. A. Yost and J. Hector, *Anal. Chem.*, **61**, 1564 (1989).
243. (a) C. Pepe, P. Dizabo, J. Dagaut, N. Balcar and M. F. Lautier, *Eur. Mass Spectrom.*, **1**, 209 (1995).
(b) C. Pepe, H. Sayer, J. Dagaut and R. Couffignal, *Rapid Commun. Mass Spectrom.*, **11**, 919 (1997).
(c) C. Pepe, H. Sayer and J. Dagaut, *Rapid Commun. Mass Spectrom.*, **12**, 565 (1998).
244. D. C. Young, P. Vouros, B. Decosta and M. F. Holick, *Anal. Chem.*, **59**, 1954 (1987).
245. L. R. Hogge, E. W. Underhill and J. W. Wong, *J. Chromatogr. Sci.*, **23**, 171 (1985).
246. W. Vetter, W. Meister and G. Oesterheld, *J. Mass Spectrom.*, **33**, 461 (1998).

247. J. Adams, *Mass Spectrom. Rev.*, **9**, 141 (1990).
248. (a) A. J. V. Ferrer-Correia, K. R. Jennings and D. K. Sen Sharma, *J. Chem. Soc., Chem. Commun.*, 973 (1975).
(b) A. J. V. Ferrer-Correia, K. R. Jennings and D. K. Sen Sharma, *Org. Mass Spectrom.*, **11**, 867 (1976).
(c) A. J. V. Ferrer-Correia, K. R. Jennings and D. K. Sen Sharma, *Adv. Mass Spectrom.*, **7A**, 287 (1977).
249. F. Hunt and T. M. Harvey, *Anal. Chem.*, **47**, 2136 (1975).
250. D. F. Hunt, C. N. McEwen and T. M. Harvey, *Anal. Chem.*, **47**, 1730 (1975).
251. (a) H. Budzikiewicz, *Fresenius Z. Anal. Chem.*, **321**, 150 (1985).
(b) H. Budzikiewicz, in *Analytiker-Taschenbuch* (Eds. W. Fresenius, H. Günzler, W. Huber, I. Lüderwald, G. Tölg and H. Wisser) Vol. 5, Springer, Berlin, 1985, pp. 135ff.
(c) H. Budzikiewicz, *Spectrosc. Int.*, **5**, 183 (1987).
(d) H. Budzikiewicz, in *Studies in Natural Products Chemistry*, Vol. 2 (Ed. Atta-ur-Rahman), Elsevier, Amsterdam, 1988, pp. 3–18.
252. A. G. Harrison, *Chemical Ionization Mass Spectrometry*, 2nd edn., Chap. 5, CRC Press, Boca Raton, FL, 1992, pp. 113–120.
253. M. Vairamani, U. A. Mirza and R. Srinivas, *Mass Spectrom. Rev.*, **9**, 235 (1990).
254. M. Vairamani, *Org. Mass Spectrom.*, **25**, 271 (1990).
255. J. Einhorn, H. I. Kenttämää and R. G. Cooks, *J. Am. Soc. Mass Spectrom.*, **2**, 305 (1991).
256. (a) D. A. Peake, S.-K. Huang and M. L. Gross, *Anal. Chem.*, **59**, 1557 (1987).
(b) M. L. Gross, *Adv. Mass Spectrom.*, **11A**, 792 (1989).
257. R. E. Doolittle, J. H. Tumlinson and A. Proveaux, *Anal. Chem.*, **57**, 1625 (1985).
258. J. Einhorn, H. Virelizier, A. L. Gemal and J.-C. Tabet, *Tetrahedron Lett.*, **26**, 1445 (1985).
259. J. Einhorn, H. Virelizier, A. Guerrero and J.-C. Tabet, *Biomed. Mass Spectrom.*, **12**, 200 (1985).
260. D. A. Peake, S.-K. Hunang and M. L. Gross, *Anal. Chem.*, **57**, 115 (1985).
261. D. A. Peake, S.-K. Hunang and M. L. Gross, *Anal. Chem.*, **59**, 1557 (1987).
262. A. J. Canty and R. Colton, *Inorg. Chim. Acta*, **220**, 99 (1994).
263. T. Keough, *Anal. Chem.*, **54**, 2540 (1982).
264. (a) C. Lange, *Org. Mass Spectrom.*, **28**, 1285 (1993).
(b) C. Lange, *Org. Mass Spectrom.*, **22**, 55 (1987).
265. M. Vairamani, K. V. Siva Kumar and G. K. Viswanadha Roa, *Org. Mass Spectrom.*, **25**, 363 (1990).
266. H. Budzikiewicz, S. Blech and B. Schneider, *Org. Mass Spectrom.*, **26**, 1057 (1991).
267. D. Kuck, in *Proceedings of the 8th ISMAS Symposium on Mass Spectrometry*, Vol. I (Ed. S. K. Aggarwal) Indian Society for Mass Spectrometry (ISMS), Mumbai, 1999, pp. 245–260.
268. R. Kaufmann, T. Wingerath, D. Kirsch, W. Stahl and H. Sies, *Anal. Biochem.*, **238**, 117 (1996).
269. K. Aitzetmüller, H. H. Strain, W. A. Svec, M. Gandolfi and J. J. Katz, *Phytochemistry*, **8**, 1761 (1969).
270. J. Carnevale, E. R. Cole, D. Nelson and J. S. Shannon, *Biomed. Mass Spectrom.*, **5**, 641 (1978).
271. M. T. Fernandez, C. Williams, R. S. Mason and B. J. C. Cabral, *J. Chem. Soc., Faraday Trans.*, **94**, 1427 (1998).
272. C. Basic and A. G. Harrison, *Can. J. Chem.*, **36**, 33 (1991).
273. J. J. Brophy and A. Maccoll, *Org. Mass Spectrom.*, **27**, 1042 (1992).
274. H. Schwarz, F. Borchers and K. Levsen, *Z. Naturforsch. B*, **31**, 935 (1976).
275. L. Friedman and A. P. Wolf, *J. Am. Chem. Soc.*, **80**, 2424 (1958).
276. M. Mormann and D. Kuck, to be published.
277. B. C. L. Weedon, *Fortschr. Chem. Org. Naturst.*, **27**, 81 (1969).
278. W. Vetter, G. Englert, N. Rigassi and U. Schwieter, in *Carotenoids* (Eds. O. Isler, H. Gutmann and U. Solms), Chap. 4, Birkhäuser Verlag, Stuttgart, 1971, pp. 189–266.
279. C. R. Enzell, R. A. Appleton and I. Wahlberg, in *Biochemical Applications of Mass Spectrometry* (Ed. G. R. Waller), Chap. 13, Wiley-Interscience, New York, 1972, pp. 315–385.
280. W. H. Elliott and G. R. Waller, in *Biochemical Applications of Mass Spectrometry* (Ed. G. R. Waller), Chap. 18, Wiley-Interscience, New York, 1972, pp. 499–536.
281. H. Budzikiewicz, *Adv. Mass Spectrom.*, **6**, 163 (1974).

282. C. R. Enzell and I. Wahlberg, in *Biochemical Applications of Mass Spectrometry*, 1st Suppl. Vol. (Eds. G. R. Waller and O. C. Dermer), Chap. 13A, Wiley, New York, 1980, pp. 311–405.
283. C. R. Enzell and I. Wahlberg, in *Biochemical Applications of Mass Spectrometry*, 1st Suppl. Vol. (Eds. G. R. Waller and O. C. Dermer), Chap. 13B, Wiley, New York, 1980, pp. 407–438.
284. C. R. Enzell, I. Wahlberg and R. Ryhage, *Mass Spectrom. Rev.*, **3**, 395 (1984).
285. C. R. Enzell, O. Dahlman and J. Bielawski, in *Applications of Mass Spectrometry to Organic Stereochemistry* (Ed. J. S. Splitter), Chap. 18, VCH, New York, 1994, pp. 509–542.
286. D. Joulain and W. A. König, *The Atlas of Spectral Data of Sesquiterpene Hydrocarbons*, E. B. Verlag, Hamburg, 1998.
287. C. R. Enzell and S. Back, in *Carotenoids*, Vol. 1B: Spectroscopy (Eds. G. Britton, S. Liaanen-Jensen and H. Pfander), Chap. 7, Birkhäuser Verlag, Basel, 1995, pp. 261–320.
288. T. Wingerath, D. Kirsch, R. Kaufmann, W. Stahl and H. Sies, *Meth. Enzymol.*, **299**, 390 (1999).
289. T. D. McClure and D. C. Liebler, *J. Mass Spectrom.*, **30**, 1480 (1995).
290. G. Tang, B. A. Andrien, G. D. Dolnikowski and R. M. Russell, *Meth. Enzymol.*, **282**, 140 (1997).
291. G. Tang, J. Qin and G. G. Dolnikowski, *J. Nutr. Biochem.*, **9**, 408 (1998).
292. M. Careri, P. Lombardi, C. Mucchino and E. Cantoni, *Rapid Commun. Mass Spectrom.*, **13**, 118 (1999).
293. (a) H. H. Schmitz, R. B. van Breemen and S. J. Schwartz, *Meth. Enzymol.*, **213**, 322 (1992).
(b) R. B. Van Breemen, H. H. Schmitz and S. J. Schwartz, *Anal. Chem.*, **65**, 695 (1993).
294. G. J. Van Berkel, K. G. Asano and S. A. McLuckey, *J. Am. Soc. Mass Spectrom.*, **5**, 689 (1994).
295. (a) R. B. van Breemen, D. Nikolic, X. Xu, J. Xiong, M. van Lieshout, C. E. West and A. B. Schilling, *J. Chromatogr. A*, **794**, 245 (1998).
(b) T. Hagiwara, T. Yasumo, K. Funayama and S. Suzuki, *J. Chromatogr. B*, **708**, 67 (1998).
296. (a) C. D. Watts, J. R. Maxwell, D. E. Games and M. Rossiter, *Org. Mass Spectrom.*, **10**, 1102 (1975).
(b) S. Takaichi, *Org. Mass Spectrom.*, **28**, 785 (1993).
297. E. R. Hilf, W. Tuszynski, B. Curdes, J. Curdes, M. Wagner and K. Wien, *Int. J. Mass Spectrom. Ion Processes*, **126**, 101 (1993).
298. A. Mele and A. Selva, *Eur. Mass Spectrom.*, **3**, 161 (1997).
299. A. Selva, F. Cardini and M. Chelli, *Org. Mass Spectrom.*, **29**, 695 (1994).
300. A. Selva and F. Cardini, *Org. Mass Spectrom.*, **28**, 570 (1993).
301. A. Mele, W. Panzeri, A. Selva and E. Canu, *Eur. Mass Spectrom.*, **5**, 7 (1999).
302. A. Selva, A. Mele and G. Vago, *Eur. Mass Spectrom.*, **1**, 215 (1995).

CHAPTER 2

NMR spectroscopy of dienes and polyenes

YOSHITO TAKEUCHI

Department of Chemistry, Faculty of Science, Kanagawa University, 2946 Tsuchiya, Hiratsuka, Japan 259-1293

e-mail: yoshito@chem.kanagawa-u.ac.jp

and

TOSHIO TAKAYAMA

Department of Applied Chemistry, Faculty of Engineering, Kanagawa University, 3-27-1 Rokkakubashi, Yokohama, Japan 221-8686

e-mail: takayt1@kanagawa-u.ac.jp

I. INTRODUCTION	60
A. Scope and Limitation	60
B. Chemical Shifts and Coupling Constants	60
II. THEORY OF NMR CHEMICAL SHIFTS OF POLYENES	65
III. RECENT APPLICATIONS	72
A. Solution NMR	72
1. Linear conjugated dienes	72
2. Polymers containing polyenes	86
3. Antibiotic polyenes	89
4. Metal bound polyenes	133
B. Solid State NMR	140
1. ¹³ C CP/MAS NMR	140
2. ² H static NMR	156
IV. SPECIAL TOPICS	165
A. Allenes	165
B. Solitons	182
C. Fullerenes	186
V. REFERENCES	194

I. INTRODUCTION

A. Scope and Limitation

From the advent of organic chemistry, dienes (and polyenes) have played a very important role in both the theoretical and synthetic aspects. For example, 1,4-addition of bromine to 1,3-butadiene to form 1,4-dibromo-2-butene rather than 3,4-dibromo-1-butene as the major product was a challenging problem for theoretical chemists, who interpreted the phenomenon in terms of resonance or delocalization of π -electrons¹.

Later, the structural chemists determined the structure of 1,3-butadiene (the bond lengths C1–C2 and C2–C3 are 1.467 and 1.349 Å, respectively, which can be compared with the corresponding values of *trans*-2-butene (1.508 and 1.347 Å), respectively). Another significant aspect of dienes is the Diels–Alder reaction, the reaction between a diene and an olefin with electron-withdrawing substituents to give a six-membered ring². The reaction is designated as 4 + 2 cycloaddition since the diene has four carbon atoms while the olefin, a dienophile, may represent a two-carbon unit. The mechanism of this useful reaction was not clear until 1964, when Woodward and Hoffmann proposed the so-called Woodward–Hoffmann rule³. This proposal has opened a wide world of electrocyclic reactions in which the symmetry of orbitals plays an important role.

NMR spectroscopy has been extensively used in diene chemistry not only for conventional structural analysis but also in dealing with theoretical problems. Among a variety of examples in which NMR spectroscopy played an important role in the latter application, is the unusually large high- and low-field shifts observed for inner protons of cyclic conjugated polyenes (annulenes). Thus, the high-field shifts for $[4n + 2]$ annulenes and corresponding low-field shifts for $[4n]$ annulenes were interpreted as the indication of aromaticity and antiaromaticity, respectively, of these compounds⁴.

Previously, the NMR spectroscopic data for dienes and polyenes were treated as a part of a chapter on alkenes⁵, and have not been treated as an independent topic. In view of the important role which dienes and polyenes have generally played in chemistry, the authors believe that the topic can, and should, be treated in an independent chapter.

In this review, chemical shifts and coupling constants of simple dienes will first be summarized, and the theory of chemical shift for dienes and polyenes will then be reviewed. Finally, the recent applications of NMR spectroscopy to a variety of polyenes and dienes and specific systems (allenes, solitons and fullerenes) will be reviewed.

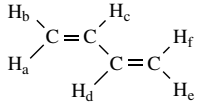
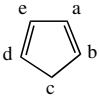
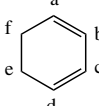
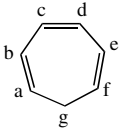
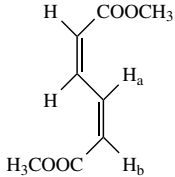

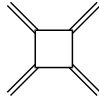
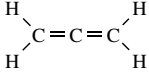
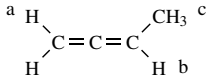
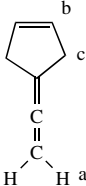
Although we have tried to cover the literature on standard data as much as possible, our emphasis have been focused on new developments of application of NMR spectroscopy to dienes and polyenes. Readers who seek more basic data rather than recent advances are advised to consult books and journal articles dealing with this topic.

B. Chemical Shifts and Coupling Constants

It would be convenient for the readers if a limited amount of selected data are summarized at the beginning of this chapter so that they can have some general idea on the chemical shifts and coupling constants observed for dienes and polyenes.

i. Protons bonded to conjugated carbon atoms. Collections of data on chemical shifts in linear dienes, cyclic dienes and exocyclic multi-methylene systems are given in Table 1 together with references to selected compounds. The characteristic values of the geminal and allylic coupling constants and chemical shifts assembled in Table 1 make these signals very informative. The chemical shifts of some allenic protons are also included in Table 1⁶.

TABLE 1. ^1H chemical shifts and coupling constants of linear and cyclic dienes, exocyclic methylenes and allenes

Compound	^1H chemical shift (ppm)	Coupling constant (Hz)	Reference
	(a,f) 5.16 (b,e) 5.06 (c,d) 6.27	$J_{ab} = 1.8, J_{bc} = 10.2, J_{ac} = 17.1,$ $J_{ad} = -0.8, J_{be} = 1.3, J_{ae} = 0.6,$ $J_{af} = 0.7, J_{bd} = -0.9, J_{ed} = 10.4$	6a
	(a,e) 6.5 (b,d) 6.4 (c) 2.90	$J_{ab} = 5.1, J_{bc} = 1.2, J_{ac} = -1.3,$ $J_{ad} = 1.1, J_{ae} = 1.9, J_{bd} = 1.9$	6a
	(a,d) 5.8 (b,c) 5.9 (e,f) 2.15	$J_{ab} = 9.4, J_{bc} = 5.1, J_{ac} = 1.1,$ $J_{ad} = 0.9$	6a
	(a,f) 5.26 (b,e) 6.09 (c,d) 6.50 (g) 2.22	$J_{ab} = 8.9, J_{bc} = 5.5, J_{bd} = 0.8,$ $J_{be} = -0.6, J_{ac} = 0.6, J_{af} = 0, J_{ed} = 11.2,$ $J_{gg} = -13.0, J_{ag} = 6.7, J_{ac} + J_{ad} = 1.5$	6a
	(a) 7.87 (b) 5.94		6b
	5.02		6b
	5.19		6b
	4.67		6b
	(a) 4.50 (b) 4.94 (c) 1.59		6b
	(a) 4.60 (b) 5.52 (c) 3.13		6b

The chemical shifts of exocyclic methylene protons are very close to the calculated value of 4.65 ppm for four-, five- and six-membered rings; not surprisingly the three-membered ring proves to be exceptional. There are also some differences in the effect exerted by carbonyl substitution in rings of different size and in the chemical shifts of radialenes.

In the case of 1,3-butadiene, the chemical shifts of inner (H2, H3) protons and outer (H1, H4) is large, while in the case of cycloalkadienes (e.g. 1,3-cyclopentadiene and 1,3-cyclohexadiene), the difference is very small. It is interesting to note that in 1,3,5-cycloheptatriene, the chemical shifts of three kinds of olefinic protons are very diverse. The effect of the ring size and in the chemical shifts of radialenes was also included.

ii. Carbon atoms of linear and branched conjugated dienes. The ^{13}C chemical shifts of simple linear and branched dienes are collected in Table 2⁷. The ^{13}C chemical shifts of conjugated dienes such as 1,3-butadiene or 1,3,5-hexatriene are not significantly different from those in the monoenes.

iii. Unsubstituted cyclopolyenes. The chemical shifts of simple unsubstituted cyclopolyenes are listed in Table 3⁷.

In the spirodiene **3** and tetraene **4** the spiroconjugated carbon nuclei are shifted downfield on going from **3** to **4**, an effect which is due to the interaction between the two π -systems.

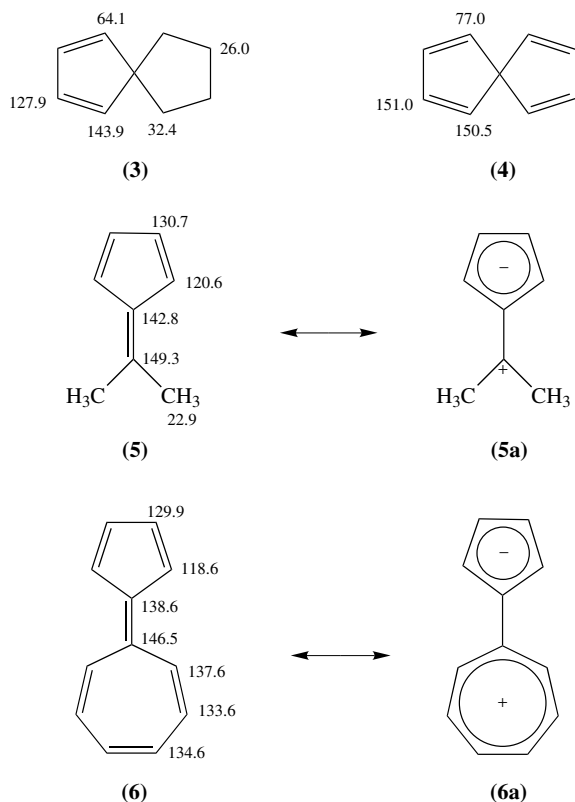


TABLE 2. ^{13}C chemical shifts for linear and branched dienes⁷

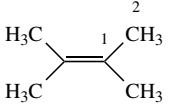
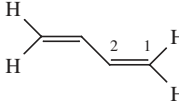
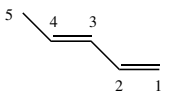
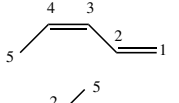
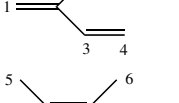
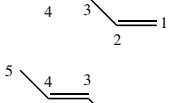
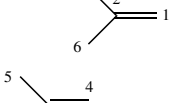
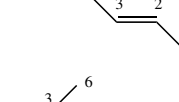
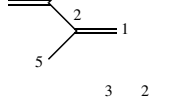
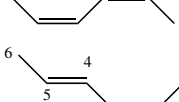
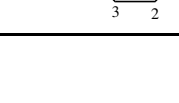
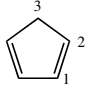
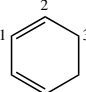
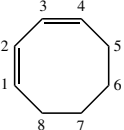
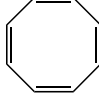
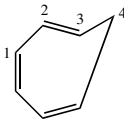
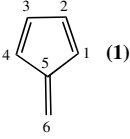
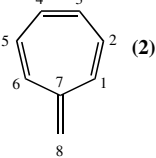
Compound	δ_c (ppm)					
	C1	C2	C3	C4	C5	C6
	123.5	20.4				
	116.6	137.2				
	114.4	137.8	129.5	133.2	17.2	
	116.5	132.5	130.9	126.4	12.8	
	113.0	142.9	140.3	116.4	17.6	
	110.3	142.1	135.5	127.1	11.1	13.6
	114.5	142.2	135.5	125.1	18.8	18.3
	17.5	126.2	132.5			
	113.0	143.8			20.3	
	12.9	124.9	125.3			
	13.0	123.1	127.4	130.2	128.3	18.0

TABLE 3. ^{13}C chemical shifts for unsubstituted cyclopolyenes

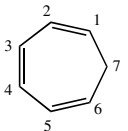
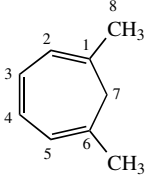
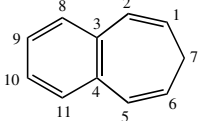
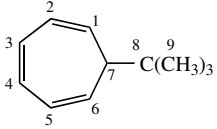
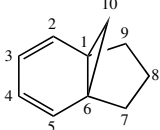
Compound	C1	C2	C3	C4	C5	C6	C7	C8
	132.2	132.8	41.6					
	126.1	124.6	22.3					
	126.5	132.1			23.4	28.5		
	131.5							
	131.0	126.8	120.4	28.1				
	124.9	134.3			152.6	123.4		
	138.3	126.8 ^a	130.8 ^a				146.6	111.9

^aAssignment uncertain.

The ^{13}C NMR data for pentafulvene (**1**) and heptafulvene (**2**) (Table 3) and for 6,6-dimethylpentafulvene (**5**) and sesquifulvalene (**6**), afford evidence of the extent to which polar structures of the types **5a** and **6a** contribute to the ground state. If the chemical shifts are analyzed on the basis of electron density, these hydrocarbons are to be considered as olefinic systems with only a small contribution (10% at most) from the polar structures **5a** and **6a**.

iv. Cyclic conjugated polyenes. Table 4⁸ gives the ^{13}C chemical shifts for cycloheptatriene and related compounds. The internal olefinic carbons C3 and C4 of the triene

TABLE 4. ^{13}C chemical shifts of cycloheptatriene and norcadiene compounds

	C1	C2	C3	C7	C8	C9	C10
	120.4	126.8	131.0	28.1			
	130.6	122.2	128.8	40.1	24.6		
	125.9	127.7	137.2	26.6	130.3	130.8	
	123.0	124.6	130.8	49.4	31.1	27.3	
	37.7	129.0	119.2	32.3	15.7		19.7

system are the most deshielded in cycloheptatriene. Methyl substitution at C1 deshields C1 and C7 and shields C2 and C3.

v. *Allenes*. Allenes form a unique class of compounds because of the extremely low field shift of the central allenic carbon C2 (200 to 220 ppm). Table 5⁸ presents representative data for a number of substituted allenes. For a given alkyl substituent, there is a linear relationship between the number of substituents and the chemical shift of the central carbon. The shielding is regarded as an additive property, a methyl group shields that carbon by 3.3 ppm, an ethyl group by 4.8 ppm and a *sec*-alkyl group by 7 ppm. Carbons C1 and C3 are shielded by some 30 ppm relative to corresponding ethylene carbons but otherwise display similar substituent effects. Strain in cyclic allenes appears to have little effect.

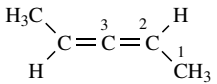
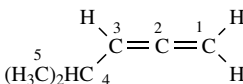
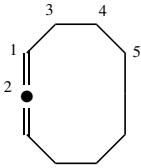
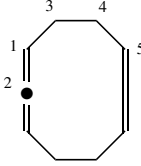
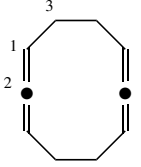
II. THEORY OF NMR CHEMICAL SHIFTS OF POLYENES

Recently, *ab initio* shielding calculations based on well-established theories, IGLO (individual gauge for localized orbitals)⁹, GIAO (gauge including atomic orbital)¹⁰ and LORG

TABLE 5. ^{13}C chemical shift of allenes

$$\begin{array}{c} \text{R}^1 \\ \diagdown \\ \text{C}^1 = \text{C}^2 = \text{C}^3 \\ \diagup \\ \text{R}^2 \end{array} \begin{array}{c} \text{R}^3 \\ \diagup \\ \text{C}^3 \\ \diagdown \\ \text{R}^4 \end{array}$$

R ¹	R ²	R ³	R ⁴	C1	C2	C3
H ^a	H ^a	H ^a	H ^a	74.8	213.5	74.8
Me	H	H	H	84.4	210.4	74.1
Me	Me	H	H	93.4	207.3	72.1
Me	H	Me	H	85.4	207.1	85.4
Me	Me	Me	Me	92.6	200.2	92.6
Me	SMe	H	H	99.9	203.6	80.1
Ph	Ph	Ph	Ph	113.6	209.5	113.6
OMe	H	H	H	123.1	202.0	90.3
Br	H	H	H	72.7	207.6	83.8
CN	H	H	H	80.5	218.7	67.2

Compound	C1	C2	C3	C4	C5
	14.6	84.5	206.5		
	76.2	207.8	97.8	27.9	22.9
	92.7	206.5	27.9	25.8 ^b	27.2 ^b
	90.4	206.7	27.4 ^b	29.2 ^b	130.4
	90.2	208.3	26.8		

^a $^{13}\text{C}-^1\text{H}$ coupling (in hertz) in allene: $^1J(\text{C}-\text{H})$ [167.8], $^2J(\text{C}-\text{H})$ [3.9], $^3J(\text{C}-\text{H})$ [7.7].

^bAssignments uncertain.

(localized orbital/local origin) methods¹¹ have been widely used not only to assist signal assignments but also to elucidate the electronic structure and conformation of molecules. The use of high-quality basis sets in these types of shielding calculations leads to reasonable results which are within the experimental accuracy.

Inoue and coworkers¹² reported an *ab initio* calculation of the ¹³C shieldings for some polyenals and their Schiff bases using the LORG method. They reported the results for some polyenes with basis sets of various quality. It was shown that the introduction of polarization functions substantially improves agreement between experiment and theory. They used the program RPAC9.0, which was developed by Bouman and Hansen¹³ for *ab initio* shielding calculations, interfacing to the Gaussian-90 program¹⁴. The geometrical parameters of all the molecules studied were optimized by using 6-31G basis sets and planar frameworks were then assumed for the backbone. The basis sets they used for shielding calculations were the Pople type 6-31G, 6-31+G, 6-31++G, 6-31G*, 6-31G**, 6-311G* and 6-311G**¹⁵.

In the LORG theory, occupied orbitals are localized according to the Foster–Boys criterion¹⁶. In the calculations described above they chose the LORG centroid assignment^{11a}.

Table 6 gives the calculated and experimental ¹³C shieldings for acrolein, crotonaldehyde and hexa-2,4-dienal. The numbering of the carbon atoms is given in Figure 1. The calculated and experimental ¹³C chemical shift data were converted to the methane reference using the data in Table 7 and in the standard reference¹⁷, respectively.

The author examined the correlation between the calculated and experimental isotropic shieldings. The 6-31G shielding data are in qualitative agreement with the experimental data and completely reproduce the relative order of all the carbon shieldings studied. The 6-31G shieldings for the carbonyl carbons shift are about 20 ppm downfield of the experimental values. If the experimental data are converted to the methane reference using the data reported by Jameson and Jameson¹⁸, this discrepancy still remains large (about 16 ppm).

The RMS error for the 6-31G data is relatively large (9.8 ppm). The origin of this error has been considered to be attributable to electron correlation effects, which were not included in the calculations. The results for the carbonyl shieldings could be improved by using *d*-type polarization functions on carbon and oxygen atoms. The results using 6-31G* and 6-31G** basis sets exhibited a good reproducibility for all the carbons including the carbonyl carbons. The RMS errors for the 6-31G* and 6-31G** results are 3.7 and 3.8 ppm, respectively.

As shown in Table 6, the addition of *p*-type polarization functions to hydrogen atoms in the 6-31G** basis has little effect on the calculated data.

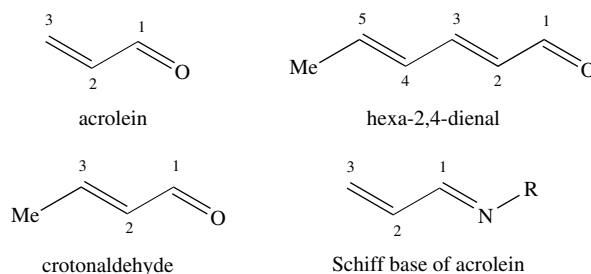


FIGURE 1. Numbering system of carbon atoms for the compounds in Table 6

TABLE 6. Comparison of calculated and experimental ^{13}C chemical shifts for acrolein, crotonaldehyde and hexa-2,4-dienal

Compound	Carbon ^d	Element	6-31G	6-31+G	6-31++G	6-31G*	6-31G**	6-311G*	6-311G**	6-311G**	Exp. ^b
Acrolein	C1	σ_{iso}	212.0	213.6	211.9	196.0	194.7	197.2	196.9	193.2	
		σ_{11}	75.8	75.0	73.4	91.6	89.5	87.5	85.8		
		σ_{22}	196.4	212.4	210.8	197.1	197.5	194.9	197.8		
	C2	σ_{33}	353.7	353.5	351.5	299.4	297.1	309.3	306.9		
		σ_{anis}	217.6	209.8	209.4	155.0	153.6	168.1	165.1		
		σ_{iso}	143.7	149.8	148.0	135.6	135.2	141.5	141.5		141.7
	C3	σ_{11}	29.0	36.9	34.9	34.6	33.1	39.4	36.5		
		σ_{22}	126.5	133.4	131.7	118.6	118.0	123.3	124.1		
		σ_{33}	275.7	279.2	277.4	253.8	254.6	261.7	263.8		
		σ_{anis}	197.9	194.0	194.0	177.2	179.0	180.3	183.5		
		σ_{iso}	141.3	143.1	141.5	137.6	136.9	140.4	141.5		136.2
		σ_{11}	8.7	11.7	10.4	12.1	11.5	13.9	11.9		
		σ_{22}	134.7	135.7	134.5	130.9	130.0	130.8	133.9		
Crotonaldehyde	C1	σ_{33}	280.5	281.6	279.7	269.7	269.1	276.5	278.6		
		σ_{anis}	208.8	207.8	207.2	198.2	198.4	204.2	205.7		
		σ_{iso}	211.3	212.7	211.0	195.5	194.3	196.8	196.6		192.1
	C2	σ_{11}	76.1	75.2	73.6	91.9	89.7	87.9	86.0		
		σ_{22}	206.7	212.6	211.1	196.6	197.1	194.7	198.1		
		σ_{33}	351.0	350.2	348.4	297.9	295.9	307.8	305.7		
	C3	σ_{anis}	209.6	206.2	206.0	153.6	152.4	166.5	163.7		
		σ_{iso}	140.9	146.5	144.9	133.4	132.6	138.7	137.9		137.8
		σ_{11}	38.9	47.1	45.5	43.2	42.0	47.5	44.9		
		σ_{22}	119.6	126.9	125.4	111.2	110.4	116.1	116.3		
		σ_{33}	264.1	265.5	263.9	245.8	245.4	252.4	252.4		
		σ_{anis}	184.8	178.5	178.5	168.6	169.2	170.6	171.8		
		σ_{iso}	153.3	156.5	154.9	151.4	150.8	158.6	157.9		151.9
Me	σ_{11}	12.1	15.5	14.1	18.2	17.2	23.3	20.1			
	σ_{22}	157.8	162.1	160.7	153.8	153.4	159.4	159.9			
	σ_{33}	290.0	292.0	290.1	282.1	281.8	293.2	293.6			
	σ_{anis}	205.1	203.1	202.7	196.0	196.5	201.9	203.6		19.9	
	σ_{iso}	15.0	16.8	16.0	14.5	14.3	16.7	16.1			
σ_{11}	-5.4	-6.0	-5.6	-5.6	-4.7	-0.4	-1.2				
σ_{22}	23.3	27.0	25.8	22.4	21.5	20.9	20.7				

Hexa-2,4-dienal		σ_{33}	27.0	29.3	28.0	26.8	26.2	29.6	28.9
C1	σ_{anis}	18.1	18.8	17.9	18.4	17.8	19.3	19.2	19.2
	σ_{iso}	211.7	213.0	211.4	195.8	194.6	197.2	197.0	192.5
	σ_{11}	75.4	74.6	73.0	91.2	89.0	86.9	85.0	85.0
	σ_{22}	207.7	213.5	211.9	196.9	197.6	195.3	198.9	198.9
	σ_{33}	352.0	351.0	349.2	299.2	297.2	309.3	307.2	307.2
	σ_{anis}	210.5	207.0	206.7	155.2	153.9	168.2	198.9	198.9
	σ_{iso}	136.1	140.5	138.9	129.1	128.5	132.1	131.3	132.9
	σ_{11}	39.1	46.6	45.2	43.8	42.5	47.2	44.3	44.3
	σ_{22}	123.7	129.5	127.9	114.5	113.7	117.4	117.7	117.7
	σ_{33}	245.6	245.3	243.5	229.1	228.6	231.7	231.9	231.9
C3	σ_{anis}	164.1	157.3	157.0	150.0	150.5	139.4	150.8	150.8
	σ_{iso}	156.2	159.8	158.2	153.6	152.7	158.9	158.3	151.8
	σ_{11}	33.1	37.3	35.7	36.5	35.2	37.4	34.4	34.4
	σ_{22}	155.3	159.9	158.4	150.3	149.7	156.0	156.9	156.9
	σ_{33}	280.1	282.2	280.5	273.9	273.3	283.4	283.5	283.5
	σ_{anis}	185.8	183.6	183.4	180.5	180.8	186.7	187.8	187.8
	σ_{iso}	137.9	141.2	139.6	131.7	130.7	136.7	135.6	133.3
	σ_{11}	34.9	39.5	38.0	38.1	36.9	40.4	37.5	37.5
	σ_{22}	114.4	118.4	116.9	108.9	107.9	113.0	113.0	113.0
	σ_{33}	264.4	265.6	263.9	247.9	247.4	256.8	256.4	256.4
C5	σ_{anis}	189.7	186.7	186.5	174.4	175.0	180.1	181.1	181.1
	σ_{iso}	145.2	147.8	146.3	140.5	140.0	146.8	145.9	142.2
	σ_{11}	20.5	23.9	22.7	27.1	26.1	32.9	29.7	29.7
	σ_{22}	139.7	142.2	140.8	134.5	134.0	138.3	138.6	138.6
	σ_{33}	275.4	277.3	275.3	260.0	259.9	269.3	269.5	269.5
	σ_{anis}	195.3	194.3	193.6	179.2	179.9	183.7	185.4	185.4
	σ_{iso}	15.1	17.1	16.3	14.4	14.2	16.7	16.1	20.4
	σ_{11}	-6.1	-6.5	-6.5	-6.3	-5.5	-1.2	-2.1	-2.1
	σ_{22}	24.6	28.5	27.2	23.5	22.8	22.3	22.0	22.0
	σ_{33}	27.0	29.3	28.1	26.0	25.4	29.0	28.4	28.4
Me	σ_{anis}	17.8	18.3	17.8	17.4	16.7	-18.5	18.4	18.4
	σ_{iso}	9.8	11.5	10.2	3.7	3.8	4.2	4.1	4.1
	RMS error ^c								

^aFor numbering of atoms, see Figure 1.

^bTaken from Reference 18.

^cRMS: Root mean square.

TABLE 7. ^{13}C shielding of methane (ppm)

Calc. ^a	
6-31G//6-31G	222.1
6-31+G//6-31G	224.5
6-31++G//6-31G	222.9
6-31G*//6-31G	213.5
6-31G**//6-31G	210.8
6-311G*//6-31G	202.5
6-311G**//6-31G	198.4
Exp. ^b	-2.1 ^c
	-7.0 ^d

^a Absolute value.^b Relative to tetramethylsilane.^c Taken from Reference 17.^d Taken from Reference 18.

By applying polarization functions, *ab initio* shielding calculations for some polyenals and their Schiff bases reproduce the experimental values well even on the carbonyl and the imine carbons using the LORG theory without including correlation effects. In addition, there is a trend that the calculation with polarization functions yields smaller anisotropies of chemical shieldings than those without polarization functions.

Recently Inoue and coworkers¹⁹ also reported *ab initio* study of ^{13}C shieldings for linear π -conjugated systems. A photoreceptive protein such as rhodopsin (Rh) or bacteriorhodopsin (bR) possesses a retinal isomer bound to a lysine residue via the protonated Schiff base linkage. Rh exists in the rod cell of the retina of vertebrate and possesses 11-*cis*-retinal (Figure 2), which is isomerized into the all-*trans* form by the absorption of photons, finally leading to signal transduction.

On the other hand, bR, which exists in the purple membrane (PM) of *Halobacterium halobium*, functions as a light-driven proton pump through a photocycle including the conversion of all-*trans* retinal into the 13-*cis* isomer. In both pigments, the conformation of retinal closely relates to the biological function, especially to the regulation of their absorption maxima. For example, in bR₅₆₈, the C6–C7 bond is likely to be planar *s-trans*, which essentially contributes to the fact that this pigment absorbs yellow-green light. The observation of ^{13}C NMR chemical shifts for the chromophore provides a good insight not only into its conformation but also into the interaction of the chromophore with the surrounding protein matrix. The solid-state NMR technique has been applied to Rh, bR and their photo-intermediates. Consequently, it was revealed that the chemical shifts for the chromophore are significantly different from those for the free protonated retinal Schiff base. As for bR, the chemical shifts of C5 and C8 are displaced significantly downfield and upfield, respectively, relative to those of model compounds.

Figure 2 shows the 10 diene derivatives examined in the work: (*E,E*)-2,4-hexadiene (HEX), (*E,E*)-3-methyl-2,4-hexadiene (3MET), (*E,Z*)-2,4-hexadiene (1CIS), (*E,Z*)-3-methyl-2,4-hexadiene (1C3M), (*E*)-2-methyl-2,4-hexadiene (4MET), (*E*)-2,3-dimethyl-2,4-hexadiene (34DME), (*E,E*)-3-*tert*-butyl-2,4-hexadiene (3TBU), (*E*)-2-methyl-3-*tert*-butyl-2,4-hexadiene (3TB4M), (*E,E*)-2,4-hexadienal (HEXAL) and (*E,Z*)-3-methyl-2,4-hexadienal (1C3MAL). These compounds are selected as minimal analogues of partial structures of 11-*cis*-retinal. The numbering of the carbon atoms and the abbreviations (in parentheses) of these dienes are not the IUPAC numbering, but given in order to easily compare the chemical shifts of corresponding carbons between different compounds.

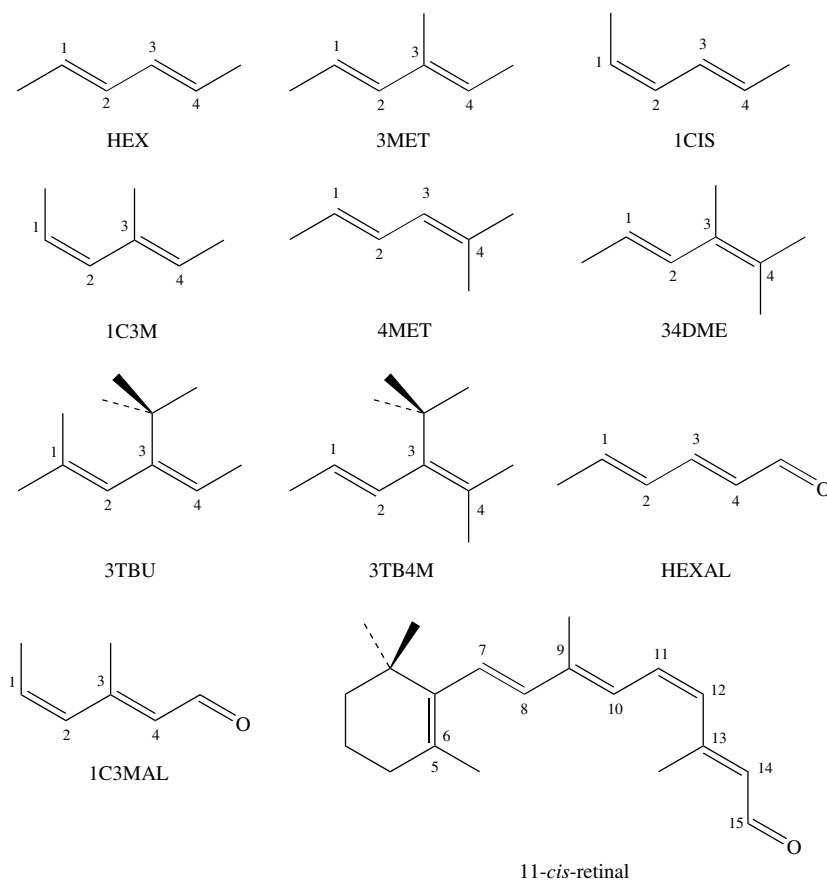


FIGURE 2. Molecular structures of the linear π -conjugated compounds studied

The *ab initio* shielding calculations are carried out in order to investigate the conformation dependence of ^{13}C chemical shifts for conjugated compounds such as the chromophore of a visual pigment Rh. First, the calculations are applied systematically to 10 diene derivatives in order to obtain basic and universal relationships between their conformation and the shieldings of unsaturated carbons. It is indicated that the conjugated carbons are classified into two types according to the profiles of the conformation dependence of the shieldings. The shieldings of the carbons composing the rotating bond exhibit complicated angular dependence. There is strong evidence that the behavior of such carbon shieldings can be understood by considering the effect of π -orbital modification, a new concept introduced in the work. On the other hand, the shieldings of the other carbons essentially follow well-known effects including the steric and charge density effects. One of the most important findings is that the steric effects are reflected predominantly on the σ_{11} component, and the effects that originated in electronic perturbation are on the σ_{22} and σ_{33} terms. This classification is hardly affected even when both types of effects act simultaneously during a conformational change. It is indicated that these basic data

for the dienes are available for interpretation of the conformational dependence of ^{13}C shieldings for more complicated compounds like retinal. Finally, by combining the data for the direct *ab initio* shielding calculations of 11-*cis*-retinal and for those of the dienes, they successfully determine the preferred conformation around the C12–C13 bond of the chromophore in Rh. It is concluded that the chromophore takes *s-trans* conformation around this bond.

III. RECENT APPLICATIONS

A. Solution NMR

1. Linear conjugated dienes

Tsuboi and coworkers²⁰ reported a stereoselective synthesis of 3,5-alkadienic ester obtained from 2,4-dienoic isomers and their NMR data.

The treatment of (2*E*,4*Z*)-2,4-alkadienoic esters (**7**) with lithium diisopropylamide (LDA) at -80°C gave the (3*E*,5*E*)-isomers (**8**) with 81–98% stereoselectivity. In contrast, the treatment of (2*E*,4*E*)-isomers (**9**) under the same conditions gave the (3*E*,5*Z*)-isomers (**10**) with 72–80% stereoselectivity. ^{13}C NMR data on 3,5-dienoates are given in Tables 8a and 8b. The stereoselectivity decreased slightly as the substituent became larger. The geometry of the rearrangement products was determined by ^1H NMR spectral data with the aid of a shift reagent $\text{Eu}(\text{dpm})_3$ and a proton decoupling technique. For example, both $J(\text{H}3\text{H}4)$ and $J(\text{H}5\text{H}6)$ in ethyl(3*E*,5*E*)-3,5-decadienoate (**8c**) were 15 Hz, which shows a *trans* geometry. The coupling constants of ethyl (3*E*,5*Z*)-3,5-decadienoate were $J(\text{H}3\text{H}4) = 15.4$ Hz and $J(\text{H}5\text{H}6) = 10.8$ Hz. The ^{13}C NMR spectra of compounds prepared in this work were measured and tentatively assigned as shown in Table 9.

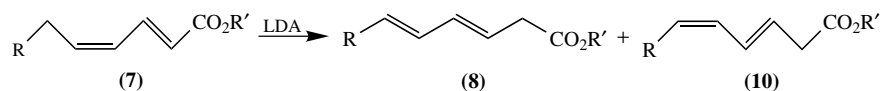
In general, signals of *cis* olefinic carbons of **10** appeared at a higher field than those of *trans,trans*-olefins **8** as a result of a steric effect²¹. These data afford an additional support for the structural assignment of **8** and **10**.

Bushby and Jarecki²² reported a preparation of precursors to conformationally constrained 8π non-Kekule polyenes and their NMR data.

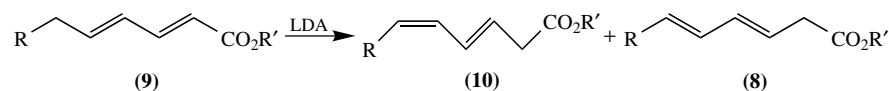
A synthesis is described for the *Z* and *E* isomers of 2-(2'-butylallylidene)-6,7-diazabicyclo[3.2.2]nona-3,6-diene **11** and **12**, which are potential precursors to conformationally constrained 8π non-Kekule polyenes.

Their ^1H NMR spectra were assigned with the help of two-dimensional NMR (COSY) experiments and the stereochemistry of the exocyclic double bonds through NOE experiments as detailed in Table 10.

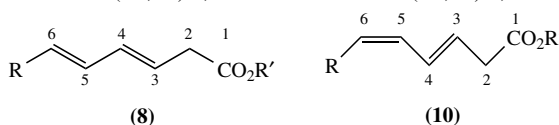
TABLE 8a. Transformation of (2*E*,4*Z*)-2,4-alkadienoates **7** to the (3*E*,5*E*)-isomers **8**



No.	7		Yields of products (%)			Stereoselectivity 8/10 (%)
	R	R'	7	8	10	
a	C_2H_5	CH_3	2	77	3	96
b	<i>n</i> - C_3H_5	CH_3	0	56	1	98
c	<i>n</i> - C_4H_9	C_2H_5	0	87	10	90
d	<i>n</i> - C_7H_{15}	C_2H_5	0	68	12	85
e	<i>n</i> - C_8H_{17}	CH_3	23	62	15	81

TABLE 8b. Transformation of (2*E*,4*E*)-2,4-alkadienoates **9** to the (3*E*,5*Z*)-isomers **10**

No.	9		Yields of products (%)		Stereoselectivity 10/8 (%)
	R	R'	10	8	
a	C ₂ H ₅	CH ₃	51	13	80
b	<i>n</i> -C ₃ H ₇	CH ₃	66	22	75
c	<i>n</i> -C ₄ H ₉	C ₂ H ₅	72	28	72
d	<i>n</i> -C ₈ H ₁₇	CH ₃	75	19	80

TABLE 9. ¹³CNMR data of (3*E*,5*E*)-3,5-alkadienoates **8** and (3*E*,5*Z*)-3,5-alkadienoates **10**

Compd	C ₁	C ₂	C ₃	C ₄	C ₅	C ₆	C ₇	C ₈	C ₉	C ₁₀	C ₁₁	C ₁₂	C ₁₃	C ₁₄
8a	171.9	38.0	122.4	134.2	128.4	136.4	25.6	13.5						
8b	172.1	37.9	122.3	134.7	129.7	134.2	34.7	22.4	13.7					
8c	171.8	38.2	122.5	134.8	129.6	134.1	29.1	31.4	22.3	14.0				
8d	172.1	37.8	122.2	134.4	129.4	134.1	18.3	29.5 ^a	29.3 ^a	28.5 ^a	28.5 ^a	31.9	22.7	14.1
10a	171.9	38.2	124.6	134.0	127.2	129.3	21.2	14.3						
10b	172.1	38.1	124.5	132.1	127.9	129.3	29.8	22.8	13.7					
10c	171.8	38.2	123.9	132.4	126.9	128.0	28.3	31.7	22.3	14.0				
10d	172.0	38.1	124.5	132.4	127.7	129.8	27.8	29.3 ^a	29.3 ^a	29.6 ^a	29.6 ^a	31.9	22.7	14.1

^aMay be exchangeable.

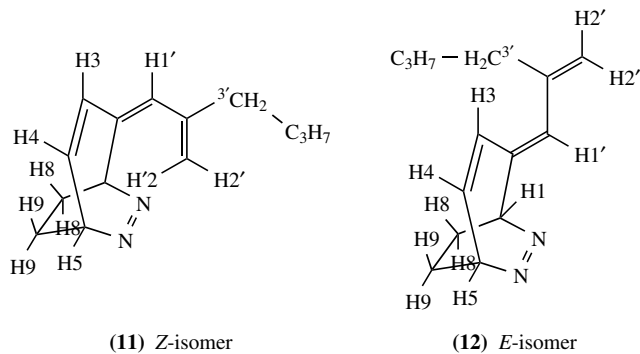
Roth and coworkers²³ reported NMR data of the orthogonal butadiene (*Z,Z*)-3,4-dimethylhexa-2,4-diene. (*Z,Z*)-**13** having the planes of the double bonds at a dihedral angle not far from 90°. This diene serves as the model for 'conjugated' diene lacking π -electron delocalization and for the transition state for interconversion of antiperiplanar (*trans*) and synperiplanar (*cis* or *gauche*) butadiene.

From the ¹H NMR and ¹³C NMR spectra reported in Table 11, it is immediately apparent which isomer has the nonsymmetrical (*E,Z*) configuration.

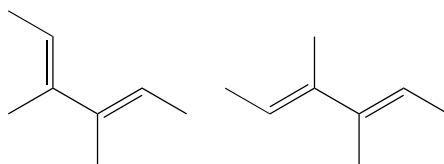
Two features in the ¹H spectra are distinctive: rotation of an (*E*) double bond out of the plane shifts the vinyl proton from 5.58 ppm in (*E,E*)-**13** to 5.20 ppm in (*E,Z*)-**13**; replacement of a (*Z*) double bond in nonplanar (*Z,Z*)-**13** by an (*E*) double bond in nonplanar (*E,Z*)-**13** causes the (*Z*)-C1 CH₃ group to be shifted downfield from 1.45 to 1.56 ppm.

In the ¹³C spectra, assignment of C1(4) and C2(3) rests not only on the larger intensity of the former but also on multiplicities found with the INEPT pulse sequence. (*E*)- and (*Z*)-methyl groups are distinguished in C2(3) CH₃.

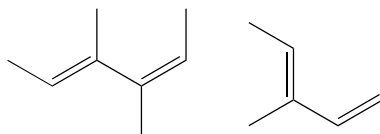
Despite identical values of the angle between the planes containing the two double bonds found by electron diffraction in (*E,Z*)-**13** and (*Z,Z*)-**13**, only the latter fails to react with sulfur dioxide or maleic anhydride. Apparently, the second α,δ -dimethyl repulsion

TABLE 10. ^1H NMR assignments for compounds **11** and **12**

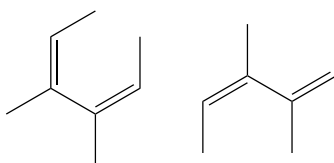
Position	$\delta(\text{CDCl}_3)$	COSY	NOE	Position	$\delta(\text{CDCl}_3)$	COSY	NOE
1	6.21	8/9	2'	1/5	5.43	4, 8/9	1'
3	5.96	4		3	6.50	4	
4	5.75	3, 5		4	5.78	1/5, 3	
5	5.45	8/9		8/9	1.5, 1.8	1/5	
8/9	1.85, 1.70	5, 1					
1'	5.90	2'		1'	5.98	2'	1
2'	5.2, 5.1	1', 3'	1	2'	5.05, 4.84	1', 3'	
3'	2.0	2'		3'	2.1	2'	



(E,E-13)



(E,Z-13)



(Z,Z-13)

TABLE 11. ^1H and ^{13}C NMR spectra of the 1,2,3,4-tetramethylbutadienes^a

Group ^a	(<i>E,E</i>)- 13	(<i>E,Z</i>)- 13	(<i>Z,Z</i>)- 13
^1H NMR (270 MHz, CDCl_3) ^{b,c}			
C1 CH_3	1.71 (d, <i>J</i> 6.6)	1.56 (dq, <i>J</i> 6.6, 1.3)	1.45 (dq, <i>J</i> 6.6, 1.3)
C4 CH_3		1.65 (d, <i>J</i> 6.9)	
C2 CH_3	1.76 (s)	1.66 (s)	1.71 (dq, <i>J</i> 1.3, 1.4)
C3 CH_3		1.73 (dq, <i>J</i> 1.3)	
C1(4)	5.58 (q, <i>J</i> 6.6)	5.20 (m)	5.26 (qq, <i>J</i> 6.6, 1.4)
^{13}C NMR (67.8 MHz, CDCl_3)			
C2(3)	137.1 (0.21) ^d	140.7 (0.15) 135.8 (0.12)	136.6 (0.21)
C1(4)	119.1 (1.00)	121.1 (0.83) 118.9 (1.00)	119.6 (0.52)
C2(3) CH_3		23.3 (1.00)	22.1 (1.00)
C1(4) CH_3	14.0(0.62)	15.1 (0.47) 14.5 (0.66)	1.41 (0.67)
	13.5 (0.75)	13.3 (0.48)	

^aNames and numbering are based on butadiene for convenience.

^bPpm relative to TMS.

^cSplittings (*J*) in hertz.

^dValues in parentheses are relative intensities.

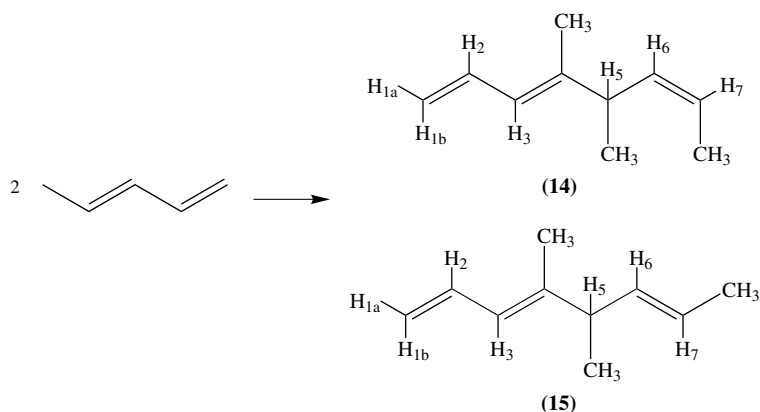
in (*Z,Z*)-**13** makes attainment of a planar *cis* conformation sufficiently less favorable so that the transition state for a Diels–Alder reaction is no longer within reach.

Denis and coworkers²⁴ reported a linear dimerization of conjugated dienes catalyzed by Ni(0)-aminophosphinite systems and their NMR data. This reaction occurs at a rather low temperature with high turnover numbers, especially with butadiene and piperylene. The reaction with butadiene gives the 1,3,6-octatriene isomers, which are further isomerized to the conjugated 2,4,6-octatrienes. With isoprene, a competitive cyclodimerization reaction occurs, but the linear dimers are obtained regioselectively by a tail-to-tail linkage. Piperylene gives rise only to head-to-head products **14** and **15**, without forming cyclodimers, which are optically active. The ee values were *ca* 90% and 35% for **14** and **15**, respectively (Scheme 1).

The LIS (Lanthanide Induced Shift) NMR technique is useful for such analysis²⁵ and the separation of olefin enantiomers such as limonene, α -camphene and β -pinene has been performed upon addition of silver salts such as Ag(fod)* or Ag(hfc)** to the commonly used lanthanide chiral salts such as Ln(tfc***)₃ or Ln(hfc)₃, where *fod = 6,6,7,7,8,8,8-heptafluoro-2,2-dimethyloctanedione, **hfc = heptafluoro-3-butyrylcamphorato and ***tfc = trifluoroacetylcamphorato.

Table 12 gives the chemical shifts of the olefinic protons in compound **15** in the presence of different shift reagents. Upon using the racemic **15** and that obtained with (D)-2'-Ph₂POCH(Ph)CH(Me)ND(Me)(EPHOSNH) [Ephedrine PHOSphine NH] as ligand, an enantiomeric shift is observed in the 5.3–5.6 ppm region where resonance of the three protons (H3, H6 and H7) occurs. Splitting occurs on the H6, and upon integration of the signals the ee of this *E,E* isomer can be estimated as 35 ± 5% (Figure 3).

The same procedure was used to analyze the *E,Z* isomer **14**. The higher optical rotation obtained with this compound (−143°) could suggest a higher optical yield. Indeed, integration of the same signals in the spectrum using Eu(tfc)₃ and Ag(fod) gave an optical yield of more than 90%.



SCHEME 1

TABLE 12. Olefinic protons chemical shifts of **15** in the presence of LIS reagents (vs TMS)

Complex (0.1 M)	H1a	H1b	H2	H3	H5	H6	H7
None	5.00	5.12	6.58	5.89	2.77	5.40	5.40
Eu(tfc) ₃	5.00	5.12	6.58	5.89	2.77	5.40	5.40
Ag(fod)	4.96	5.10	6.82	5.96	2.9	5.60	5.60
Eu(tfc) ₃ + Ag(fod)	4.32	4.45	6.60	5.50	2.7	5.4–5.5	

Chen and coworkers²⁶ reported the structures of spiral hexatrienes and the NMR data.

Steric crowding in the *cis* isomer of Mini-3 (**16**), a chain shortened triene analog of β -carotene, and hexakis (2,2',4,4',6,6'-trifluoromethyl)stilbene (**17**) forces the polyene chromophores to adopt a spiral conformation. Some of the associated unusual spectroscopic properties (UV-VIS and NMR) of these compounds and a rare 1,7-H shift process were described.

The unusual conformation is also in agreement with the dynamic NMR behavior exhibited by compounds **16** and **17**. For **16**, the geminal dimethyl singlet (0.98 ppm) in its room temperature ¹H NMR spectrum (in toluene-d₈, 500 MHz spectra) splits into two singlets ($\Delta\delta = 68.8$ Hz) upon cooling indicating that the two methyl groups are now nonequivalent, as indicated in structures **16'** and **16''**. The coalescence temperature ($T_c = -69^\circ\text{C}$), and the calculated ΔG^\ddagger values (9.9 kcal mol⁻¹) based on the equation²⁷:

$$\Delta G^\ddagger = 4.57 T_c [9.97 + \log T_c / (\Delta\nu \text{ values} + 6J)^{-1/2}],$$

(J being zero for both **16** and **17**) are, somewhat surprisingly, lower than those of the 7-*cis* retinoids (coalescence temperatures usually near 0°C)²⁸.

The ¹⁹F NMR spectra (in THF-d₈, 283 MHz) of compound **17** also exhibits dynamic NMR behavior; of **17'** and **17''**. At room temperature, two singlets ($\delta = 60.97$ and -65.05 ppm) of 2 : 1 relative intensities were observed corresponding to the *o*- and *p*-CF₃'s. At lower temperatures, the major peak split into two singlets ($\Delta\delta = 136$ Hz) with the coalescence temperature being -90°C , giving $\Delta G^\ddagger = 9.3$ kcal mol⁻¹. The higher field peak is most likely due to that of the inward CF₃ group of **17''**, now frozen in a direction above the plane of second phenyl ring. The activation parameters

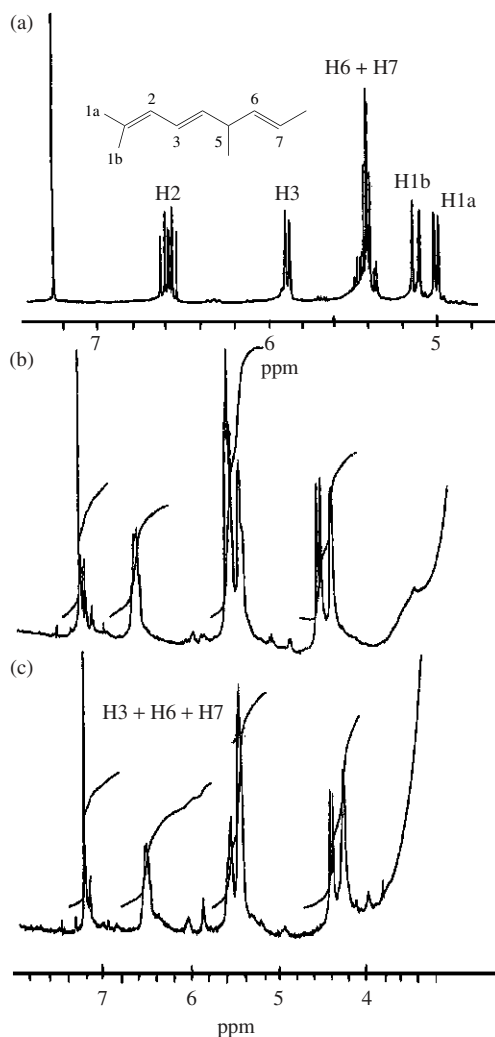
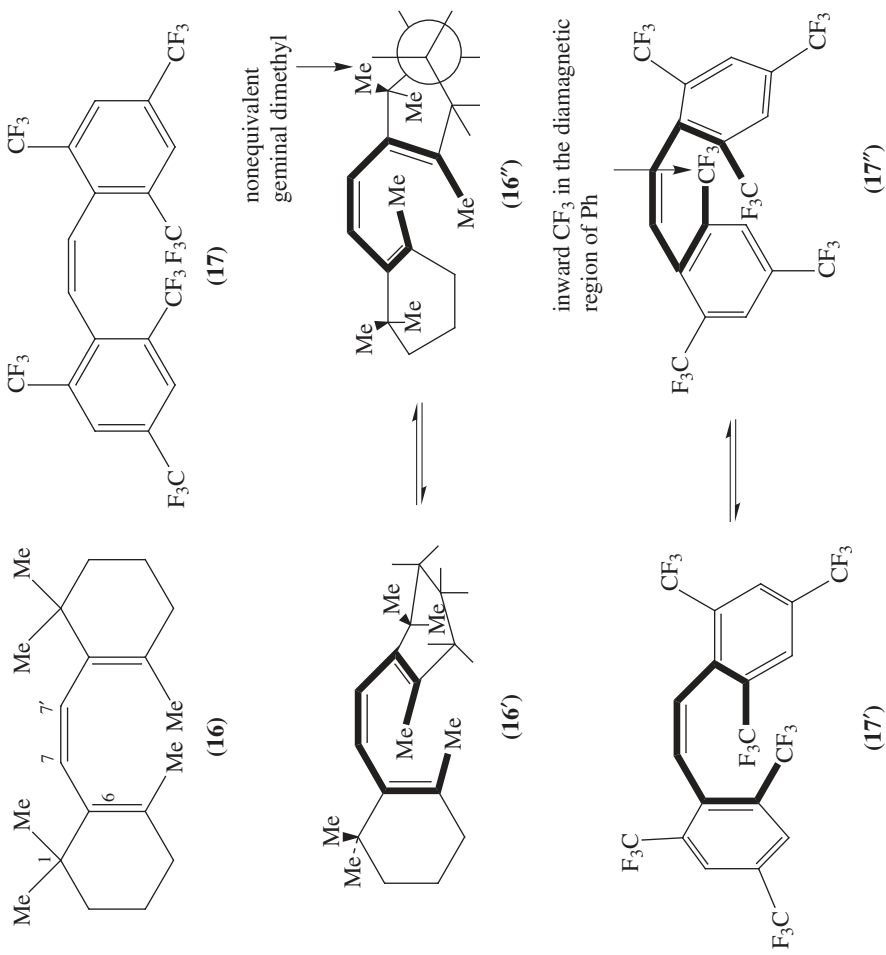


FIGURE 3. 400 MHz proton NMR spectrum of **15** in CDCl_3 (olefinic protons) with (a) no shift reagent, (b) racemic **15** with $\text{Eu}(\text{tfc})_3$ and $\text{Ag}(\text{fod})$, (c) **15** produced from piperylene with $\text{Ni}(\text{COD})_2$ and D-EPHOSNH , with $\text{Eu}(\text{tfc})_3$ and $\text{Ag}(\text{fod})$. Reproduced by permission of Elsevier Sequoia S.A. from Reference 24

($\Delta H^\ddagger = 4.4 \text{ kcal mol}^{-1}$, $\Delta S^\ddagger = -19.8 \text{ eu}$) are similar to those of **16**, suggesting that a concerted motion is also involved in the equilibration process.

Taskinen²⁹ reported a ^{17}O NMR study of p - π conjugation in methoxybutadienes and related compounds.

The ^{17}O NMR spectra of some monomethoxy and dimethoxy derivatives of buta-1,3-diene, hexa-2,4-diene, cyclohexa-1,3-diene and cyclohexa-1,4-diene were recorded in CDCl_3 . The $\delta(^{17}\text{O})$ values show that in 2-methoxybuta-1,3-diene the efficiency of p - π

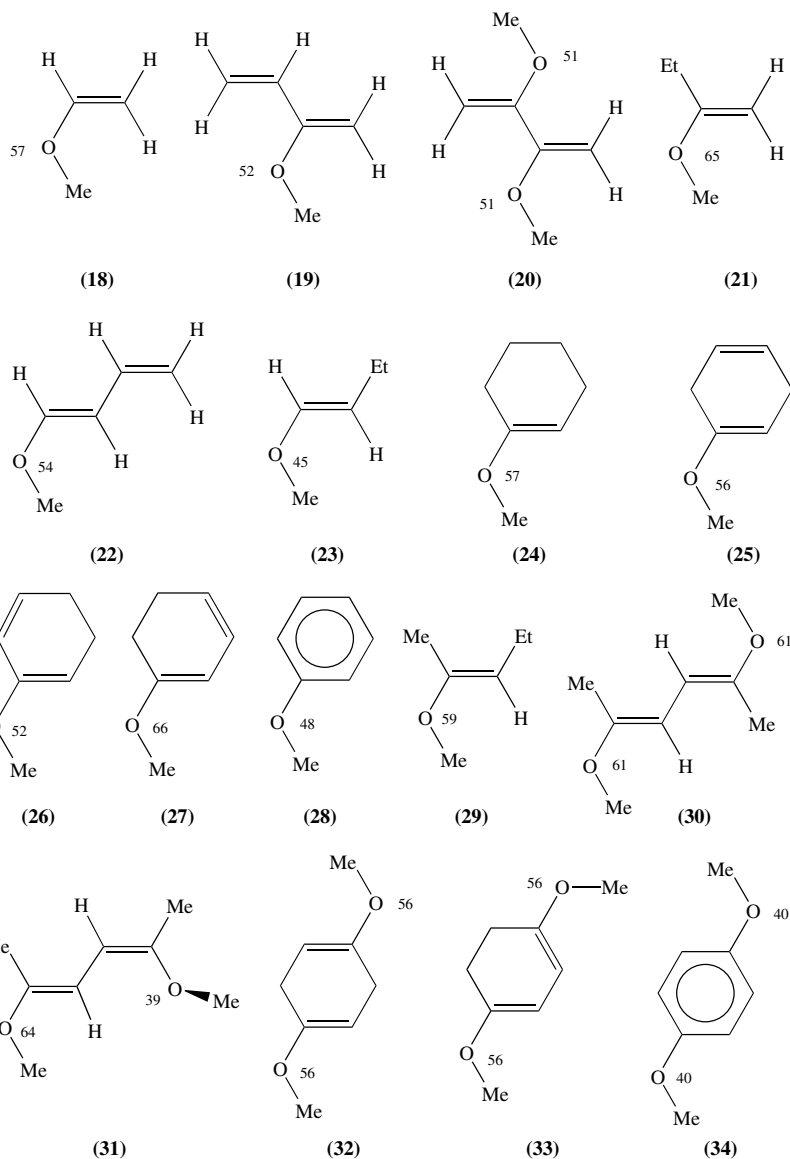


conjugation in the $-\text{O}-\text{C}=\text{C}$ moiety is significantly lowered by cross-conjugation of the $\text{C}=\text{C}$ bond with the other olefinic linkage. In the related system of 2-methoxycyclohexa-1,3-diene, however, the corresponding effect is much smaller, apparently because of weak conjugative $\pi-\pi$ interaction in the olefinic system. On the other hand, the strength of the $p-\pi$ conjugation appears to be the same in the $-\text{O}-\text{C}=\text{C}-\text{C}=\text{C}$ moieties of both 1-methoxycyclohexa-1,3-diene and 1-methoxycyclohexa-1,4-diene. Moreover, as a transmitter of substituent effects, the unsaturated system of cyclohexa-1,3-diene is comparable to that of the benzene nucleus. The $\delta(^{17}\text{O})$ values, relative to external water, are given in Scheme 2, which shows that when the α -H atom of **18** is replaced with either a vinyl group (**19**) or a MeO-substituted vinyl group (**20**), a decrease of 5–6 ppm in $\delta(^{17}\text{O})$ is observed. For comparison, an Et-substituent in the α -position (**21**) causes an 8 ppm increase in $\delta(^{17}\text{O})$. Thus there is a difference of 13 ppm in $\delta(^{17}\text{O})$ between **21** and **19**, which suggests the $p-\pi$ conjugation to be less efficient in the latter compound. As it seems likely that the MeO group of **19** can readily adopt the planar *s-cis* conformation, the reduction in $p-\pi$ conjugation is likely to arise from electronic rather than steric factors.

As expected, $\delta(^{17}\text{O})$ of **24** is not significantly affected by the introduction of another $\text{C}=\text{C}$ linkage into a nonconjugated position in the six-membered ring (**25**; $\delta = 56$ ppm), or when the oxygen is at the center rather than at the terminus of the conjugated system (**26**; $\delta = 52$ ppm). However, the presence of an $-\text{O}-\text{C}=\text{C}-\text{C}=\text{C}$ system in **27** increases $\delta(^{17}\text{O})$ by 9 ppm, with the shift value of **24** as a reference. This agrees with the 9 ppm difference in chemical shift between the respective open-chain compounds **22** and **23**. The buta-1,3-diene skeleton of **22** is known to assume the planar *s-trans* conformation with a normal buta-1,3-diene stability while the 1,3-diene moiety of **27** behaves like that of the parent cyclohexa-1,3-diene, i.e. devoid of conjugative stabilization. Thus the ^{17}O NMR data suggest that in an $-\text{O}-\text{C}=\text{C}-\text{C}=\text{C}$ system the oxygen chemical shift, and hence the strength of $p-\pi$ conjugation, do not essentially depend on whether or not there is any actual conjugative $\pi-\pi$ interaction between the two $\text{C}=\text{C}$ bonds.

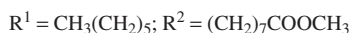
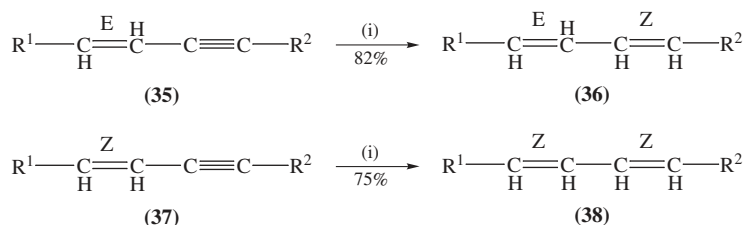
The $\delta(^{17}\text{O})$ data in Scheme 2 show that replacement of the Et group of **23** by a vinyl substituent (**22**) leads to an increase of 9 ppm in $\delta(^{17}\text{O})$. On the other hand, if the Et group of **29** is replaced with a MeO- and Me-substituted vinyl group (leading to **30**), the increase in $\delta(^{17}\text{O})$ is only 2 ppm. Clearly, in the latter case the smaller effect of substitution must be due to the combined electron-releasing power of the MeO and Me groups at the end of the 1,3-diene system of **30**, which opposes the electron transfer due to the similar groups at the other end of the conjugated system. In **31**, however, one of the MeO groups is forced by steric reasons to assume a nonplanar *gauche* conformation about the $\text{O}-\text{C}(\text{sp}^2)$ bond, which leads to reduced $p-\pi$ conjugation between this MeO group and the adjacent $\text{C}=\text{C}$ bond. The shift of the *gauche* MeO group is decreased by 22 ppm, whereas that of the other MeO group is increased by 3 ppm as a result of the weaker electron transfer to the 1,3-diene system by the *gauche* MeO group. It is noteworthy that the shift difference of 25 ppm between the two O atoms of **31** is in line with $\delta(^{17}\text{O})$ data observed previously for some related pairs of geometrical isomers, such as the 2-methoxybut-2-enes, for which the shift difference is also 25 ppm³⁰. A comparison of the $\delta(^{17}\text{O})$ values of **27** and **33** (66 and 56 ppm, respectively) shows that introduction of an additional MeO group at the other end of the $-\text{O}-\text{C}=\text{C}-\text{C}=\text{C}$ system of **27** decreases the oxygen chemical shift by 10 ppm, making it comparable to that of **32**, in which the $\text{C}=\text{C}$ bonds are isolated.

Similarly, $\delta(^{17}\text{O})$ of **34** is 8 ppm lower than that of **28**. Accordingly, although the 1,3-diene system of **33** does not possess the nature and thermochemical stability of ordinary conjugated 1,3-dienes, substituent effects are transmitted at least as efficiently through this system as they are transmitted through the aromatic system of **34**.

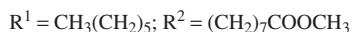
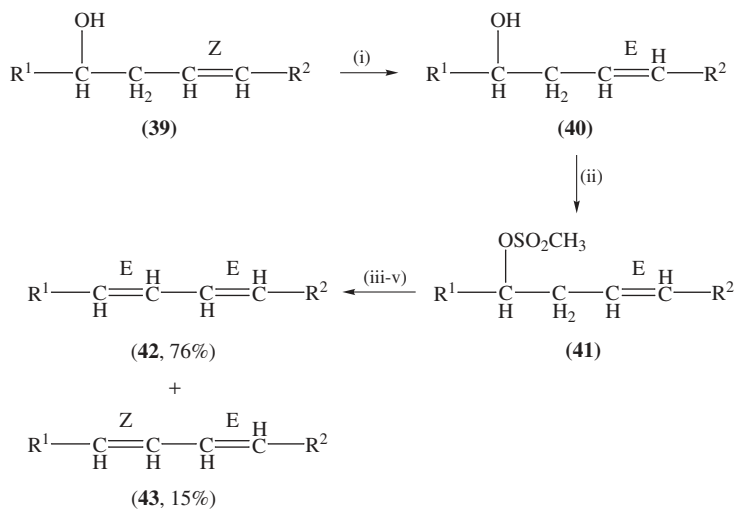
SCHEME 2. ^{17}O NMR chemical shift values (ppm) in CDCl_3 solution for compounds 18–34

Lie and coworkers³¹ reported the synthesis and NMR properties of all geometrical isomers of conjugated linoleic acids. Pure geometric isomers of conjugated linoleic acid (CLA) were prepared from castor oil as the primary starting material. Methyl octadeca-9*Z*,11*E*-dienoate (**36**) and methyl octadeca-9*Z*,11*Z*-dienoate (**38**) were obtained by zinc reduction of methyl santalbate (**35**, methyl octadec-11*E*-en-9-ynoate) and methyl

octadec-11*Z*-en-9-ynoate (**37**), respectively, as the key intermediates. Methyl octadeca-9*E*,11*E*-dienoate (**42**) and methyl octadeca-9*E*,11*Z*-dienoate (**43**) were prepared by demesylation of the mesyloxy derivative (**41**) of methyl ricinelaidate (**40**, methyl 12-hydroxyoctadec-9*E*-enoate) which was obtained in turn from the *Z*-isomer **39** (Scheme 3).



Reagents and conditions: (i) zinc, *n*-propanol, reflux, 10 h.



Reagents and conditions:

- (i) *p*-toluenesulfonic acid, dioxane, reflux, 1 h;
- (ii) methanesulfonyl chloride, triethylamine, dichloromethane;
- (iii) 1,8-diazabicyclo[5.4.0]undec-7-ene, dimethyl sulfoxide, reflux, 12 h;
- (iv) crystallization from ethanol and urea fractionation of mother liquid;
- (v) BF_3 -methanol, reflux.

SCHEME 3

A study of the NMR spectra was carried out, and the shifts of the olefinic carbon atoms of 18 : 2 (9*Z*,11*E*) (**36**) and (9*E*,11*Z*) (**43**) were readily identified by a combination of incredible natural abundance double quantum transfer experiment (INADEQUATE),

heteronuclear multiple bond correlation and $^1\text{H}-^{13}\text{C}$ correlation spectroscopy techniques. Doubts remain in the absolute identification of the individual olefinic carbon atoms of the (9Z,11Z) (**38**) and (9E,11E) (**42**), except for the fact that the shifts of the 'inner' (C10 and C11) and 'outer' (C9 and C12) olefinic carbon atoms of the conjugated diene system are distinguishable.

In order to assign the chemical shifts of the carbon atoms of the conjugated diene system of each CLA isomer, it was necessary to conduct INADEQUATE, HMBC (heteronuclear multiple bond correlation) and two-dimensional $^1\text{H}-^{13}\text{C}$ correlation spectroscopy (COSY) techniques on the carbon signals of the diene system of the *E,Z*-isomers. The results of these experiments for the CLA isomers are summarized in Table 13.

The *E,Z*-, *Z,E*-, *E,E*- and *Z,Z*-isomers can be characterized in sufficient detail by a combination of NMR techniques.

Shtarev and coworkers³² established the structures of substituted F-polyenes on the basis of *J*(FF) coupling constants. 1-Aryl-1,3-butadienes-F₅ **44** (Figure 4) and α,ω -diaryl-F₆-polyenes **45**, **46** (Figure 5) were formed as mixtures of *E* and *Z* isomers, where *E* isomers predominated, as established on the basis of ^{19}F NMR chemical shifts, *J*(FF) coupling constants and integration of the assigned signals. There are significant differences in coupling constants between the F_a and F_b, or the F_a and F_c nuclei, due to the specific configurations and conformations of the individual isomers. The long-range coupling $^5J(\text{a-e}) = 20-22$ Hz in (*E*)-**44** is relatively large, although smaller than $^5J(\text{F1F4})$ and $^5J(\text{F3F6}) = 29.7-32.6$ Hz for the case of the diaryl systems **45** and **46**, apparently due to a significant contribution of the cisoid conformation (Figure 6).

The assumed out-of-plane s-cisoid conformations with the dihedral angles $\phi = 5-23^\circ$ and $\theta = 47-49^\circ$, which were found in structurally similar systems and confirmed by X-ray and other spectral characteristics, are supported by relatively large $^5J(\text{F1F4})$ and $^5J(\text{F3F6})$

TABLE 13. ^{13}C NMR chemical shift values of conjugated linoleic acid isomers

Carbon nucleus	Isomer			
	(9Z,11E) (36)	(9E,11Z) (43)	(9E,11E) (42)	(9Z,11Z) (38)
C1	174.32	174.34	174.22	174.27
C2	34.1	34.1	34.09	34.1
C3	24.95	24.95	24.95	24.97
C4	29.06	28.97	29.04	29.14
C5/C6/C7	29.12-29.67	29.13-29.45	29.14-29.77	29.11-29.60
C8	27.66	32.86	32.61a ^a	27.46
C9	129.89	134.51	132.16b ^a	131.87d ^a
C10	128.71	125.72	130.37c ^a	123.58e ^a
C11	125.58	128.57	130.51c' ^a	123.72e' ^a
C12	134.76	130.17	132.43b' ^a	132.14d' ^a
C13	32.92	27.72	32.68a' ^a	27.54
C14	29.41	29.73	29.4	29.68
C15	28.95	28.97	28.97	29.04
C16	31.77	31.77	31.82	31.81
C17	22.65	22.65	22.68	22.69
C18	14.12	14.12	14.13	14.13
COOCH ₃	51.44	51.45	51.39	51.42

^aThe assignments a and a', b and b', c and c', d and d', e and e' can be interchanged

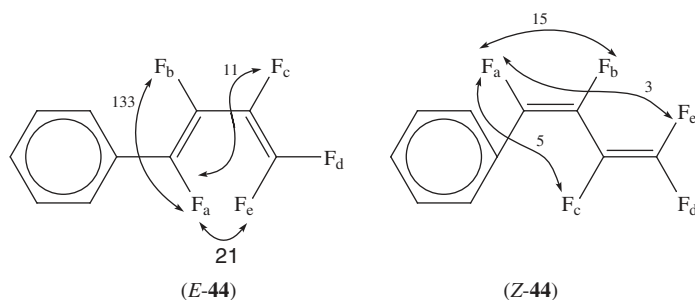


FIGURE 4. Selected $J(FF)$ for *E*- and *Z*-44. Reprinted with permission from Reference 32. Copyright (1997) American Chemical Society

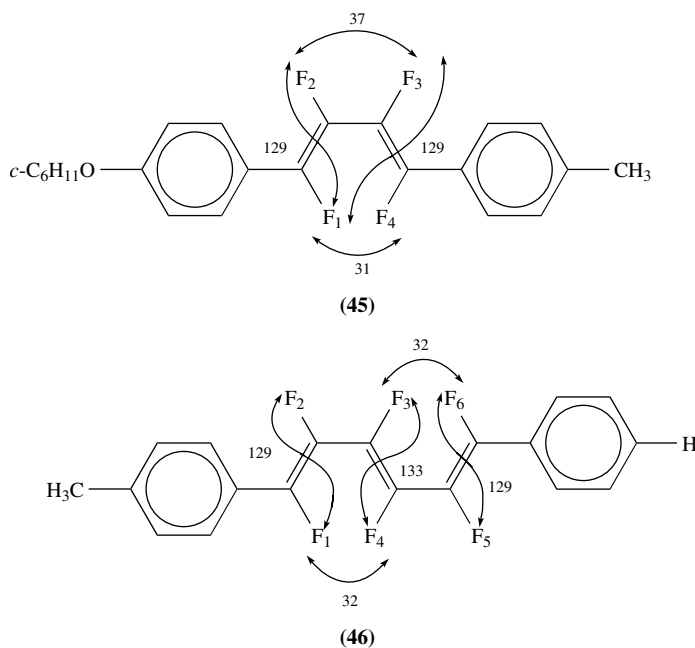


FIGURE 5. Selected $J(FF)$ for (*E,E*)-45 and (*E,E,E*)-46. Reprinted with permission from Reference 32. Copyright (1997) American Chemical Society

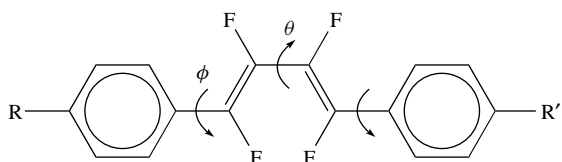
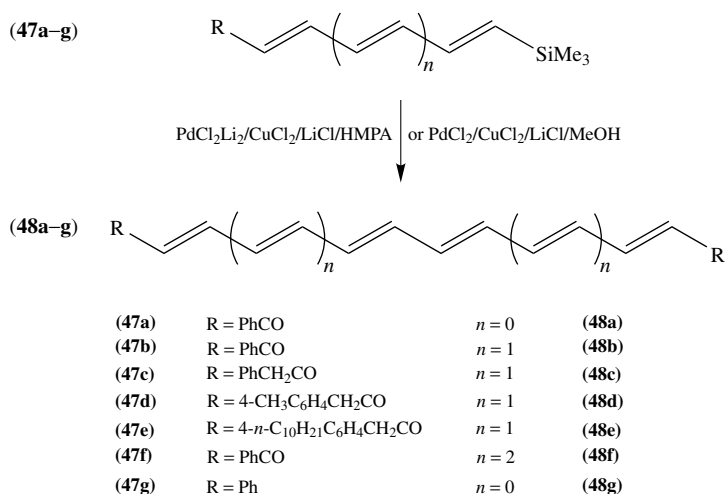


FIGURE 6. Geometry of an (*all-E*)- α,ω -diaryl- F_4 -polyene. Reprinted with permission from Reference 32. Copyright (1997) American Chemical Society

coupling constants observed in the ^{19}F NMR spectra. Their magnitude is apparently due to through-space interaction, as shown for **45** and **46** in Figure 5.

Babudri and coworkers³³ reported a highly stereoselective synthesis of conjugated polyenes and their NMR data. They reported a new method for the synthesis of conjugated polyenes containing up to eight double bonds with all-*E* configuration based upon a homocoupling reaction of dieny-, trieny- or tetraenylsilanes, promoted by PdCl_2 in methanol in the presence of LiCl and CuCl_2 .

Configurational and conformational assignments were made rigorously on the basis of NMR spectra. By applying a similar procedure to more complex systems, they prepared the series of polyenylsilanes **47a–g** and investigated their transformation into longer polyenes **48a–g** (Scheme 4). The configuration of compounds **48a–f** was determined by ^1H NMR spectroscopy. The analysis of the ^1H NMR spectrum of compound **48a** was straightforward.

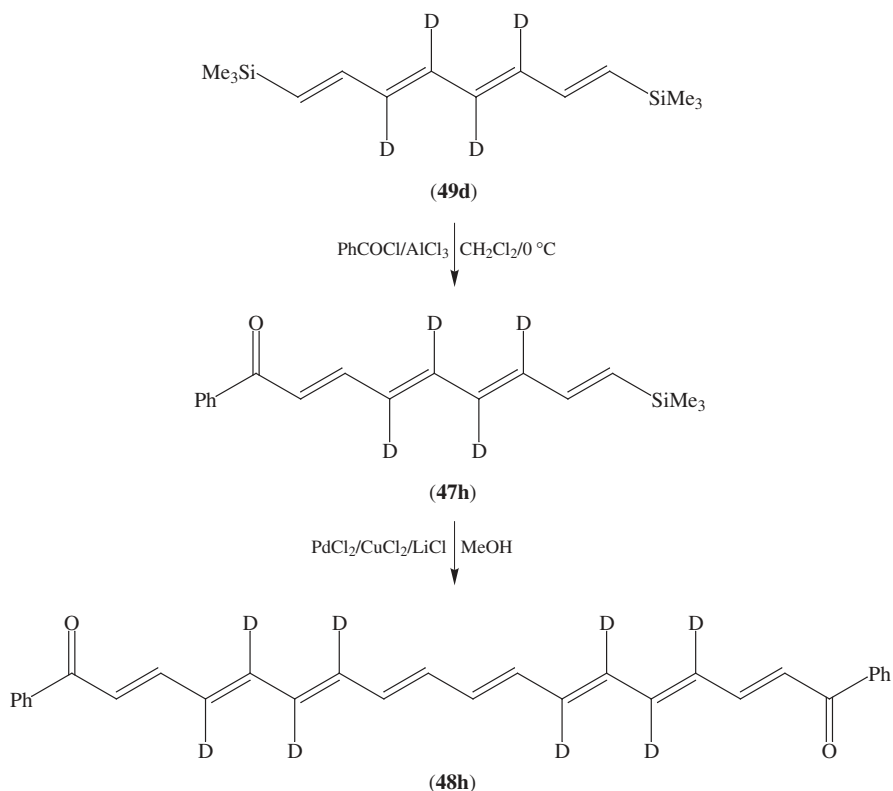


SCHEME 4

For compounds **48b–f** the complexity and the extensive overlap of resonance signals limit the amount of information that can be obtained from single resonance spectra. H1/H1' protons give distinct doublet in all the compounds examined and H2/H2', H3/H3', H4/H4' resonances were assigned by homonuclear decoupling experiments. H1/H1' and H2/H2' were in all cases obtained directly from ^1H single resonance spectra. For the hydrogen atoms bonded to the central carbon atoms, NMR parameters could not be extracted by direct inspection of the spectra, because of second-order effects and extensive overlap of the resonance signals. Even in COSY spectra, cross-peaks originated from second-order effects precluded the possibility of obtaining vicinal coupling constants $^3J(\text{HH})$ reliable enough to assign the configuration at the central double bonds of the polyenic chain. Least-squares analysis of the spectra was the only way to obtain chemical shifts and $^3J(\text{HH})$ values which permitted the required configurations to be determined unambiguously.

The eight central protons H3/H3', H4/H4', H5/H5' and H6/H6' of the polyenic chains in compounds **48b–e** were analyzed as an AA'BB'CC'DD' spin system. The resonances of H3/H3', H5/H5' and H6/H6' are located in a narrow range (50 Hz), and spin-tickling

experiments were necessary for a correct assignment of the experimental frequencies to the calculated transitions. COSY spectra were helpful in estimating transitions and the proton chemical shift values used to start the iterative analysis. For compound **48f**, decoupling of H4/H4' allowed the H3/H3' and H5/H5' resonances to be localized; these resonances strongly overlap with H6/H6', H7/H7' and H8/H8' resonances. Since the signals arising from these 10 protons are located in a range of 90 Hz, it was not possible to carry out the spectral analysis of the spin system H5/H5', H6/H6', H7/H7' and H8/H8'. The stereochemistry of the fragment C7–C8–C8'–C7' was determined for the partially and selectively deuteriated octaene **48h**, prepared from the tetradeuteriated **49d** as shown in Scheme 5.



SCHEME 5

The ^1H NMR spectrum of the four central protons of **48h** was analyzed as an AA'BB' spin system. The coupling constants between H7/H7' and the deuterium nuclei on C6/C6' (ca 2 Hz) were taken into account as first-order perturbations. In all cases coupling constants over four (–0.58 to –0.87 Hz) and five (+0.32 to +0.69 Hz) bonds were also considered in performing the spectral analysis. Chemical shifts and vicinal coupling constants for **48a–f** are reported in Table 14.

Vicinal coupling constants across double bonds are in the range 14.2–15.3 Hz, thus indicating the all-*E* configuration of the conjugated system. The $^3J(\text{HH})$ values across

TABLE 14. ^1H NMR chemical shifts^a and vicinal coupling constants^b for polyenes **48a–f**

Compd	H1	H2	H3	H4	H5	H6	H7	H8
48a	7.07 (14.82)	7.48 (10.74)	6.65 (14.99)	6.76 (11.23)				
48b	6.99 (14.89)	7.48 (11.40)	6.53 (14.80)	6.69 (10.16)	6.43 (14.12)	6.48 (11.95)		
48c	6.23 (15.23)	7.25 (11.39)	6.33 (14.74)	6.65 (10.65)	6.38 (15.12)	6.46 (10.79)		
48d	6.21 (15.28)	7.25 (11.42)	6.33 (14.69)	6.64 (11.19)	6.38 (14.09)	6.45 (11.85)		
48e	6.22 (15.23)	7.26 (11.34)	6.34 (14.78)	6.65 (11.0)	6.38 (14.19)	6.45 (11.09)		
48f	6.97 (14.9)	7.47 (11.5)	6.49 (14.7)	6.72 (11.0)	6.42 (15.0)	6.48 (10.0)	6.43 (14.83)	6.40 (11.40)

^a ^1H NMR chemical shifts are listed in ppm vs TMS in CDCl_3 .

^bVicinal coupling constants of each proton with the following one in the polyenic chain are reported in parentheses (in Hz).

single carbon–carbon bonds, which are in the range 10.0–11.8, suggest the occurrence of a nearly planar arrangement of the polyenic chains. However, on this basis a distinction between *s-trans* or *s-cis* conformation was not possible. The conformation of **48a** was fully determined by ^{13}C NMR and 2D NOESY spectra. The 2D NOESY spectrum shows correlation peaks of significant intensities between the pairs of protons H1/H1'–H3/H3' and H2/H2'–H4/H4'. This suggests an *s-trans* (a) conformation of the polyenic chain. Such a conformation is confirmed also by the $^3J(\text{CH})$ values between C1/C1' and H3/H3' of 3.8 Hz, and between C2/C2' and H4/H4' of 5.0 Hz.

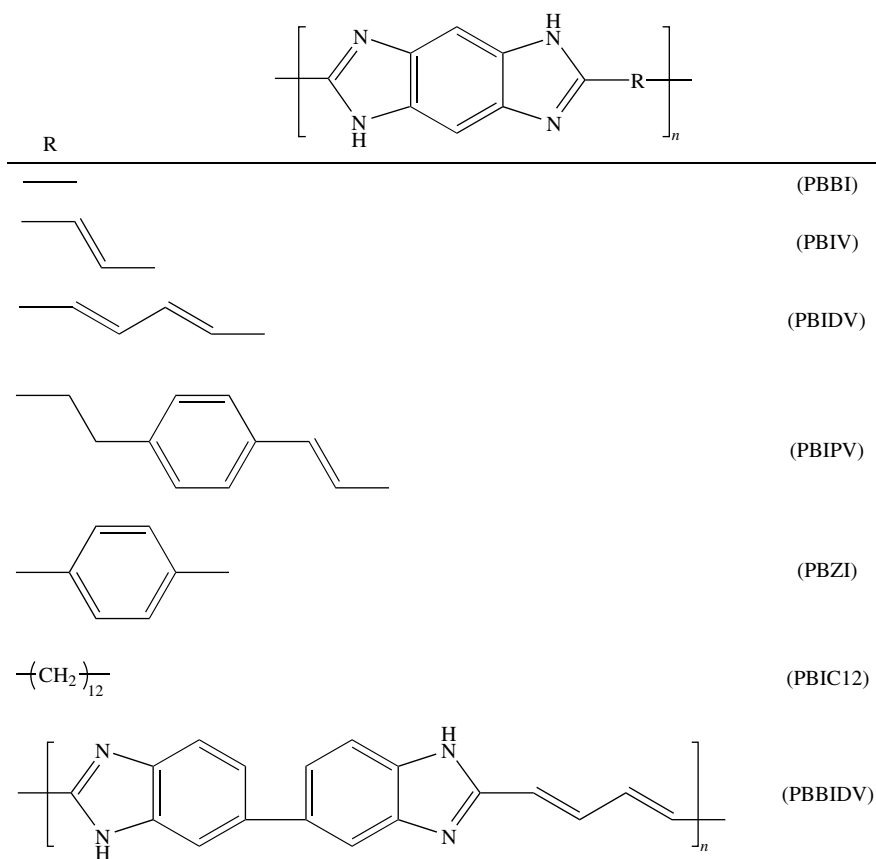
2. Polymers containing polyenes

Osaheni and Jenekhe³⁴ reported a synthesis of conjugated rigid-rod polymers and their NMR data. The conjugated rigid-rod polymers have interesting photoconductive, light-emitting and third-order nonlinear optical properties that have some potential for applications in optoelectronics and photonics.

New conjugated rigid-rod poly(benzobis(imidazole)s incorporating varying lengths of *trans*-polyene segments and 1,4-phenylenebis(vinylene) linkages have been synthesized and characterized by ^1H NMR spectra. The synthesis, characterization, thin film processing and optical properties of the conjugated poly(benzobis(imidazole)s shown in Scheme 6 were reported.

The series of polymers includes the parent poly(benzobis(imidazole)) (PBBI), poly(benzobis(imidazole)vinylene) (PBIV), poly(benzobis(imidazole)divinylene) (PBIDV), poly(benzobis(imidazole)-1,4-phenylenebis(vinylene)) (PBIPV) and poly(benzimidazole-divinylene) (PBBIDV). The new nonconjugated polymer poly(benzobis(imidazole)(dodecamethylene) (PBIC12) as well as the previously reported poly(*p*-phenylenebenzobis(imidazole)) (PBZI) were also synthesized for the purposes of comparative studies. The ^1H NMR spectrum of PBIDV in deuteriated nitromethane containing aluminum trichloride, shown in Figure 7, exemplifies the results.

The assignment of the resonances is also shown in Figure 7, in agreement with the proposed structure, including the *trans,trans*-divinylidene conformation. However, the integration of the amine (N–H) protons of the ring was not very accurate due to the rapid



SCHEME 6

proton exchange. The N–H proton resonance in the conjugated poly(benzobisimidazole)s was at 9.0–9.2 ppm whereas the resonance of this proton in the nonconjugated PBIC12 was at 6.9 ppm.

The ^1H NMR spectra were all in good agreement with the proposed structures of the polymers in Figure 7.

Jin and coworkers³⁵ reported a synthesis and characterization of new thermotropic side-chain liquid crystal polymers containing 1,6-heptadiyne backbone. Poly(1,6-heptadiyne) derivatives with side-group liquid crystalline mesogens are prepared by ring-forming metathesis polymerization with transition metal catalysts. MoCl_5 -based catalyst systems are more effective for the polymerization of 1,6-heptadiyne monomers with various mesogenic groups than are WCl_6 -based catalyst systems. The resulting polymers exhibit good solubility in common organic solvents such as chloroform and THF. The ^1H and ^{13}C NMR spectra of the resulting polymers indicate that side-chain liquid crystal polymers with a 1,6-heptadiyne backbone possess a polyene structure, presumably with cyclic recurring units in the polymer backbone. Thermal behaviors, morphology and electrical conductivities are investigated by using differential scanning calorimetry and cross-polarized optical

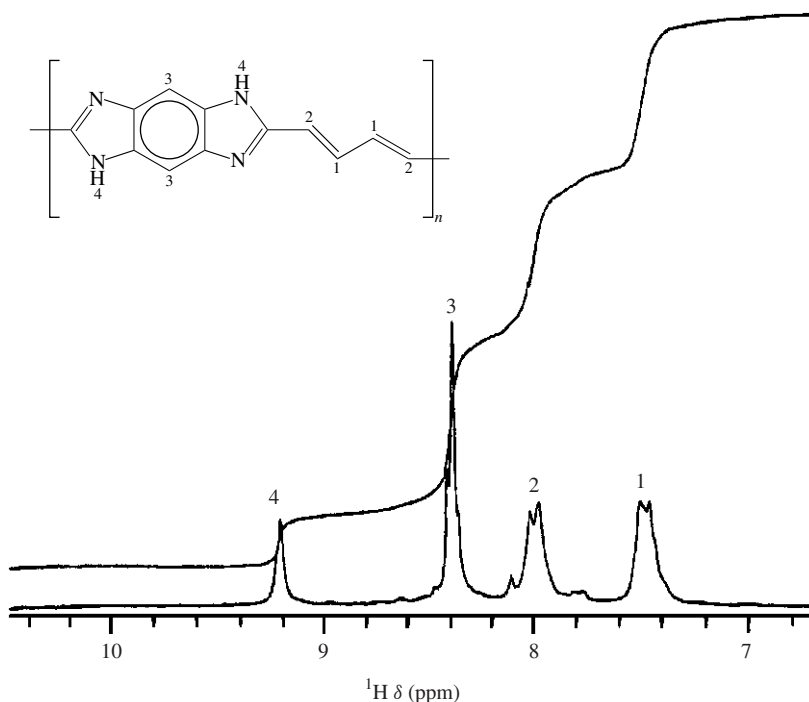


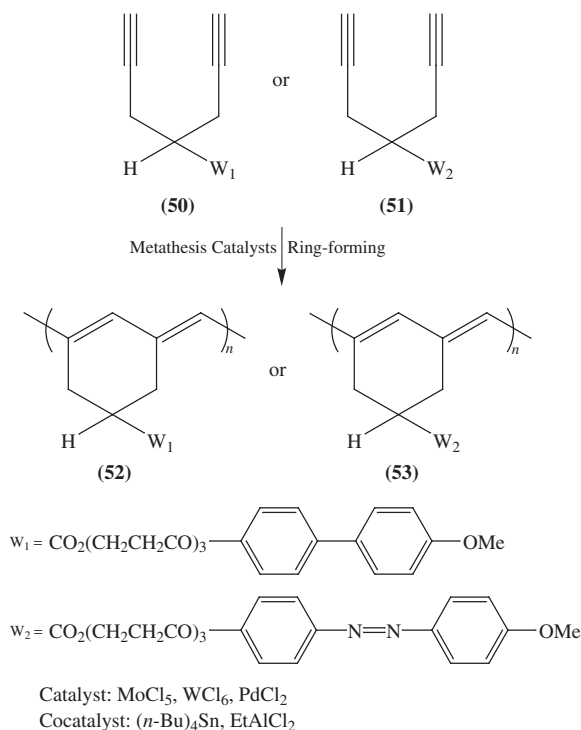
FIGURE 7. ^1H NMR spectrum of PBIDV in $\text{CD}_3\text{NO}_2/\text{AlCl}_3$ and its assignment. Reprinted with permission from Reference 34. Copyright (1995) American Chemical Society

microscopy. Compounds **50** and **52** displayed enantiotropic liquid crystallinity showing reversible phase transition. Compounds **51** and **53** displayed no mesophase. The electrical conductivities of the film-type polymers are in the 10^{-4} to 10^{-2} S/cm range.

The polymerization of the monomers **50** and **51** with ring-forming metathesis catalysts give **52** and **53**. The polymerization of **50** was carried out with transition metal catalysts; with MoCl_5 as catalyst and $(n\text{-Bu})_4\text{Sn}$ as a cocatalyst, the yield of **52** was quantitative (Scheme 7).

Careful ^1H and ^{13}C NMR analyses were carried out for both monomers and polymers in order to prove the chemical structures of the polymers. The ^1H NMR spectra of **50** and **52** are shown in Figure 8. As polymerization proceeded, an acetylenic proton peak at 2.0–2.2 ppm disappeared, while a new vinylic proton peak appeared broadly in the 6.8–7.2 ppm range. Since the new peak is weaker than those for the aromatic biphenyl rings and the two peaks are superimposed, it is hard to separate them clearly. The broad peaks at 2.6 and 3.4 ppm are assignable to the methylene protons and methine proton in the ring, respectively.

Figure 9 exhibits the ^{13}C NMR spectra of **50** and **52**. The monomer has acetylenic carbon peaks at 70 and 82 ppm, but **52** does not show these peaks. Instead, the olefinic carbon peaks of the **52** backbone appear at 123 and 141 ppm, although the value for the quaternary carbon is very weak. The peak of the methylene carbon adjacent to the polymer backbone is shifted from 20 to 43 ppm on polymerization.



SCHEME 7

3. Antibiotic polyenes

Ghirlando and coworkers³⁶ reported interactions between a protonated retinal Schiff base and various counterions using two-dimensional NOE NMR. Bacteriorhodopsin (bR) is the protein pigment (a constituent of the purple membrane) of *Halobacterium halobium*. Its role is to convert light energy directly into a gradient of hydrogen ion concentration across the membrane, which is subsequently used, via a chemiosmotic mechanism, to synthesize adenosine-5'-triphosphate. bR consists of a chromophore, all-*trans*-retinal, covalently bound to the polypeptide backbone through a protonated Schiff base link to the ϵ -amino group of a lysine. The protonated *n*-butylamine Schiff base of all-*trans*-retinal in methanol absorbs at 440 nm, whereas in bR, in its light-adapted form, it has an absorption maximum of 570 nm. This absorption maxima difference between the chromophore in the natural pigment and in methanol is defined as the opsin shift³⁷. A better understanding of the mechanism through which the protein shifts the absorption maximum to longer wavelengths, in addition to accounting for the absorption maxima in various visual pigments ranging from 440 to 625 nm, is of great interest.

At present the opsin shift in bR is interpreted as a result of a combination of different factors: (i) weaker hydrogen bonding in the pigment between the positively charged nitrogen and its counterion relative to the hydrogen bonding existing in methanol solution, (ii) *s-trans* ring-chain planarity and (iii) interaction of the retinal chromophore with a nonconjugated dipole introduced by the protein.

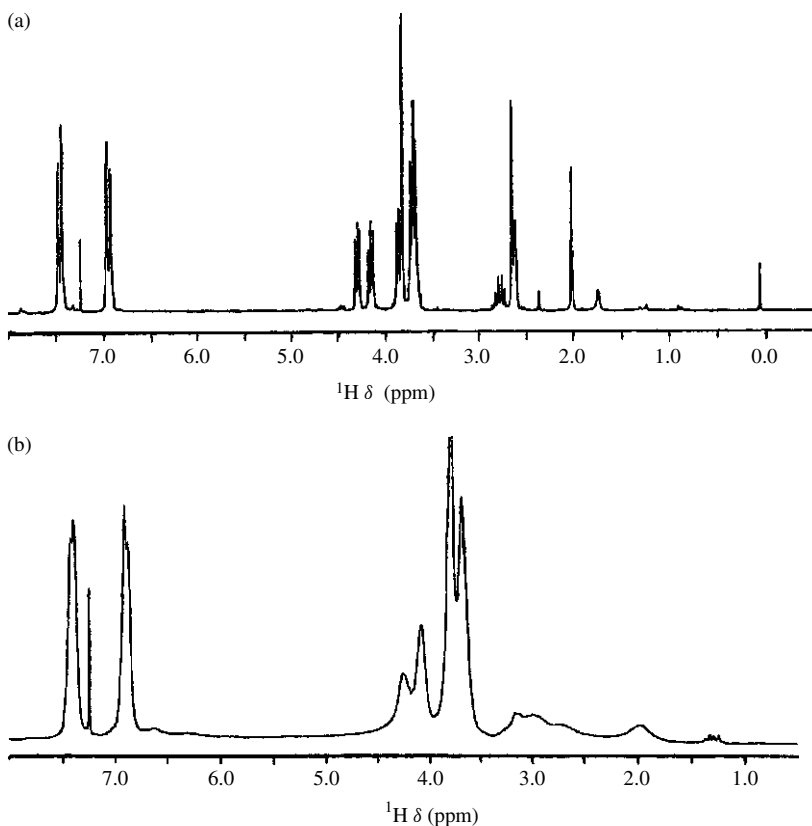
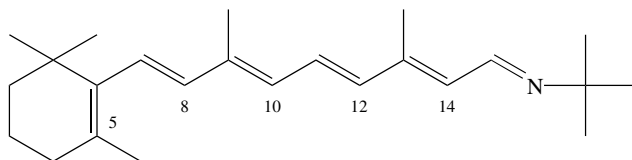
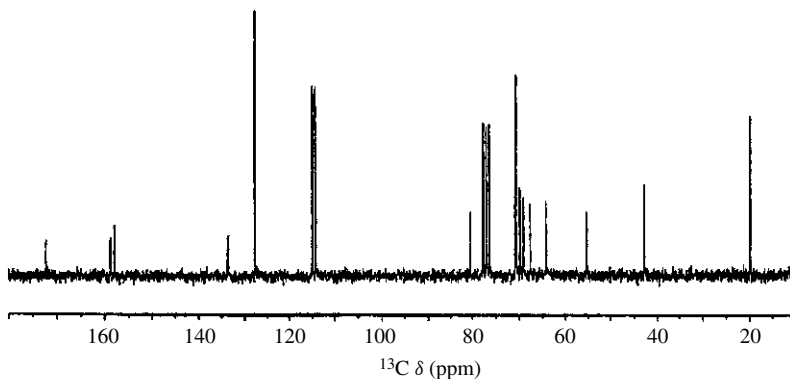


FIGURE 8. ^1H NMR spectrum of (a): **50** and (b): **52** in CDCl_3 . Reproduced by permission of Marcel Dekker, Inc. from Reference 35

The importance of the interaction between the protonated retinal Schiff base and its counterion for determining the absorption maxima was pointed out by Blatz and Mohler³⁸, who first noticed a correlation between the type of counterion used and the change in the wavelength of the absorption maximum in aprotic solvents. Excess of trifluoroacetic acid, in methylene chloride as a solvent, introduced a red shift due to the weakening of the electrostatic interaction between the positively charged nitrogen and its counterion. It is therefore important to determine directly the actual spatial location of the counterion along the polyene chain of the all-*trans* protonated retinal Schiff base in solution. The structure of a retinal Schiff base of *t*-butylamine is given below.



(a) Liquid crystal polymers



(b)

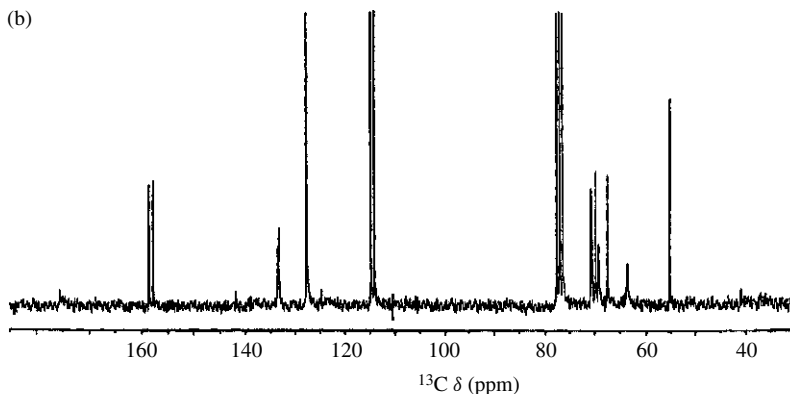


FIGURE 9. ^{13}C NMR spectrum of (a): **50** and (b): **52** in CDCl_3 . Reproduced by permission of Marcel Dekker, Inc. from Reference 35

Blatz and Mohler³⁸ have performed 2D NOE NMR experiments on the protonated *t*-butylamine Schiff base of all-*trans*-retinal using different counterions, each carrying at least one nonexchangeable proton. The study has indicated that a proton on the counterion molecule is spatially close, in aprotic solvents, to the protons of the chromophore near the positively charged nitrogen. It has also shown that the ion-pair formation is relaxed in either the presence of excess carboxylic acid (the counterion) or when using methanol as a solvent.

Experiments were performed at 5°C in order to arrest the *cis*–*trans* isomerization of the protonated Schiff base. Spectra with one equivalent of acid and different mixing times showed one NOE cross-peak between H15 of the retinal molecule and the proton on the counterion, as shown for a mixing time of 0.4 s in Figure 10. The strong chemical shift dependence of the H15 resonance on the concentration of the acid dictated the use of less than one equivalent of the protonating formic acid, and therefore an incomplete protonation (>80%) of the retinal, in order to avoid an overlap between the formate and the H15 peaks in the spectrum. This should not affect the observed result since an average chemical shift, between those of H15 of the retinal in its nonprotonated and protonated

states, was observed, suggesting a fast exchange. Electrostatic considerations imply that the formate counterion will only interact with the charged protonated retinal Schiff base molecules.

The discrepancy between the intensities of the signals of the formyl proton and of H15 (Figure 10) arises from the large difference in the relaxation times of the two molecules. This has a more pronounced effect on the observed intensity in the 2D NMR projection than in the normal NMR spectrum.

Using two-dimensional NMR spectroscopy, the spatial location of various carboxylate anions relative to the polyene chain of the protonated Schiff base of all-*trans*-retinal was determined. The observed intermolecular NOE cross-peaks between a proton on the counterion and a proton near the nitrogen atom indicate the existence of ion-pair formation between the protonated retinal Schiff base and various counterions in chloroform. The results suggest that the most likely site of the carboxylate group of the counterion is in the immediate vicinity of the positively charged nitrogen atom of the retinal Schiff base.

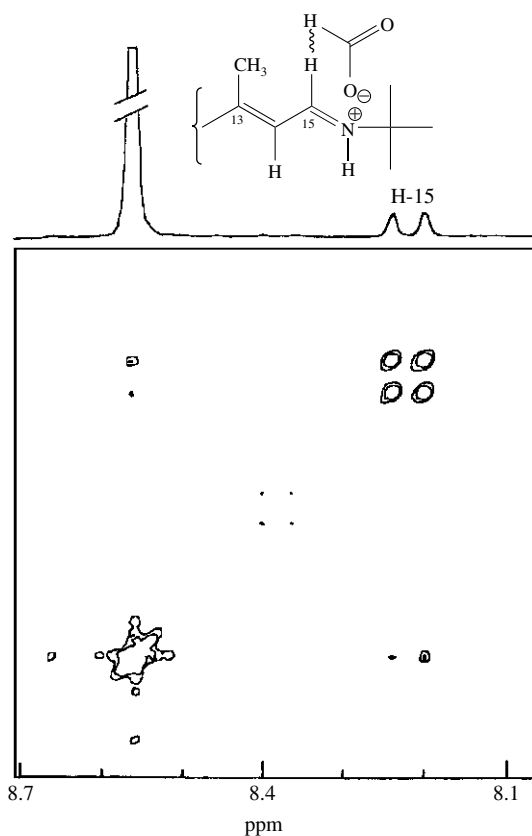


FIGURE 10. Contour plot of two-dimensional nuclear Overhauser effect ¹H NMR (NOESY) of the protonated Schiff base of all-*trans*-retinal, in chloroform, with formate as the counterion. The intermolecular NOE cross-peak observed between H15 of the retinal and the counterion proton, at a mixing time of 0.4 s, is shown. Top trace: *f*₂ projection of the 2D NOE spectrum. Reproduced by permission of John Wiley & Sons from Reference 36

Li and coworkers³⁹ reported the production of new polyene antibiotics. Ethyl (*Z*)-16-phenylhexadeca-9-enoate (**56**), an analog of ethyl oleate (**55**), was synthesized and added to cultures of *Streptomyces cellulosa* ATC C12625, which normally produce fungichromin (**54**) as the principal polyene antibiotic (Figure 11). These cultures showed drastic reduction of fungichromin biosynthesis but afforded four new polyene antibiotics with a truncated four-carbon side chain which are designated as isochainin (**58**) [an isomer of chainin (**57**)], 14-hydroxyisochainin (**59**), 1'-hydroxyisochainin (**60**) and 1',14-dihydroxyisochainin (**61**). The close correspondence of ¹³C NMR chemical shifts between these compounds and fungichromin and the coproduction of compounds **58–61** and fungichromin (**54**) suggest that the stereochemistry at every site is exactly analogous (Table 15).

Recently, the absolute stereochemistry of pentamycin, an antibiotic from *Streptomyces pentaticus* with the same gross structure as fungichromin (**54**), has been reported as being either **62a** or **62b**. Elucidation of the stereochemical relationship between pentamycin (**62**)

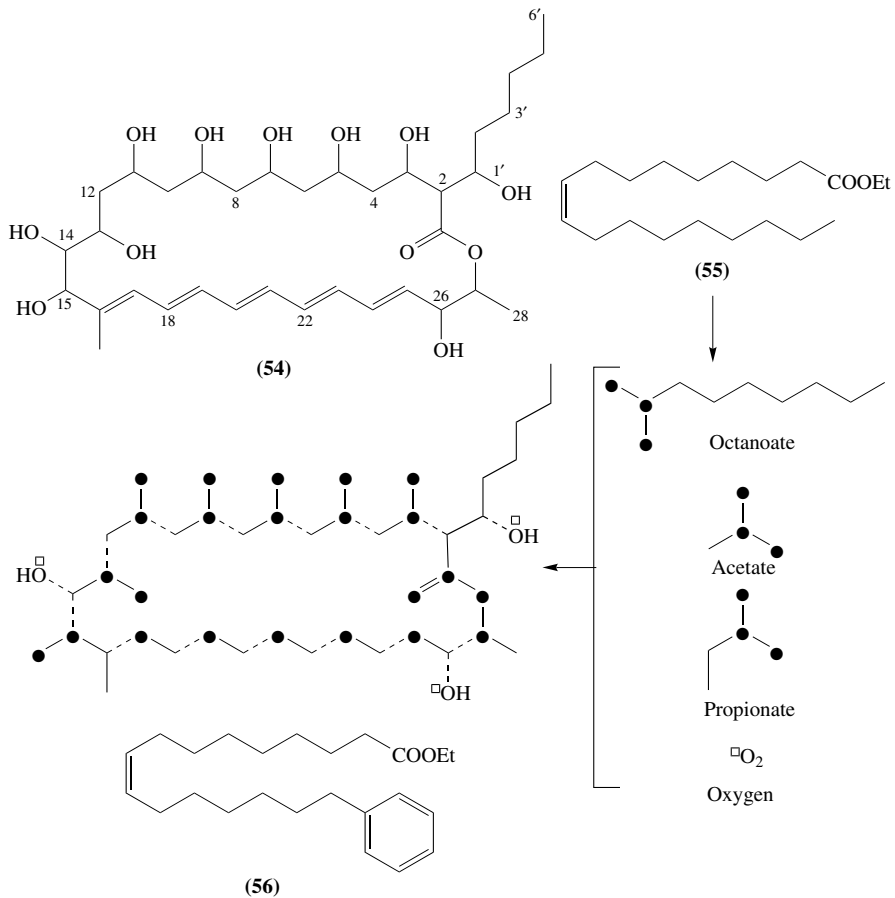


FIGURE 11. Biosynthetic origin of fungichromin (**54**) and structure of oleate analog (**56**). Reproduced by permission of Japan Antibiotics Research Association from Reference 39

TABLE 15. ^{13}C chemical shifts (δ) for fungichromin (**54**), isochainin (**58**), 14-hydroxyisochainin (**59**), 1'-hydroxyisochainin (**60**) and 1',14'-dihydroisochainin (**61**)^a

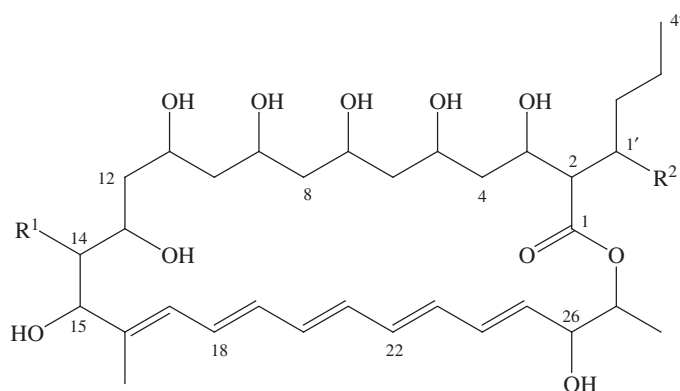
Carbon	54	58	59	60	61
29	11.74	11.45	11.80	11.08	11.70
6'	14.38	—	—	—	—
28	17.96	18.29	18.30	17.95	17.91
5'	23.65	—	—	—	—
3'	26.01	23.60	23.61	19.51	19.52
4'	32.88	14.21	14.25	14.23	14.23
2'	36.22	29.87	30.18	38.36	38.40
12	39.58	42.52	39.50	41.58	39.54
4	41.38	42.70	42.33	42.86	41.34
10	44.34	44.20	44.15	44.18	44.36
6	45.17	44.91	44.83	45.17	45.21
8	45.33	45.11	45.16	45.26	45.36
2	60.35	54.26	54.40	60.31	60.46
13	70.34	67.50	70.26	67.47	70.38
11	71.45	71.00	71.35	71.12	71.46
1'	72.59	30.60	30.57	72.28	72.21
26	73.25	73.15	73.44	73.15	73.30
3	73.41	73.29	73.55	73.60	73.30
7	73.92	73.38	73.56	73.65	73.90
5	74.08	73.55	73.64	73.65	74.08
9	74.20	74.24	74.02	73.91	74.17
27	75.25	74.47	74.58	75.10	75.25
14	78.31	45.21	78.20	45.29	78.32
15	80.43	75.63	80.32	75.83	80.50
18	129.06	128.04	129.25	128.35	129.05
17	129.91	129.57	129.79	129.31	129.93
24	131.97	132.43	131.99	132.25	132.03
22	133.66	133.62	133.74	133.82	133.67
20	134.13	134.15	133.96	134.12	134.13
23	134.21	134.19	134.32	134.12	134.17
25	134.28	134.44	134.37	134.28	134.27
21	134.81	134.57	134.45	134.59	134.85
19	135.36	134.68	135.18	134.96	135.41
16	138.55	140.64	138.71	140.34	138.53
1	172.98	175.43	175.37	173.02	173.01

^a100.6 MHz ^{13}C NMR spectrum in methanol- d_4 with solvent reference at 49.00 ppm.

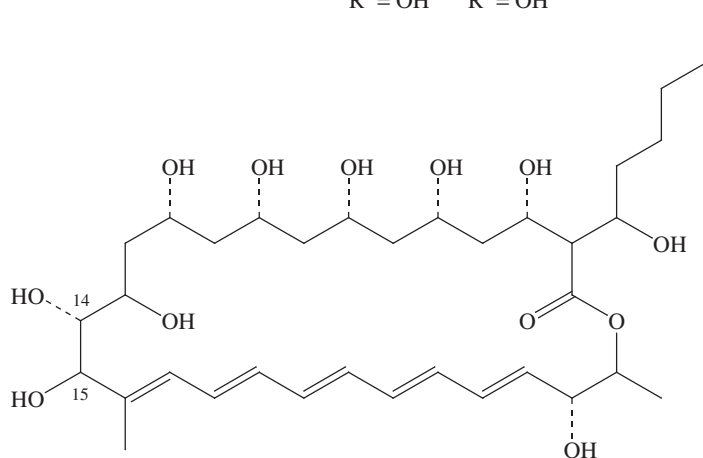
and fungichromin (**54**) should allow stereochemical assignment of isochainin (**58**) and its hydroxylated derivatives **59–61** with reasonable confidence.

Sowinski and coworkers⁴⁰ reported a structure of vacidin A (**63**), an aromatic heptaene macrolide antibiotic. The constitution of vacidin A, a representative of the aromatic heptaene macrolide antibiotics, was established on the basis of ^{13}C and ^1H – ^1H double quantum filtered correlated spectroscopy, rotating frame nuclear Overhauser effect spectroscopy, J -resolved ^1H as well as ^1H – ^{13}C correlation NMR spectra. The geometry of the polyene chromophore was determined as 22*E*, 24*E*, 26*E*, 28*Z*, 30*Z*, 32*E*, 34*E*.

The ^{13}C NMR spectrum of **64**, an amide of **63**, showed sixty-two carbon signals of which partial assignments, shown in Table 16, were made based upon distortionless enhancement by polarization transfer(DEPT), ^1H – ^{13}C correlation experiments and literature data describing ^{13}C NMR analysis of polyene macrolides.



Chainin	(57)	R ¹ = H	R ² = H
Isochainin	(58)	R ¹ = H	R ² = H
	(59)	R ¹ = OH	R ² = H
	(60)	R ¹ = H	R ² = OH
	(61)	R ¹ = OH	R ² = OH

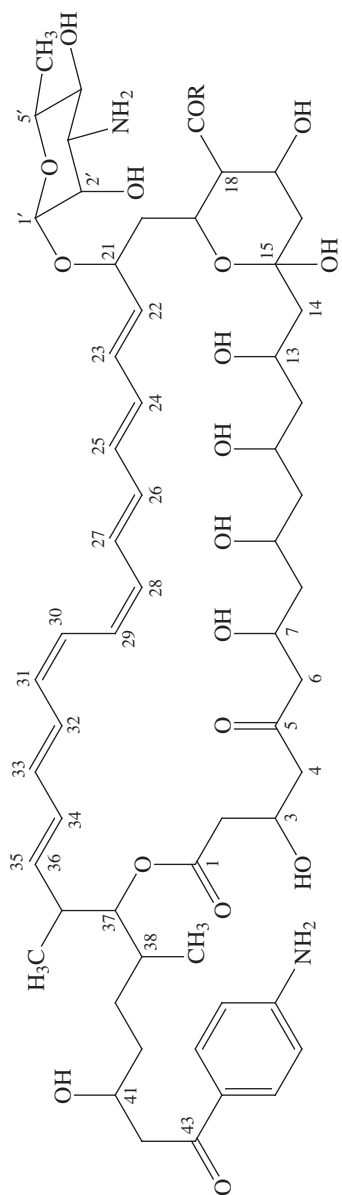


(62a) 14-OH is in a dashed line and 15-OH in a full bond

(62b) 14-OH is in a full line and 15-OH in a dashed bond

The data from ¹H NMR studies of **63**, which included double quantum filtered phase sensitive correlated spectroscopy (DQF-COSY) and rotating frame nuclear Overhauser effect spectroscopy (ROESY) experiments (Figure 12), are collected in Table 17.

The latter, in contrast to nuclear Overhauser enhancement and exchange spectroscopy (NOESY), always feature positive NOEs (negative cross-peaks with respect to diagonal), eliminating known problems of NOEs vanishing or spin diffusion, depending on correlation time, when high field spectrometers are used for measurements of medium-size compounds.

vacidin A (**63**)vacidin A methoxycarbonylmethylamide (**64**)

R = OH

R = NHCH₂COOCH₃

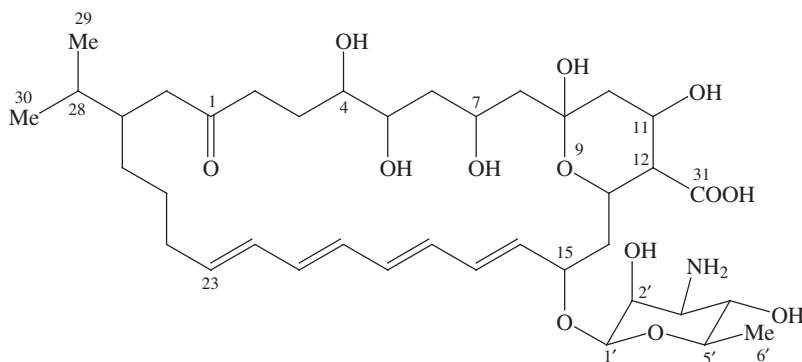
TABLE 16. ^{13}C NMR data for vacidin A methoxycarbonylmethylamide (**64**)

Description	No. of carbon atoms	δ (ppm)	Description	No. of carbon atoms	δ (ppm)
CH ₃	4	13.5, 16.7, 18.6, 52.4	C27		128.58
CH ₂	13	31–52	C28		130.91
CH:			C29		125.53
CHCH ₃	2	34.3, 40.4	C30 (C24)		125.28
CHNH ₂	1	57.9	C31		130.84
CHCONHR	1	59.3	C32		128.62
CHOR	13	64–79	C33 (C23)		134.42
Acetal	1	97.7	C34		133.67
CH Ar	4	113.7, 131.6	C35		137.88
=CH–			Nonprotonated:		
(olefinic) ^a :C22		113.67	Hemiketal	1	98.2
C23 (C33)		130.00	C Ar	2	127.0, 171.2
C24 (C30)		134.80	COXR	3	171.8, 174.6, 174.7
C25		133.10	C=O	2	198.1, 208.9
C26		135.64			

^aAssignment by H, C-COSY. Interchangeable assignments are shown in parentheses.

The coupling constants listed in Table 17 were assigned on the basis of the 1D ^1H NMR spectrum of **63**, but for a few cases the analysis of phase structure of the cross-peaks in the DQF-COSY spectrum was carried out to attribute correct values to the appropriate protons. Also, the analysis of the NOE effects yields the same results (Figure 13).

Hirota and coworkers⁴¹ reported a planar structure of new polyene macrolide antibiotic YS-822A (**65**), which they isolated. ^1H and ^{13}C NMR spectra of **65** showed a number of broad and overlapping signals, but the ^1H – ^1H and ^{13}C – ^1H COSY spectra implied the existence of a mycosamine moiety and several other partial structures. The connectivity of these partial structures was established by extensive 2D NMR experiments, including homonuclear Hartmann–Hahn and heteronuclear multiple-bond connectivity measurements, which led to the determination of the gross planar structure of **65**.



(65) YS-822A

Although 1D ^1H and ^{13}C NMR spectra of **65** in DMSO- d_6 showed a number of broad and overlapping signals, the ^{13}C – ^1H COSY spectrum afforded the assignment

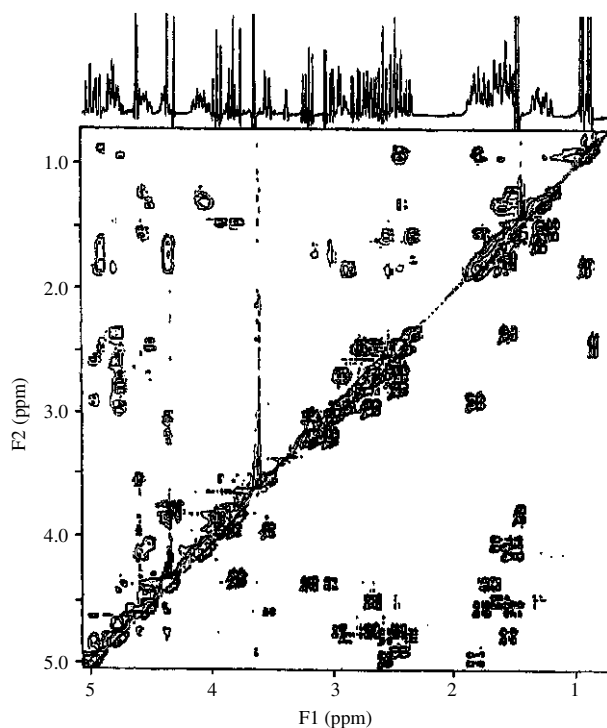


FIGURE 12. Spectra of vacidin A methoxycarbonylmethylamide **64**. Spectral region 0.72–5.06 ppm of 300 MHz ROESY (upper triangle) and DQF-COSY (lower triangle) spectra of VacGlyOMe (15 mg ml^{-1} , pyridine- d_5 -methanol- d_4 , 9 : 1) combined along the diagonal. Reproduced by permission of Japan Antibiotics Research Association from Reference 40

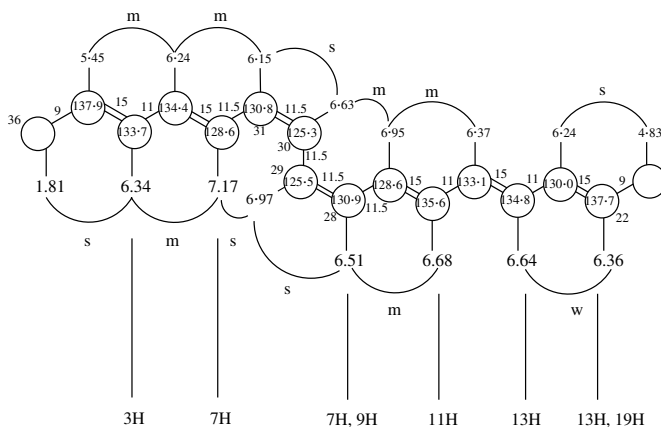


FIGURE 13. Polyene part of vacidin A. NOE's, $J(\text{HH})$ and ^1H , and ^{13}C chemical shifts. Reproduced by permission of Japan Antibiotics Research Association from Reference 40

TABLE 17. ^1H NMR data for the vacidin A and NOE effects^d

No. of proton	δ (ppm)	$J(\text{HH})$ (Hz) (coupling partner)	NOE to protons (intensity)
2a	2.80	15.1 (2b), 3.7 (3)	3 (m)
2b	2.45	15.1 (2a), 9.3 (3)	3 (w)
3	4.78	9.3 (2b), 8.1 (4b), 5.6 (4a), 3.7 (2a)	38-CH ₃ (w), 2a (m), 4a (m), 4b (m), 2b (w), 34 (m)
4a	2.96	17.5 (4b), 5.6 (3)	3 (m), 4b (s)
4b	2.68	17.5 (4a), 8.1 (3)	3 (m), 4a (s)
6a	2.68	16.8 (6b), 9.6 (7)	6b (s), 8a (w)
6b	2.44	16.8 (6a), ~2 (7)	6a (s), 8b (w), 7 (m)
7	4.54	9.6 (6a), 9.6 (8a), ~2 (6b), ~2 (8b)	8b (m), 6b (m), 9 (s), 28(m), 29(m)
8a	1.62	~ 13 (8b), 9.6 (7), 10.0 (9)	6a (w)
8b	1.30	~ 13 (8a), ~2 (7), ~2 (9)	7 (m), ^c (m), 6b (w)
9	4.06	10.0 (8a), 10.0 (10a), ~2 (8b), ~2 (10b)	[10b or 8b] ^c (m), 7 (s), 28 (m)
10a	1.51	~13 (10b), 10.0 (9), 10.3 (11)	
10b	1.27	~13 (10a), ~2 (9), ~2 (11)	^c (m), ^d (m)
11	4.11	10.3 (10a), 10.3 (12a), ~2 (10b), ~2 (12b)	[12b or 10b] ^d (m), 13 (s), 26 (m)
12a	1.51	10.3 (11), 10.5 (13), 13.5 (12b), ~2 (11), ~2 (13), 13.5 (12a)	13 (m), ^d (m)
12b	1.21	10.5 (12a), 10.5 (14a) ^b , 2 (12b), 2 (14b) ^b	12b (m), 14b (w), 11 (s), 23 (w), 22 (m), 24 (m)
14a	1.78	10.5 (13)	16a (w)
14b	1.54	2 (13)	13 (m)
16a	2.35	12.2 (16b), 4.7 (17)	16b (m), 14a (w), 17 (m)
16b	1.56	12.2 (16a), 10.3 (17)	18 (m), 16a (m)
17	4.82	10.3 (16b), 10.3 (18)	16a (m), 18 (m), 19 (m)
18	2.56	10.3 (17), 10.1 (19)	16b (m), 20b (w), 19 (m), 17(m)
19	5.00	10.1 (18), 10.1 (20b) ^b	18 (m), 20 (m), 2' (m), 1' (m), 17 (m), 23 (w), 22 (m)
20a	2.90	~9 (21)	20b (m), 21 (w), 19 (m), 1' (m)
20b	1.82	10.1 (19)	18 (w), 21 (w), 20 (m)
21	4.83	9 (22), ~9 (20a) ^b	20a (w), 20b (w), 1' (s), 23 (s), 22 (m)
22	6.36	9 (21), 15 (23)	19 (m), 21 (m), 24 (w), 13 (m)
23	6.24	11 (24), 15 (22)	19 (w), 21 (s), 13 (w), [24 or 30 or none] ^e (w)
24	6.64	11 (25), 15 (23)	13 (m), 22 (w), ^e (w)
25	6.37	11 (26), 15 (24)	27 (m)
26	6.68	11 (25), 15 (27)	11 (m), 28 (m)
27	6.95	11.5 (28), 15(26)	30 (m), 25 (m)
28	6.51	11.5 (27), 11.5 (29)	7 (m), 9(m), 26 (m), 29 (s)
29	6.97	11.5 (28), 11.5 (30)	7 (m), 28 (s), 32 (s)
30	6.63	11.5 (29), 11.5 (31)	31 (s), 27 (m), [33 or 23 or none] ^e (w)
31	6.15	11.5 (30), 11.5 (32)	33 (m), 30 (s)
32	7.17	11.5 (31), 15 (33)	34 (m), 33 (w), 29 (s)
33	6.24	11 (34), 15 (32)	35 (m), 31 (m), 32 (w), ^e (w)
34	6.34	11 (33), 15 (35)	35 (m), 3 (m), 36 (s), 32 (m)

(continued overleaf)

TABLE 17. (continued)

No. of proton	δ (ppm)	J (HH) (Hz) (coupling partner)	NOE to protons (intensity)
35	5.45	9 (36), 15 (34)	36-CH ₃ (m), 37 (m), 33 (m), 34 (m)
36	1.81	9 (35), 9.8 (37)	38-CH ₃ (m), 36-CH ₃ (m), 38(w), 37 (m), 34 (s)
37	4.94	9.8 (36), 2.2 (38)	36-CH ₃ (m), 38 (m), [40 or 39] ^f (m), 36 (m), 35 (m)
38	1.81	6.7 (39) ^g , 2.2 (37) ^g	36-CH ₃ (m), 38-CH ₃ (m), 36 (w), 37 (m)
39a	1.61		^f (m)
39b			
40a	1.70		^f (m)
40b			
41	4.37	8.1 (42a), 4.2 (42b)	40a/b (m), 42a (m), 42b (m)
42a	3.20	15.6 (42b), 8.1 (41)	41 (m), 42b (s)
42b	3.02	15.6 (42a), 4.2 (41)	41 (m), 42a (s)
36-CH ₃	0.87	6.6 (36)	35 (w), 37 (m), 38 (m), 36 (m)
38-CH ₃	0.94	6.8 (38)	3 (w), 38 (m), [39 or 40] ^f (m), 36 (m)
1'	5.14	~0 (2')	20a (m), 3' (s), 5' (s), 2' (s), 21 (s), 19 (m)
2'	4.63	3.3 (3'), 0 (1')	3' (s), 1' (s), 19 (m)
3'	3.55	9.7 (4'), 3.3 (3')	1' (s), 2' (s)
4'	3.97	9.7 (3'), 9.7 (5')	6' (m)
5'	3.82	9.7 (4'), 5.9 (6')	6' (m), 1' (s)
6'	1.45	5.9 (5')	4' (m), 5' (m)
Aromatic protons	6.81	8.6	
	7.95	8.6	
Glycine methyl ester protons			
OCH ₃	3.66 (s)		
CH ₂	3.81/4.35	17.6	

^aNOE scale: 100% for CH₂CO; 10–20% (w), 20–75% (m), 75–200% (s).

^bThe correct values of coupling constants were attributed to the appropriate protons by the analysis of antiphase structures of cross-peaks in DQF-COSY spectrum.

^cH10a and H8b have nearly the same chemical shifts. NOE between (H10b or/and H8b) and H9.

^dH12b and H10b have nearly the same chemical shifts. NOE between (H12b or/and H10b) and 11-H.

^eThe pairs H23, H33 and H24, H30 have nearly the same chemical shifts. NOE between (H23 or H33) and (H24 or H30).

^fH39 and H40 have nearly the same chemical shifts. NOE between (H39 or/and H40) and H37.

^gValues from ¹H NMR spectrum in 35% DMSO-d₆ in methanol-d₄.

of directly bonded carbons and protons (see Table 18), and the ¹H–¹H COSY (see Figure 14) spectrum implied the existence of several partial structures (A, B, C, D and E) as shown in Figure 15). The presence of mycosamine moiety (a partial structure A) was deduced from ¹H–¹H COSY correlation peaks [H1'(δ 4.55)/H2'(δ 3.80), H2'/H3'(δ 2.92), H3'/H4'(δ 3.22), H4'/H5'(δ 3.32), and H5'/Me6'(δ 1.17)], and comparison of its ¹H and ¹³C chemical shifts. One side of the all-*trans*-tetraene moiety, the presence of which was predicted from the UV spectrum and was confirmed by these NMR spectra, was

TABLE 18. ^{13}C and ^1H NMR data for YS-882A (**65**)

Carbon	^{13}C	^1H	Carbon	^{13}C	^1H
1	173.2 s		20	131.8 d	6.28
2	30.7 t	2.38, 2.52	21	131.5 d	6.15
3	28.1 t	1.65, 1.75	22	130.9 d	5.95
4	72.2 d	3.20	23	133.4 d	5.73
5	72.7 d	3.55	24	29.8 t	1.98, 2.10
6	38.9 t	1.42, 1.58	25	24.4 t	1.20, 1.48
7	67.4 d	4.31	26	29.8 t	1.45, 1.55
8	45.8 t	1.55, 1.61	27	76.0 d	4.78
9	97.0 s		28	31.4 d	1.75
10	44.3 t	1.10, 1.85	29	17.7 q	0.84 (3H, d, $J = 7$ Hz)
11	65.6 d	4.00	30	18.5 q	0.86 (3H, d, $J = 7$ Hz)
12	58.8 d	1.82	31	177.5 s	
13	65.2 d	4.20	1'	95.4 d	4.55
14	36.1 t	1.45, 2.18	2'	67.8 d	3.80
15	74.0 d	4.40	3'	56.2 d	2.92
16	136.2 d	6.05	4'	69.6 d	3.22
17	128.3 d	6.12	5'	72.4 d	3.32
18	132.9 d	6.35	6'	17.9 q	1.17 (3H, d, $J = 6$ Hz)
19	131.2 d	6.20			

attached with a methylene ($\delta_{\text{C}} 29.8$ t, $\delta_{\text{H}} 1.98$ and 2.10), which was in turn connected with a methylene ($\delta_{\text{C}2} 4.4$ t, $\delta_{\text{H}} 1.20$ and 1.48). The other side of the tetraene moiety was connected with a methine ($\delta_{\text{C}7} 4.0$ d, $\delta_{\text{H}} 4.40$; adjacent to an oxygen), and it was probable from the ^1H - ^1H COSY spectrum that this methine was connected with a unit consisting of two methylenes and three methines to compose a partial structure B. The partial structures C and D were also deduced from ^1H - ^1H COSY correlations, even though there were several severely overlapping signals; for example there were 11 proton signals between $\delta_{\text{H}} 1.4$ and 1.8 . The ambiguity and the poor reliability of the assignments and proposed partial structures C and D were dissolved by homonuclear Hartmann-Hahn (HOHAHA) and heteronuclear multiple-bond connectivity (HMBC) spectra. HOHAHA and HMBC measurements not only confirmed the deductions above but also connected all the remaining fragments and quaternary carbons (Figure 16). That is, the distinct correlation peaks of a carbonyl carbon (C1; $\delta 173.2$) with H2 ($\delta 2.38$ and 2.52) and H27 ($\delta 4.78$) appeared on the HMBC spectrum, which established the connection between partial structures C and D through an ester group. In the HOHAHA spectrum, a methine proton at $\delta 4.78$ (H27) showed correlation peaks with protons at $\delta 1.98$ and 2.10 (H24) through 1.45 and 1.55 (H26), and 1.20 and 1.48 (H25), and two methyl protons at $\delta 0.84$ and 0.86 through 1.75 (H28), which not only confirmed the partial structure D but also established the connection between D and B. Correlation peaks between C15 ($\delta 74.0$) and H1' ($\delta 4.55$) and between C31 ($\delta 177.5$) and H12 ($\delta 1.82$) on the HMBC spectrum supported the partial structure E.

YS-822A had nine degrees of unsaturation, all of which have already been assigned to four double bonds, two carbonyls (a lactone and a carboxylic acid) and three rings. Consequently, all the oxygen functional groups at C should be hydroxyls. Thus, the planar structure of YS-822A was determined as **65**.

Gebhard and coworkers⁴² reported a synthesis and spectroscopy of chemically modified spheroidenes. The structure and numbering of the system is shown in **66**. The syntheses and spectroscopic properties of the all-*E* isomers of 11',12'-dihydrospheroidene (**67**),

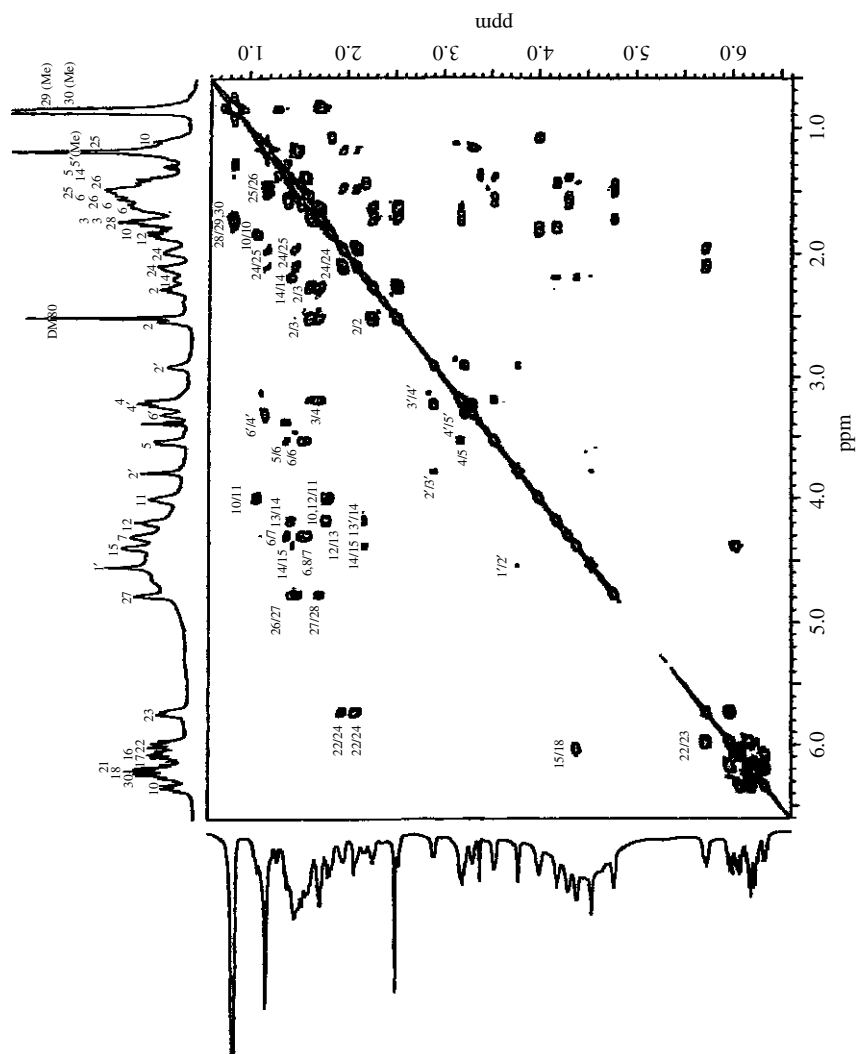


FIGURE 14. ^1H - ^1H COSY spectrum of YS-822A (65) in DMSO-d_6 (300 K). Reproduced by permission of Japan Antibiotics Research Association from Reference 41

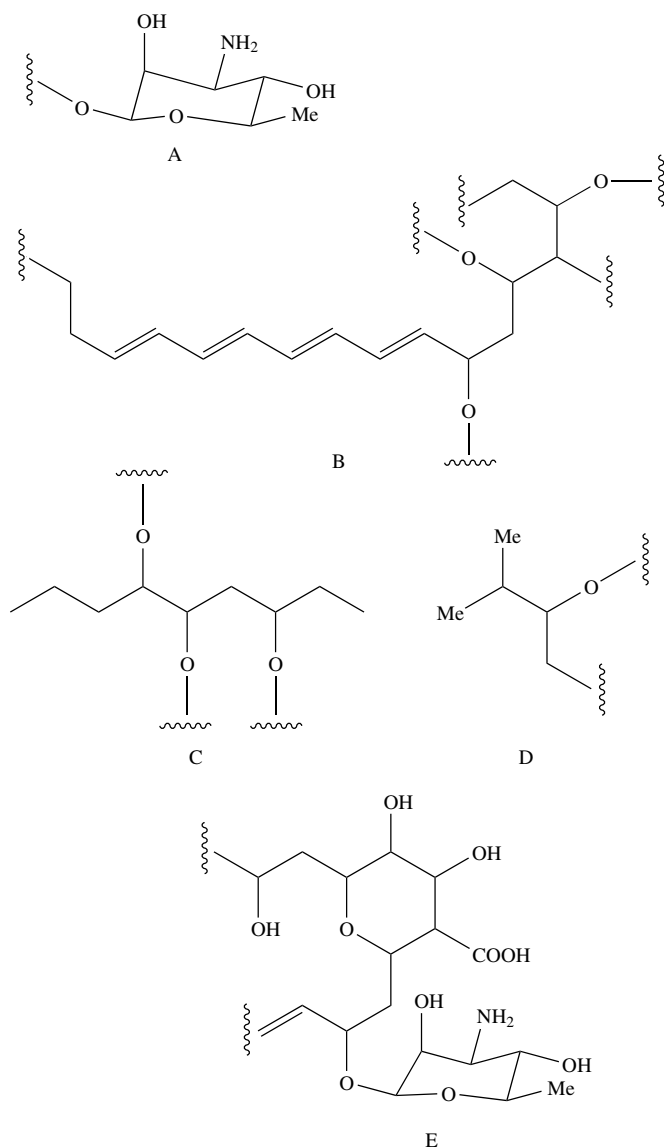


FIGURE 15. Partial structures of YS-822A (**65**). Reproduced by permission of Japan Antibiotics Research Association from Reference 41

3,4,11',12'-tetrahydrospheroidene (**68**), 3,4-dihydrospheroidene (**69**), 3,4,5,6-tetrahydrospheroidene (**70**), 3,4,7,8-tetrahydrospheroidene (**71**) and 15,15'-didehydrospheroidene (**72**) are described.

Spheroidenes **67–71** have the same overall shape as native all-*trans* spheroidene (**66**), which is the carotenoid bound in the photosynthetic reaction center of *Rhodobacter*

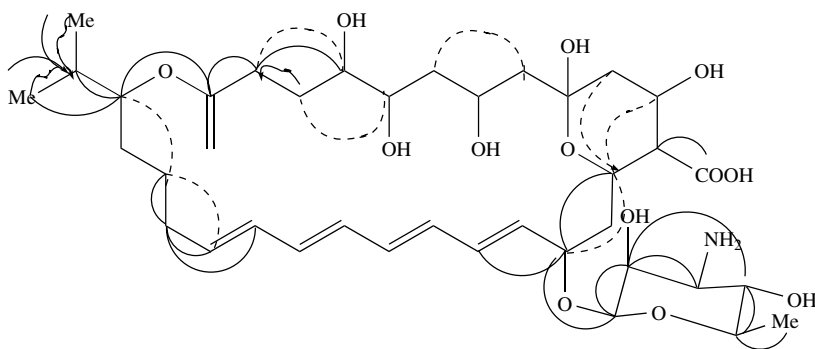


FIGURE 16. Results of HMBC and ^1H - ^1H HOHAHA measurements of YS-822A in DMSO-d_6 (300 K). Solid arrows denote correlation peaks between carbons (tail) and protons (head) in the HMBC spectrum. Dotted lines indicate ^1H - ^1H HOHAHA correlations after removal of ^1H - ^1H COSY ones. Reproduced by permission of Japan Antibiotics Research Association from Reference 41

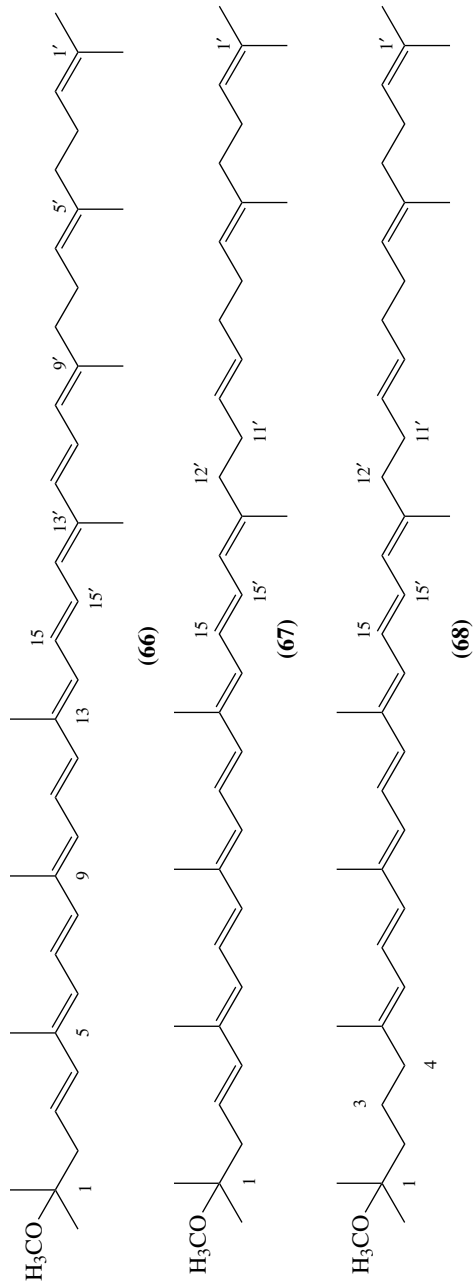
sphaeroides. They have instead polyene chromophores of nine (**69**), eight (**67**, **70**) or seven (**68**, **71**) conjugated double bonds. In **72**, the central double bond is substituted by a triple bond. A detailed analysis of the ^1H and ^{13}C NMR spectra of **66**–**72** has been achieved by mutual comparison.

The 300 MHz ^1H NMR spectra of the all-*E* isomers of **67**–**72** were measured in CDCl_3 . The signals were assigned using the COSY technique. The chemical shift values and the values of the coupling constants are completely in agreement with their all-*trans* structures and are summarized in Tables 19 and 20, respectively, together with the values for **66** which are included for comparison.

As can be seen from Table 19, the saturation between C11' and C12' in **67** causes an upfield shift of H14' (*ca* 0.2 ppm) and of H15 and H15' (*ca* 0.1 ppm) compared with **66**. The remaining polyene protons in **67** are only slightly affected. Similar features are observed upon comparison of the chemical shift values of the protons of the polyene chains of **68**, **69**, **70** and **71** with those of **66**. Thus, saturation of a double bond in a polyene chain generally leads to an upfield shift of *ca* 0.2 ppm for the protons connected to the γ - and the δ -carbons; the upfield shift of the remaining polyene protons is generally less than 0.05 ppm. Comparison of the chemical shift values of **72** with those of **66** shows that the introduction of the 15,15'-triple bond in **72** leads to an upfield shift of the signals of H14 and H14' (*ca* 0.5 ppm), whereas the chemical shift values of the other polyene protons are only slightly affected.

In the ^1H -noise-decoupled 75 MHz ^{13}C NMR spectra of the all-*trans* isomers of **67**–**70** and **72**, the expected 40 different signals are present. In the spectrum of 3,4,7,8-tetrahydro-spheroidene (**71**), only 29 separated signals are observed due to the almost perfect twofold symmetry of the C7–C7' part of the molecule. The signals of the proton-bearing carbon atoms were assigned using the attached proton test (ATP) and the ^{13}C - ^1H correlated technique. The signals of the quaternary carbon atoms were assigned by comparison with the spectrum of **66** and by using chemical shift increments. The ^{13}C chemical shift values of **67**–**72** are completely in agreement with the all-*E* structures of **67**–**72** and are collected with their assignments in Table 21. For comparison, the chemical shift values of **66** and the chemical shift differences between **67**–**72** and **66** are also given.

In the spectrum of **67**, the signals of C11' and C12' (changed to sp^3 hybridization from sp^2) are shifted to the high-field part of the spectrum, i.e. the saturation of the 11', 12'



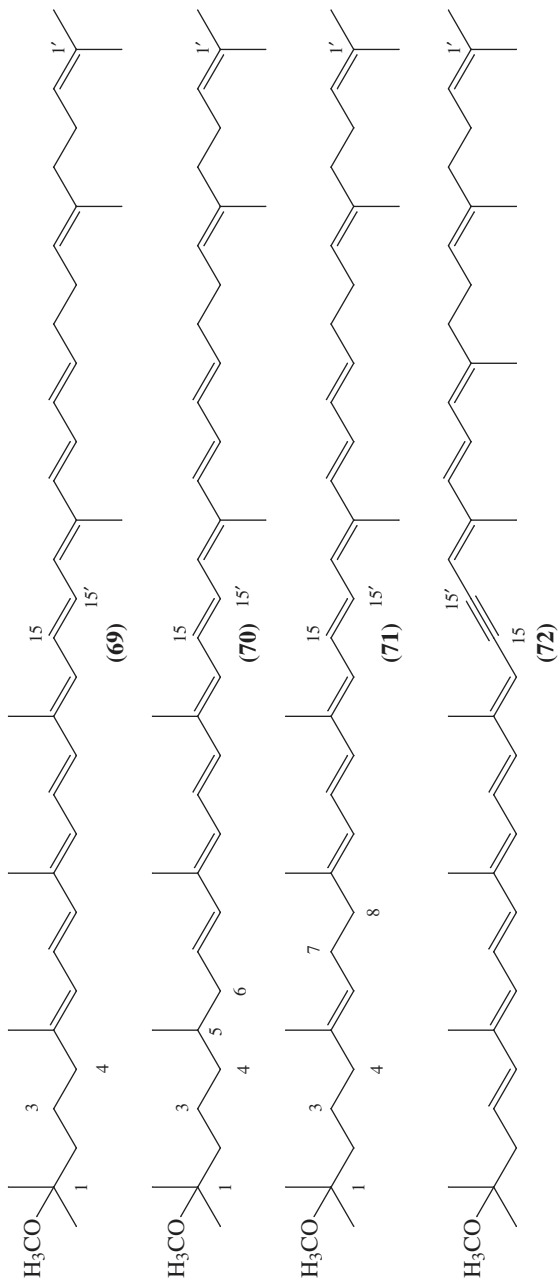


TABLE 19. ^1H NMR chemical shift values (ppm) of all-*E* **66**–**72**^a

H	66	67	68	69	70	71	72
2	2.32	2.32	1.45	1.45	1.30	1.40	2.32
3	5.72	5.71	1.45	1.45	1.30	1.40	5.73
4	6.16	6.15	2.10	2.10	1.15/1.3	1.95	6.16
5	—	—	—	—	1.54	—	—
6	6.11	6.10	5.96	5.95	1.95/2.1	5.12	6.10
			(−0.15)	(−0.16)			
7	6.60	6.58	6.47	6.50	5.69	2.10	6.63
			(−0.13)	(−0.10)	(+0.09)		
8	6.35	6.34	6.24	6.24	6.12	2.10	6.33
			(−0.09)	(−0.09)	(−0.23)		
10	6.22	6.21	6.17	6.18	6.09	5.95	6.19
					(−0.13)	(−0.27)	
11	6.63	6.59	6.59	6.62	6.59	6.48	6.38
						(−0.15)	(+0.07)
12	6.37	6.35	6.34	6.35	6.33	6.24	6.38
						(−0.13)	
14	6.26	6.21	6.19	6.27	6.23	6.19	5.72
			(−0.07)			(−0.07)	(−0.54)
15	6.61	6.49	6.49	6.61	6.60	6.59	—
		(−0.12)	(−0.12)				
15'	6.62	6.49	6.49	6.61	6.60	6.59	—
		(−0.13)	(−0.13)				
14'	6.20	5.98	5.96	6.22	6.19	6.19	5.68
		(−0.22)	(−0.24)				(−0.52)
12'	6.23	2.12	2.12	6.25	6.24	6.24	6.25
11'	6.50	2.05	2.06	6.48	6.50	6.48	6.57
							(+0.07)
10'	5.95	5.10	5.10	5.95	5.95	5.95	5.93
8'	2.12	2.05	2.05	2.10	2.15	2.10	2.05
7'	2.05	2.05	2.05	2.10	2.05	2.10	2.05
6'	5.12	5.10	5.10	5.10	5.12	5.12	5.12
4'	2.05	2.05	2.05	2.10	2.05	2.10	2.05
3'	2.05	2.05	2.05	2.10	2.05	2.10	2.05
2'	5.10	5.10	5.10	5.10	5.10	5.10	5.10
1-(CH ₃)	1.16	1.15	1.14	1.14	1.14	1.13	1.16
5-CH ₃	1.93	1.92	1.81	1.81	0.88	1.61	1.93
			(−0.12)	(−0.12)		(−0.32)	
9-CH ₃	1.98	1.97	1.96	1.96	1.91	1.82	1.99
					(−0.07)	(−0.16)	
13-CH ₃	1.95	1.93	1.94	1.96	1.94	1.94	2.10
							(+0.15)
13'-CH ₃	1.97	1.80	1.81	1.95	1.95	1.94	2.09
		(−0.17)	(−0.16)				(+0.12)
9'-CH ₃	1.82	1.60	1.60	1.82	1.82	1.82	1.83
		(−0.22)	(−0.22)				
5'-CH ₃	1.61	1.60	1.60	1.60	1.61	1.61	1.62
1'-CH ₃ (<i>E</i>)	1.68	1.68	1.68	1.68	1.68	1.68	1.68
1'-CH ₃ (<i>Z</i>)	1.60	1.60	1.60	1.60	1.60	1.60	1.61
OCH ₃	3.25	3.25	3.17	3.17	3.17	3.16	3.23

^aIn parentheses relevant chemical shift differences from **66** of more than ± 0.05 ppm are given.

TABLE 20. Values of the $^1\text{H}-^1\text{H}$ coupling constants as obtained from the spectra of **66**–**72** (*, obtained by spectral simulation; nd, not determined, due to overlap of signals)

$^3J(\text{HH})$	66	67	68	69	70	71	72
H2H1	7.5	7.4	—	—	—	—	7.4
H3H4	15.5	15.6	—	—	—	—	15.8
H6H7	11.9	11.3	10.9	11.3	6.3	—	11.3
H7H8	15.0	14.9	15.2	15.0	15.3	—	15.0
H10H11	11.3	11.3	11.3	11.7	11.2	10.9	11.3
H11H12	14.8	14.8	15.0	14.9	15.5	15.1	14.9
H14H15*	10.7	11.0	11.0	nd	11.5	11.5	—
H15H15 ^{/*}	14.0	14.6	14.6	nd	14.5	14.5	—
H15'H14 ^{/*}	11.0	11.0	11.0	nd	11.5	11.5	—
H13'H11'	15.0	—	—	15.2	15.1	15.1	15.1
$^4J(\text{HH})$							
H14'H15*	nd	-1.1	-1.1	nd	-0.9	-0.9	—
H14H15 ^{/*}	nd	-1.1	-1.1	nd	-0.9	-0.9	—

bond in **67** shows a pronounced effect on the carbon atoms of the polyene chain compared with **66**. C13' is shifted downfield by 3.7 ppm and an upfield shift of 5.6 ppm is observed for C14'. The chemical shift values of the carbon atoms 10, 12, 14, 15' are not affected, while an upfield shift is observed for C9 (0.4 ppm), C11 (0.5 ppm), C13 (0.6 ppm) and C15 (2.2 ppm). The 11', 12' single bond in **67** also affects the chemical shift of the 13'-CH₃ group: it is located 4.2 ppm downfield from the 13'-CH₃ group in **66**. As can be seen in Table 21, similar effects are observed for the chemical shifts of the polyene carbons 3, 4, 5 and 6 upon saturation of the 3, 4 bond, the 5, 6 bond and the 7, 8 bond, respectively. This effect, which has previously been noted for short polyenes, can be generalized as follows: removal of a double bond in a polyene chain leads to a downfield shift of *ca* 4 ppm of the signal of the α -carbon atom. An upfield shift is observed for the chemical shift of the β , δ and ζ olefinic carbon atoms (decreasing with increasing distance), while the chemical shift values of the γ , ϵ and η carbon atoms changed only slightly.

In the ^1H noise-decoupled 75.5 MHz ^{13}C NMR spectrum of **72**, the signals of the sp-hybridized carbon atoms C15 and C15' are found at 98.3 and 97.3 ppm. This is in the expected region for substituted alkynes and the chemical shifts agree very well with those of other didehydrocarotenoids. As can be seen in Table 21, the 15,15'-triple bond leads to an upfield shift of *ca* 22 ppm for the directly connected C14 and C14'. The chemical shifts of the other carbon atoms of the polyene chain are also affected: a downfield shift is observed for the odd carbon atoms and a (slight) upfield shift for the even carbon atoms, both decreasing with increasing distance from the central part.

Hand and coworkers⁴³ reported an effect of electron-donating and electron-withdrawing substituents on ^1H and ^{13}C NMR chemical shifts of novel 7'-aryl-substituted 7'-apo- β -carotenes. Their synthesis, where aryl(Ar) is C₆F₅, 4-O₂NC₆H₄, 4-(MeO₂C)₆H₄, 2,4,6-Me₃C₆H₂, Ph and 4-MeOC₆H₄ (**73a–f**), was described. NMR chemical shifts of all H- and C-nuclei are presented, together with specific examples of the spectra. In contrast to ^1H chemical shifts which, except for HC8' and HC7', did not differ greatly from those of β , β -carotene, considerable variations in ^{13}C chemical shifts were observed.

In **73a–f**, 13 of the 14 olefinic protons give rise to ^1H NMR signals within 0.50 ppm of each other; in the spectrum of **73d** all olefinic signals fall within this range. Thus, even at relatively high frequency (360 MHz), extensive overlap occurs (Figures 17–20).

TABLE 21. ^{13}C NMR chemical shift values (ppm) of all-*E* 66–72^a

C	66	67	68	69	70	71	72
1	75.0	75.0	74.5	74.5	74.6	74.6	75.0
2	43.7	43.7	39.3	39.3	40.0	39.2	43.7
3	125.3	125.2	22.1	22.1	21.3	22.1	125.6 (+0.3)
4	137.5	137.5	40.5	40.5	37.2	40.1	137.5
5	135.2	135.0	139.2 (+4.0)	139.4 (+4.2)	33.5	135.4	135.7 (+0.5)
6	130.6	130.6	125.8 (-4.8)	125.7 (-4.9)	40.7	124.0	130.4
7	124.6	124.4	124.4	124.6	128.8 (+4.2)	26.7	125.3 (+0.7)
8	137.5	137.5	135.4 (-2.1)	135.4 (-2.1)	136.1 (-1.4)	40.2	137.5
9	135.9	135.5 (-0.4)	135.4 (-0.5)	136.0	135.4 (-0.5)	139.5 (+3.6)	137.2 (+1.3)
10	132.6	132.6	131.5 (-1.1)	131.6 (-1.0)	130.1 (-2.5)	125.8 (-6.8)	131.8 (-0.8)
11	124.9	124.4 (-0.5)	124.4 (-0.5)	124.9	124.8	124.9	127.0 (+2.1)
12	138.0	138.1	137.5 (-0.5)	137.4 (-0.6)	137.1 (-0.9)	135.3 (-2.7)	135.6 (-2.4)
13	136.1	135.5 (-0.6)	135.5 (-0.6)	136.1	136.1	136.1	146.3 (+10.3) ^b
14	133.0	132.8	132.5 (-0.5)	132.6 (-0.4)	132.3 (-0.7)	131.4 (-2.6)	111.0 (-22.0)
15	129.4	127.3 (-2.1)	127.3 (2.1)	129.5	129.4	129.5	98.3
15'	130.3	130.3	130.1	130.1	130.0 (-0.3)	129.5 (-0.8)	97.3
14'	131.4	125.8 (-5.6)	125.8 (-5.6)	131.4	131.4	131.4	109.6 (-22.7)
13'	136.6	140.3 (+3.7)	140.2 (+3.6)	136.5	136.4	136.1 (-0.5)	146.3 (+9.8) ^b
12'	135.2	40.2	40.2	135.3	135.3	135.3	133.0 (-2.2)
11'	125.1	26.5	26.5	125.0	125.0	124.9	127.3 (+2.2)
10'	125.8	124.1	124.2	125.8	125.8	125.8	125.3 (-0.5)
9'	139.7	134.9	134.9	139.7	139.6	139.5	141.5 (+1.8)
8'	40.2	39.7	39.7	40.2	40.2	40.2	40.2
7'	26.7	26.7	26.7	26.7	26.7	26.7	26.7
6'	123.9	123.7	123.8	123.8	123.8	123.9	123.7
5'	135.3	135.0	135.0	135.4	135.4	135.4	135.5
4'	39.7	39.7	39.7	39.7	39.7	39.7	39.7
3'	26.6	26.6	26.6	26.6	26.6	26.6	26.5
2'	124.3	124.3	124.4	124.3	124.3	124.3	124.3
1'	131.3	131.2	131.2	131.3	131.3	131.3	131.3
1-(CH ₃) ₂	24.9	24.9	25.0	25.0	25.0	25.0	24.9
5-CH ₃	13.0	13.0	16.9 (+3.9)	16.8	19.6 (+6.6)	15.9	13.0

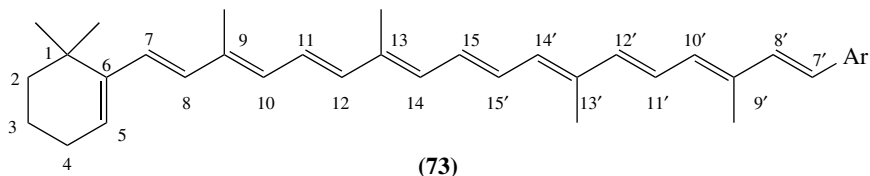
(continued overleaf)

TABLE 21. (continued)

C	66	67	68	69	70	71	72
9-CH ₃	12.9	12.8	12.8	12.8	13.0	17.0 (+4.1)	12.9
13-CH ₃	12.8	12.6	12.7	12.9	12.8	12.8	15.3
13'-CH ₃	12.7	16.9 (+4.2)	16.8 (+4.1)	12.8	12.8	12.8	15.3
9'-CH ₃	17.0	16.0	16.0	17.0	17.0	17.0	17.1
5'-CH ₃	16.0	16.0	16.0	16.0	16.0	16.0	16.0
1'-CH ₃	25.7	25.7	25.7	25.7	25.7	25.7	17.7
(E)							
1'-CH ₃	17.7	17.6	17.7	17.7	17.7	17.7	25.7
(Z)							
OCH ₃	49.3	49.3	49.1	49.1	49.1	49.1	49.3

^aIn parentheses relevant chemical shift differences from **66** of more than ± 0.03 ppm are given.

^bMight be interchanged.



- (a) Ar = C₆F₅, (b) Ar = 4-O₂NC₆H₄, (c) Ar = 4-(MeO₂CC₆H₄), (d) Ar = 2,4,6-Me₃C₆H₂,
 (e) Ar = Ph, (f) Ar = 4-MeOC₆H₄

The spectrum of the ester **73c** is similar to that of the unsubstituted phenyl compound **73e** (both not shown). It is noted that the chemical shift of the HC8' reflects the electron-withdrawing properties of the substituents. A combination of 1D and 2D techniques is used to establish the assignments shown, and the chemical shift changes as compared to β , β -carotene are listed in Tables 22 and 23.

Chemical shifts of compounds **73a**, **73d** and **73f** were deduced as described for **73b**. Comparison of the data reveals certain trends that were then utilized in the analyses of the spectra of **73c** and **73e**, for which HMBC spectra were not determined. First, apparent first-order coupling constants of corresponding protons are similar; approximate values are: $J(7, 8; 7', 8')$, *ca* 16; $J(10, 11; 10', 11')$, *ca* 10–12; $J(11, 12; 11', 12')$, *ca* 15; $J(14, 15; 14', 15')$, *ca* 10; and $J(15, 15')$, *ca* 14 Hz. Except for $J(7, 8)$, the coupling constants $J(11, 12; 11', 12')$ are considerably larger than the others, so that the doublets due to HC12, HC12', and HC10' can be identified, even in regions of overlap. Second, for the paired doublets of HC7'/HC8' in compounds **73a**, **73b**, **73f** the chemical shift of HC8' is greater than that of HC7'. Third, for a given pair with nonprimed and corresponding primed C-nuclei, δ (no *n*-primed) > δ (primed) for odd-numbered C-nuclei, whereas the opposite is true for even-numbered C-nuclei. That is, those atoms that bear a formal positive charge in the resonance structures, i.e. $-[C(\beta)^{\delta+} = C(\alpha)-]_n - Ar^{\delta-}$, are deshielded; the others are shielded. Fourth, compared with β , β -carotene, C $_{\beta}$ atoms are in general deshielded (Table 23), while C $_{\alpha}$ nuclei are shielded. Both effects decrease in a regular, albeit nonlinear manner similar to the shift changes reported for apo- β -carotenals. Exceptions are the chemical shifts of C7' and C8', which are subject to anisotropy effects

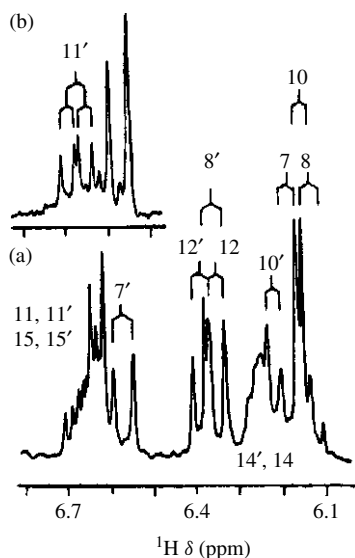


FIGURE 17. ^1H NMR spectra of **73d** (ca 25 mg ml^{-1} CDCl_3): (a) olefinic region and (b) NOE difference spectrum (irradiation at 2.06 ppm). Reproduced by permission of Neue Schweizerische Chemische Gesellschaft from Reference 43

(of the Ar substituent) that differ from those in β,β -carotene. The fact that all substituents, whether electron-donating or electron-withdrawing in the classical sense, cause shifts in the same direction suggests that in the polyene chain C electron densities are similar. Correlations of ^{13}C chemical shifts and electron densities (AM1 calculation) in these compounds was investigated.

^1H NMR data of a minor isomer of **73e** are consistent with the (7'Z)-structure that is expected on chemical grounds. Thus, the observed highfield shift of one CH_3 signal (1.70 vs 2.05 ppm) is expected if Me-C9' lies above the plane of the Ph ring.

Further, the doublets due to HC7' and HC8' in the (E)-isomer (6.57 and 6.90 ppm) are shifted upfield (6.43 and 6.27 ppm) in the (Z)-isomer, as is observed in the spectra of other (E/Z)-isomers.

Yamagishi and coworkers⁴⁴ reported a structure determination of rumbrin **74**, a new cytoprotective substance. Its structure was elucidated by NMR spectral analysis and was found to possess a novel skeleton containing α -pyrone, tetraene and pyrrole moieties.

The ^1H NMR spectrum of **74** (Figure 21) showed 14 signals, which were attributed to two singlet CH_3 (δ_{H} 1.92 and 2.05), one OCH_3 (δ_{H} 3.95), one imine (δ_{H} 11.44) and 10 olefinic methine protons. The ^{13}C NMR spectrum of **74** showed signals for 20 carbons. The distortionless enhancement by polarization transfer (DEPT) experiment assigned them to 3 methyl, 10 sp^2 methine and 7 quaternary carbons including one ester carbonyl carbon (C18) and two-oxygenated sp^2 carbons (C14 and C16). The ^1H - ^1H COSY spectrum established a tetraene structure composed of C6-C12 with E geometrical configurations for the C6-C7, C8-C9 and C10-C11 double bonds, which are apparent from the coupling constants [$J(6, 7) = 15.0\text{ Hz}$, $J(8, 9) = 14.5\text{ Hz}$ and $J(10, 11) = 14.0\text{ Hz}$]. HMBC experiment on **74** showed long-range couplings of 19-CH to C13 (δ_{C} 124.8) and C14 (δ_{C} 159.1), 21 CH_3 to C16 (δ_{C} 165.7), C17 (δ_{C} 100.3) and C18 (δ_{C} 163.4), 20- OCH_3 to

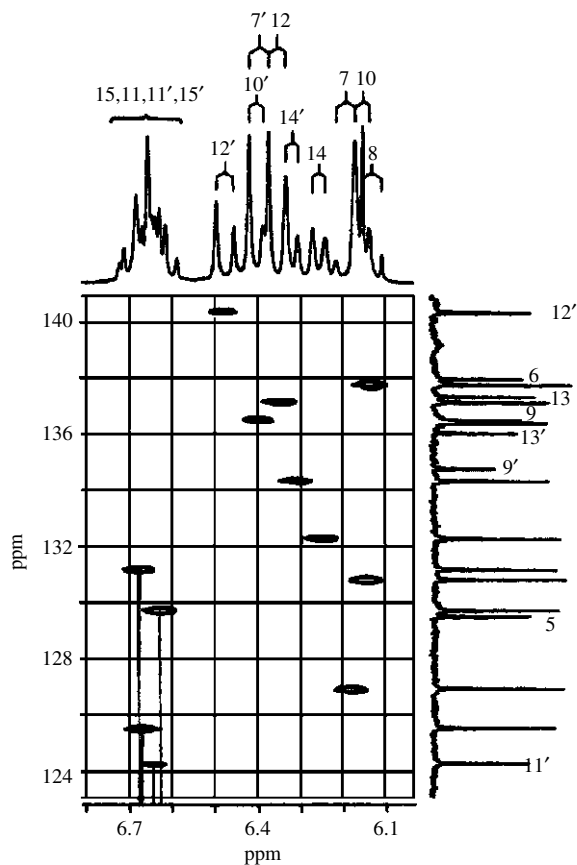


FIGURE 18. Selected portion of a HETCOR plot of **73a** ($13 \text{ mg ml}^{-1} \text{ CDCl}_3$). Projections along the axes are 1D spectra obtained at 360 MHz for ^1H and 90 MHz for ^{13}C . The spectra contain additional olefinic signals at 141.76(C(8')), 110.81(C(7')) and 7.18 (d, H-C(8')) ppm. Reproduced by permission of Neue Schweizerische Chemische Gesellschaft from Reference 43

C16 and H15 to C13, C14 and C17. These correlations established the connectivities of C13–C18. Taking into consideration the number of oxygen atoms contained in **74** and the chemical shifts of C14 and C18, one oxygen atom must be inserted between C14 and C18. Thus, the existence of an α -pyrone unit in **74** was confirmed, as shown in Figure 22.

The HMBC experiment also showed long-range couplings of 19-CH₃ to C12 (δ_{C} 134.7), C13 (δ_{C} 124.8) and C14. Thus, the tetraene and the α -pyrone units are linked through C13 (Figure 22). The diagnostic ^{13}C chemical shift for C19 (δ_{C} 21.1) and NOE between H12 and 19-CH₃ defined the configuration of the C12–C13 double bond as *Z*.

In the ^1H – ^1H COSY spectrum, cross peaks were observed among the two methine protons H2 (δ_{H} 6.90, $J = 2.6, 3.0 \text{ Hz}$) and H3 (δ_{H} 6.13, $J = 2.3, 3.0 \text{ Hz}$) and an imine proton (δ_{H} 11.44, $J = 2.3, 2.6 \text{ Hz}$). In addition, long-range couplings were observed from H3 to C2 (δ_{C} 120.2) and C4 (δ_{C} 111.5), H2 to C3 (δ_{C} 109.0), C4 and C5 (δ_{C} 125.9), H6 to C4 and H7 to C5 in the HMBC experiment. These couplings indicated the presence

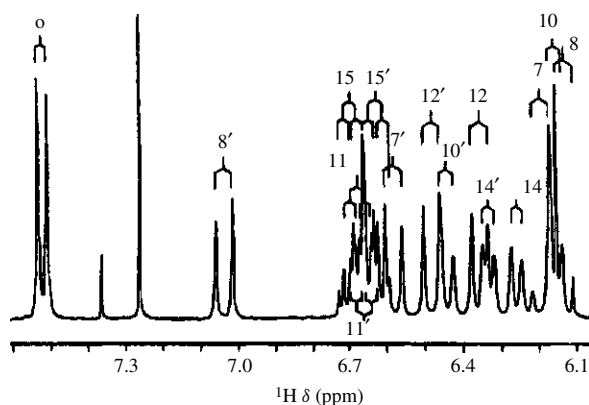


FIGURE 19. Selected portion of the ^1H NMR spectrum of **73b** (18 mg ml^{-1} CDCl_3). The d due to $\text{H}-\text{C}(3')$ and $\text{H}-\text{C}(5')$ (8.17 ppm) is not shown. Reproduced by permission of Neue Schweizerische Chemische Gesellschaft from Reference 43

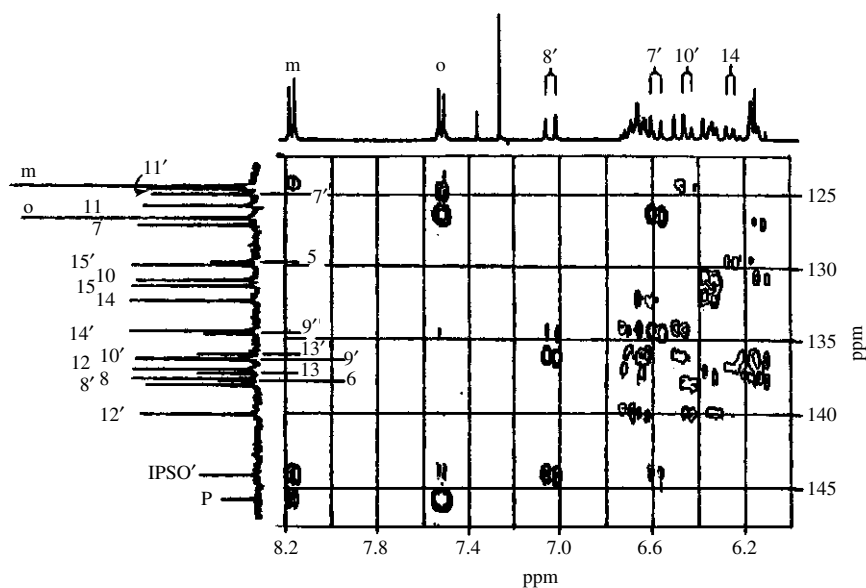


FIGURE 20. Contour plot of a selected portion of the ^{13}C , ^1H HMBC spectrum of **73b** (20 mg ml^{-1} CDCl_3). Projections along the axes are 1D spectra obtained at 360 MHz for ^1H and 90 MHz for ^{13}C . Reproduced by permission of Neue Schweizerische Chemische Gesellschaft from Reference 43

of a 2,3-disubstituted pyrrole ring consisting of $\text{C}2-\text{C}5$, and the linkage to the tetraene unit at $\text{C}5$. Therefore, attachment of the chlorine atom to the quaternary carbon $\text{C}4$ was deduced (Figure 22). Based on all these findings, the total structure of **74** was established to be (1*Z*, 3*E*, 5*E*, 7*E*)-6-(8-(3-chloro- ^1H -pyrrol-2-yl)-1,3,5,7-octatetraenyl)-4-methoxy-3-methyl-2*H*-pyran-2-one.

TABLE 22. ^1H NMR chemical shift differences (ppm) of olefinic protons of (all-*E*)-7'-aryl-7'-apo- β -carotens and β,β -carotene^a

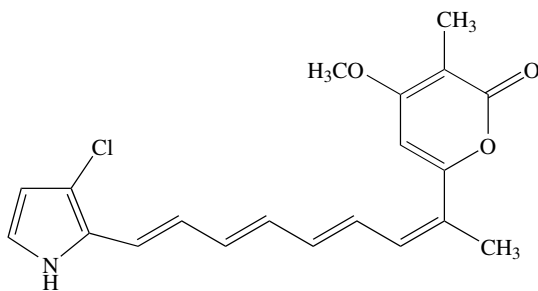
Hydrogen	73a	73b	73c	73d	73e	73f
HC15	0.05	0.07	0.03	-0.01	0.00	0.00
HC14'	0.06	0.07	0.05	0.00	0.01	-0.01
HC12'	0.11	0.12	0.08	0.02	0.06	0.03
HC11'	-0.01	0.00	0.00	0.01	0.00	0.01
HC10'	0.24	0.28	0.22	0.05	0.17	0.14
HC8'	1.04	0.90	0.84	0.21	0.76	0.63
HC7'	0.19	0.38	0.38	0.37	0.37	0.34

^aIn the symmetrical β,β -carotene, δ values of primed and nonprimed atoms are identical. Other chemical shifts of 73a-d were the same (± 0.01 ppm) as those reported for β,β -carotene, except for Me-C(9'): 73a, 2.03; 73b, 2.05; 73c, 2.04; 73d, 2.06; 73e, 2.05; 73f, 2.03; β,β -carotene, 1.98 ppm.

TABLE 23. ^{13}C NMR chemical shift differences (ppm) of compounds 73a-f (all-*E*) and β,β -carotene^a

Carbon	73a	73b	73c	73d	73e	73f
C7'	-15.93	-2.01	-0.69	-1.10	+0.61	+0.22
C9'	-1.30	-1.45	-1.03	-0.48	-0.61	-0.36
C11'	-0.86	-0.74	-0.48	-0.32	-0.25	-0.10
C13'	-0.50	-0.48	-0.34	-0.19	-0.18	-0.07
C15'	-0.38	-0.38	-0.26	-0.15	-0.16	-0.10
C14	-0.22	-0.23	-0.14	-0.07	-0.09	-0.04
C12	-0.22	-0.25	-0.17	-0.09	-0.13	-0.09
C10	-0.11	-0.13	-0.09	-0.05	-0.07	-0.05
C8	-0.09	-0.12	-0.08	-0.05	-0.07	-0.06
C6	-0.14	-0.17	-0.14	-0.09	-0.15	-0.14
C5	0.10	0.11	0.07	0.00	0.04	+0.02
C7	0.16	0.17	0.09	-0.04	0.00	-0.04
C9	0.41	0.37	0.23	0.04	0.11	0.05
C11	0.40	0.43	0.26	0.04	0.10	0.02
C13	0.80	0.85	0.55	0.15	0.27	0.13
C15	1.07	1.11	0.74	0.21	0.34	0.14
C14'	1.83	1.91	1.30	0.41	0.69	0.39
C12'	3.00	2.90	1.96	0.67	0.99	0.45
C10'	5.48	5.44	3.95	1.24	2.33	1.37
C8'	3.94	0.34	-1.66	0.71	-4.17	-6.09

^aNegative values indicate upfield shifts, compared to those of β,β -carotene, except that values of C9 and C13 are interchanged.



(74)

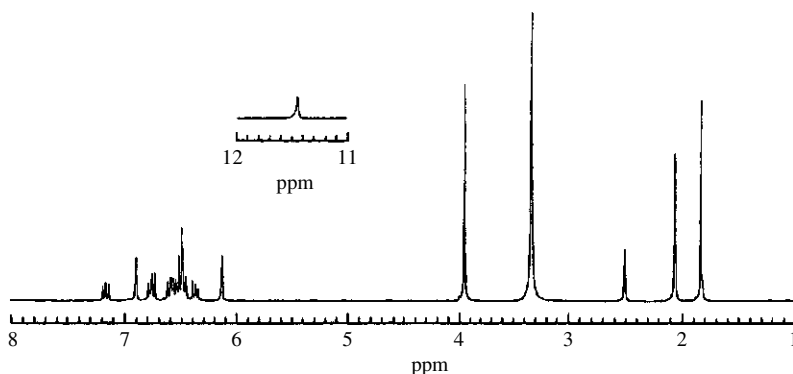


FIGURE 21. The 500 MHz ^1H NMR spectrum of rumbrin in DMSO-d_6 . Reproduced by permission of Japan Antibiotics Research Association from Reference 44

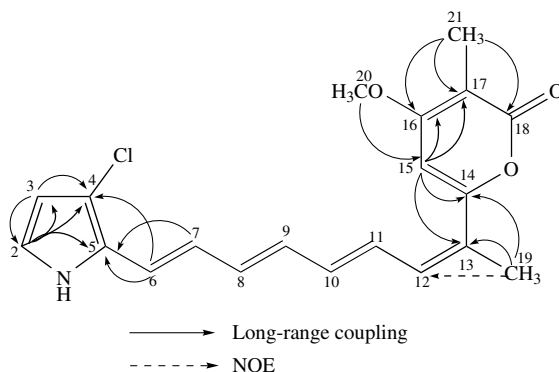


FIGURE 22. ^1H - ^{13}C long-range couplings and NOE of rumbrin (**74**). Reproduced by permission of Japan Antibiotics Research Association from Reference 44

In the ^1H - ^{13}C COSY spectrum, the olefinic carbon signals could not be unambiguously assigned because of the overlapping of their proton signals. Therefore, these carbons were assigned and the structure of **74** was confirmed using $^1J(\text{CC})$ information⁴⁴. The biosynthetic origin of the polyene and α -pyrone units was expected to be mainly acetate. Thus, an incorporation experiment with $[1,2-^{13}\text{C}_2]$ acetate was carried out with a culture of *A. umbrium* n13. By adding 1 g of sodium $[1,2-^{13}\text{C}_2]$ acetate 48 hours after the beginning of a 1-liter culture, 4 mg of labeled **74** were obtained. A 2D INADEQUATE experiment using this sample confirmed the structure of **74** and the assignments of all sp^2 carbons (Figure 23). The complete carbon and proton assignment is given in Table 24.

Chatterjee and coworkers⁴⁵ recently reported the taxonomy, production, isolation, structure elucidation and biological properties of a new antibacterial antibiotic alisamycin (**75**), a new member of the manumycin group of antibiotics obtained by the fermentation of *Streptomyces actuosus*.

Table 25 summarizes the ^1H and ^{13}C NMR spectra of **75**. The proton resonances were analyzed by double quantum filtered H-H shift-correlated COSY spectrum and

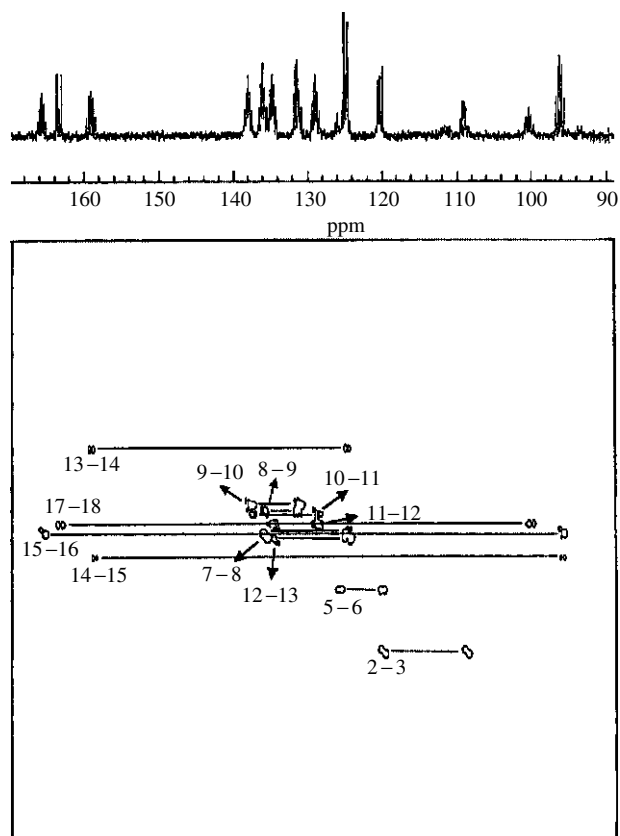


FIGURE 23. 2D INADEQUATE spectrum of $[1,2-^{13}\text{C}_2]$ acetate labeled rumbrin. Reproduced by permission of Japan Antibiotics Research Association from Reference 44

the carbon resonances were assigned by a proton-detected CH shift-correlated multiple quantum coherence (HMQC) NMR experiment. The spectral properties showed strong similarities to those reported for the manumycin group of antibiotics. From the COSY spectrum recorded in CDCl_3 , four spin systems could be extracted including a conjugated diene moiety attached to a methine multiplet ($\text{H6}'$, $\delta 2.10$) being part of a cyclohexane unit, one isolated triene moiety, three signals from the 5-epoxycyclohex-2-enone and two strongly coupled signals representing four protons.

In CDCl_3 , **75** also revealed the presence of four D_2O exchangeable singlets at $\delta 13.52$, 7.58, 7.54 and 3.25 corresponding to one enolic hydroxyl, two amides and a hydroxy proton, respectively. On addition of DMSO-d_6 as co-solvent, the first three signals underwent large downfield shifts to $\delta 14.00$, 9.60 and 8.45, respectively, and the fourth one was not observed. The amide singlet at $\delta 7.54$ showed COSY correlation to $\text{H2}'$ ($\delta 5.84$) and also to the H3 ($\delta 7.40$) which, in turn, showed coupling ($J = 2.6$ Hz) to the epoxy proton H5 . All these observations were suggestive of a carboxamide group linking the diene unit to the epoxycyclohexenone. A full confirmation was obtained by a proton-detected long-range CH shift correlation (HMBC)NMR experiment (Table 25). Thus this amide proton

TABLE 24. The 500-MHz ^1H NMR and 125-MHz ^{13}C NMR spectral data for rumbrin in DMSO- d_6^a

Position	δ_{H}	δ_{C}
1-NH	11.44 (dd 2.3, 2.6)	
2	6.90 (dd 2.6, 3.0)	120.2(d)
3	6.13 (dd 2.3, 3.0)	109.0(d)
4		111.5(s)
5		125.9(s)
6	6.49 (d 15.0)	120.2(d)
7	6.75 (dd 11.0, 15.0)	124.8(d)
8	6.59 (dd 11.0, 14.5)	135.9(d)
9	6.37 (dd 11.3, 14.5)	131.3(d)
10	6.54 (dd 11.3, 14.0)	137.9(d)
11	7.16 (dd 12.5, 14.0)	128.9(d)
12	6.47 (d 12.5)	134.7(d)
13		124.8(s)
14		159.1(s)
15	6.50 (s)	96.2(d)
16		165.7(s)
17		100.3(s)
18		163.4(s)
19	2.05 (s)	21.1(q)
20	3.95 (s)	56.6(q)
21	1.92 (s)	8.5(q)

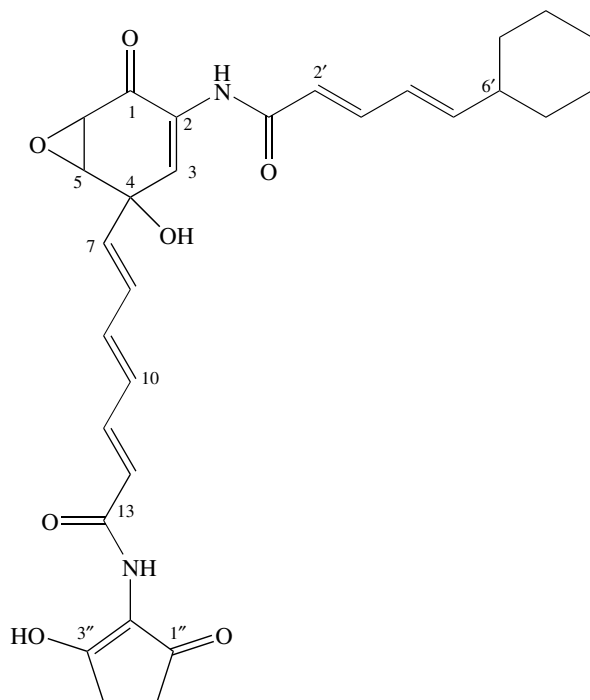
^aCoupling constants in $J(\text{Hz})$ are given in parentheses.

showed $^3J(\text{CH})$ correlation to C3 (δ 126.36), C1 (δ 188.63); and $^2J(\text{CH})$ correlation to C1' (δ 165.16), and could thereby be assigned to the 2-NH proton. The more downfield amide proton showed an exchange cross peak with the enolic proton in the NOESY spectrum and it also showed long-range COSY correlation with the H11 proton (δ 7.32).

In the HMBC spectrum this NH proton exhibited $^3J(\text{CH})$ correlation to the C3'' (δ 174.15) and $^2J(\text{CH})$ interaction to the C13 (δ 165.48) carbonyl, the latter in turn showing $^2J(\text{CH})$ interaction with H12(δ 6.05). Thus it became clear that a carboxamide group linked the conjugated triene and the cyclopentenone unit. A $^2J(\text{CH})$ coupling of the triene terminus H7 to C4 ($\delta_{\text{H}}/\delta_{\text{C}}$ 5.86/71.20) established the point of attachment of the triene unit to C4. An observed NOE interaction between the H7 and H5 lent further support to this attachment and was suggestive of proximal orientation of the *trans*- Δ^7 bond to the epoxy unit in the most preferred conformation. The absolute configuration at C4 was not established.

The double bond geometries were determined by coupling constant measurements as well as NOE studies. Large coupling constant values (14–15 Hz) observed for H12 and H2' established *E*-configuration of the corresponding double bonds. The olefinic protons H8/H9 and H4'/H5' are isochronous, appearing at δ 6.58 and 6.12, respectively, and their coupling constant values could not be measured by simple analysis of the ^1H NMR spectrum (Figure 24).

The problem of strong coupling could be resolved by simulating all the olefinic signals with the LAOCOON program and the best fitting values were taken. These values confirmed *E*-configuration for all the five disubstituted double bonds of **75**. Most of the olefinic protons also exhibited long-range couplings (Table 25). The *E*-configurations of the double bonds were further corroborated by the NOE network (Figure 24) as revealed



(75)

in a phase-sensitive 2D NOESY spectrum (300 MHz, CDCl_3 - DMSO-d_6 , 500 ms mixing time with 4% random variation).

Imai and coworkers⁴⁶ reported a structural study of lagunamycin (**76**), a novel 5-lipoxygenase inhibitor which is isolated from the culture filtrate of *Streptomyces sp.* AA0310 and showed inhibitory activity against 5-lipoxygenases and antibacterial activity against Gram-positive bacteria. The structure of **76** has been elucidated to be 6-diazo-4-[(*E*)-4,6-dimethyl-2-hepten-2-yl]-3-methyl-2,5,7,8-tetraoxoquinoline by a combination of chemical degradations and NMR studies.

The ^{13}C and ^1H NMR data are summarized in Table 26. All one-bond ^1H - ^{13}C connectivities were determined by a ^{13}C - ^1H COSY experiment. ^1H - ^1H COSY, NOESY and long-range ^{13}C - ^1H COSY experiments indicated a partial structure of $\text{C}_{13}\text{H}_{21}\text{NO}$ containing an amide as depicted in Figure 25. The geometry of the double bond (2',3') was established as *E* by measurement of the $^3J(\text{CH})$ value (8.3 Hz) between $\text{C}1'$ and $\text{H}3'$ in a nondecoupled ^{13}C NMR spectrum.

The lower field ^{13}C NMR signals of **76** suggested a substituted pyridone (δ 116.3 s, 130.0 s, 138.6 s, 151.4 s and 161.3 s) and a 2-diazo-3-oxo-1,4-benzoquinone (887.5 s, 168.8 s, 172.5 s and 173.6 s) moiety by comparison with the reported values of diazaquinomycin A and 2-diazo-3-oxo-1,4-naphthoquinone, respectively. Similar stabilities of 1- and 2-diazo-3-oxo-1,4-naphthoquinone under acidic conditions indicated the presence of a diazo group in **76**. By combining these results, the structure of **76** was assigned.

Seto and coworkers⁴⁷ reported a study on viridenomycin (**77**), a novel 24-membered macrocyclic polyene lactam antibiotic. A new antitumor antibiotic, designated AL081,

TABLE 25. ^{13}C (67.5 MHz) and (400 MHz) ^1H NMR spectral data of alisamicin (**75**) (CDCl_3 , 303 K)^a

Position	δ_{C}^b	^1H		
		δ (multiplicity, J in Hz)	HMBC partner	
			$^2J(\text{CH})$	$^3J(\text{CH})$
1	188.63	—		
2	128.08	—		
3	126.36	7.40 (d, 2.6)	C2	C1
4	71.20	—		
5	57.41	3.70 (dd, 2.6, 3.6)	C4	C7
6	52.93	3.65 (d, 3.6)	C1, C5	C2
7	136.29	5.86 (dd, 14.5, 0.3)		C3, C9
8	131.58	6.58 (dd, 11.3, 14.5)		
9	139.52	6.58 (dd, 14.8, 11.3)		
10	131.74	6.42 (ddd, 11.2, 14.8, 0.3)		
11	143.45	7.32 (dd, 11.2, 14.7)		C13
12	121.59	6.05 (d, 14.7)	C13	C10
13	165.48	—		
1'	165.16	—		
2'	120.95	5.84 (d, 14.8)	C1'	
3'	144.16	7.22 (ddm, 14.8, 10.5)		
4'	125.52	6.12 (dd, 10.5, 15.5)	C3'	
5'	150.76	6.12 (m)		C3'
6'	41.13	2.10 (m)		
7', 11'	32.25	1.76 (m) (eq), 1.13, (m) (ax)		
8', 10'	25.80	1.73 (m) (eq), 1.28 (m) (ax)		
9'	26.00	1.67 (m) (eq), 1.18 (m) (ax)		
1''	197.39	—		
2''	115.01	—		
3''	174.15	—		
4''	32.14	2.61 (m)		
5''	25.65	2.53 (m)		
3''-OH	—	13.52 (s)		
4-OH	—	3.25 (s)		
2-NH	—	7.54 (s)	C1'	C1, C3
13-NH	—	7.58 (s)	C13	C3''

^aThe ^1H and ^{13}C chemical shifts are in ppm from $(\text{CH}_3)_4\text{Si}$ and CDCl_3 as internal standards, respectively.

^bThe carbon multiplicities were determined by DEPT-135 experiment.

was obtained from the culture filtrate of an actinomycete identified as *Streptomyces ganmycius*, and found to be identical with **77** by direct comparison.

The structure was determined by NMR spectral analysis including a variety of two-dimensional NMR techniques. The 500-MHz ^1H NMR spectrum of **77** taken in CDCl_3 (Figure 26) revealed the presence of 5 aromatic protons, 15 olefinic protons, a methoxy ($\delta 3.65$), an allylic methyl ($\delta 2.14$) and a tertiary methyl group ($\delta 1.33$). The ^{13}C NMR spectrum showed signals due to all 34 carbons, which were assigned to 7 quaternary carbons, 23 methines, 1 methylene and 3 methyls by DEPT experiments. The ^{13}C and ^1H NMR spectral data are summarized in Table 27.

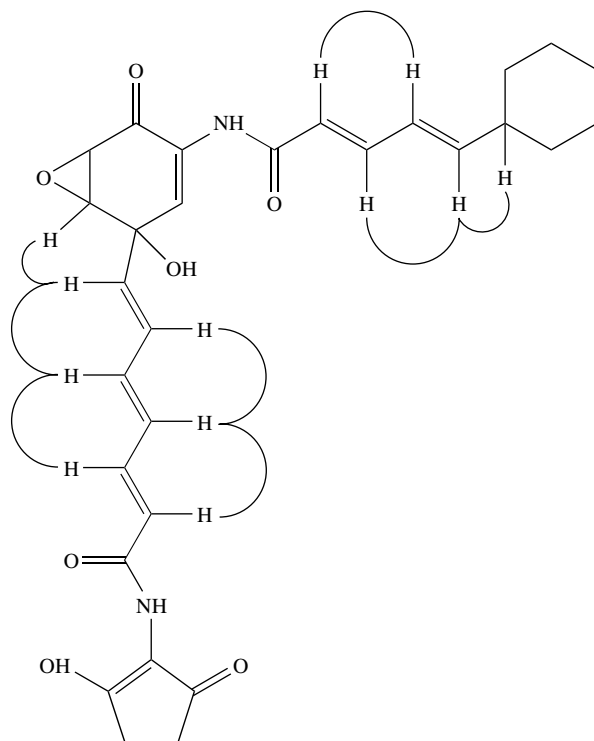


FIGURE 24. NOE network of alisamycin (**75**). Reproduced by permission of Japan Antibiotics Research Association from Reference 45

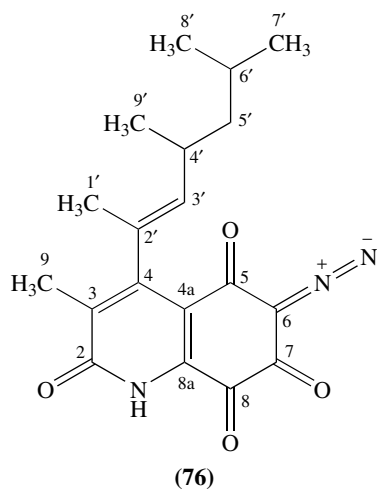


TABLE 26. ^{13}C and ^1H NMR spectra of lagunamycin (**76**) in CDCl_3

Atom	^{13}C	^1H
1		9.60 (1H, s)
2	161.3 (s)	
3	130.0 (s)	
4	151.4 (s)	
4a	116.3 (s)	
5	173.6 (s)	
6	87.5 (s)	
7	168.8 (s)	
8	172.5 (s)	
8a	138.6 (s)	
9	14.0 (q)	2.18 (3H, s)
1'	16.8 (q)	1.90 (3H, d, $J = 1.3$)
2'	137.4 (s)	
3'	135.0 (d)	4.86 (1H, dq, $J = 9.4, 1.3$)
4'	30.4 (d)	2.68 (1H, m)
5'	46.6 (t)	1.19 (2H, m)
6'	25.9 (d)	1.61 (1H, m)
7'	22.4 (q)	0.93 (3H, d, $J = 6.4$)
8'	23.2 (q)	1.93 (3H, d, $J = 6.4$)
9'	20.4 (q)	1.01 (3H, d, $J = 6.6$)

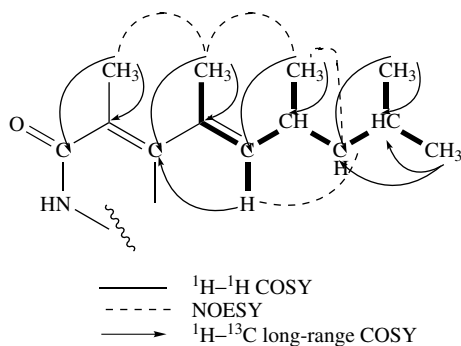


FIGURE 25. A partial structure of lagunamycin (**76**) as revealed by $^1\text{H}-^1\text{H}$ COSY, NOESY and $^1\text{H}-^{13}\text{C}$ long-range COSY experiments. Reproduced by permission of Japan Antibiotics Research Association from Reference 46

All one-bond $^1\text{H}-^{13}\text{C}$ connectivities were established by a heteronuclear multiple-quantum coherence (HMQC) experiment. Partial structures including a tetraene system, a phenyl group and a diol moiety as shown in Figure 27A were determined by a $^1\text{H}-^1\text{H}$ COSY experiment.

The remaining olefinic methine (C21), which could not be assigned due to overlapping of three olefinic protons (H20, H21 and H22) at $\delta 6.22$, was assumed to form another tetraene system together with C16–C20, C22 and C23 from their chemical shifts. $^1\text{H}-^{13}\text{C}$ long-range couplings in the heteronuclear multiple-bond correlation (HMBC) spectrum confirmed this tetraene moiety. As shown in Figure 27B, long-range couplings

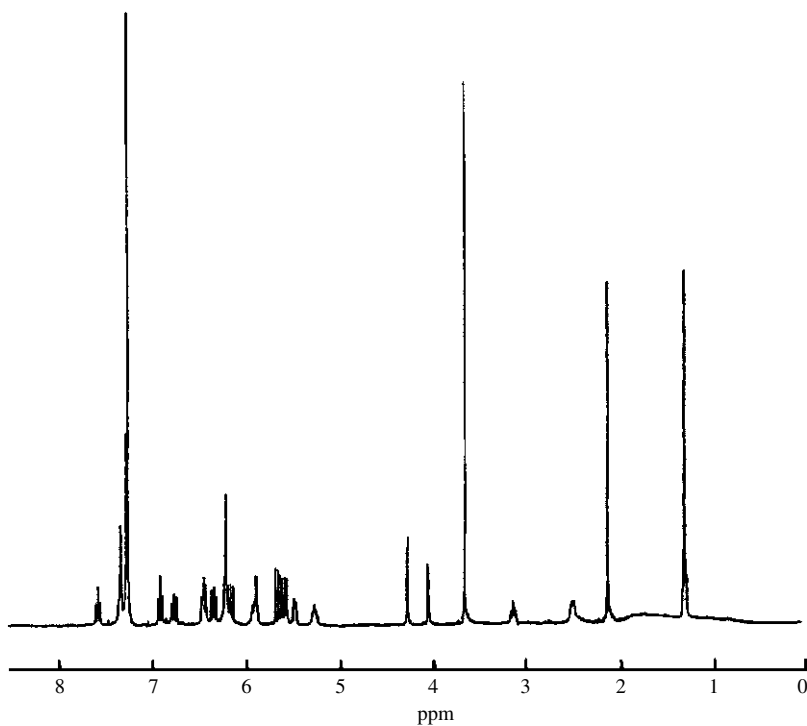
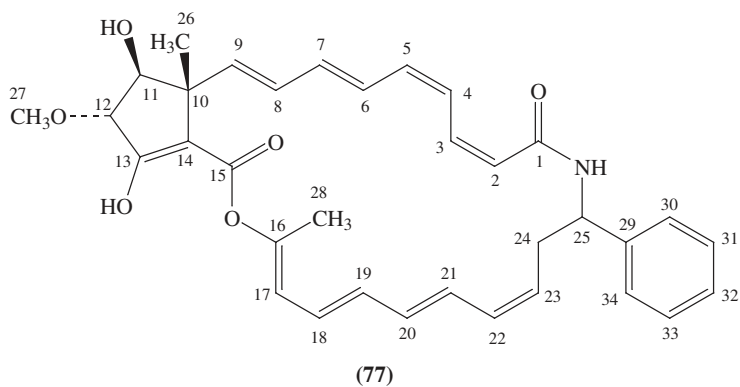


FIGURE 26. The 500-MHz ^1H NMR spectrum of viridenomycin (77) in CDCl_3 . Reproduced by permission of Japan Antibiotics Research Association from Reference 47

were observed between H20 (or H21) and the carbon at $\delta 133.7$, and H24 and the carbon at $\delta 133.7$. Therefore carbon signals at $\delta 134.3$, 128.1 and 133.7 were assigned to C20, C21 and C22, respectively.

The connectivities of the partial structures thus obtained were elucidated by observation of the ^1H - ^{13}C long-range correlations from H2, H3 and NH25 to a carbonyl carbon (C1,

TABLE 27. ^{13}C and ^1H NMR assignments for viridenomycin (**76**) in CDCl_3

No.	δ_{C}^a	δ_{H}	(J , Hz) ^a
1	166.2 s		
2	120.8 d	5.59	(d, 11.5)
3	134.9 d	6.92	(t, 11.5)
4	124.6 d	7.57	(t, 11.5)
5	135.8 d	6.45	(t, 11.5)
6	126.3 d	6.77	(dd, 15.0, 11.5)
7	136.3 d	6.46	(dd, 15.0, 10.5)
8	131.4 d	6.34	(dd, 15.0, 10.5)
9	141.7 d	5.68	(d, 15.0)
10	46.8 s		
11	83.4 d	4.06	(d, 6.5)
12	85.3 d	4.29	(d, 6.5)
13	171.1 s		
14	105.9 s		
15	167.1 s		
16	147.7 s		
17	119.1 d	5.63	(d, 11.5)
18	126.3 d	6.17	(dd, 14.5, 11.5)
19	133.7 d	5.91	(dd, 14.5, 10.0)
20	134.3 d	6.22	(br s)
21	128.1 d	6.22	(br s)
22	133.7 d	6.22	(br s)
23	125.7 d	5.28	(ddd, 11.0, 10.0, 6.5)
24	33.7 t	3.12	(ddd, 13.5, 10.0, 4.5)
		2.50	(ddd, 13.5, 6.5, 3.5)
25	51.5 d	5.49	(ddd, 9.5, 4.5, 3.5)
25-NH		5.90	(d, 9.5)
26	17.0 q	1.33	(s)
27	59.1 q	3.65	(s)
28	15.9 q	2.14	(s)
29	139.5 s		
30, 34	126.3 d	7.28	(d, 7.0)
31, 33	128.5 d	7.34	(t, 7.0)
32	127.3 d	7.28	(d, 7.0)

^as, singlet; d, doublet; t, triplet; q, quartet.

δ 166.2), and from H30 and H34 to a methine carbon (C25, δ 51.5), thereby showing that the tetraene moiety consisting of C2 to C9 was attached to C25 through an amide linkage, and the phenyl group is connected to C25.

The remaining functional groups including a tertiary methyl, a methoxy, a diol moiety and three quaternary carbons were assembled as shown in Figure 27C by analysis of the HMBC spectral data, which revealed the ^1H - ^{13}C long-range couplings from the tertiary methyl (H26) to C9, C10, C11 and C14, from the oxymethine (H12) to C13 and C14, and from the methoxy (H27) to C12. These correlations established a cyclopentene ring structure (C10-C14) substituted with a methoxy group at C12 and a tetraene moiety at C9. The only remaining carbon (C15) was assignable to an ester from its chemical shift (δ 167.1) and an IR absorption at 1700 cm^{-1} . In order to explain the chemical shifts of C13 (δ 171.1) and C14 (δ 105.9), and a positive ferric chloride reaction for viridenomycin, C13 and C14 must form an enol group conjugated to the ester carbonyl (C15). The ester linkage between C15 and C16 was determined by the chemical shift of C16

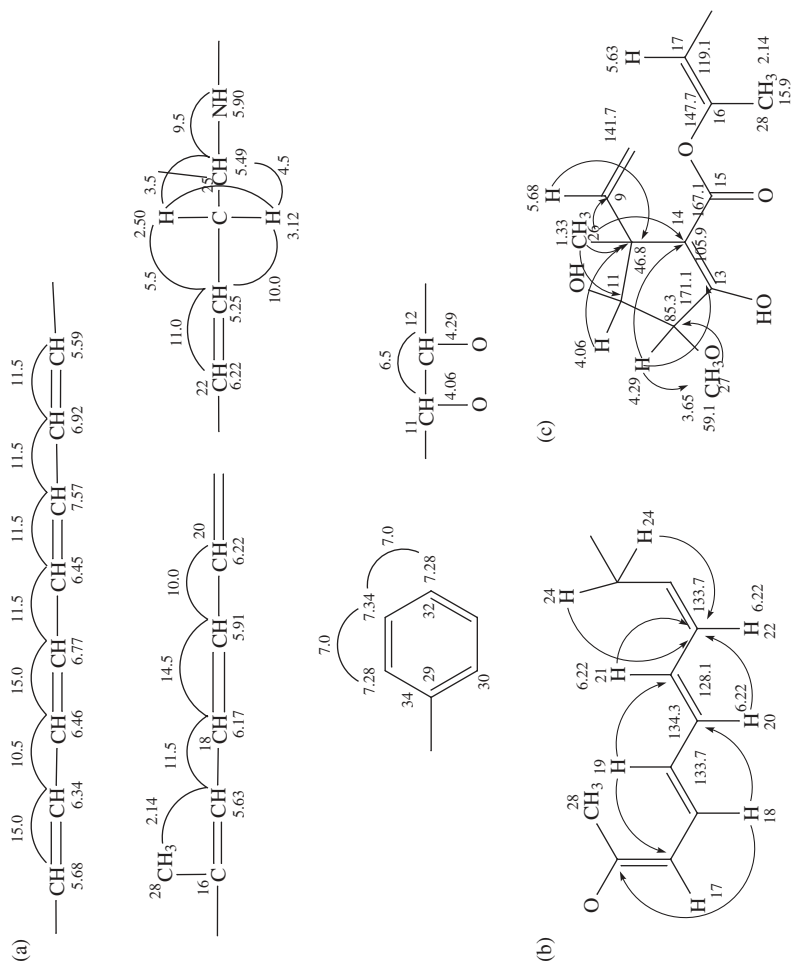


FIGURE 27. Partial structures of viridenomycin. (a): Data from $^1\text{H}-^1\text{H}$ COSY experiment; (b), (c): The solid line arrows indicate $^1\text{H}-^{13}\text{C}$ long-range coupling detected by HMBC

(δ 147.7) and long-range couplings from the allylic methyl (H28) to only two carbons, C16 and C17.

Six of the eight geometries of the two tetraene systems were established to be *2Z,4Z,6E,8E,18E* and *2Z* by the coupling constants $J(23) = 11.5$ Hz, $J(45) = 11.5$ Hz, $J(67) = 15.0$ Hz, $J(1819) = 14.5$ Hz and $J(2223) = 11.0$ Hz. An upfield chemical shift of C-28 (δ 15.9) and no NOE between H17 and H28 showed the *E* configuration for C16. The remaining stereochemistry at C20 proved to be *20E* by the chemical shifts of C19 (δ 133.7) and C22 (δ 133.7) observed at a low-field region free from the γ effects in comparison with C21 (δ 128.1) and C23 (δ 125.7). NOEs observed from H26 to H12 but not to H11 indicated that the relative configuration of the cyclopentene ring was as shown in Figure 27B. The stereochemistry at C25 remains to be determined.

Thus, the structure of viridenomycin was established except for the absolute configuration. This antibiotic is partially related to hitachimycin, which is a 19-membered lactam antibiotic possessing a phenyl group and a cyclopentene ring, but devoid of the tetraene systems and ester linkage.

Colmenares and coworkers⁴⁸ reported a ^{19}F NMR study of rhodopsin analogs. ^{19}F NMR spectra of 11-*cis* and 9-*cis* isomers of six fluorinated rhodopsin analogs with the label(s) located at the vinylic positions of the polyene chain (8F, 10F, 12F, 14F, 8,12F₂, 10,14F₂) are reported along with their UV-Vis and CD spectra. The regiospecific F chemical shift data are analyzed in terms of chromophore changes and local perturbation resulting from specific interactions with the protein. Two analogs (11-*cis*-12-F and 11-*cis*-8-F) and also 9,11-di-*cis*-12-F display FOS (fluorine opsin shift) values uniquely different from others. *Ab initio* ^{19}F NMR chemical shielding calculations of model structures provide support to the assumption that a strong protein perturbation to the 12F position prevails in the binding cavity and that the F8 shift is sensitive to variation of the nearby dihedral angle(s). Possible causes for the broad line width of the F signals of these membrane proteins are discussed.

Freshly reconstituted and concentrated pigment analogs were used for ^{19}F NMR studies for recording the 'before photoirradiation' and 'after irradiation' spectra. Representative spectra of the 8-F and 14-F monofluoro analogs are shown in Figures 28 and 29. The signal that disappears upon photobleaching is identified as that of the pigment analog, the new signal that appears upon irradiation of the photobleaching product, stereochemistry identified by their F shifts and the HPLC retention time and UV data of the extracted retinal analog. Chemical shifts are listed in Table 28.

The fluorine chemical shift is very sensitive to changes in the environment. In this study, the F shift of each fluorinated pigment (a protonated Schiff base PSB) is compared to that of the solution value of the corresponding free PSB. The difference in their ^{19}F NMR chemical shifts represents the change imposed by the local environment (the protein binding cavity) on the F probe. This value is now termed the ^{19}F NMR opsin shift (FOS). The FOS values for the 9-*cis* as well as the 11-*cis* pigments are listed in Table 28. They have a mean value of 6.6 ppm with 95% of them distributed between 4.6 and 8.6 ppm. Only three FOS values are exceptional, falling outside this range: those of 9,11-di-*cis*-12-F (-2.1 ppm), 11-*cis*-8-F (13.1 ppm) and 11-*cis*-12-F (13.2 ppm) and, to a lesser degree, also those for the disubstituted 11-*cis*-8,12-F₂ (11.8, 11.7 ppm). The trends are evident in the plot of FOS values vs the F position along the chromophore chain shown in Figure 30.

Li and coworkers⁴⁹ reported a molecular motion of β -carotene and a carotenoporphyryrin dyad (composed of a porphyrin, a trimethylene bridge and a carotenoid polyene) in solution. Internal rotational motions in carotenoid polyenes and porphyrins are of interest because they can mediate energy and electron transfer between these two moieties when the pigments are joined by covalent bonds. Such internal motions can affect the performance of synthetic model systems which mimic photosynthetic antenna function,

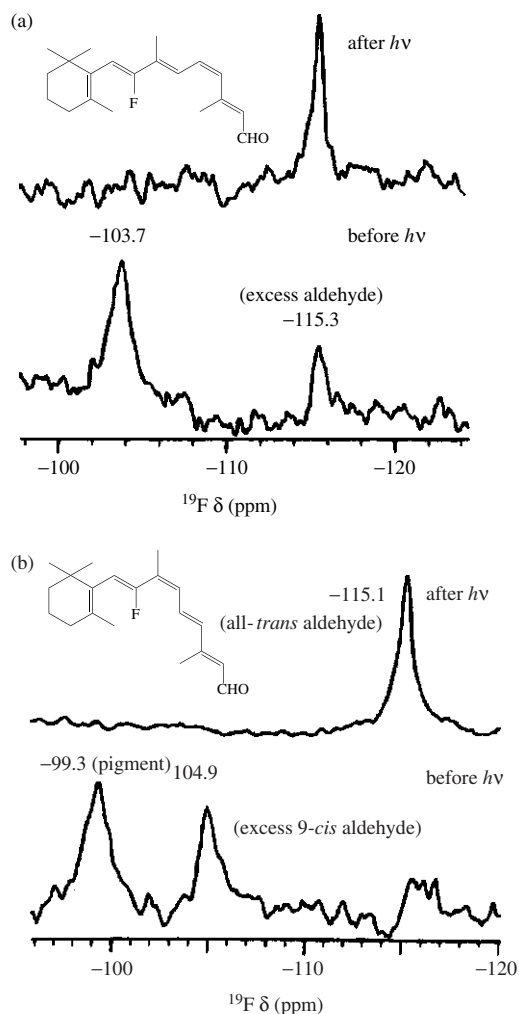


FIGURE 28. 283-MHz ^{19}F NMR spectra of isomers of 8-F-rhodopsin in CHAPS before (lower) and after photoirradiation (upper): (a) 11-*cis* (pulse delay, $D5 = 5.0$ s, number of acquisitions, $NA = 5200$, line broadening, $LB = 80$ Hz); (b) 9-*cis* ($D5 = 50$ ms, $NA = 160000$, $LB = 80$ Hz). Disappearance of the excess 9-*cis* aldehyde was due to repeated formation and bleaching of pigment during the irradiation process. Reprinted with permission from Reference 48. Copyright (1996) American Chemical Society

photoprotection and photoinduced electron transfer. Analysis of ^{13}C NMR spin-lattice relaxation times (T_1) yields information concerning both overall tumbling of molecules in solution and internal rotations about single bonds. Relaxation time and nuclear Overhauser effect data have been obtained for β -carotene (**78**) and the related molecules, squalene (**82**) and carotenoporphyryn (**80**) which is a zinc *meso*-tetraphenylporphyrin (**79**) covalently linked to a carotenoid polyene through a trimethylene bridge. Squalene (**81**)

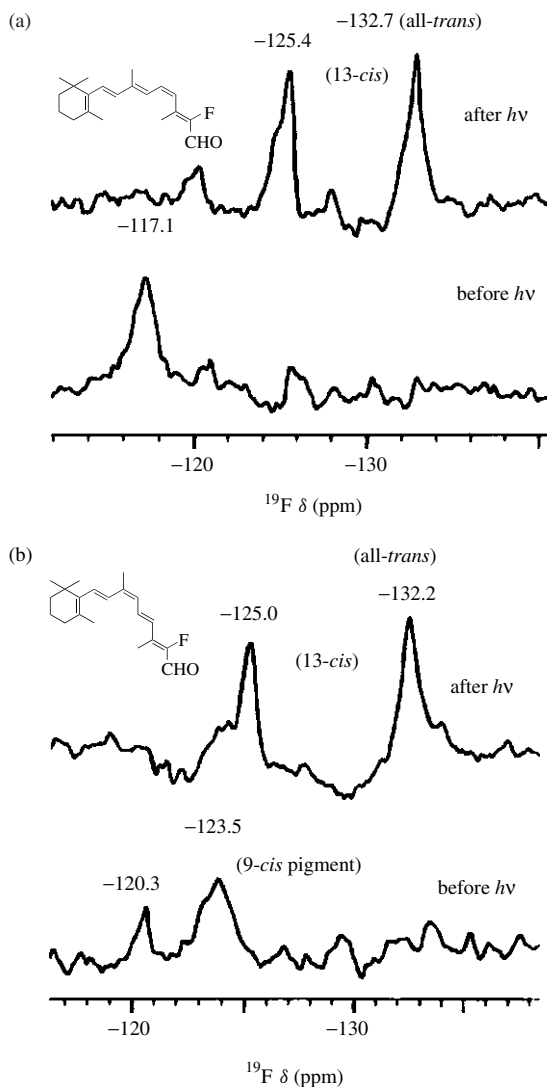


FIGURE 29. 283-MHz ^{19}F NMR spectra of 14-F-rhodopsin in CHAPS before and after photoirradiation: (a) 11-*cis* (D5 = 50 ms, NA = 196136, LB = 80 Hz); (b) 9-*cis* (D5 = 50 ms, NA = 200000, LB = 80 Hz). The 13-*cis* isomer was from dark isomerization. Reprinted with permission from Reference 48. Copyright (1996) American Chemical Society

and squalene (**82**), which lack conjugated double bonds, behave essentially as limp string, with internal rotations at least as rapid as overall isotropic tumbling motions. In contrast, β -carotene reorients as a rigid rod, with internal motions which are too slow to affect relaxation times. Modeling it as an anisotropic rotor yields a rotational diffusion coefficient for motion about the major axis, which is 14 times larger than that for rotation

TABLE 28. ^{19}F NMR chemical shifts of retinylidene PSBs, (protonated Schiff bases), rhodopsin pigments and corresponding ^{19}F NMR opsin shifts

Analog	PSB (CD_2Cl_2)	Pigment (CHAPS) ^c	F NMR OS ^a
11- <i>cis</i> -8-F	-116.8	-103.7	13.1
11- <i>cis</i> -10-F	-112.2 ^b	-107.4	4.8
11- <i>cis</i> -12-F	-107.8 ^b	-94.6	13.2
11- <i>cis</i> -14-F	-125.5	-117.1	8.4
11- <i>cis</i> -8, 12-F ₂	-117.0	-105.2	11.8
	-104.6	-92.9	11.7
11- <i>cis</i> -10, 14-F ₂	-115.3	-111.8	3.5
	-122.7	-117.6	5.1
9- <i>cis</i> -8-F	-105.9	-99.3	6.6
9- <i>cis</i> -10-F	-119.7 ^b	-115.3	4.4
9- <i>cis</i> -12-F	-120.9	-114.3	6.6
9- <i>cis</i> -14-F	-131.4	-123.5	7.9
9- <i>cis</i> -10, 14-F ₂	-119.1	-115.4	3.7
	-128.8	-121.2	7.6
9, 11-di- <i>cis</i> -12-F	-108.7	-110.8	-2.1
9- <i>cis</i> -9-CF ₃	-64.6	-60.2	4.4

^a ^{19}F NMR opsin shift = (column 3 - column 2) in δ (ppm).

^bIn CDCl_3 .

^cCHAPS = A membrane protein solubilizing agent: *N,N*-Dimethyl-*N*-(3-sulfopropyl)-3-[(3 α , 5 β , 7 α , 12 α)-3,7,12-trihydroxy-24-oxocholan-24-yl]amino]-1-propanaminium inner salts.

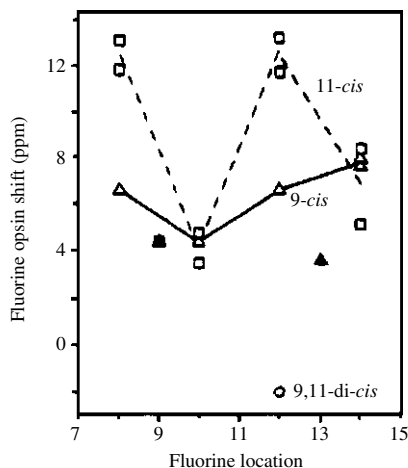
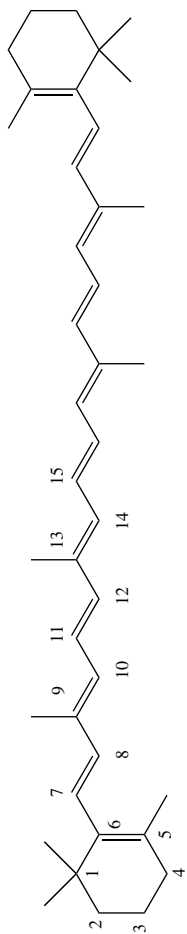
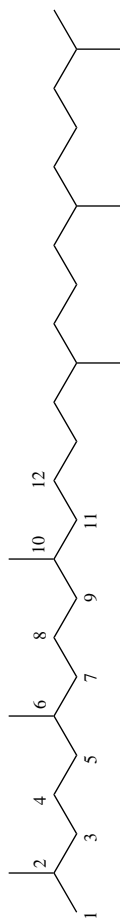


FIGURE 30. Plot of FOS (ppm) for vinyl-F labels at several locations on the chain of the retinyl chromophore in the (\square) 11-*cis*, dashed line, (Δ) 9-*cis*, solid line, and (\circ) 9,11-di-*cis* configurations. Where appropriate, the averaged FOS values from mono- and dilabeled analogs were used for connecting lines. Solid symbols are for CF₃. Reprinted with permission from Reference 48. Copyright (1996) American Chemical Society

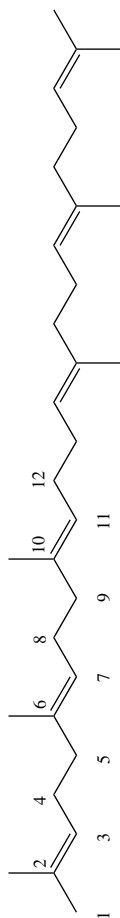
about axes perpendicular to that axis. The porphyrin reorients more nearly isotropically and features internal librational motions about the single bonds to the phenyl groups. The relaxation time data for the carotenoporphyrin are consistent with internal motions similar to those of a medieval military flail, consisting of a rigid, rod-like carotenoid



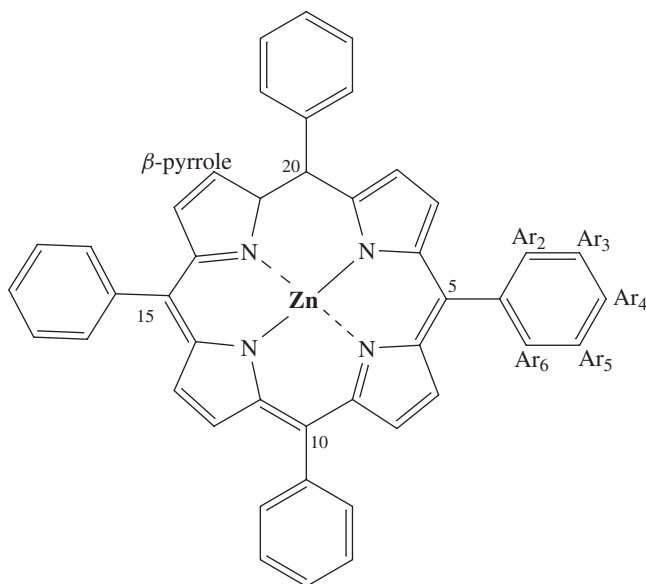
β -Carotene (78)



Squalane (81)



Squalene (82)

Zinc *meso*-tetraphenylporphyrin (**79**)

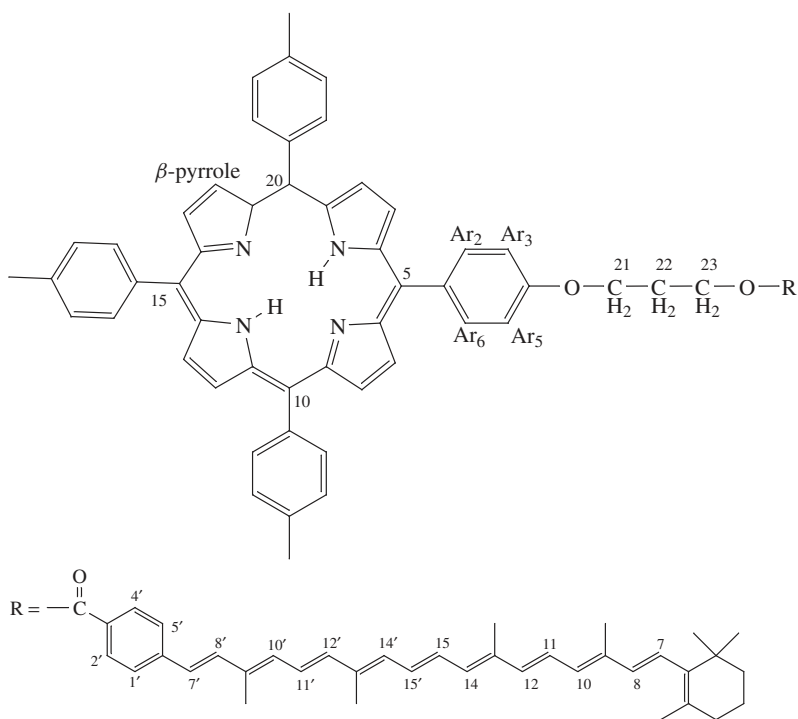
and ball-like porphyrin linked by a flexible chain of single bonds. Internal reorientation about this linkage is approximately 100 times faster than triplet-triplet energy transfer from the porphyrin to the carotenoid, which is mediated by such motions. The chemical shift assignments for the carbon nuclei of interest are given in Tables 29–32.

The assignments have been achieved using COSY, NOESY, ROESY, HMQC and HMBC experiments.

Spin–lattice relaxation time- T_1 and nuclear Overhauser effect ($1 + \eta$) for relevant carbon nuclei of **78–82** were determined in deoxygenated CDCl_3 at 297 ± 2 K. Three magnetic field strengths (7.0, 9.4, and 11.7 T) were employed. For T_1 measurements the inversion recovery technique was used, e.g. for **78** (Figure 31), whereas NOE values were determined by a gated decoupling method. Results for squalane (**81**) and squalene (**82**) appear in Table 29, whereas those for **78–80** are given in Tables 30–32, respectively. The reported T_1 values are averages of at least three separate determinations and are reproducible to within 5%. The NOE values are less reliable (15%), due in part to a less than optimal signal-to-noise ratio.

The T_1 and NOE results for the monoprotonated carbon atoms of the β -carotene backbone of **78** at three magnetic field strengths are given in Table 30. An obvious difference from the results for **81** and **82** is that the T_1 values do not increase dramatically as one moves along the carbon chain away from the center of mass. In fact, the T_1 values for carbons 10, 11, 12, 14 and 15 are identical, within experimental error, while those for carbons 7 and 8 at the end of the chain are only slightly longer. This result indicates that the overall tumbling of the β -carotene molecule about its center of mass is substantially faster than internal rotations about the carbon–carbon bonds in the backbone, so that internal motions no longer affect relaxation significantly. The molecule behaves essentially as a rigid rotor.

Given the fact that β -carotene behaves essentially as a rigid rotor, the linear geometry of the molecule as shown by X-ray studies suggests that it should not tumble



isotropically. Indeed, to a first approximation, it might be expected to rotate more like an ellipsoid of rotation, with a major axis lying more or less along the conjugated carbon backbone. The field dependence of the T_1 and NOE data shown in Table 30 is consistent with this interpretation. In the first place, it will be noted that the NOE values are not maximal (2.99) and that they decrease with increasing magnetic field. At first glance, this might be taken to mean that a second relaxation mechanism, which becomes more important at higher fields, is contributing. The most likely candidate is chemical shift anisotropy. The chemical shift anisotropy relaxation rate is proportional to the square of the spectrometer magnetic field strength, and the mechanism should therefore be more effective at the higher fields. However, it can be seen in Table 30 that the spin–lattice relaxation times increase with magnetic field. Relaxation is becoming less effective rather than more effective. Any additional relaxation mechanism coming into play at higher field strengths could only decrease relaxation times. Thus chemical shift anisotropy, and indeed any other mechanism competing with dipole–dipole relaxation, may be ruled out.

An alternative explanation, consistent with the data, is that dipole–dipole relaxation dominates for β -carotene, but that molecular reorientation is anisotropic and occurs in a time range where the NOE is less than the maximum of 2.99 that is found in the ‘extreme narrowing’ region. For a rigid isotropic rotor, the correlation times are such that $\omega^2\tau_c^2 \ll 1$ and T_1 will be independent of magnetic field strength and the NOE will be full (2.99). For the field strengths used in this study, this extreme narrowing region includes diffusion coefficient values greater than about $5 \times 10^9 \text{ s}^{-1}$. For smaller values

TABLE 29. ^{13}C NMR chemical shift values (δ), observed and calculated^a spin–lattice relaxation times (T_1) and observed nuclear Overhauser effects (NOE) for squalane (**81**) and squalene (**82**) in CDCl_3 solution at 11.7 T

Carbon	81				82			
	δ (ppm) ^b	obsd T_1 (s)	calcd T_1 (s)	obsd NOE ($1 + \eta$)	δ (ppm)	obsd T_1 (s)	calcd T_1 (s)	obsd NOE ($1 + \eta$)
2	28.05	4.85	3.70	2.83				
3	39.47	2.50	1.76	2.09	124.46	4.31	3.99	2.85
4	24.88	1.75	1.66	2.54	26.81	1.85	1.83	3.13
	24.89							
5	37.39	1.33	1.57	2.69	39.75	1.62	1.73	3.05
6	32.86	1.86	2.96	2.76				
7	37.48	1.24	1.39	2.81	124.32	2.26	3.05	2.85
	37.52							
8	24.56	1.02	1.30	2.85	26.69	1.14	1.36	3.13
9	37.50	1.03	1.21	2.69	39.77	1.17	1.27	3.05
	37.55							
10	32.86	1.83	2.23	2.76				
11	37.20	0.88	1.03	2.75	124.35	1.77	2.15	2.85
	37.21							
	37.29							
	37.30							
12	27.52	0.91	0.91	2.78	28.30	0.90	0.90	3.17
	27.53							
	27.54							

^aThe rotational diffusion coefficients used to calculate the various T_1 values are discussed in the text.

^bAs discussed in the text, this sample is a mixture of stereoisomers and, as a result, resonances for some carbons appear as clusters of closely spaced peaks with chemical shift values as listed in this column. The reported experimental T_1 and NOE values are averages for these clusters.

TABLE 30. ^{13}C NMR chemical shift values (δ), spin–lattice relaxation times (T_1) and nuclear Overhauser effects (NOE) for β -carotene (**78**) in CDCl_3 at various magnetic field strengths

Carbon	δ (ppm)	7.0 T		9.4 T		11.7 T	
		T_1 (s)	NOE ($1 + \eta$)	T_1 (s)	NOE ($1 + \eta$)	T_1 (s)	NOE ($1 + \eta$)
7	126.67	0.58	2.55	0.67	2.46	0.71	2.25
8	137.28	0.59	2.48	0.66	2.49	0.70	2.34
10	130.85	0.54	2.49	0.61	2.38	0.67	2.29
11	125.05	0.51	2.46	0.57	2.43	0.61	2.18
12	137.25	0.52	2.54	0.60	2.53	0.65	2.30
14	132.43	0.54	2.53	0.59	2.42	0.63	2.37
15	130.00	0.51	2.69	0.57	2.44	0.59	2.38

of the diffusion coefficient, T_1 will increase with increasing magnetic field strength, and NOE will decrease until it reaches a limiting minimum value.

Rochet and Lancelin⁵⁰ reported revised ^1H and ^{13}C NMR assignments of the polyene antibiotic Filipin III (**83**). This macrolide which was isolated from *Streptomyces filipinensis* was reinvestigated in DMSO-d_6 solution using homonuclear and heteronuclear correlation spectroscopy. In addition to several corrections to previous ^1H NMR

TABLE 31. ^{13}C NMR chemical shift values (δ), observed and calculated spin–lattice relaxation times (T_1) and observed nuclear Overhauser effects (NOE) for zinc *meso*-tetraphenylporphyrin (**79**) in CDCl_3 solution at 9.4 T

Carbon	δ (ppm)	Obsd T_1 (s)	Calcd T_1 (s)	NOE ($1 + \eta$)
β -pyrrole	131.99	0.40	0.40	2.85
Ar 2, 6	134.45	0.64	0.64	2.72
Ar 3, 5	126.55	0.63	0.64	3.10
Ar 4	127.49	0.41	0.40	2.61

TABLE 32. ^{13}C NMR chemical shift values (δ) and observed and calculated^a spin–lattice relaxation times (T_1) for carotenoporphyrin (**80**) in CDCl_3 solution at 11.7 T

Carbon	δ (ppm)	Obsd T_1 (s)	Calcd T_1 (s)
β -pyrrole	130.6–130.8 ^b	0.30	0.30
5-Ar 2, 6	135.59	0.31	0.32
5-Ar 3, 5	112.70	0.32	0.32
10, 15, 20-Ar 2, 6	134.51	0.37	0.38
10, 15, 20-Ar 3, 5	127.39	0.38	0.38
21	64.78	0.26	0.26
22	29.02	0.44	0.44
23	61.89	0.24	0.24
1', 5'	126.09	0.37	0.41
2', 4'	130.06	0.34	0.41
12'	139.26	0.44	0.41
8	137.74	0.52	0.41
12	137.14	0.45	0.41
8'	136.20	0.40	0.41
10'	134.78	0.42	0.41
14'	133.74	0.40	0.41
14	132.31	0.38	0.41
10	130.82	0.40	0.41
15	130.78	0.32	0.41
15'	129.79	0.36	0.41
7	126.83	0.54	0.41
7'	126.09	0.37	0.41
11	125.36	0.40	0.41
11'	124.58	0.39	0.41

^aThe rotational diffusion coefficients used to calculate the variations in T_1 values are discussed in the text.

^bAs discussed in the text, the β -pyrrole resonances for this molecule appeared as a broad singlet. The reported T_1 value is therefore an average for all β -pyrrole resonances.

assignments (Figure 32), the nine exchangeable hydroxylic protons were structure-specifically assigned together with ^{13}C NMR lines using proton-detected HSQC spectroscopy (Table 33). The magnitudes of the $^3J(\text{HH})$ indicated a probable constrained geometry of the macrocyclic lactone.

4. Metal bound polyenes

Yasuda and coworkers⁵¹ reported a route to niobocene-allyl compounds by hydrometalation of conjugated dienes with niobium hydrido-olefin complexes, $\text{NbH}(\text{C}_5\text{H}_5)_2(\text{olefin})$,

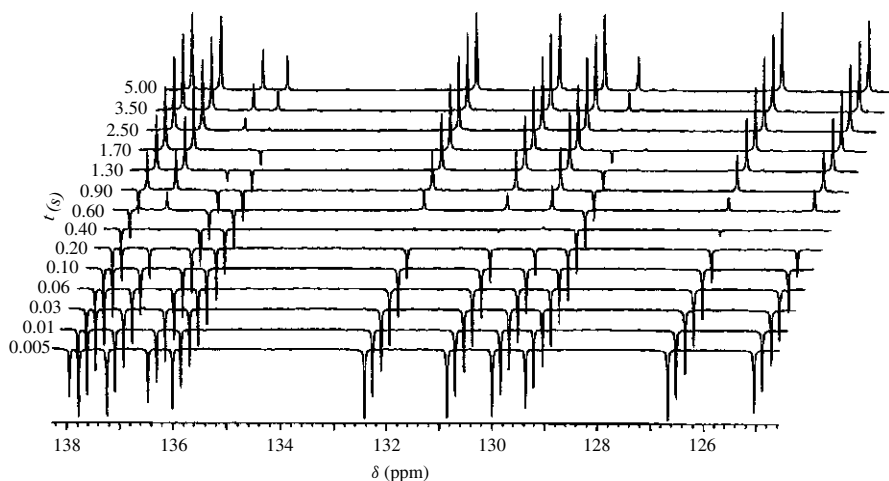
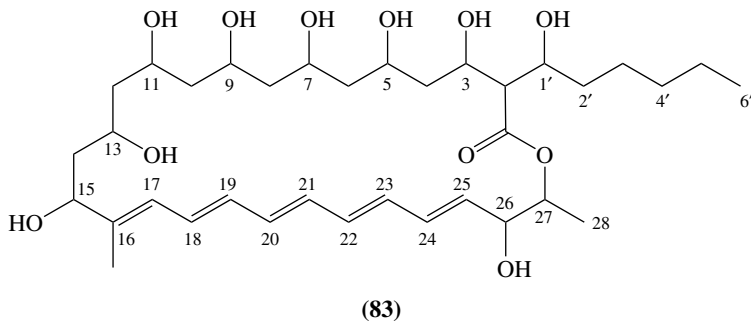


FIGURE 31. Typical data set for measurement of the spin–lattice relaxation times of the sp^2 -hybridized carbon atoms of β -carotene at 11.7 T. The chemical shift values are shown across the bottom of the figure. The t -value for each spectrum is the delay time in the inversion-recovery pulse sequence. Reprinted with permission from Reference 49. Copyright (1995) American Chemical Society



which readily react with conjugated dienes such as butadiene, isoprene and pentadiene, to give $Nb(C_5H_5)_2(\eta^3\text{-allyl})$ derivatives of *syn* or *syn,syn* geometry, in 80%–90% yields with high regioselectivity. All the complexes were isolated as crystals and their structures were determined by NMR spectroscopy (equations 1 and 2).

The coordinated ethylene is readily expelled at 25 °C by the attack of a conjugated diene and the hydride is transferred to the sterically less crowded diene terminus. Thus the niobium hydrido-olefin complexes serve as convenient reagents for the preparation of 1,2- or 1,3-dialkyl-substituted allylniobium compounds starting from butadiene, (*E,E*)- and (*E,Z*)-2,4-hexadiene, (*E*)- and (*Z*)-1,3-pentadiene (equation 1), 3-methyl-1,3-pentadiene and isoprene (equation 2). All the allyl niobium compounds synthesized were isolated as air-sensitive pale-yellow crystals by crystallization from hexane.

All of the allylniobium compounds are monomeric, as revealed by the mass spectroscopic analysis, and always exist in the thermodynamically more favored *syn*- or

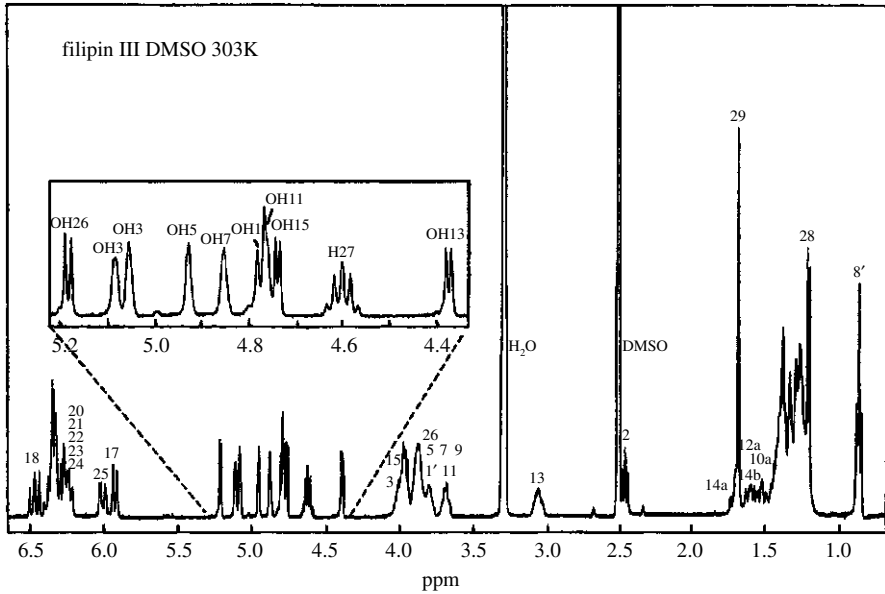


FIGURE 32. ^1H NMR spectrum of filipin III, 3 mM in DMSO-d_6 , recorded at 400 MHz and 25°C . The expanded region contains nine hydroxyl proton resonances that fully exchange with deuterium oxide and correspond to the nine hydroxyl groups of filipin III. No apodization functions were applied prior to the Fourier transformation. Reproduced by permission of John Wiley & Sons from Reference 50

syn,syn-allyl structure as deduced from one or more ^1H NMR parameters, such as $J(\text{H1R2})$ and/or $J(\text{R2H3})$ of 13.5–14.2 Hz (Table 34).

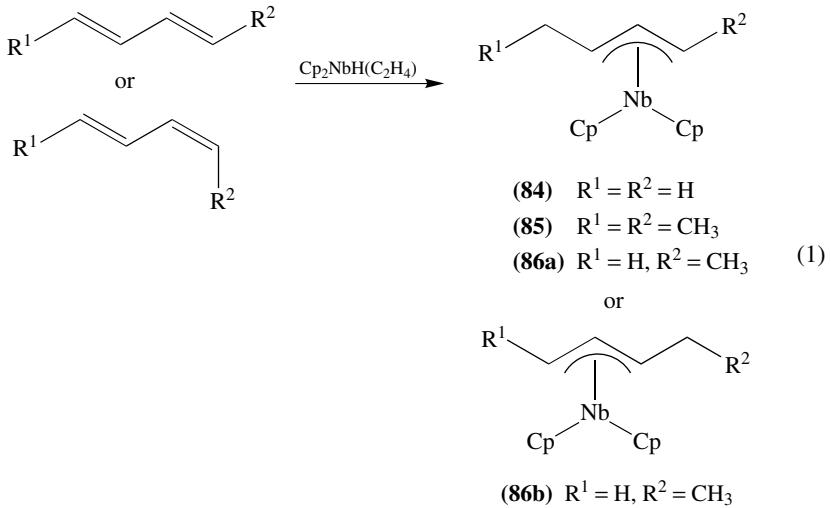
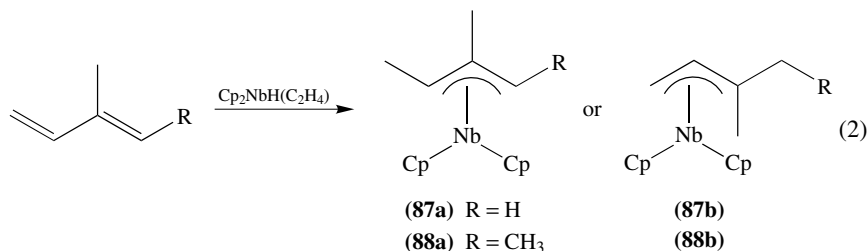


TABLE 33. ^1H and ^{13}C chemical shifts (ppm) of filipin III in $\text{DMSO}-d_6$ solution at 303 K.^a

Position	$\delta^1\text{H}$	$\delta^{13}\text{C}$
2	2.44	58.1
3	3.98, 5.08 (OH)	69.9
4	1.36, 1.36	40.0
5	3.87, 4.93 (OH)	69.4
6	1.30, 1.30	43.4
7	3.85, 5.85 (OH)	69.4
8	1.30, 1.38	43.4
9	3.84, 5.06 (OH)	69.9
10	1.26, 1.36	42.3
11	3.77, 4.76 (OH)	68.3
12	1.28, 1.58	44.3
13	3.04, 4.37 (OH)	64.7
14	1.49, 1.68	42.4
15	3.94, 4.74 (OH)	71.0
17	5.91	125.4
18	6.44	127.7
19	6.22	131.0
20	6.30	128.8*
21	6.30	131.0*
22	6.30	132.0*
23	6.30	132.7*
24	6.30	132.8*
25	5.98	134.8
26	3.94, 5.19 (OH)	73.0
27	4.60	72.6
28	1.18	17.0
29	1.67	10.0
1'	3.66, 4.77 (OH)	69.5
2'	1.25, 1.34	33.6
3'	1.18, 1.22	30.6
4'	1.24, 1.42	24.0
5'	1.23	21.3
6'	0.83	12.9

^aAsterisked resonances can be interchanged. Quaternary C-1 and C-16 are not assigned.

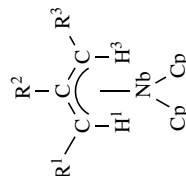


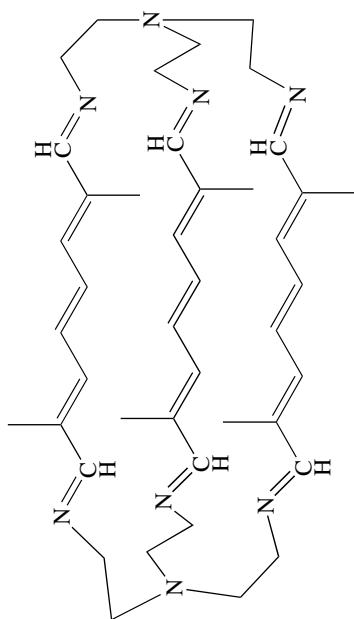
Lehn and coworkers⁵² reported the synthesis, crystal structure and dinuclear copper(I) complexes of tris-carotenoid macrobicyclic ligands. The macrobicycles **89** and **90** were obtained in good yields in a one-step macrobicyclisation condensation between the tripod $\text{N}(\text{CH}_2\text{CH}_2\text{NH}_2)_3$ and the polyolefinic dialdehydes **93** and **94**.

TABLE 34. ¹H NMR parameters for niobocene-allyl compounds^a

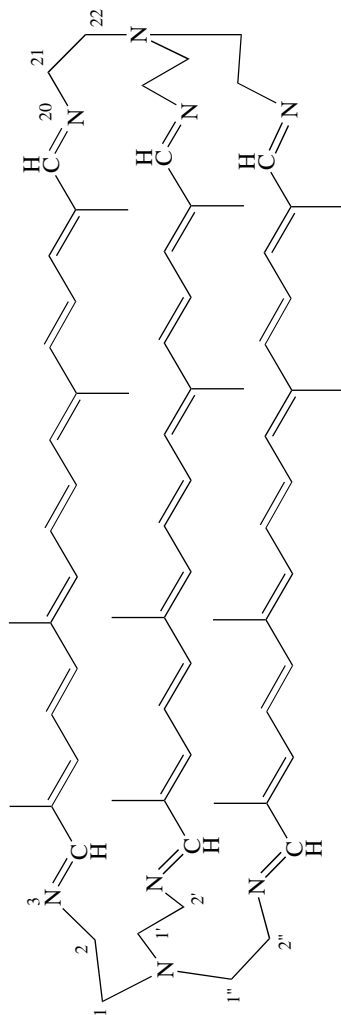
Cp ₂ Nb(R ¹ CH ¹ CR ² CH ³ R ³)		Chemical shifts (δ, ppm)						Coupling constants (Hz) ^c					
R ¹	R ²	R ³	ν (H1)	ν (R1)	ν (R2)	ν (H3)	ν (R3)	ν (Cp)	J (H ¹ , R ¹)	J (H ¹ , R ²)	J (R ¹ , R ²)	J (R ² , H ³)	J (H ³ , R ³)
H	H	CH ₃ (84)	0.51	2.65	2.29	1.46	2.01	4.54	-4.4	13.6	9.5	11.5	5.6
CH ₃	H	C ₂ H ₅ (85)	1.17	1.95	2.33	1.61	2.28	4.14	5.5	13.8		13.7	5.7
CH ₃	H	CH ₃ (86a)	1.17	1.97	2.34	1.17	1.97	4.11	5.5	13.9		13.9	5.5
CH ₃	CH ₃	CH ₃ (87a)	0.97	1.88	1.52	0.97	1.88	4.50	5.8				5.8
H	CH ₃	CH ₃ (88a)	0.62	2.73	1.59		1.89	4.15	-5.0				5.5
H	H	H ^b	0.75	2.95	2.18	0.75	2.95	4.04	-4.5	14.9	9.5	14.9	-4.5
H	CH ₃	H ^b	0.86	2.90	1.60	0.86	1.60	4.08	-4.8				-4.8
								4.49					
								4.10					

Numbering scheme

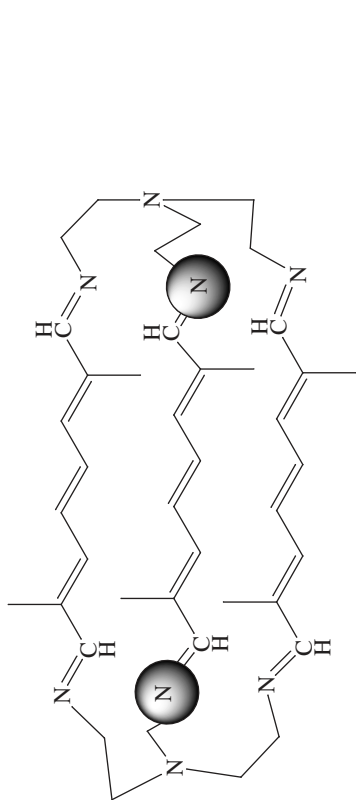
^aParameters were determined by the computer simulation of the 100 MHz NMR spectra (C₆D₆ at 30 °C). Chemical shifts are expressed in ppm downfield from TMS with calibration with C₆H₆ assumed to be at 7.2 ppm as internal standard.^bPrepared by reaction of Cp₂NbCl₂ with allylmagnesium bromide.^cJ(H1H3) and J(H1R3) (R = H) are in the ranges -0.5 to -0.9 and -0.1 to -0.2 Hz, respectively.



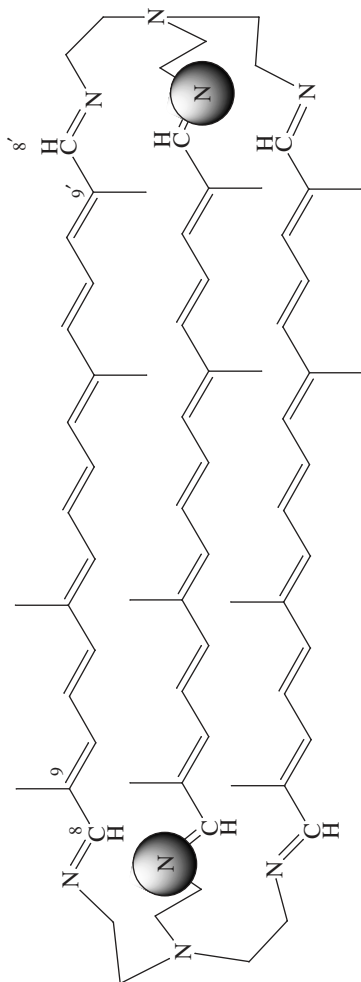
(89)



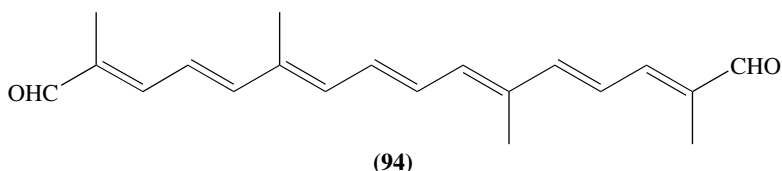
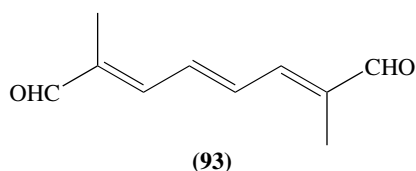
(90) (arbitrary numbering)



(91)



(92) (carotenoid numbering)



89 and **90** form dinuclear cryptates by complexation of two Cu(I) ions. The crystal structure of the tris-carotenoid **90** confirms that it contains three parallel polyolefinic strands. These substances may formally be considered as prototypes of molecular 'cables' formed by three electron-conducting molecular wires. The ^1H NMR spectra of the free ligands **89** and **90** and of their complexes **91** and **92** (the darkened circle represents the Cu atom) show notable differences (Figures 33 and 34).

In particular, the CH_2CH_2 unit of the free ligands **89** and **90** presents signals of the ABCD type, all four protons being different; this indicates an unsymmetrical structure which is also sufficiently rigid so as not to undergo conformational averaging by a twisting motion around the *N,N*-bridgehead axis. This agrees with the conformation found in the crystal structure when it is motionally frozen on the NMR time scale. High-temperature NMR measurements of **89** in $\text{C}_2\text{D}_2\text{Cl}_4$ indeed show coalescence of the four CH_2CH_2 signals at 2.33 and 2.92 ppm and at 3.23 ppm into two broad resonances at *ca* 2.7 and 3.5 ppm, respectively, with a coalescence temperature of *ca* 340 K. The corresponding free energy of activation ΔG_c^\ddagger is calculated to be *ca* 16 kcal mol $^{-1}$.

In contrast, the CH_2CH_2 resonances of the corresponding complexes **91** and **92** are of A_2X_2 type indicating a highly symmetrical averaging by rapid torsional oscillation around the *N,N*-bridgehead axis. The olefinic protons display a compression of signals into a narrower ppm range, and the $\text{CH}=\text{N}$ signal undergoes a downfield shift of *ca* 0.5 ppm on complexation.

In comparison, both the free ligand and the dinuclear Cu(I) cryptate of an analogous macrobicyclic structure possessing a diphenylmethane group as a central unit display only two resonances for the CH_2CH_2 fragment, as is the case here only for the complexes **91** and **92**. This points to the special conformation features of the free macrobicycles **89** and **90**.

B. Solid State NMR

1. ^{13}C CP/MAS NMR

Polydiacetylenes are obtained as single crystals by topochemical solid-state polymerization of the monomer single crystal. These compounds have received considerable attention because of their one-dimensionally π -conjugated structure. Their unique π -electron structures, and therefore superior third-order nonlinear optical properties, have been extensively investigated.

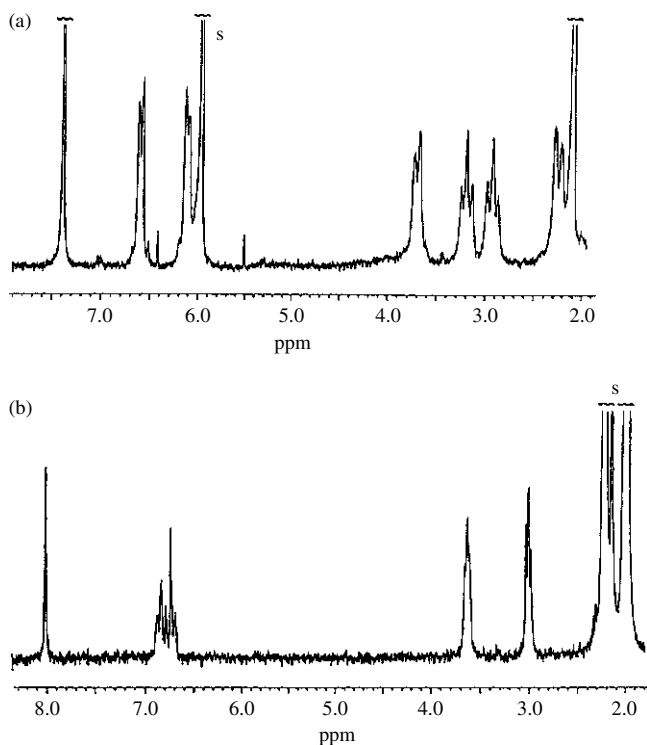


FIGURE 33. ^1H NMR spectra (200 MHz): (a) of cryptand **89** in $\text{C}_2\text{D}_2\text{Cl}_4$ and (b) of its dinuclear Cu^{I} complex **91** in CD_3CN (s = solvent). Reproduced by permission of Neue Schweizerische Chemische Gesellschaft from Reference 52

Hayamizu and coworkers⁵³ reported the polymerization of the octatetrayne monomer 15,17,19,21-hexatriacontatetrayne (HTY) (**95**) to the polydiacetylene **96** with butadiynyl substituents ($\text{R} = \text{H}$) as presented in Figure 35 as an example.

It was found that solid-state polymerization of these monomers always proceeds by 1,4-addition. Furthermore, polydiacetylene **96** could be thermally reacted and the structure of the final polymer was proposed to be that of the ladder polymer **97** where the repeating unit is 1,6-didehydro[10]annulene (**98**), i.e. two conjugated polydiacetylenes. However, the annulene **98** is expected to be unstable. In fact, its cycloaromatization reaction to the 1,5-dehydronaphthalene diradical **99** was recently reported. The instability is considered to be due to in-plane repulsion of the face to face π -orbitals at sp -hybridized carbon in the annulene ring. Thus, the final structure of the polymers from octatetrayne derivatives after the thermal reaction may be either a planar cycloaromatized polymer and/or a three-dimensional polymer, which would be obtained if the polymerization proceeded in a different direction from that of the same column of the polymer side chain. To obtain the ladder polymer where two polydiacetylenes are conjugated in each repeating unit, it is necessary to keep the polydiacetylene backbones separated by conjugated divalent groups.

In this study, a dodecahexayne derivative with long alkyl substituents, i.e. 15,17,19,21,23,25-tetracontahexayne (THY), was also synthesized as an extension of the study of the octatetrayne system. Its solid-state polymerization behavior was investigated using

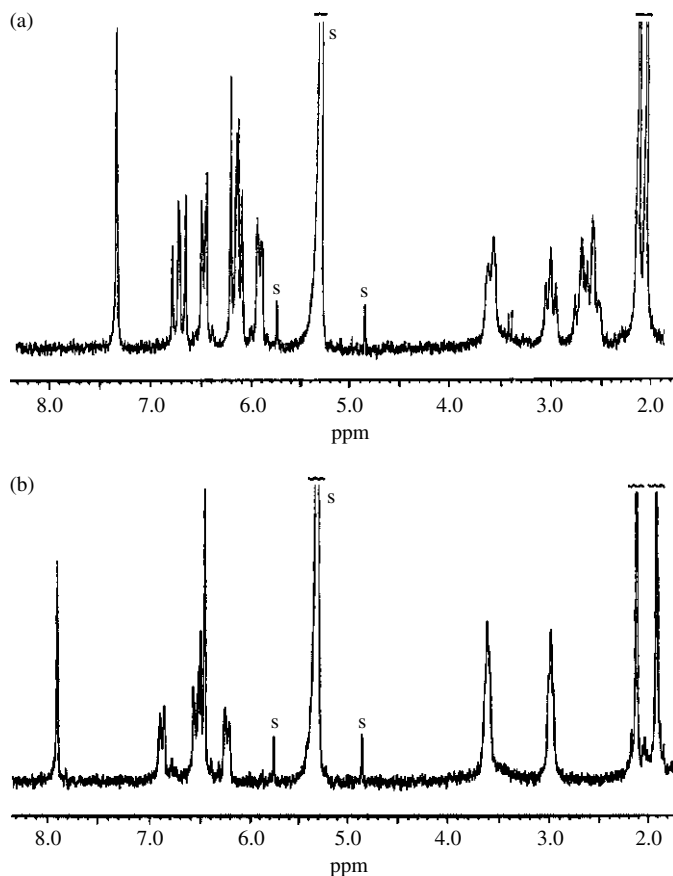


FIGURE 34. ^1H NMR spectra (200 MHz): (a) of cryptand **90** and (b) of its dinuclear Cu^{I} complex **92** in $\text{C}_2\text{D}_2\text{Cl}_4$. (s = solvent). Reproduced by permission of Neue Schweizerische Chemische Gesellschaft from Reference 52

IR and visible near-IR absorption, NMR, ESR and X-ray diffraction. It was emphasized that solid-state high-resolution ^{13}C NMR spectroscopy is a powerful tool for the structure analysis of polydiacetylenes. THY is particularly attractive because of its potential for forming the polydiacetylene ladder polymer.

The ^{13}C CP/MAS NMR spectrum taken 30 min after recrystallization of THY is shown in Figure 36A, and the ^{13}C chemical shift values of this spectrum together with those of the THY monomer in CDCl_3 solution are summarized in Table 35.

The assignment of the monomer solution spectrum was performed by using an NMR spectral database system (SDBS-NMR)⁵⁴. The signals of the six acetylene carbons from 60.34 to 81.91 ppm in the solution spectrum indicated the monomer structure of a dodecahexyne derivative substituted symmetrically by alkyl groups. Since the spectral patterns in Figure 36A are almost the same as those of the monomer, only a small extent of polymerization had occurred during the 30 min after recrystallization. The signal at about

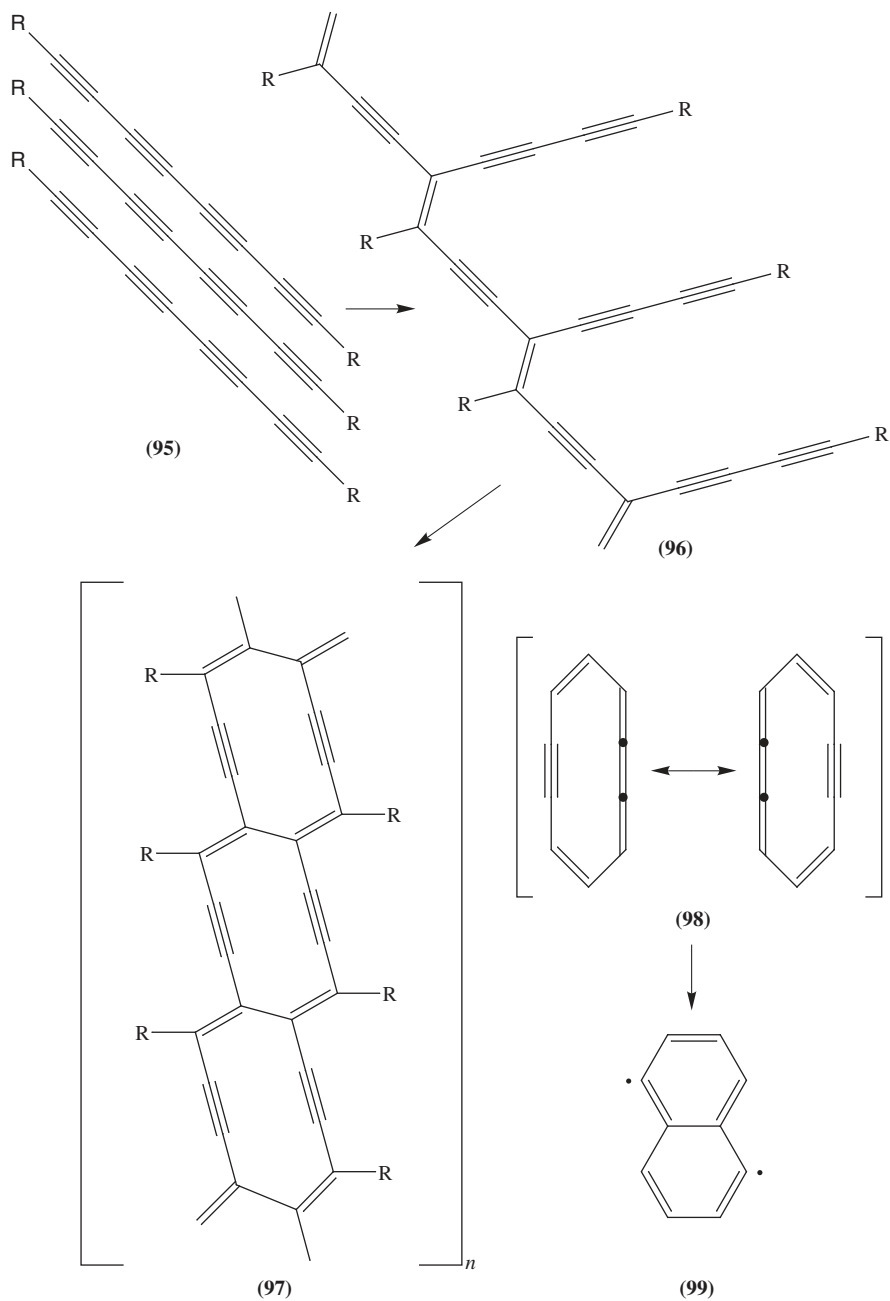


FIGURE 35. Polymerization schemes of octatetraene derivatives and cycloaromatization of 1,6-didehydro[10]annulene (98). Reprinted with permission from Reference 53. Copyright (1994) American Chemical Society

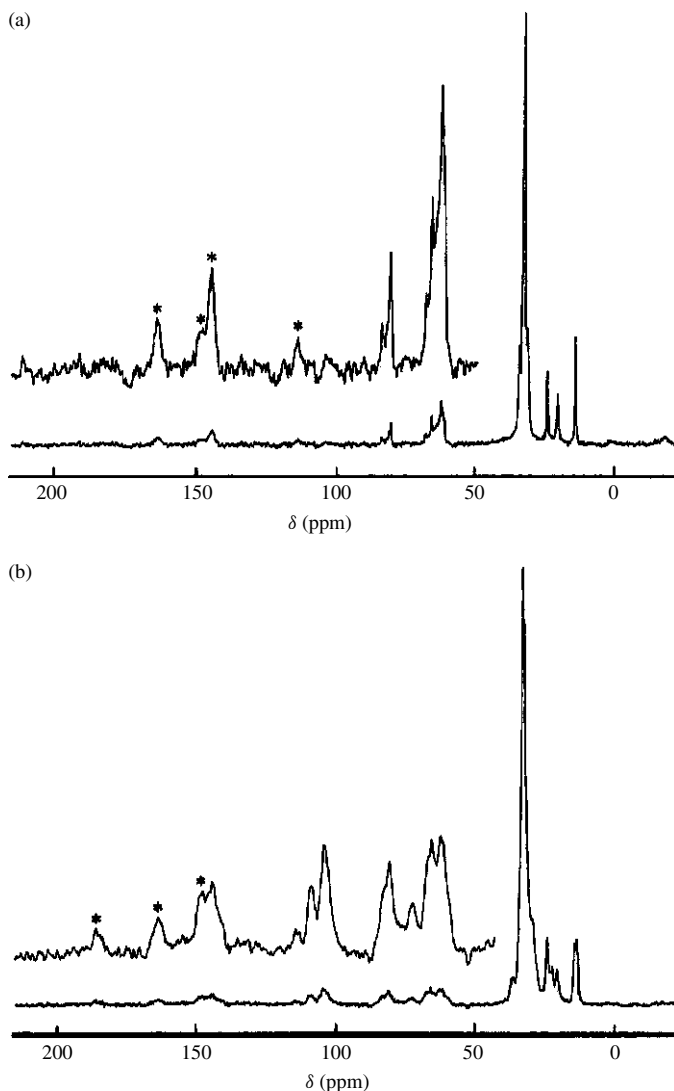


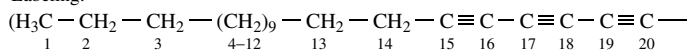
FIGURE 36. (a) ^{13}C CP/MAS spectrum of THY 30 min after recrystallization. Asterisks indicate spinning sidebands. The signals can be assigned to the THY monomer. (b) The spectrum after 22 h. The signals can be assigned to structure **100** shown in Figure 37. Reprinted with permission from Reference 53. Copyright (1994) American Chemical Society

82 ppm is assigned to the acetylene carbons at position 15 next to the alkyl chain, which splits into two peaks with a separation of 3.3 ppm. Similarly, the signal of the acetylene carbons at position 16 splits with a smaller separation of 2.2 ppm.

Although the signals of other acetylene carbons are split, they overlap in a very small range between 62 and 64 ppm and are too complicated to be distinguished from each other.

TABLE 35. ^{13}C chemical shifts of the THY monomer in solution and THY in the solid state after 30 min

In solution ^a (δ_{sn})	In the solid state ^b (δ_{sd})	$\delta_{\text{sd}} - \delta_{\text{sn}}$	Assignment ^c
81.91	85.2	3.3	15
	81.9	0	
	69.2	3.6	16
65.61	67.0	1.4	
62.70	62–64 ^d	1–2	17
62.36	d		18
61.46	d		19
60.34	d		20
31.92	35.4	3.5	3
28.82–29.64 ^e	33.8 ^f	4	4–12
27.83	32.5	4.7	13
22.69	25.6	2.9	2
19.52	21.8	2.3	14
14.14	15.4	1.3	1

^aCDCl₃ solution.^bCP/MAS.^cLabeling:^dOverlap each other.^eSeparated seven peaks for nine carbons.^fMany peaks overlap.

The splitting of the resonances from carbons in the same position is due to polymorphism of the monomer in the solid state. A similar ^{13}C signal splitting was found in monomers of octatetrayne derivatives containing urethane groups. It was not observed, however, in the corresponding alkyl-substituted octatetrayne monomer of HTY (**95**). In the THY monomer spectrum, the ^{13}C chemical shifts in the solid state (δ_{sd}) move to the low-field side from those in solution (δ_{sn}), and these differences ($\delta_{\text{sd}} - \delta_{\text{sn}}$) are shown in Table 35. Large low-field shifts are generally observed when the packing of alkyl chains is tight. In the case of the corresponding alkyl-substituted octatetrayne derivative of HTY, a signal of the carbons originating from the mobile chains was observed as a sharp line with a ^{13}C chemical shift similar to that found in the solution spectrum. Since the THY monomer did not show such mobile carbon signals, it is suggested that the stacking of the alkyl chains of the THY monomer is more rigid than in the HTY monomer.

After about 3 h, additional peaks at 146, 111 and 106 ppm appeared and their intensities gradually increased. These three peaks were assigned to the unsaturated carbons in the asymmetrically-substituted polydiacetylene backbone with acetylene substituents. A ^{13}C spectrum obtained after 22 h, when those three peaks were clearly observed, is shown in Figure 36B.

The structure of the polymer in the first step of polymerization is presented in Figure 37. The symbols defining the carbons are given in this figure. In the spectrum in Figure 36B, the peak at 73 ppm was assigned to the acetylene carbon (α) of the side chain. These assignments were based on the ^{13}C spectra of the polymer obtained from HTY. Spectral changes also occurred in the alkyl carbon region. The peak at 38 ppm was assigned to the methylene carbon (14') next to the olefin carbon in the polymer backbone. The intensity of the signal increased gradually concomitantly with those of the peaks for the polymer-backbone carbons. Simultaneously, the peak of the methylene carbon attached

to the acetylene moiety at 22 ppm decreased in intensity, and the relative intensities of the two peaks at 22 and 38 ppm became almost the same, as shown in Figure 36(b). The methyl carbon signal at 15.4 ppm came to have a shoulder on the higher field side and eventually separated to form a new peak at 14.6 ppm. After 22 h, the relative intensities of these two methyl carbon peaks became almost equivalent.

At this stage the main part of the crystals had changed from that of the monomer to **100** by the 1,4-addition. The ^{13}C chemical shifts of **100** are summarized in Table 36 together with those of the polydiacetylene with butadiynyl substituents (**96**) obtained from HTY.

The only difference between **100** and **96** is the acetylene carbon numbers in the side chains, i.e. six for **100** and four for **96**. However, the alkyl signals of **100** have a more complicated pattern than those of **96**. The signal positions of alkyl carbons attached to the acetylene side chain are assumed to be near those of the monomer, and those attached directly to the backbone may move to the higher field near those of the monomer in solution. The alkyl carbons bound to the polymer backbone and the acetylene group in **96** may be in similar situations since the ^{13}C peaks of the alkyl chain carbons in **96** do not split.

The ^{13}C spectral pattern for both the alkyl and the unsaturated carbon signals changed continuously. The ^{13}C spectrum measured after 56 h is shown in Figure 38(a).

The terminal methyl and methylene signals for the $-\text{CH}_2-\text{CH}_3$ moiety have become single lines, and the decreasing signals adjacent to the acetylene carbon around 22 ppm have disappeared, while the intensities of the signals at about 38 ppm from the newly formed methylene groups have increased. At the same time, the signal intensities of the main chain acetylene and olefin carbons in the region of 100–150 ppm have increased

TABLE 36. ^{13}C chemical shifts (CP/MAS) of **100** from THY and **96** from HTY

100	96	Assignment ^a
146	146.3	A
111.0	110.2	D
105.7	105	B, C
84		θ
82.1	80.7	β
73.2	72.6	α
67.0		ζ
67.0		η
65		ε
63.6	65.4	γ
63.6	88.7	δ
37.7	37.3	14'
35.2	^b	3
33.8 ^c	33.7 ^c , 31.3 ^{c,d}	4–12
32.5	^b	13
25.4	24.4	2
23.5		
21.9	22.3	14
15.4	14.8	1
14.6		

^aFor labeling of **100** see Figure 37.

^bBroad signal.

^cMany overlapping peaks.

^dMobile methylene carbons.

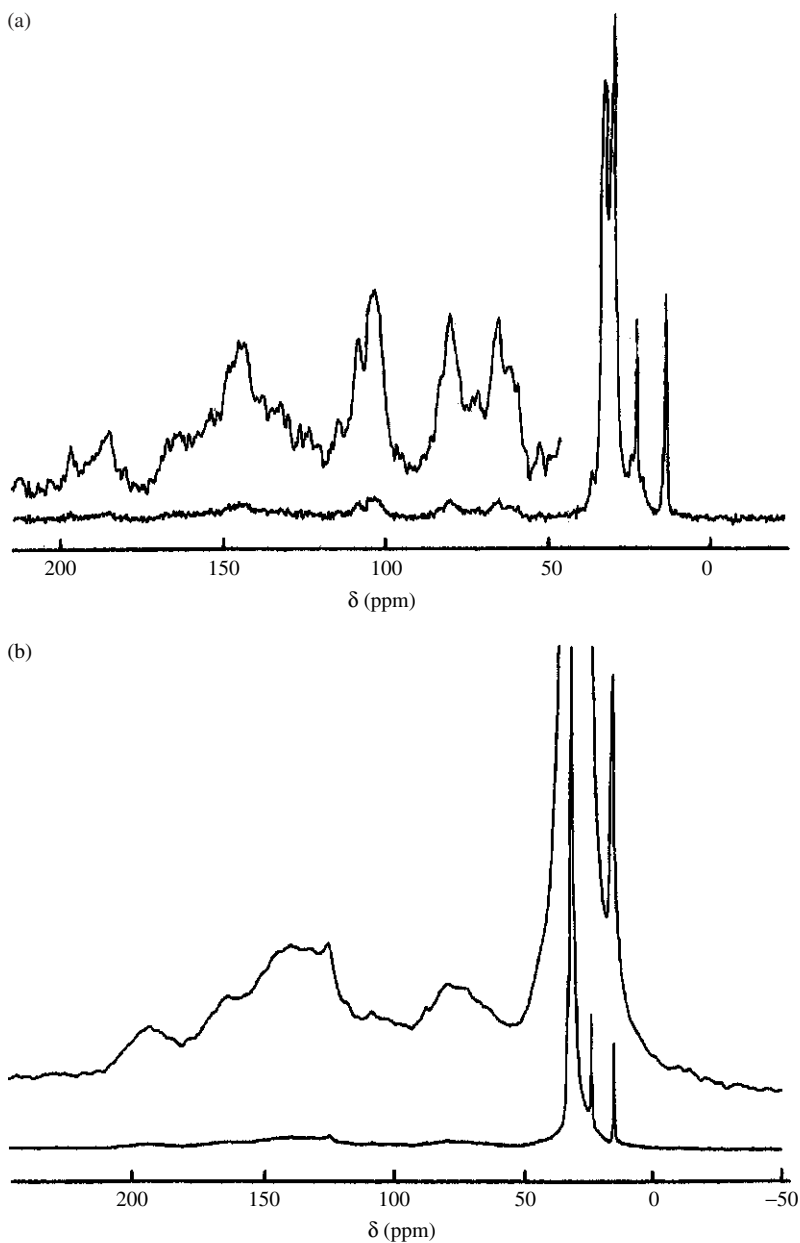


FIGURE 38. (a) ^{13}C CP/MAS spectrum of THY after 56 h. The proposed structure from this spectrum is the ladder polymer **101** shown in Figure 37. (b) The spectrum after 11 days. The proposed structure from this spectrum is the ladder polymer **102** shown in Figure 37. Reprinted with permission from Reference 53. Copyright (1994) American Chemical Society

relative to those of the side chain acetylene carbons (60–95 ppm), and signal patterns in the region for the unsaturated carbons became simpler than in the spectrum in Figure 36(b). The spectra measured successively during these periods indicate that the second step of polymerization occurred at the ξ - and θ -positions of **100** in the 1,4-polymerization scheme to produce a new ladder polymer (**101**), as presented in Figure 37 (the symbols defining the carbons are also indicated). Such a ladder-type structure with an extended π -electron system was also supported by the absorption in the >900 nm region described above. The ^{13}C chemical shifts of **101** are summarized in Table 37.

Since polymer **101** has a symmetrical structure, the number of nonequivalent carbons in the conjugated system was expected to be five with an intensity ratio of 1 : 1 : 2 : 1 : 1, which corresponds to the carbon positions A : D : B + C : β : α . The ^{13}C chemical shift values are also expected to remain similar to those of **100**. Subsequently, five peaks were observed at 147, 110, 105, 82 and 67 ppm having relative intensities of 1 : 1 : 2 : 1 : 1, as shown in Figure 38. The signals at 82 and 67 ppm were assigned to the ladder carbons at the β - and α -positions of the polydiacetylene chains, respectively. The three different methylene peaks from 30 to 34 ppm were assigned to the long chain carbons 3–13 in different stacked states in the solid state. In Figure 38, broad signals were observed around 120–170 and 190 ppm, and their intensity gradually increased. The rate of spectral change slowed down at this stage.

After 11 days, the alkyl carbon signals became simpler and only four peaks were observed, as shown in Figure 38(b). In this spectrum, the backbone acetylene and olefin carbon signals (100–150 ppm) were observed. The integrated intensity of the ladder carbon signals between 60 and 90 ppm accounted for 30% of the signals for unsaturated carbons (60–220 ppm).

Since the starting monomer of THY is a hydrocarbon and the reactions took place spontaneously in the solid state, the resulting polymer should be a hydrocarbon. No oxidation was confirmed from the IR spectra. The most likely chemical structures giving signals in the region >180 ppm are allenes. It was assumed⁵⁴ that the predominant structures of the final polymer are allene-type ladder polymers **102**, as shown in Figure 37. There are few ^{13}C shift data to examine for these allene structures. It has been confirmed that the solid-state ^{13}C shifts of tetraphenylbutatriene agree well with the solution data for the α - and β -cumulene carbons to the phenyl groups, which are at 124.1 and 152.9 ppm,

TABLE 37. ^{13}C chemical shifts (CP/MAS) of **101**

101	Assignment ^a
147	A
110	D
107	B, C
82	β
67	α
37 ^b	14
33.8 ^c , 30.6 ^{c,d}	4–13
32.5	3
23.4	2
14.5	1

^aFor labeling of structure **101** see Figure 37.

^bBroad signal.

^cMany overlapping peaks.

^dMobile methylene carbons.

respectively. The effect of the number of double bonds has been studied in solution, and the carbons at the β -position from the substituents in the allenes having an even number of double bonds with an odd number of sp-carbons give peaks between 180 and 210 ppm. From comparison with the data of 2,4-dimethyl-2,3-pentadiene and tetraphenylpropadiene, the ^{13}C chemical shift values of the α - and β -carbons of the methyl derivative shift about 20 and 10 ppm to a lower field, respectively. Although model compounds for the proposed structure of **102** could not be found and the substituent effects on the ^{13}C chemical shifts for longer allene systems are uncertain, the ^{13}C chemical shift values observed in Figure 38(a) seem reasonable.

The ^{13}C NMR spectra were measured regularly over 6 months (190 days) and the polymer structure became almost stable after this period. After 6 months, the relative intensities in the unsaturated carbon region were independent of CP time. The alkyl signal positions became constant after 11 days (Figure 38(b)). However, their line width gradually broadened to double the width after 6 months.

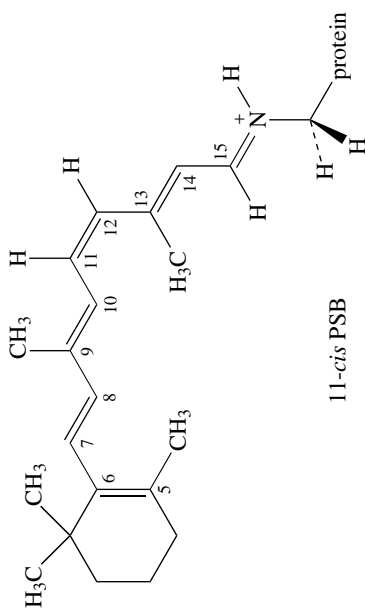
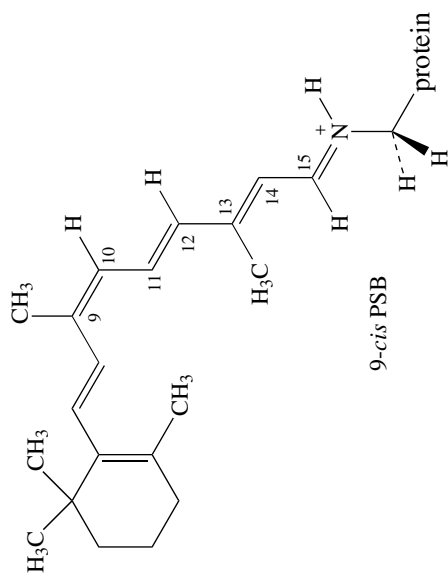
Smith and coworkers⁵⁵ reported a solid-state NMR study of the mechanism of the opsin shift in the visual pigment rhodopsin. They have presented solid-state NMR spectra of rhodopsin and isorhodopsin regenerated with retinal containing ^{13}C labels at each position along the conjugated chain of the chromophore. Comparison of the $^{13}\text{C}^*$ chemical shifts observed in the pigment with the corresponding chemical shifts of retinal PSB model compounds allowed them to examine the mechanism of the opsin shift in these pigments.

The chemical shifts for $^{13}\text{C}5$, $^{13}\text{C}6$, $^{13}\text{C}14$ and $^{13}\text{C}15$ correspond closely to the chemical shifts observed in the 9-*cis* and 11-*cis* PSB model compounds (shown below), while differences in chemical shifts are observed for C8 through C13, with the largest differences in both pigments localized at C13. These data provide support for the model of the opsin shift, which relies on a protein perturbation in the vicinity of C13. Concurrently, the results argue that the factors regulating the absorption wavelength in another well-studied retinal protein, bacteriorhodopsin, namely protein perturbations near the β -ionone ring (C5...C7), a 6-*s-trans* single bond and a weak hydrogen-bonding interaction with the Schiff base counterion, are not important in rhodopsin and isorhodopsin. Finally, in isorhodopsin a substantial shift is observed at C7, and only a small shift is present at C12. Taken together with resonance Raman results, these observations suggest that 9-*cis*- and 11-*cis*-retinals reside differently in the opsin binding pocket, in line with their significantly different opsin shifts (*ca* 1000 cm^{-1} less for isorhodopsin).

The general strategy for establishing the sites of protein–chromophore interactions in rhodopsin involves introduction of selective ^{13}C labels at each position along the length of the retinal chromophore.

Differences in the ^{13}C chemical shifts between rhodopsin and retinal PSB model compounds reveal the regions of the chromophore where changes occur in the retinal's structure or environment. Figure 39 presents several solid-state ^{13}C NMR spectra of rhodopsin that illustrate the resolution and sensitivity which can be obtained by using MAS methods.

In these spectra, the protein has been regenerated with retinal specifically ^{13}C labeled at positions 11, 12 and 13, and in each case the retinal resonance exhibits a sharp centerband at the isotropic chemical shift and is flanked by rotational sidebands. Other lines in the spectrum are the natural-abundance ^{13}C resonances of the protein carbonyls (*ca* 175 ppm) and aliphatic carbons (0–100 ppm). Contributions from the Ammonyx-LO detergent in these spectra are seen in the different intensities in the 0–100 ppm region. Ammonyx-LO does not exhibit NMR resonances above 100 ppm. Spectra of the 9-*cis* pigment isorhodopsin are similar. Table 38 summarizes the isotropic chemical shifts from the solid-state NMR spectra of rhodopsin regenerated with retinal ^{13}C labeled at each position along



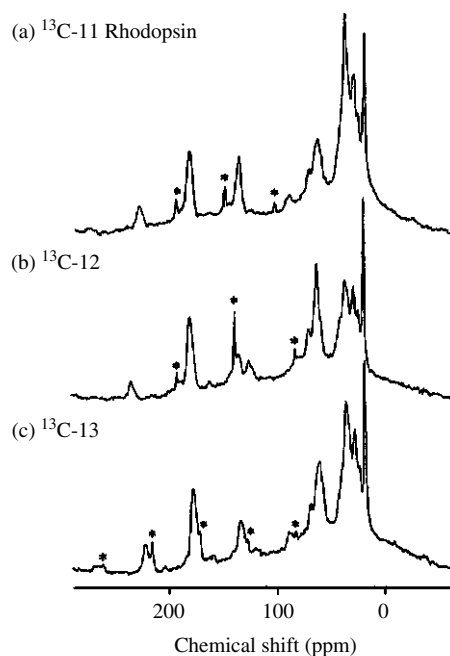


FIGURE 39. MAS ^{13}C NMR spectra of (a) ^{13}C -11, (b) ^{13}C -12 and (c) ^{13}C -13 rhodopsin. Centerbands and rotational sidebands of the retinal resonances are marked with asterisks. Reprinted with permission from Reference 55. Copyright (1990) American Chemical Society

TABLE 38. ^{13}C chemical shifts (ppm)^a for rhodopsin and 11-*cis* PSB model compounds

Position	Rhodopsin	11- <i>cis</i> -PSB	
		Cl^{-b} , <i>n</i> -propyl ^c	ClO_4^{-b} , <i>t</i> -butyl ^c
5	130.3	131.7	132.0
6	137.7	137.2	137.5
7	132.3	132.3	132.2
8	139.2	137.2	137.0
9	148.5	146.6	146.8
10	127.8	126.4	127.7
11	141.6	137.5	139.1
12	132.1	129.0	129.4
13	168.9	162.7	166.0
14	121.2	121.3	119.5
15	165.4	163.9	160.0
19	12.0	12.5	12.5
20	168.8	18.8	18.0

^aChemical shifts are referenced to TMS.

^bDesignates the counterion to the PSB.

^cAmine used to form the Schiff base.

the conjugated polyene chain. These data are compared with chemical shifts from two 11-*cis* PSB salts which differ in the amine and acid used to form the protonated Schiff base. The λ_{max} for the all-*trans*-retinal PSB perchlorate salt is at *ca* 470 nm in CCl_4 compared to *ca* 440 nm for the chloride salt. Thus, the bulky ClO_4^- counterion and *t*-butyl group may be inducing a weaker hydrogen bond at the Schiff base.

The differences in chemical shift observed between rhodopsin and the 11-*cis* PSB chloride salt are plotted in Figure 40. The shifts of $^{13}\text{C}5$ through $^{13}\text{C}7$, $^{13}\text{C}14$ and $^{13}\text{C}15$ in rhodopsin are close to their values in the 11-*cis* PSB model compound, while larger shift differences are observed at $^{13}\text{C}11$ (4.1 ppm), $^{13}\text{C}12$ (3.1 ppm) and $^{13}\text{C}13$ (6.2 ppm).

Table 39 summarizes the isotropic chemical shifts from the ^{13}C NMR spectra of isorhodopsin along with chemical shift data from the 9-*cis* PSB chloride salt. The difference in chemical shifts between isorhodopsin and the 9-*cis* PSB are qualitatively similar to the differences observed between rhodopsin and the 11-*cis* PSB with the exception of C7, where a 4.3 ppm chemical shift difference is observed, and C12, where the difference, amounting to about 3 ppm in rhodopsin, has now vanished.

Some possible explanations for these differences in isorhodopsin are considered below. In both rhodopsin and isorhodopsin, the largest chemical shift difference is observed at C13. Recently, an analysis of the solid-state NMR spectrum of $^{13}\text{C}12$ rhodopsin suggested that both the isotropic chemical shift and individual shift tensor elements shifted relatively to their values in bR⁵⁶. These results were interpreted as indicating a strong protein interaction at C12. The authors have reexamined these shifts and found that, although the isotropic chemical shift moves slightly in comparison to the PSB model compounds (129 \rightarrow 132 ppm), the principal values of the chemical shift tensor are largely unperturbed ($\sigma_{11} = 58$ ppm, $\sigma_{22} = 133$ ppm, $\sigma_{33} = 212$ ppm). This is illustrated in Figure 41, where difference spectra between labeled and unlabeled rhodopsin highlight the retinal resonance, and are compared with simulations using the shift tensor values obtained from the all-*trans* PSB model compound (Figure 41b) and from the previous $^{13}\text{C}12$ rhodopsin spectra of Mollevanger and coworkers⁵⁶ (Figure 41c). In these spectra, the centerband (at the isotropic chemical shift) is at *ca* 130 ppm and is flanked by rotational sidebands spaced at the spinning frequency. The relative intensities of the centerbands and sidebands determine

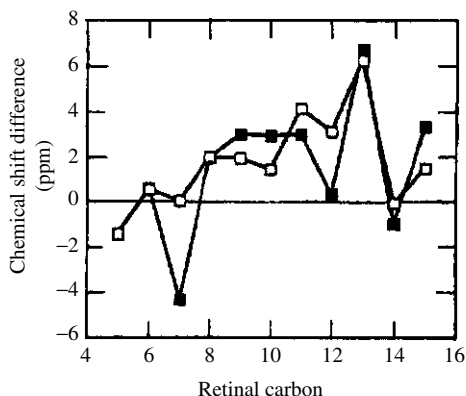


FIGURE 40. Plot of the differences in chemical shift observed between rhodopsin and the 11-*cis*-retinal PSB chloride salt (open squares), and between isorhodopsin and the 9-*cis*-retinal PSB chloride salt (closed squares), for retinal carbons along the polyene chain. Reprinted with permission from Reference 55. Copyright (1990) American Chemical Society

TABLE 39. ^{13}C chemical shifts (ppm)^a for isorhodopsin and the 9-*cis* PSB *n*-butylammonium chloride salt

	Isorhodopsin	9- <i>cis</i> PSB
5	130.5	132.0
6	137.0	136.4
7	128.2	132.5 ^b
8	131.1	129.2
9	147.5	144.5
10	130.8	127.9
11	139.3	136.3
12	133.9	133.6 ^b
13	169.2	162.5
14	119.0	120.0
15	166.5	163.2
19	19.8	20.9
20	13.6	14.3

^aAll chemical shifts are referenced to TMS.

^bThe assignments of the C7 and C12 resonances in the 9-*cis* PSB may be reversed since on-resonance decoupling affects both resonances.

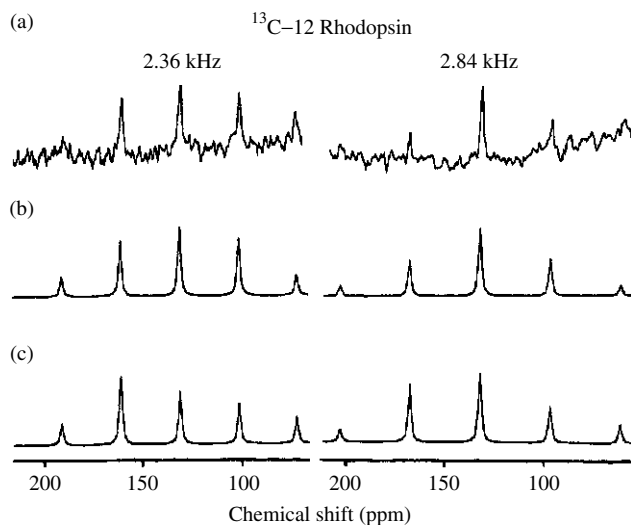


FIGURE 41. Solid-state NMR spectra of the ^{13}C -12 retinal resonance in rhodopsin (a) obtained by taking the difference between ^{13}C -12 rhodopsin and unlabeled rhodopsin spectra. Spectra were obtained at two spinning speeds, 2.36 kHz (left) and 2.84 kHz (right), and are compared with simulations (b and c) based on different chemical shift tensors. The simulations in (b) are for a chemical shift tensor having the principal tensor elements of the all-*trans* PSB chloride salt ($\sigma_{11} = 58$, $\sigma_{22} = 133$, $\sigma_{33} = 212$), while the simulations in (c) use the shift tensor values ($\sigma_{11} = 41$, $\sigma_{22} = 149$, $\sigma_{33} = 209$) obtained for ^{13}C 12 rhodopsin by Mollevanger and coworkers⁵⁶. Reprinted with permission from Reference 55. Copyright (1990) American Chemical Society

the chemical shift tensor. Comparison of the intensity of the first sideband with the centerband intensity clearly shows the difference between the two simulations.

The experimental data closely resemble the simulation based on the all-*trans* PSB values. The discrepancy between the two solid-state NMR studies on rhodopsin arises in part from a difference, in signal-to-noise ratio and in part from possible problems associated with a fatty acid resonance which overlaps with the centerband in the previous study. The simulations illustrate the sensitivity of the sideband intensities to changes in the chemical shift tensor, as well as the quality of data necessary to accurately determine the shift tensor values.

2. ^2H static NMR

Ulrich and coworkers⁵⁷ reported a distorted structure analysis of the retinal chromophore in bacteriorhodopsin resolved by ^2H NMR. Measuring the orientations of its individual methyl groups reveals structural details about the geometry of the retinal chromophore in the binding pocket of bacteriorhodopsin. Solid-state ^2H NMR measurements were performed on macroscopically oriented samples of purple membrane patches, containing retina specifically deuterium-labeled at one of the three methyl groups along the polyene chain (C18, C19, C20). The deuterium quadrupole splitting of each 'zero-tilt' spectrum is used to calculate the orientation of the corresponding C-CD₃ bond vector with respect to the membrane normal; however, two possible solutions may arise. These ambiguities in angle could be resolved by recording a tilt series of spectra at different sample inclinations to the magnetic field and analyzing the resulting complex line shapes with the aid of computer simulations. The angles for the C18, C19 and C20 group are found to be $37 \pm 1^\circ$, $40 \pm 1^\circ$ and $32 \pm 1^\circ$, respectively. These highly accurate values imply that the polyene chain of the retinal chromophore is not straight but rather has an in-plane curvature and possibly an out-of-plane twist. Together with the angles of the remaining methyl groups on the cyclohexene ring that have been measured previously, an overall picture has thus emerged of the intramolecular conformation and the three-dimensional orientation of retinal within bacteriorhodopsin. The deduced geometry confirms and refines the known structural information on the chromophore, suggesting that this ^2H NMR strategy may serve as a valuable tool for other membrane proteins.

Immobilized proteins in uniaxially oriented membrane samples give rise to highly characteristic ^2H NMR spectra, when labeled at one specific position such as an individual methyl group. The deuterium quadrupole splitting and the spectral line shapes contain information about the bond vector that can be used for the structure determination⁵⁸. Note that, due to the rapid spinning of the methyl group in the otherwise immobilized sample, the orientation of the three deuterium atoms are time-averaged and the effective bond vector corresponds to the methyl-rotor axis. Generally, there exists a simple relationship between the spectral quadrupole splitting $\Delta\nu_Q$ and the angle θ of a C-CD₃ bond vector with respect to the magnetic field direction (equation 3):

$$\Delta\nu_Q = 40(3\cos^2\theta - 1) \quad (\text{kHz}) \quad (3)$$

The scaling factor of 40 kHz was independently determined at -60°C from the powder spectrum of a random dispersion of a deuteriated PM sample⁵⁹. This value was further confirmed in the simulations of the ^2H NMR tilt series for each of the three labeled methyl groups, according to the total spectral width and line-shape arguments discussed by Ulrich and Watts⁵⁸.

Simple ^2H NMR spectra that can be readily interpreted are observed when the uniaxially oriented sample is aligned with its normal parallel to the spectrometer magnetic field

direction ('zero-tilt' spectrum). These spectra consist of a pair of resonances, separated by a certain quadrupole splitting which is determined by the orientation of the methyl group on the protein. In this experimental geometry, all the labeled bond vectors make the same angle θ with the sample normal and therefore also with the spectrometer field direction. All deuteriomethyl groups thus contribute the same quadrupole splitting $\Delta\nu Q$ to the overall spectral line shape. In practice, when the alignment of the membrane fragments in the sample plane is less than perfect, the mosaic spread of the sample gives rise to a certain degree of spectral line broadening.

From the quadrupole splitting in the zero-tilt spectrum of a single labeled methyl group, it should be straightforward to calculate the angle of that group relative to the membrane normal, using equation 3. However, only the absolute value and not the sign of the quadrupole splitting is measured from the spectrum, and positive and negative splittings cannot be discriminated.

Therefore, two solutions to equation 3 are obtained whenever $\Delta\nu Q < 40$ kHz, which corresponds to the range of angles between 35° and 90° . To resolve this ambiguity, Ulrich and Watts⁵⁸ have recently developed a strategy by which the value of the angle θ can be extracted uniquely from a series of measurements of the oriented sample at different inclinations to the spectrometer field. The line shapes of such a tilt series are considerably more complex than the simple zero-tilt spectrum described above, because the bond vectors are distributed over a range of different angles. Consider a cone of methyl group bond vectors being progressively tilted with respect to the reference direction of the spectrometer field. Depending on the cone opening angle θ , at any particular alignment relative to the field, the bond vectors assume a discrete range of angles. They all contribute their respective quadrupole splitting to the overall spectral line shape, which can be computed by summing up these overlapping contributions weighted by their corresponding probability density. A full tilt series can thus be analyzed quantitatively with the aid of computer simulations, or qualitatively by eye, revealing both the value and the sign of the quadrupole splitting, from which the angle is unambiguously defined between 0° and 90° with respect to the membrane normal.

The ^2H NMR spectra from three different bR samples (dark adapted) are shown in Figure 42, where the retinal is selectively deuteriated in the C18, C19 or C20 methyl group, respectively. The uniaxially oriented PM patches were measured with the membrane normal parallel to the spectrometer magnetic field, at -60°C . Measurements at room temperature gave essentially the same spectra but with a poorer signal-to-noise ratio, and the line shapes were obscured by an isotropic resonance from the residual deuterium in the water. In each of the zero-tilt spectra in Figure 42, two broad resonances are seen with a respective quadrupole splitting (absolute value) of 36 kHz (for C18), 30 kHz (for C19) and 46 kHz (for C20). The initial step in the analysis consists of calculating the corresponding value(s) for θ from equation 3. In the case of the C20-labeled retinal with a (46 ± 1) -kHz splitting, the angle between the C- CD_3 vector and the membrane normal is found to be $\theta = 32 \pm 1^\circ$. This solution is unambiguous, because the quadrupole splitting is larger than 40 kHz and must therefore be positive. The other two quadrupole splittings of 36 and 30 kHz from the C18 and C19 deuteriomethyl groups, on the other hand, each gives rise to two possible bond angles, depending on the sign of the splitting, which is not known. That is, with a measured $\Delta\nu Q$ of 36 kHz, a bond angle of $\theta = 37^\circ$ or 73° is calculated for the C18 group, and a $\Delta\nu Q$ of 30 kHz for C19 gives $\theta = 40^\circ$ or 73° , for positive or negative splitting, respectively. The correct bond angle can be distinguished by measuring a tilt series of ^2H NMR spectra, as illustrated in Figure 43.

The experimental data from the C19 deuteriomethyl group are given in the middle column, at seven different sample inclinations (α , angle between sample normal and spectrometer field direction) from 0° to 90° in the spectrometer. For comparison, the line shapes predicted by computer simulation are shown on either side of the experimental

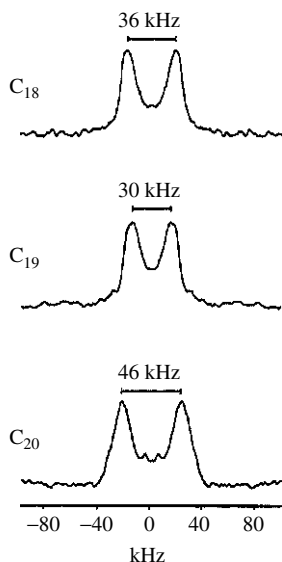


FIGURE 42. ^2H NMR spectra from three different bR samples containing retinals with the individually deuterium-labeled methyl groups C18, C19 and C20. Reprinted with permission from Reference 57. Copyright (1994) American Chemical Society

tilt series, with the simulation for $\theta = 40^\circ$ in the left-hand column and for $\theta = 73^\circ$ in the right-hand column. Note that only the zero-tilt simulations at $\alpha = 0^\circ$ in the top row are indistinguishable, regardless of the sign of the 30 kHz quadrupole splitting, which is positive in the left column ($\theta = 40^\circ$) and negative in the right column ($\theta = 73^\circ$).

Across the whole tilt series in Figure 43, a close resemblance is seen between the experimental spectra in the middle column with the simulated line shapes on the left ($\theta = 40^\circ$) but not with those on the right ($\theta = 73^\circ$). Therefore, the angle θ is uniquely identified to be $40 \pm 1^\circ$ for the deuteriated C19 group on retinal. A similar analysis for the C18 group ($\Delta\nu Q = 36$ kHz) yields an angle of $37 \pm 1^\circ$, and the other possible value of 79° is rejected. The experimental spectra of that tilt series plus those of C20 ($\Delta\nu Q = 46$ kHz, $\theta = 32^\circ$, see above) are shown in Figure 44, together with the superimposed best-fit line shape simulations.

The analysis of a full tilt series of ^2H NMR spectra not only allows the determination of the unique bond angle for a deuteriated methyl group, but also provides an internal check for the consistency of the spectral interpretation. In particular, simulations provide a means for the analysis of line-broadening effects, which arise from the sample mosaic spread as well as the intrinsic line width of the nuclear transition and instrumental factors. When line shapes are fitted to a full tilt series of spectra in a concerted manner and are also compared with the powder spectrum of an unoriented sample, the different contributions can be discerned. In that way an intrinsic line width of around 2 kHz is found for the spectra shown here, together with a mosaic spread between $\pm 8^\circ$ and $\pm 10^\circ$ for the three samples.

From the good fit to the experimental spectra it is thus evident that one characteristic angle θ describes the whole tilt series and that the underlying cone model for the bond vectors is consistent. The accuracy of the angles determined is estimated to be within

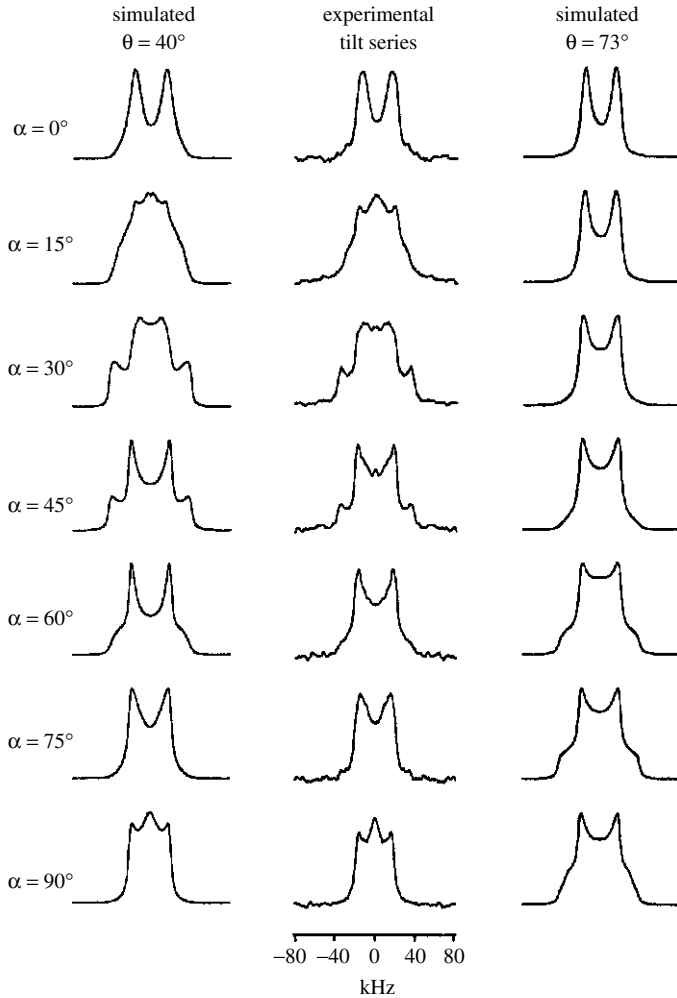


FIGURE 43. Tilt series of ^2H NMR spectra from the C19 deuteriomethyl group of retinal in oriented purple membranes, recorded at seven different inclinations (α) of the sample normal relative to the spectrometer field. Both the experimental data (middle column) and the two simulated series (outer columns) are characterized by an absolute quadrupole splitting of 30 kHz in the zero-tilt spectrum ($\alpha = 0^\circ$, top row). The simulations on the left are based on a methyl group angle of $\theta = 40^\circ$ which corresponds to a positive splitting, while the simulations on the right are based on $\theta = 73^\circ$ with a negative quadrupole splitting. Reprinted with permission from Reference 57. Copyright (1994) American Chemical Society

$\pm 1^\circ$, since the range around 45° is particularly sensitive as is seen from equation 3. A small change of 1° in θ would lead to a significant change in the quadrupole splitting of around 2 kHz in the zero-tilt spectrum. When the labeled segment is undergoing any small oscillations with a correlation time of less than $1/\Delta\nu_Q$, *ca* 10^{-5} s, the angle obtained represents the time-averaged orientation of the methyl group.

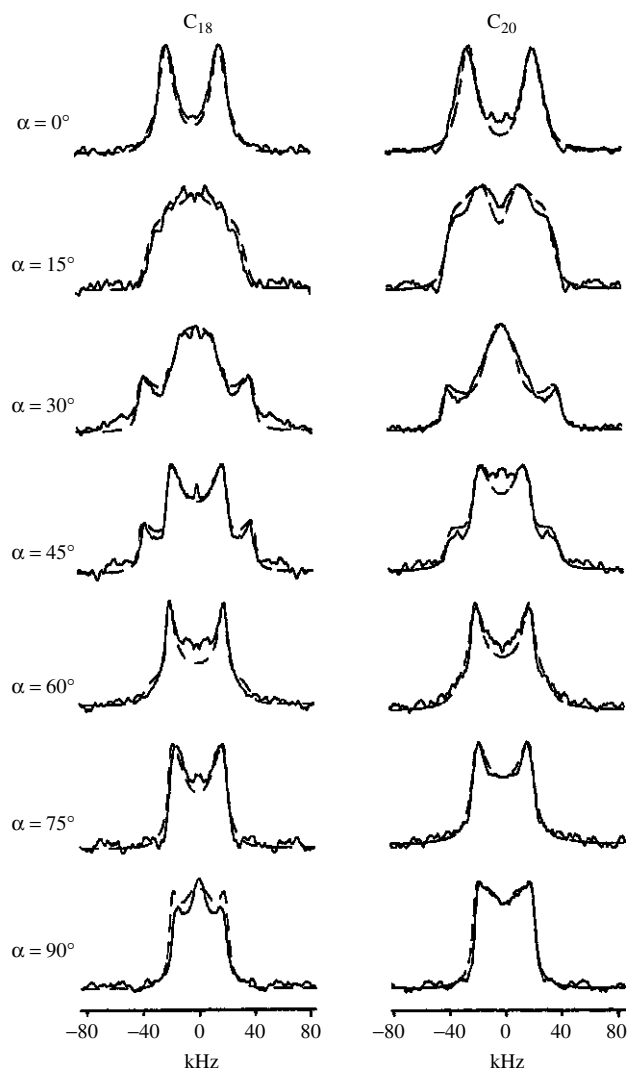


FIGURE 44. Tilt series of ^2H NMR spectra from the deuteriomethyl groups C18 (left column) and C20 (right column) of retinal in oriented purple membranes, at seven different sample inclination (α) in the spectrometer field. The line-shape simulations are superimposed over the experimental spectra in order to illustrate the good line fit obtained by the prediction method. Reprinted with permission from Reference 57. Copyright (1994) American Chemical Society

Figure 45 illustrates how all the different methyl group orientations with respect to the membrane normal N are accommodated in space by the proposed structure of retinal within bR. This picture is clear from the measured values of θ , which are indicated as labels to the individual methyl groups. The roughly parallel orientations of the two methyl groups, C18 ($\theta = 37^\circ$) and C19 ($\theta = 40^\circ$), demonstrate that retinal must have a

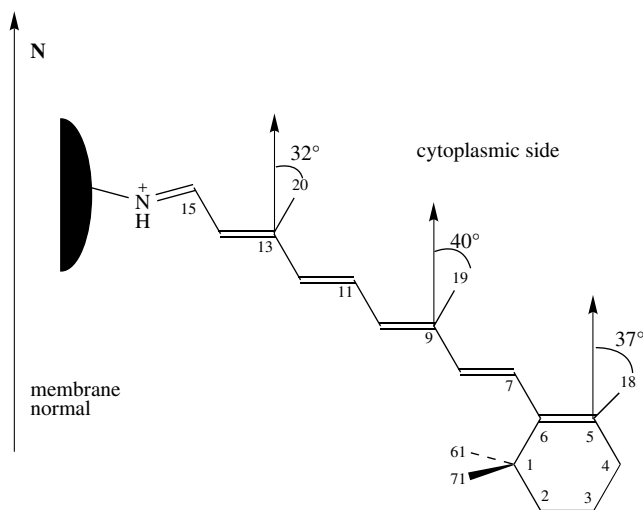


FIGURE 45. Orientation and conformation of retinal in bR, constructed from the individual methyl group orientations that have been determined by solid-state ^2H NMR. The angles θ of the C- CD_3 bond vectors with respect to the membrane normal (N) were evaluated for C_{18} (37°), C_{19} (40°) and C_{20} (32°) from the zero-tilt spectra shown in Figure 44 and with the aid of line-shape simulation of the tilt series in Figure 42 and 43. Reprinted with permission from Reference 57. Copyright (1994) American Chemical Society

$6s$ -*trans* rather than a $6s$ -*cis* conformation when bound to bacteriorhodopsin. That is, a 180° rotation around the C6–C7 bond, which has a substantially lower energy barrier compared to the other single bonds of the conjugated system, would produce a structure that is incompatible with the measured angles. This conclusion confirms previous solid-state NMR studies that have proposed a $6s$ -*trans* chromophore from comparison with crystalline model compounds. By focussing on the specific angles of the three methyl groups, C18, C19 and C20, along the polyene chain, it is apparent that the chromophore backbone cannot be perfectly straight.

In an undistorted system of conjugated double bonds, the three methyl groups would be expected to be exactly parallel; however, in this case their individual orientations are not the same with respect to the membrane. In particular, the two neighboring methyl groups, C19 ($\theta = 40^\circ$) and C20 ($\theta = 32^\circ$), show that the carbon framework of the polyene chain must be distorted by an in-plane curvature and possibly an out-of-plane twist. The fact that the two methyl groups, C18 ($\theta = 37^\circ$) and C19 ($\theta = 40^\circ$), are not entirely parallel may be partially attributed to the additional rotational flexibility around the C6–C7 bond. It thus appears that the observed in-plane curvature, and possibly an out-of-plane twist, relieve the steric crowding of the three methyl groups (C18, C19 and C20) along the retinal chain, as well as the interference of the *gem*-dimethyl groups (C16 and C17) on the ring with the proton on C8. A more refined picture of the chromophore in terms of the individual bond and torsion angles could be obtained by computer modeling of the molecular framework to the set of geometrical constraints, i.e. to the measured methyl group orientations. However, since the in-plane and out-of-plane distortional modes are interdependent, it is not possible to quantify the contribution of each, and a family of plausible retinal structures which are compatible with the ^2H NMR results would emerge.

Ulrich and coworkers⁵⁹ reported the orientation and conformation of the cyclohexene ring of retinal in bacteriorhodopsin of the purple membrane of *Halobacterium halobium* by solid-state ^2H NMR spectroscopy, through the determination of individual chemical bond vectors (Figure 46). The chromophore ([2,4,4,16,16,16,17,17,17,18,18- ^2H 11] retinal) was specifically deuterium-labeled on the cyclohexene ring and incorporated into the protein. A uniaxially oriented sample of purple membrane patches was prepared and measured at a series of inclinations relative to the spectrometer field. Computer simulations were applied in the analysis of the ^2H NMR spectrum line shapes. From the deuterium quadrupole splittings, the specific orientations of the three labeled methyl groups on the cyclohexene ring could be calculated. The two adjacent methyl groups (on C1) of the retinal were found to be approximately horizontal to the membrane and make respective angles of $94^\circ \pm 2^\circ$ and $75^\circ \pm 2^\circ$ with the membrane normal. The third group (on C5) points toward the cytoplasmic side with an angle of $46^\circ \pm 3^\circ$. These intramolecular constraints indicate that the cyclohexene ring lies approximately perpendicular to the membrane surface and that it has a *6s-trans* conformation. From the estimated angle of the tilt of the chromophore long axis, it is concluded that the polyene chain is slightly curved downward to the extracellular side of the membrane (Figure 47).

Figure 48 shows representative experimental ^2H NMR spectra from the labeled retinal in bR in a dark-adapted PM sample. The line shape simulations are superimposed on the experimental spectra. The powder pattern [Figure 48(a)] serves as a general reference for the tilt series of spectra recorded at various sample inclinations [Figure 48(b)], because it defines the accessible frequency region over which the spectral intensity can occur. The oriented sample was measured at every 22.5° between 0° and 90° , of which three inclinations are represented in Figure 48(b) with $\alpha = 0^\circ, 45^\circ$ and 90° .

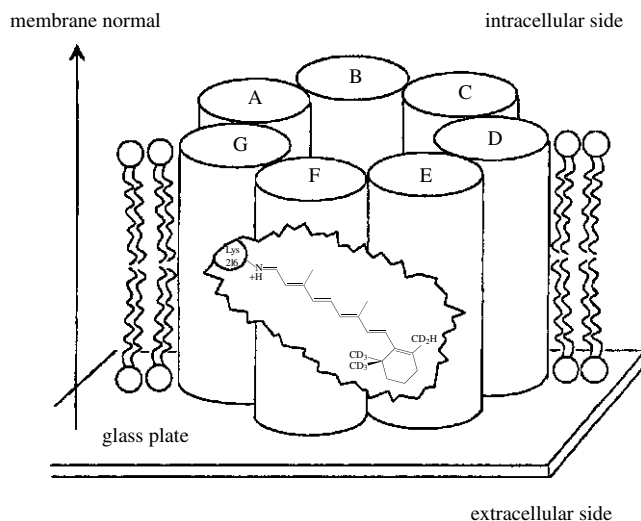


FIGURE 46. Retinal chromophore in bR is attached via a protonated Schiff base to Lys-216 on helix G and is tilted toward the extracellular side. To determine its detailed structure, retinal was selectively deuteriated on the three methyl groups on the cyclohexene ring and incorporated into bR from *H. Halobium*. Reprinted with permission from Reference 60. Copyright (1997) American Chemical Society

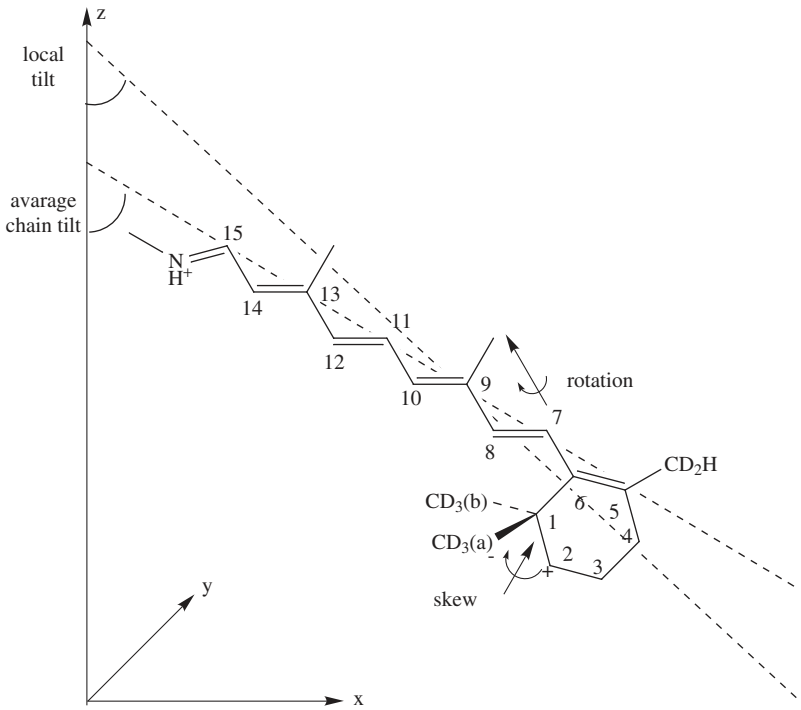


FIGURE 47. Three-dimensional structure of the cyclohexene ring of retinal in bR as determined by ^2H NMR, relative to the membrane surface in the x - y plane. Analysis of the orientations of the three deuterium labeled methyl groups on the puckered ring (skew around C1-C6) indicates that the chromophore has a *6s-trans* conformation around the C6-C7 bond. Reprinted with permission from Reference 60. Copyright (1997) American Chemical Society

With the sample aligned horizontally in the magnet, further spectra were recorded over a range of temperatures from 30° down to -120°C . Representative line shapes are compared in Figure 48 for 21°C (c) and -60°C (b). The signal-to-noise ratio improves dramatically with decreasing temperature, and therefore the spectral analysis was based on the set of data acquired at -60°C . The central resonance line which appears at temperatures above 0°C is due to HDO. Two components appear to be resolved at 21°C , but they are found to broaden and merge to give the unresolved line shape at -60°C . A possible interpretation of this observation could be that some small local fluctuations within the puckered cyclohexene ring are frozen out in a slight glassy disorder, which is commonly found in crystalline retinal derivatives. Nevertheless, the overall line shape does not change significantly over the whole range of temperatures examined, and therefore the structure of the chromophore appears to remain relatively unaffected by freezing.

The characteristic shape of the ^2H NMR powder pattern [Figure 48(a)] indicates that the dynamics of the rotating methyl groups is within the fast-motional limit at temperatures down to -120°C . This assumption is further supported by the increasing signal-to-noise ratio with decreasing temperature, since no loss, but rather a gain, in intensity is observed on cooling. It is also clear that the cyclohexene ring does not undergo significant librational

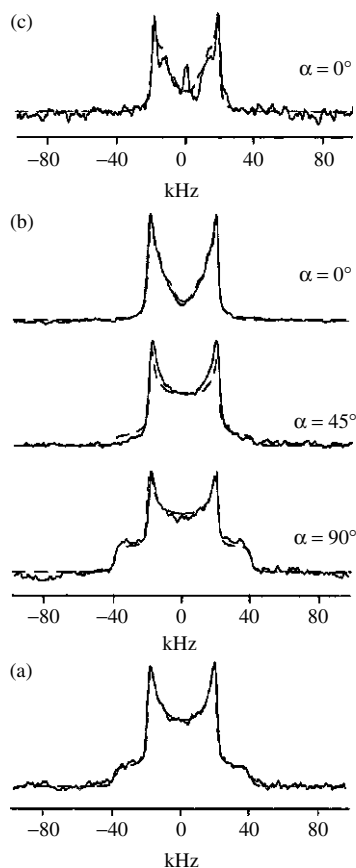


FIGURE 48. Representative ^2H NMR spectra (full lines) of dark-adapted bR (90 mg) containing deuterated retinal, with line shape simulations (dashed lines) superimposed. Both the powder spectrum (a) from randomly oriented PM patches and the tilt series (b) over sample inclinations, $\alpha = 0^\circ$, 45° and 90° , were recorded at -60°C (number of scans, 1.7×10^5 , for $\alpha = 0^\circ$). Spectrum (c) was measured at 21°C with $\alpha = 0^\circ$ (number of scans, 3×10^5). Reprinted with permission from Reference 60. Copyright (1997) American Chemical Society

motion within its binding pocket, since the ^2H NMR spectra are not time-averaged by this type of random oscillation (with a correlation time $\tau_c < 10^{-6}$ s). The polyene chain of the chromophore has been shown to be completely immobilized on the time scale of 10^{-9} – 10^{-2} s, indicating the absence of any rotational freedom.

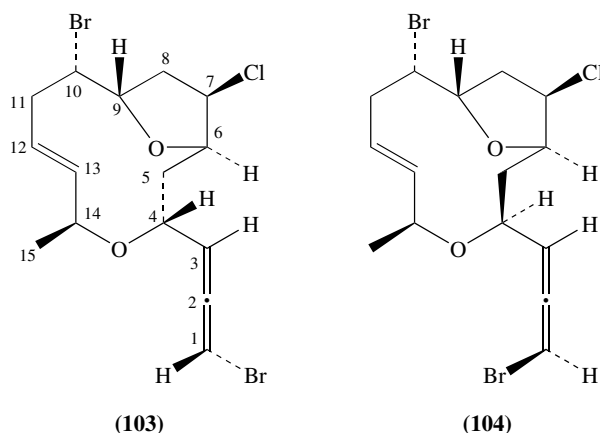
With a horizontally oriented sample ($\alpha = 0^\circ$), the spectrum of the labeled bR in Figure 48(b) should display three quadrupole splittings corresponding to the three labeled methyl groups on the retinal. It is apparent, however, that the expected three pairs of resonances are not resolved because of spectral overlap of the broadened lines. A computer simulation approach was used to analyze the spectral line shapes despite the overlap, but much qualitative information about the cyclohexene ring can be gained by simple inspection of the experimental data in Figure 48.

IV. SPECIAL TOPICS

A. Allenes

Allenes form a unique class of compounds which are dienes (or polyenes), but simultaneously they are the parent compounds for the interesting family of cumulenes. The NMR investigation of these compounds is interesting in view of their unique electronic and structural properties.

A new C15 bromoallene⁶⁰, dactylallene (**103**), was isolated from the digestive gland of the anaspidean mollusc *Aplysia dactylomela*. The structure was established by using mainly one- and two-dimensional NMR techniques, whereas the absolute stereochemistry was determined by X-ray diffractometric analysis. Ichthyotoxicity and antifeedant activity suggests a defensive role of **103** against predators. The structure of **103** is given below together with that of its stereoisomer **104**.



The ¹H NMR spectrum displayed signals attributable to a secondary methyl at δ 1.33 (H15, d, $J = 7.0$ Hz), six deshielded methines at δ 4.00 (H-6), δ 4.19 (H-4), δ 4.38 (H-7), δ 4.42 (H-14), δ 4.48 (H-10), δ 4.73 (H-9) and three methylenes at δ 1.59 (H-5a, ddd, $J = 14.0, 10.7$ and 1.9 Hz) and δ 1.69 (H-5b, m), δ 2.40 (H-8a, m), and δ 2.43 (H-8b, m), δ 2.43 (H-11a, m) and δ 2.89 (H-11b, m), strongly suggesting a nonterpenoid structure containing heteroatoms.

The presence of a bromoallene function was indicated both by two long-range coupled methine signals in the ¹H NMR spectrum at δ 6.01 (H1, dd, $J = 5.8$ Hz and 1.7 Hz) and δ 5.35 (H3, dd, $J = 5.8$ and 6.0 Hz) and by the resonances in the ¹³C NMR spectrum at δ 73.66 (C1), δ 103.62 (C3) and δ 200.99 (C2) (Table 40).

However, dactylallene (**103**) differs from **104** mainly in the chemical shifts of C14 (δ 70.54 in **103**, δ 61.26 in **104**), C4 (δ 64.68 in **103**, δ 76.34 in **104**) and C15 (δ 14.05 in **103**, δ 21.19 in **104**), suggesting a different relative stereochemistry for C4 or C14. However, the difference between the δ values for C4 and C14 in **103** and **104** is too large to be justified only by a different relative stereochemistry at the chiral center C4 or C14; it is most likely that these assignments in **104** should be reversed. In addition, the sign of $[\alpha]_D$ of **103**, opposite to that of **104**, indicated a different absolute stereochemistry of the allene residue, which could be predicted as S according to the Lowe–Brewster's rule⁶¹.

Barretta and coworkers⁶² reported an assignment of the absolute configuration of chiral allenes, which is usually a difficult task. The problem has been solved by suitable chemical

TABLE 40. ^1H and ^{13}C NMR data^{a,b} for dactylallene (**103**)

Position	$\delta^1\text{H}$	m	$J(\text{Hz})$	$\delta^{13}\text{C}$	m ^c	Long-range connectivities ^d
1	6.01	dd	5.8 and 1.7	73.66	d	H3
2				200.99	s	H1, H3, H4
3	5.35	dd	5.8 and 6.0	103.62	d	H1, H4, H5a
4	4.19	m		64.68	d	H1, H3, H5a, H14
5	1.59	ddd	14.0, 10.7, 1.9	37.05	t	H4
	1.69					
6	4.00	m		76.69	d	H5b, H7, H8, H9
7	4.38	m		62.51	d	H6, H8
8	2.40	m		38.61	t	
	2.43					
9	4.73	m		78.26	d	H7, H11
10	4.48	m		49.96	d	H8, H11
11	2.43	m		37.84	t	H9
	2.89					
12	5.79	m		128.23	d	H11, H14, H15
13	5.72	m		128.23	d	H11, H14, H15
14	4.42	m		70.54	d	H4, H12, H13, H15
15	1.33	d	7.0	14.05	q	

^aBruker AMX 500 MHz, CDCl_3 ; δ values are reported in ppm referred to CHCl_3 (δ_{H} 7.26) and to CDCl_3 (δ_{C} 77.0).

^bAssignments determined by $^1\text{H}^{13}\text{C}$ CHETCOR, $^1\text{H}^1\text{H}$ COSY, $^1\text{H}-^1\text{H}$ decoupling experiments.

^cDetermine by DEPT sequence.

^dBy HMBC ($J = 10$ Hz).

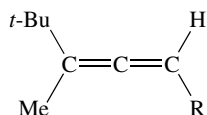
correlations of allenes with centrosymmetric molecules of known absolute configuration or by developing semiempirical rules, which relate the absolute configuration to the sign of the rotatory power or CD bands.

An alternative approach is provided by NMR spectroscopy. Separate NMR signals can be in principle obtained for stable or short-lived diastereomeric derivatives of the enantiomeric mixtures, the intensities of which are correlated with the enantiomeric composition and their relative stereochemistry to the absolute configuration. For this reason, great effort has been continually devoted to the development of new chiral auxiliaries for NMR spectroscopy. The majority of these are dedicated to the chiral assay of molecules having polar functional groups.

Recently, it was found that the commercially available heptakis(2,3,6-tri-*O*-methyl)- β -cyclodextrin (permethylated β -cyclodextrin, TRIMEB), induced nonequivalence in the ^1H NMR spectra, in CD_3OD , of enantiomeric mixtures of trisubstituted allenes devoid of polar functional groups, thus affording a simple and general way to determinations of their enantiomeric purity⁶³.

The authors reported that a consistent correlation exists between the absolute configuration of the trisubstituted allenes **105a–e** and the permethylated β -cyclodextrin induced shifts of their proton signals. Hence the use of TRIMEB as chiral auxiliary for the rapid and reliable NMR determination of their absolute configuration was proposed. The enantiomeric purities of the samples have been determined by analyzing the ^1H NMR spectra of their mixtures with permethylated β -cyclodextrin (with TRIMEB/allene molar ratios of 1–2) in CD_3OD solutions. In all cases TRIMEB distinguished between the two enantiomers of each of the allenes **105a–e**. The corresponding spectral regions relative to the resonances of the allene protons of the substrates in the presence of the cyclodextrin are reported in Figure 49. The bromoallene (*R*)-**105a** showed the major signal at 6.10 ppm, at

higher field than the minor signal corresponding to the (*S*)-allene at 6.14 ppm. The allenes **105b–e**, having (*S*)-absolute configuration, generated from the bromoallene **105a**, showed a major signal (at 6.12, 6.13, 7.02 and 6.09 ppm for **105b**, **105c**, **105d** and **105e**, respectively), which was at lower field than the minor signal due to the (*R*)-allene (at 6.09 ppm for **105b–c**, 6.95 ppm for **105d** and 6.06 ppm for **105e**). For the (*R*)-allenes **105b–e**, it has been also verified that the allene absorption of the (*R*)-enantiomers resonates at higher field with respect to the same signal of the (*S*)-enantiomer. It is noteworthy that the same kind of correlation between the sense of nonequivalence, i.e., the relative position of the absorption of one enantiomer with respect to the other, and the absolute configuration has been found for the alkyl protons: all the proton signals due to the (*S*)-enantiomer are lower field shifted with respect to the corresponding signals due to the (*R*)-enantiomer (Table 41).



(105)

- (a) R = Br
- (b) R = Ph
- (c) R = *p*-FC₆H₄
- (d) R = α -Naph
- (e) R = *p*-MeOC₆H₄

In conclusion, the most important result is that the use of permethylated cyclodextrin as chiral solvating agent for NMR spectroscopy not only affords a simple and practical way for the determination of the stereochemical purities of trisubstituted allenes, but also allows one to simultaneously determine their absolute configuration. Indeed, TRIMEB induced only positive complexation shifts of all the allene protons, which are greater for the (*S*)-enantiomer than for the (*R*)-enantiomer, independent of the structure of the allene. This empirical correlation seems to be reliable since it has been satisfied by a large number of trisubstituted allenes.

The method is undoubtedly very attractive from the practical point of view: it only requires the acquisition of a routine NMR spectrum for the suitable allene/TRIMEB mixture.

With the aid of ¹³C NMR, ⁶Li NMR and ¹H HOESY (heteronuclear Overhauser effect spectroscopy) NMR of α -lithiomethoxyallene (**106**) and 1-lithio-1-ethoxy-3-*t*-butyllallene (**107**) as well as by *ab initio* model calculations on monomeric and dimeric α -lithiohydroxyallene, Schleyer and coworkers⁶⁴ proved that **106** and **107** are dimeric in THF (**106** forms a tetramer in diethyl ether) with a nonclassical 1,3-bridged structure. The ¹³C NMR spectrum of allenyllithium in THF is also in agreement with the allenic-type structure: the chemical shift of C2 (196.4 ppm) resembles that of neutral allene (212.6 ppm), rather than C2 of propyne (82.4 ppm).

The structures of **106** and **107** were also investigated in ether and THF solutions by using IR and NMR methods. Compound **107** was synthesized in order to avoid problems with the rapid rearrangement at > -20 °C of **106** to an alkynyllithium derivative. The lithiomethoxyallene had to be synthesized at *ca* -78 °C in THF or diethyl ether and it was measured *in situ* without isolation of the metalated product. Its NMR data are given in Table 42.

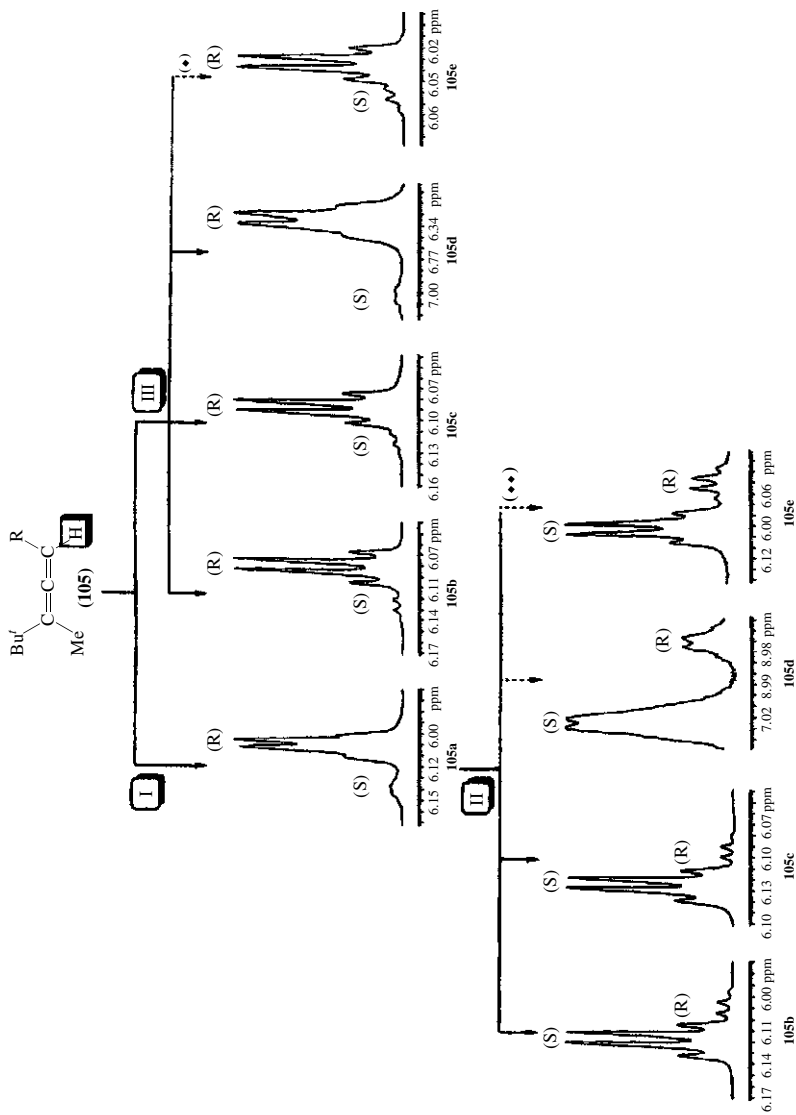
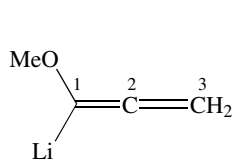


FIGURE 49. ^1H NMR (300 MHz, CD_3OD) spectra of samples of allenes **105a-e** obtained by starting from (*S*)-**105** (ee 89%): Spectral regions corresponding to the allene proton absorptions for mixtures TRIMEB/allene (molar ratio 1 : 1 for **105a-c**, **e** and 2 : 1 for **105d**), at -20°C for **105a-c**, **e** and at -40°C for **105d**. (♦) (*R*)-**105e** was obtained by starting from a sample of (*S*)-**105** with lower enantiomeric purity (81%). (◆◆) (*S*)-**105d-e** were obtained by starting from a sample of **105a** with lower enantiomeric purity (64%). Reprinted with permission from Reference 62. Copyright (1995) American Chemical Society

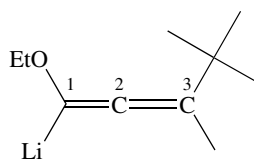
TABLE 41. Complexation shifts ($\Delta\delta^a$, 300 MHz, CD₃OD) induced by TRIMEB on the two enantiomers of allenes **105a–e**

Allene	$\Delta\delta_S$			$\Delta\delta_R$			$T(^{\circ}\text{C})$	Molar ratio
	H	Me	<i>t</i> -Bu	H	Me	<i>t</i> -Bu		
105a	9.88	3.48	3.30	7.69	2.38	2.93	25	1 : 1
	40.55	11.16	8.20	29.88	7.93	6.55	–20	1 : 1
105b	7.05	5.14	4.12	5.43	4.18	3.68	25	1 : 1
	23.83	12.52	10.27	15.59	9.22	7.89	–20	1 : 1
105c	4.86	1.72	1.62	2.21	0.47	0.59	25	1 : 1
	22.75	9.02	7.78	11.58	5.01	4.49	–20	1 : 1
105d	9.15	4.40	4.40	5.67	2.20	2.57	25	1 : 2
	67.41	21.70	25.35	42.05	10.99	14.55	–40	1 : 2
105e	8.23	4.03	3.66	3.94	1.83	1.47	25	1 : 1
	26.85	11.88	10.50	10.14	5.42	4.64	–20	1 : 1

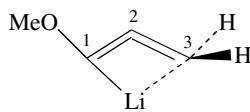
^a $\Delta\delta = \delta_{\text{mixture}} - \delta_{\text{free}}$, Hz.



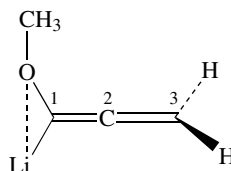
(106)



(107)



(108)



(109)

In **106**, the ¹³C signal of C1 is shifted *ca* 30 ppm downfield and the C3 signal is shifted *ca* 20 ppm upfield compared with the parent compound. The essentially unchanged C2 signal at *ca* 195 ppm proves an allenic structure for **106** both in THF and in diethyl ether. The C1 ¹³C signal of a ⁶Li-labeled lithiomethoxyallene exhibits scalar ¹³C⁶Li coupling, a quintuplet [¹*J*(¹³C⁶Li) = 6.0 Hz] at –100 °C in THF indicates a dimer and a septuplet [¹*J*(¹³C⁶Li) = 4.5 Hz] at –93° in diethyl ether indicates a tetrameric aggregate (Figure 50).

In addition, the C3–H coupling constant (from a gated decoupling NMR experiment) of 161.8 Hz in **106** compared with 162 Hz in allenyllithium vs 167.5 Hz in methoxyallene and 168 Hz in allene is also in agreement with an allenic structure. However, neither the C–H coupling constant nor the NMR chemical shifts distinguish between the alternatives that **106** has a nonclassical 1,3-bridged structure **108** (M = Li) or an *O*-coordinated allenic structure **109**. Hence the ⁶Li, ¹H-HOESY NMR technique which can be used to detect close proximities (*ca* < 3.5 Å) between ¹H and ⁶Li nuclei was applied. The HOESY spectrum of α -lithiomethoxyallene in THF solution (in which **106** is dimeric) is shown

TABLE 42. NMR data (δ in ppm) of α -lithiomethoxyallene (**106**) and 1-lithio-1-ethoxy-3-*tert*-butyllallene (**109**) and their neutral parent compounds

	C1	C2	C3	C4	C5	OCH ₂ /OCH ₃	OCH ₂ CH ₃
Methoxyallene	6.77 (t, 6.1 Hz)		5.48 (d, 6.1 Hz)			3.41 (s)	
Methoxyallene 106	122.8	201.1	91.2			55.8 3.31 (s)	
106	154.1	194.1	67.0			57.7	
106	150.4	195.4	69.8			56.7	
1-Ethoxy-3- <i>tert</i> - butyllallene	6.7 (d, 6 Hz)		5.8 (d, 6 Hz)		1.1 (s)	3.6 (q, 6 Hz)	1.3 (t, 6 Hz)
1-Ethoxy-3- <i>tert</i> - butyllallene	122.5	190.1	117.1	32.9	29.2	63.4	14.3
107 -TMEDA _{0,5}			4.34 (s)		0.95 (s)	3.59 (q, 6.0 Hz)	1.14 (t, 6.0 Hz)
107 -TMEDA _{0,5}	159.3	188.1	96.8	32.7	31.6	64.6	16.1
107	157.9 158.0	186.5 186.4	95.4	31.8	30.5	63.7 63.6	14.6

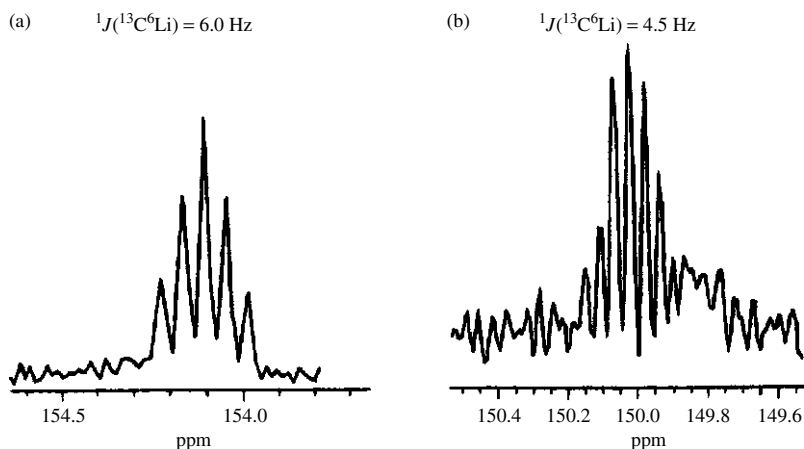


FIGURE 50. C1 ^{13}C NMR signal of ^6Li -labeled α -lithiomethoxyallene (**106**) in THF- d_8 at -100°C and (b) in diethyl ether at -93°C . Reprinted with permission from Reference 64. Copyright (1993) American Chemical Society

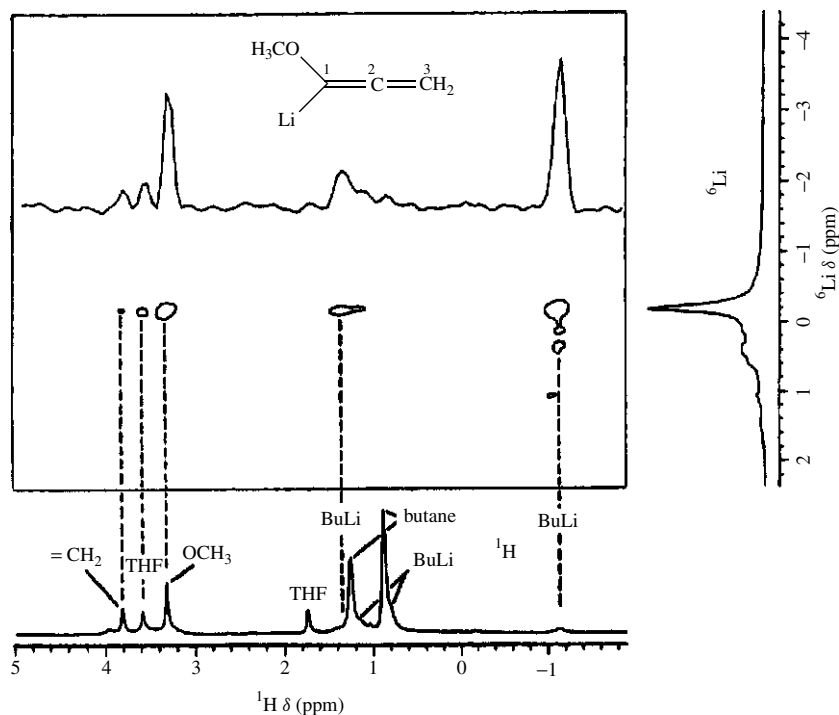


FIGURE 51. ^6Li ^1H -HOESY spectrum of ^6Li -labeled α -lithiomethoxyallene (**106**) (0.71 M) in THF- d_8 at 6°C . Mixing time 2.0 s. Reprinted with permission from Reference 64. Copyright (1993) American Chemical Society

in Figure 51. Besides cross peaks between the Li signal and the protons of excessive *n*-BuLi and of THF, there are two cross peaks involving the lithioallene: one to the methoxy protons at 3.31 ppm and one to the CH₂ protons of the allenic moiety at 3.81 ppm.

In analogy to **106**, significant changes in the ¹³C NMR spectrum of **107** in THF are only observed for C1 and C3 compared with the neutral parent compound. The C1 ¹³C signal of a ⁶Li-labeled compound **107** is split into a six-line multiplet (Figure 52).

This is interpreted as the superposition of two quintuplets [¹*J*(¹³C⁶Li) = 6.5 Hz] which are separated by *ca* 6.5 Hz.

Since **107** is chiral, the two quintuplets are assigned to a pair of enantiomeric dimers (*RR*-dimer and *SS*-dimer) and to the diastereomeric *meso* form of a dimer (*RS*-dimer). Because both diastereomeric dimers of **107** are formed in approximately equal amounts, the difference in the chemical shift of C1 of both diastereomers is approximately equal to the coupling constant, and a six-line multiplet results. In addition, two equally intense singlets are observed for each C2 and OCH₂ carbon atoms of the two diastereomers. A ⁶Li ¹H-HOESY spectrum of 8-TMEDA_{0.5} in THF (Figure 53; TMEDA = tetramethylethylenediamine) shows ⁶Li cross peaks to all protons of the lithioallene and the TMEDA molecules. Again, the cross peak due to the H3 proton at 4.34 ppm indicates a 1,3-bridged structure for **107**.

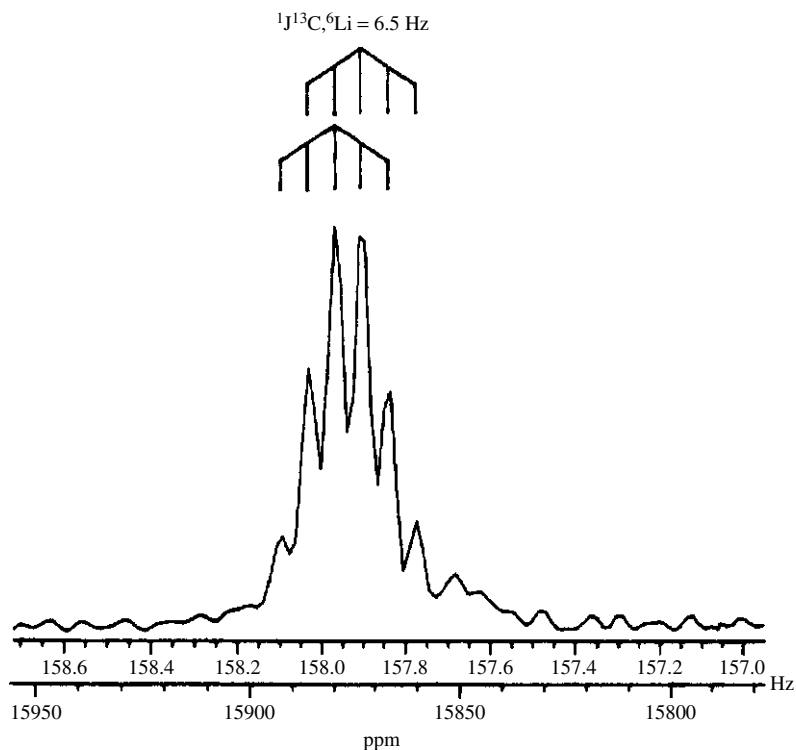


FIGURE 52. C1 ¹³C NMR signal of ⁶Li-labeled 1-lithio-1-ethoxy-*t*-butylallene (**107**) in THF-*d*₈ at -92 °C. Reprinted with permission from Reference 64. Copyright (1994) American Chemical Society

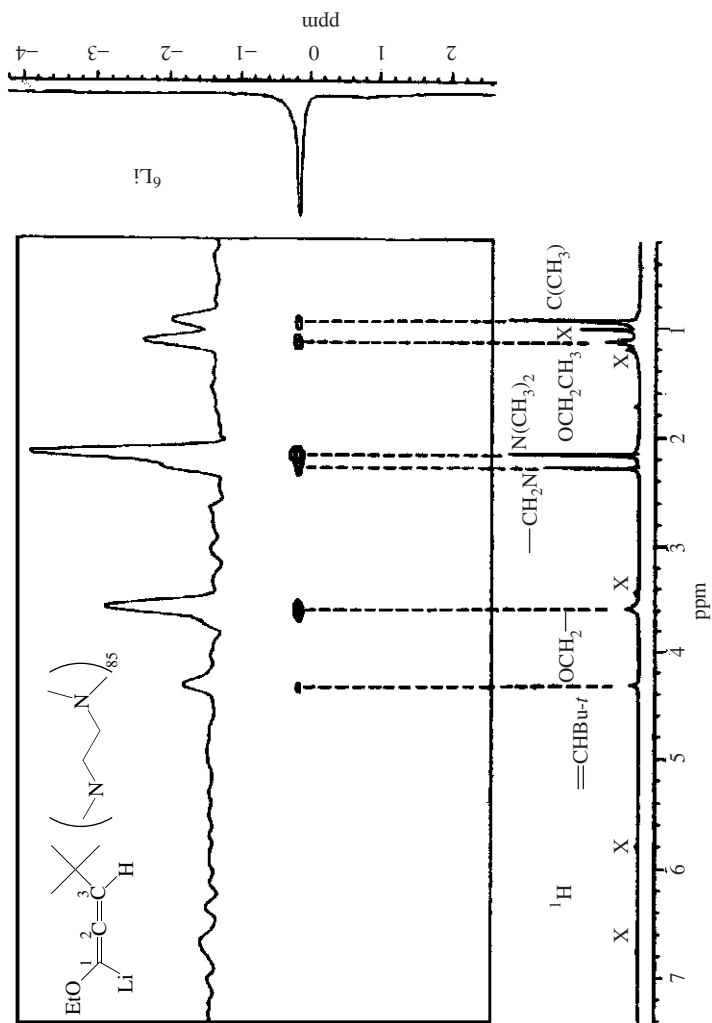
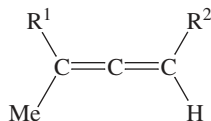


FIGURE 53. ${}^6\text{Li}$ - ${}^1\text{H}$ -HOESY spectrum of ${}^6\text{Li}$ -labeled 1-lithio-1-ethoxy-*r*-butyllallene (**107**). TMEDA_{0.5} in THF-*d*₈ at -60°C . X denotes signals of the allene. Mixing time 2.0 s. Reprinted with permission from Reference 64. Copyright (1993) American Chemical Society

Barretta and coworkers⁶³ reported a direct determination of the enantiomeric purity of chiral trisubstituted allenes by using permethylated cyclodextrin as a chiral solvating agent. They found that the heptakis β -cyclodextrin TRIMEB discussed above can be successfully used as a chiral solvating agent (CSA) for the NMR determination of the enantiomeric purity of trisubstituted allenes **110a–f**. An accurate analysis of the experimental conditions (molar ratio allene/TRIMEB, temperature and solvent) required to optimize the enantioseparation has been carried out. The ¹H NMR spectra of TRIMEB, allenes **110a–f**, and the mixtures TRIMEB/allene have been recorded at 300 MHz in CD₃OD as solvent.



(110)

- (a) R¹ = *t*-Bu, R² = Br
- (b) R¹ = Et, R² = Br
- (c) R¹ = Pr, R² = Br
- (d) R¹ = *t*-Bu, R² = Ph
- (e) R¹ = Et, R² = Ph
- (f) R¹ = R² = *t*-Bu

The proton spectrum of the permethylated cyclodextrin at room temperature is completely restricted to the region between 3.0 and 4.0 ppm, with the exclusion of the sharp doublet centered at 5.14 ppm. The free allene **110a** shows a well-recognizable singlet at 1.09 ppm, due to the absorption of the *t*-butyl group, and a doublet ($J = 2.2$ Hz) centered at 1.82 ppm, corresponding to the resonance of the methyl group; in the low-field spectral region, only the quartet centered at 6.01 ppm is present, arising from the proton directly bound to the allene moiety. Similarly, allenes **110b–f** show resonances between 0.9 and 2.2 ppm due to the methyl, the alkyl protons R¹ (and R² for **110f**) and a well-resolved signal, near 6.0 ppm for **110b–e** and near 5.0 ppm for **110f** which is due to the allene proton. In the case of allenes **110d** and **110e**, absorptions between 7.0 and 7.7 ppm are observed, arising from the phenyl protons. Therefore, the absorptions of the allenes and cyclodextrin fall in distinct spectral regions and mutual interference is not observed in the spectra.

By comparing the spectra of the racemic allenes **110a–f** in the free state and in the presence of the cyclodextrin, it has been observed that TRIMEB produced duplication of almost all signals of allene. As an example, the well-resolved quartet of the allene proton of free **110a** (at 6.01 ppm at 25 °C in CD₃OD, Figure 54a) gives two partially superimposed quartets centered at 6.04 and 6.03 ppm (Figure 54b, $\Delta\delta = 3.9$ Hz) in the presence of equimolar amounts of TRIMEB. These two absorptions correspond in position to those obtained starting from each enantiomer of allene, respectively, at same allene/TRIMEB molar ratio, total concentration and temperature (Figure 54c,d).

Consequently, the splitting observed is due to the fact that TRIMEB induces nonequivalence in the proton nuclei of the two enantiomers of the allenes, thus enabling one to determine the enantiomeric purities by using a chiral solvating agent. In all cases examined the extent of the nonequivalence, i.e. the difference of the proton chemical shifts of the two enantiomers in the presence of TRIMEB, can be increased by increasing the

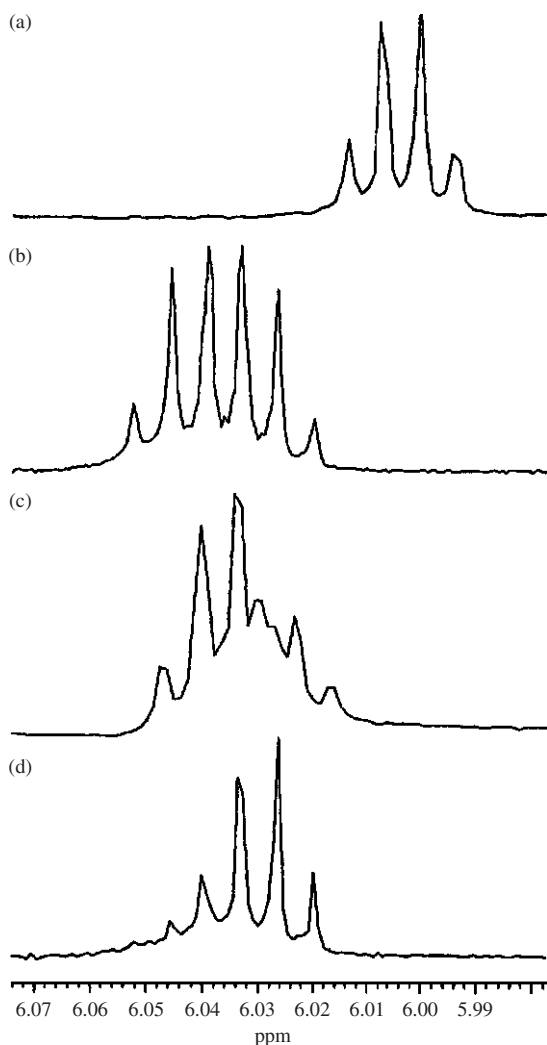


FIGURE 54. ¹H NMR spectra (300 MHz, CD₃OD), ppm referred to TMS as external standard, 25 °C) of (a) free compound **110a** (40 mM), (b) equimolar mixture of (*R,S*)-**110a**/TRIMEB, (c) equimolar mixture as in (b) starting from a sample of **110a** enriched in the (+)-(*S*)-enantiomer and (d) equimolar mixture as in (b) starting from a sample of enantiomerically pure (–)-(*R*)-**110a**. Reprinted with permission from Reference 63. Copyright (1994) American Chemical Society

TRIMEB/allene molar ratio. Data relative to the allene proton of **110a–f** are summarized in Table 43.

As shown in Figure 55 for the allene proton of **110a**, the nonequivalence increases from 3.9 Hz (Figure 55a) in an equimolar solution to 7.0 Hz (Figure 55b) by adding an additional equivalent of TRIMEB and to 10.9 Hz (Figure 55c) in the presence of 3 equivalents of the cyclodextrin, giving rise to two completely separated signals.

TABLE 43. Unequivalence ($\Delta\delta^a$ at 300 MHz, CD₃OD) induced in the allene proton of trisubstituted allene (40 mM) in the presence of TRIMEB, as a function of the temperature and of the allene/TRIMEB molar ratio

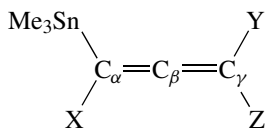
Allene	25 °C		-40 °C
	molar ratio 1 : 1	molar ratio 1 : 2	molar ratio 1 : 1
110a	3.9	7.0	18.1
110b	1.8	2.0	7.4
110c	1.1	4.2	5.9
110d	3.3	7.0	23.4
110e	2.9	3.3	11.7
110f	0.5	2.9	4.9

^a $\Delta\delta$ = difference between the proton chemical shifts (Hz) of the two enantiomers in the presence of TRIMEB.

The use of CD₃OD as a solvent also allowed one to affect the nonequivalence by temperature variations: the absorptions of the allene proton of **110a** in the two enantiomers are separated by 11.9 Hz at -20 °C (Figure 56a) and by 18.1 Hz at -40 °C (Figure 56b). The possibility of increasing the nonequivalence by decreasing the temperature instead of increasing the CSA/allene molar ratio represents a double advantage: the measurement requires a minor amount of TRIMEB, thus becoming less expensive, and better results are obtained taking into account that the non-equivalence is very sensitive to temperature variations.

On the basis of the results above it can be concluded that, at least for the allenes investigated, the complete separation of the two allene absorptions can be achieved both by varying the molar ratio and by lowering the temperature, and hence the enantiomeric composition can be accurately determined by comparing the areas of the two absorptions by integration.

A series of stannylallene derivatives (**111**) was studied by means of ¹³C, ²⁹Si and ¹¹⁹Sn NMR spectroscopy by Lukevics and coworkers⁶⁵. The effects of substituents on chemical shift values and *J* (SSCC) in **111** are additive. A set of linear correlations between the isotope shifts (IS) and SSCC for **111** demonstrates the interrelation of these values.



(111)

X = H, SnMe₃, SiMe₃, GeMe₃, SC₂H₅, Br

Y = H, SnMe₃

Z = H, SnMe₃, SiMe₃, GeMe₃, SC₂H₅

The ¹³C, ²⁹Si and ¹¹⁹Sn NMR chemical shifts measured for stannylallenes and silylstannylallenes are presented in Tables 44 and 46; ⁿ*J*(¹¹⁹Sn¹³C), ⁿ*J*(¹¹⁹Sn¹¹⁷Sn), ⁿ*J*(²⁹Si¹³C) and isotope shifts (IS) are given in Tables 45 and 46.

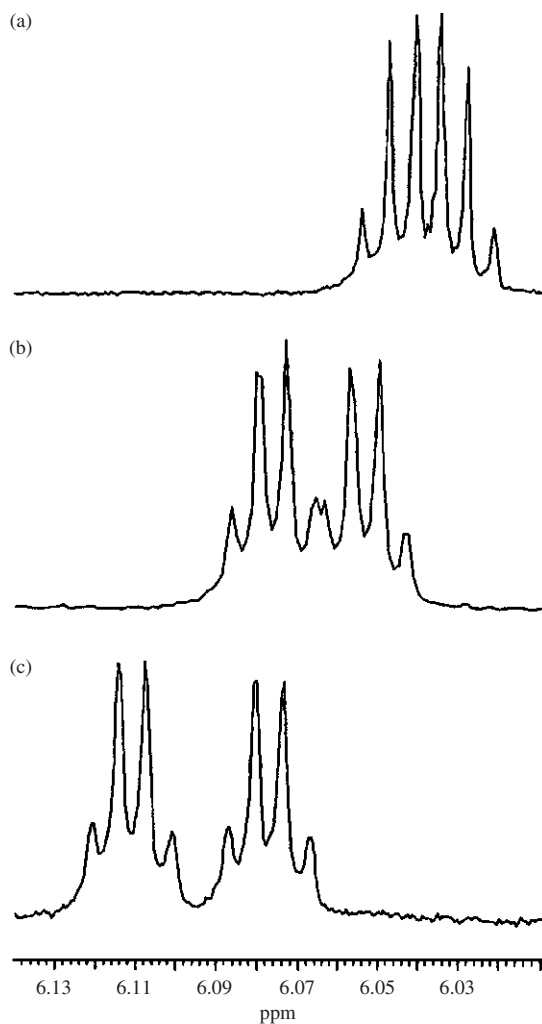


FIGURE 55. ^1H NMR spectra (300 MHz, CD_3OD , ppm referred to TMS as external standard, 25°C) of (a) equimolar mixture of (R,S) -**110a**/TRIMEB, (b) 1 : 2 mixture of (R,S) -**110a**/TRIMEB and (c) 1 : 3 mixture of (R,S) -**110a**/TRIMEB. Reprinted with permission from Reference 63. Copyright (1994) American Chemical Society

Analysis of the chemical shifts of ^{13}C and ^{119}Sn for stannylallenes **111** (Table 44) shows that these values are additive and can be described by equations 4 to 6:

$$\delta(^{13}\text{C}_\alpha, \gamma) = 81.2 + \Sigma X_\alpha + \Sigma X_\gamma \quad (4)$$

$$\delta(^{13}\text{C}_\beta) = 219.0 + \Sigma X_\beta \quad (5)$$

$$\delta(^{119}\text{Sn}) = -21.6 + X_\alpha + \Sigma X_\gamma \quad (6)$$

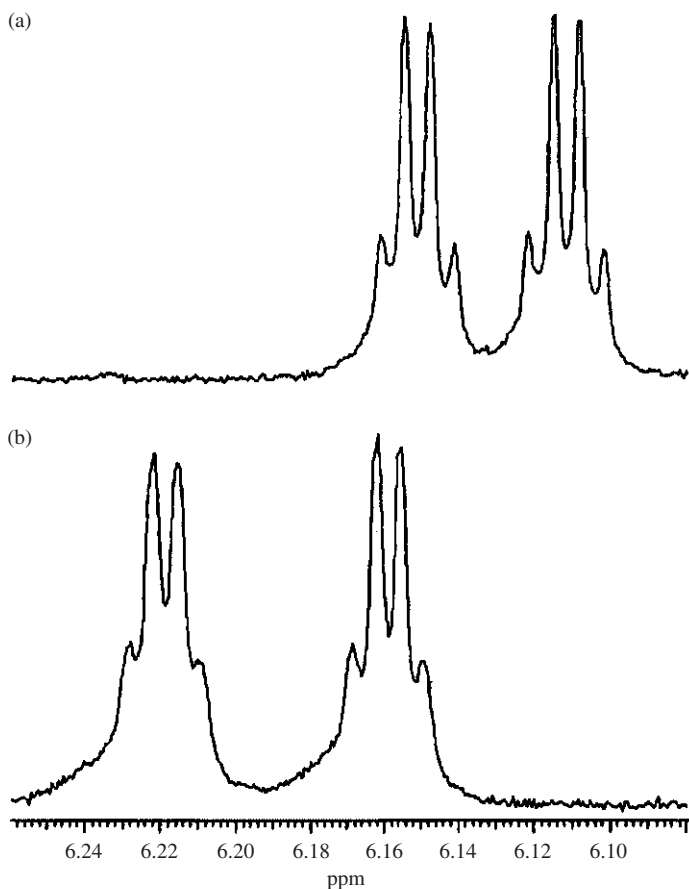


FIGURE 56. ^1H NMR spectra (300 MHz, CD_3OD , ppm referred to TMS as external standard) of an equimolar mixture of (*R,S*)-**110a**/TRIMEB recorded at (a) -20°C and (b) -40°C . Reprinted with permission from Reference 63. Copyright (1994) American Chemical Society

where X_α , X_β and X_γ are increments of the corresponding substituents in the α -, β - and γ -positions with regard to the nuclei under study. The calculated increments of substituents are presented in Table 47.

The difference between the calculated ^{13}C and ^{119}Sn CS and their experimental values for C_α , C_β and C_γ does not exceed -0.6 ppm and for ^{119}Sn CS -0.3 ppm. The relatively small values of these deviations demonstrate that the increments can be used for analytical purposes. The study of increments for ^{13}C (Table 47) provides evidence for a considerably larger influence of the MMe_3 group in the γ -position of the allene system than in the α - and β -positions. The negative sign of the γ -increment results from exponential correlation between the electronegativity of the substituent and the γ -increment value. A significant increase in the shielding of the γ -carbon nucleus (owing to the introduction of a MMe_3 group into the α -position of the allene system) is observed in the sequences $\text{CMe}_3 <$

TABLE 44. ^{13}C and ^{119}Sn chemical shifts δ (ppm) of stannylallenes in C_6D_6

X	Y	Z	δ (^{119}Sn)	$\delta(^{13}\text{C})$						
				C_α	C_β	C_γ	SnCH_3	XCH_3	$\text{C}_{\text{Y,Z}}$	
SnMe ₃	H	H	-9.55	75.23	205.98	53.01	-8.53	-8.53	—	
	H	SiMe ₃	-3.56	65.06	202.91	55.36	-8.35	-8.53	-0.06	
	H	GeMe ₃	-4.94	65.96	201.76	56.70	-8.38	-8.38	-0.82	
	H	SnMe ₃	-3.12	61.98	201.32	50.49	-8.38	-8.38	-9.03	
	H	SC ₂ H ₅	-5.07	79.59	204.08	65.14	-8.06	-8.06	29.86 (CH ₂) 15.09 (CH ₃)	
	SnMe ₃	SiMe ₃	3.40	50.78	196.08	52.69	-8.29	-8.29	-8.23(SnMe ₃) 0.67 (SiMe ₃)	
	SnMe ₃	GeMe ₃	1.87	52.06	196.13	54.20	-8.27	-8.27	-8.32(SnMe ₃) 0.01 (GeMe ₃)	
	SnMe ₃	SnMe ₃	3.73	47.36	195.58	47.36	-8.32	-8.32	-8.32	
	SnMe ₃	SC ₂ H ₅	-1.82	70.04	200.00	64.03	-8.06	-8.06	29.04 (CH ₂) 15.41 (CH ₃) -8.79 (SnMe ₃)	
	SiMe ₃	H	SiMe ₃	-5.95	71.44	204.93	59.14	-8.15	0.32	-0.09
H		GeMe ₃	-7.73	71.92	203.32	60.05	-8.21	0.32	-0.85	
H		SC ₂ H ₅	-6.08	77.92	206.13	68.63	-7.88	0.53	29.74 (CH ₂) 15.21 (CH ₃)	
SnMe ₃		SiMe ₃	0.34	56.79	197.48	56.79	-8.06	0.76	0.23 (SnMe ₃) 0.18 (SiMe ₃)	
SnMe ₃		GeMe ₃	-1.48	57.64	196.97	57.73	-8.14	0.74	-8.17 (SnMe ₃) 0.04 (GeMe ₃)	
SnMe ₃		SnMe ₃	0.02	52.69	196.08	50.78	-8.23	0.67	-8.29	
SnMe ₃		SC ₂ H ₅	-3.68	76.40	200.59	67.52	-7.88	0.38	-8.76(SnMe ₃) 28.81 (CH ₂) 15.35 (CH ₃)	
GeMe ₃		H	SiMe ₃	-7.42	71.59	203.58	59.69	-8.26	-0.29	-0.12
		H	GeMe ₃	-9.01	72.20	202.10	60.71	-8.32	-0.34	-0.89
		H	SC ₂ H ₅	-8.49	78.71	204.36	69.30	-8.00	-0.35	29.30 (CH ₂) 15.21 (CH ₃)
	SnMe ₃	SiMe ₃	-0.95	57.73	197.48	57.64	-8.17	0.04	-8.14(SnMe ₃) 0.74 (SiMe ₃)	
	SnMe ₃	GeMe ₃	-2.61	58.60	196.45	58.06	-8.21	-0.04	—	
	SnMe ₃	SnMe ₃	-1.03	54.20	196.13	52.06	-8.21	0.01	-8.27(SnMe ₃)	
	SnMe ₃	SC ₂ H ₅	-3.96	77.33	199.54	68.66	-7.97	-0.15	-8.76(SnMe ₃) 28.78 (CH ₂) 15.41 (CH ₃)	
H	SnMe ₃	SnMe ₃	-8.66	50.49	201.32	61.98	-9.03	—	-8.38	
SC ₂ H ₅	SnMe ₃	SiMe ₃	-1.88	67.52	200.59	76.40	-8.76	28.81(CH ₂) 15.36(CH ₂)	-7.88(SiMe ₃) 0.38 (SiMe ₃)	
	SnMe ₃	GeMe ₃	-3.48	68.66	199.54	77.33	-8.76	28.78(CH ₂) 15.41(CH ₂)	-7.97(SnMe ₃) -0.15(GeMe ₃)	
	SnMe ₃	SnMe ₃	-2.94	64.03	200.00	70.04	-8.79	29.04(CH ₂) 15.41(CH ₂)	-8.06(SnMe ₃)	
	Br	H	H	2.98	78.51	206.98	74.96	-8.56	—	

TABLE 45. Coupling constants and isotope shifts of stannylallenes in C₆D₆

X	Y	Z	Coupling constants (Hz)					Isotope shifts (ppb)		
			SnC _α	SnC _β	SnC _γ	¹¹⁹ Sn- ¹¹⁷ Sn	SnCCH ₃	¹ Δ ¹¹⁹ Sn(C _α)	¹ Δ ¹¹⁹ Sn (CCH ₃)	
SnMe ₃	H	H	261.7	30.5	60.6	158.5	348.2	31.8	9.0	
	H	SiMe ₃	264.4	26.3	50.1	169.1	349.4	34.3	7.1	
	H	GeMe ₃	269.9	26.8	57.1	190.9	347.6	33.8	7.7	
	H	SnMe ₃	274.1	26.0	58.9	199.4(² J)	347.0	34.2	7.7	
	H	SC ₂ H ₅	239.8	31.2	65.1	166.5	348.1	37.5	6.6	
	SnMe ₃	SiMe ₃	281.7	21.4	48.6	202.6(² J)	348.0	32.2	7.5	
						248.6(⁴ J)				
	SnMe ₃	GeMe ₃	285.1	22.7	54.5	226.2(² J)	345.9	31.9	9.2	
						250.5(⁴ J)				
	SnMe ₃	SnMe ₃	292.9	22.1	54.8	234.0(² J)	345.6	31.1	9.3	
					254.2(⁴ J)					
SnMe ₃	SC ₂ H ₅	263.2	30.5	66.4	246.3(² J)	343.0	33.2	7.5		
					202.3(⁴ J)					
SiMe ₃	H	SiMe ₃	254.4	31.6	49.6	—	348.3	35.5	8.0	
	H	GeMe ₃	261.6	^a	56.4	—	346.7	35.0	8.0	
	H	SC ₂ H ₅	233.5	36.6	64.5	—	346.5	36.5	7.4	
	SnMe ₃	SiMe ₃	270.4	27.7	47.8	241.1(⁴ J)	346.0	33.3	8.3	
	SnMe ₃	GeMe ₃	276.8	28.8	53.9	244.6(⁴ J)	344.6	32.7	8.5	
	SnMe ₃	SnMe ₃	284.0	28.2	54.8	248.7(⁴ J)	347.2	32.2	8.6	
	SnMe ₃	SC ₂ H ₅	257.7	28.4	65.7	199.3(⁴ J)	340.2	34.6	8.2	
GeMe ₃	H	SiMe ₃	280.3	23.6	48.5	—	349.1	33.4	8.2	
	H	GeMe ₃	286.9	23.0	54.6	—	347.4	30.5	8.5	
	H	SC ₂ H ₅	258.9	26.7	62.6	—	347.6	35.6	7.1	
	SnMe ₃	SiMe ₃	298.1	19.2	46.3	244.6(⁴ J)	347.0	31.7	9.2	
	SnMe ₃	GeMe ₃	304.6	20.1	52.1	247.3(⁴ J)	345.7	30.7	9.3	
	SnMe ₃	SnMe ₃	310.0	19.3	53.3	250.5(⁴ J)	344.9	30.0	9.7	
	SnMe ₃	SC ₂ H ₅	283.7	26.2	61.6	198.6(⁴ J)	341.3	33.0	7.9	
	H	SnMe ₃	SnMe ₃	423.5	6.1	44.8	248.3(⁴ J)	353.5	22.4	12.1
SC ₂ H ₅	SnMe ₃	SiMe ₃	410.6	35.2	32.2	199.3(⁴ J)	353.2	38.4	6.3	
	SnMe ₃	GeMe ₃	417.0	26.2	35.1	198.6(⁴ J)	352.6	37.6	6.6	
	SnMe ₃	SnMe ₃	433.7	32.1	36.4	202.3(⁴ J)	350.9	36.6	7.2	
Br	H	H	360.8	32.5	27.4	—	371.5	26.4	1.1	

^aNot measured.

GeMe₃ < SiMe₃ < SnMe₃. This is corrected by the increasing σ -donating capacity of substituents in this sequence, suggesting that the negative values of the γ -increment result from the σ -donating capacity of the MMe₃ group.

Generally, inverse relationships are observed between the ¹¹⁹Sn and ¹³C chemical shifts of the β -carbon atom in **111** (Table 44). This indicates a conjugation between the tin atom and the allene system as a downfield shift of the ¹³C_β signal corresponds to an upfield shift

TABLE 46. ^{29}Si NMR spectra of stannylsilyllallenes and related compounds in C_6D_6

X	Y	Z	δ (^{29}Si) (ppm)	Coupling constants (Hz)			$^1\Delta^{29}\text{Si}$ (C_α) (ppm)
				$^{29}\text{Si}-\text{CCH}_3$	$^{29}\text{Si}-\text{C}_\alpha$	$^{29}\text{Si}-^{119}\text{Sn}$	
SnMe_3	SiMe_3	H	-5.06	52.86	66.19	27.74	-9.1
GeMe_3	SiMe_3	H	-5.12	52.91	65.21	26.94	-9.5
SiMe_3	SiMe_3	H	-4.94	53.20	64.61	26.68	-9.6
SiMe_3	SnMe_3	SnMe_3	-3.59	52.75	58.69	27.56 (4J) 23.81 (2J)	-9.8
SiMe_3	SnMe_3	GeMe_3	-3.66	52.87	57.96	27.16 (4J) 20.28 (2J)	-10.0
SiMe_3	SnMe_3	SiMe_3	-3.98	53.31	57.56	18.03 (4J) 20.14 (2J)	-10.5
SiMe_3	H	SiMe_3	-3.89	52.95	55.40	18.49	-10.4
SiMe_3	H	GeMe_3	-4.01	53.06	55.58	26.26 (4J)	-10.4
SiMe_3	H	SC_2H_5	-3.41	53.31	52.91		-11.1
SiMe_3	SnMe_3	SC_2H_5	-3.34	52.98	55.61	21.64 (2J)	-10.3

	-0.31
--	-------

TABLE 47. Values of the calculated increments of substituents in stannylallenes **111** in C_6D_6

Measured value	Increment of group				
	SnMe_3	GeMe_3	SiMe_3	SC_2H_5	CMe_3
$\delta(^{13}\text{C}_\alpha)$	-2.5	+3.6	+2.6	+13.3	+28.6
$\delta(^{13}\text{C}_\beta)$	-6.1	-5.0	-4.4	-1.6	-5.6
$\delta(^{13}\text{C}_\gamma)$	14.1	-10.0	-10.8	+8.3	-3.5
$\delta(^{119}\text{Sn})$	+12.4 (α) +6.6 (γ)	+7.6 (α) +4.6 (γ)	+8.7 (α) +6.3 (γ)	+6.0 (α) +3.0 (γ)	
$^1J(^{119}\text{Sn}^{13}\text{C}_\alpha)$	+130.6 (α) +15.9 (γ)	-113.4 (α) +9.6 (γ)	+139.4 (α) +5.2 (γ)		
$^2J(^{119}\text{Sn}^{13}\text{C}_\beta)$	+16.0 (α) -4.4 (γ)	+13.0 (α) -3.6 (γ)	+22.1 (α) -4.6 (γ)		
$^3J(^{119}\text{Sn}^{13}\text{C}_\gamma)$	+10.0 (α) -2.1 (γ)	+8.0 (α) -4.0 (γ)	+9.5 (α) -10.7 (γ)		

of the ^{119}Sn resonance. In a series of structurally similar compounds, the relative changes in the shielding of nuclei under the influence of substituents are related to corresponding changes in the electron density of these nuclei. Therefore, one can assume that an increase in the negative charge on the tin atom results from a decrease in the charge of C_β in the $\text{Me}_3\text{Sn}-\text{C}_\alpha=\text{C}_\beta=\text{C}_\gamma$ system. This conclusion is in agreement with the correlation found earlier between the shielding of the central $^{13}\text{C}_\beta$ atom in the allene system and substituent resonance effects. Judging from the β -increments (Table 47), the π -acceptor capacity of the MMe_3 group increases in the sequence $\text{Sn} < \text{Ge} < \text{Si}$.

B. Solitons

Tolbert and Ogle⁶⁶ reported a ^{13}C NMR study on soliton model compounds. Although many of the qualitative aspects of charge transport in conductive polymers have their counterparts in classical organic chemistry, the concept of a mobile charge carrier ('soliton') is one of the most difficult to reconcile with the conventional understanding of resonance. According to the soliton theory, the charge carrier in reductively (or oxidatively) doped polyacetylene is a resonance-stabilized carbanion (or carbocation) of finite width with maximum charge at the center of the defect and diminishing amplitude away from the center. Charge transport is thus associated with migration of the charge density wave down the polymer chain (Figure 57).

Such migration will be isoergic only if the solitonic charge density wave has finite width relative to the unsaturation length. Although increased charge density at the center of an odd-alternant hydrocarbon anion has been a familiar aspect of the chemistry of polyenyl anions since the pioneering work of Kloosterziel and Werner⁶⁷, less widely understood is the requirement that what would ordinarily be static resonance forms become only dynamically equivalent at long chain length. Figure 57 thus represents the centers of delocalized finite domains as they migrate down the chain. The relevance of the interchain charge-transport mechanism to the overall mechanism of conductivity in bulk polymers, for which interchain charge migration ('intersoliton hopping') is apparently rate-limiting, is still the subject of controversy and is not addressed here.

In order to relate this conclusion from solid-state theoretical physics to the organic chemistry of conductive polymers, Tolbert and Ogle undertook an examination of the effect of increasing chain length on the spectral properties of polyenyl anions, using ^{13}C NMR spectroscopy. By using α , ω -diphenylpolyenyl anions (DP1, DP3, DP5, etc.), they investigated the chain length at which the properties of these anions and n-doped polyacetylene converge (Scheme 8).

Treatment of the appropriate hydrocarbon precursors DPN-H (= DP1-H, DP2-H, ...) in Me_2SO solution with potassium (methylsulfinyl)methide ('dimsyl') resulted in an immediate color formation that varied from orange to deep blue-black to colorless as the chain length increased. The higher homologues were poorly soluble and required filtration under inert atmosphere in order to obtain homogeneous solutions for NMR analysis. In the case of DP17 and higher homologues, anisotropic line broadening prevented acquisition of analyzable spectra. However, anions DP1–DP13 yield quite satisfactory ^{13}C and ^1H spectra for further analysis. Curiously, although DP3 exhibited both *E,E* and *E,Z* conformers

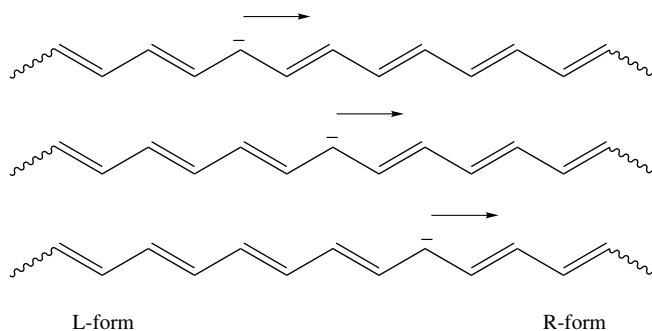
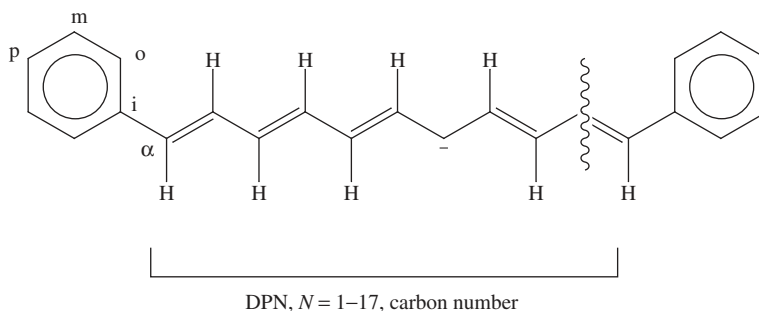


FIGURE 57. Coupled soliton modes in n-doped polyacetylene. Reprinted with permission from Reference 66. Copyright (1990) American Chemical Society



SCHEME 8

in accordance with literature studies in non-ion pairing solvents, the higher homologues showed little conformational diversity apart from absorbances of $< ca$ 5% intensity that apparently corresponded to *Z* conformers. By analogy with DP3, for which proton and carbon chemical shifts had similar frequency separation and, therefore, similar exchange kinetics, such conformers in the higher homologues should have been visible in the carbon spectra. It was concluded that the carbon chemical shifts corresponded to the single isomer represented in the proton spectra. Moreover, the coupling constants, which ranged from 11.7 Hz for central protons to 14.8 Hz for the α protons, are consistent only with the all-*trans* planar conformation in which increased bond localization at the ends of the chain leads to a higher coupling constant. The ^{13}C chemical shifts of the anions were found to be devoid of counterion effects as indicated by employing $\text{CH}_3\text{SOCH}_2^- \text{K}^+ / 18\text{-crown-6}$ in $\text{Me}_2\text{SO-d}_6$ as the base. The chemical shift of C-1 of DP1 was obtained only after addition of $\text{Me}_2\text{SO-d}_6$ to the deprotonated substrate, since facile protium/deuterium exchange led otherwise to line broadening and an isotope effect on the chemical shift. Similarly, DP3 underwent slow exchange with $\text{Me}_2\text{SO-d}_6$ to yield a deuterated anion which exhibited an isotope effect on the C1 chemical shift. Although the assignment of ^{13}C chemical shifts for anions DP1–DP7 was straightforward by the use of two-dimensional (HETCOR) spectroscopy (Figure 58a), the higher homologues required more rigorous examination. The HETCOR of DP9 with carbon and proton assignments is shown in Figure 58a.

In particular, DP9 presented ambiguities associated with the proton assignments from which the ^{13}C assignments were derived. Thus, it was necessary to use the COSY method to assign the proton absorptions first. Homonuclear COSY NMR spectroscopy allowed unambiguous assignment of proton chemical shifts in all cases.

Figure 58(b) shows a COSY spectrum of DP9 as a representative example of ^1H chemical shifts that were readily assigned from the doublet at $\delta 5.38$ ($J = 14.4$ Hz) corresponding to the C-1 proton. Heteronuclear (HETCOR) ^{13}C – ^1H spectroscopy allowed indirect assignment of the ^{13}C chemical shifts. The assignment of all chemical shifts and calculated charge densities for anions DP1–DP13 is presented in Table 48⁶⁸.

In all cases, the nuclei corresponding to the odd-numbered carbon atoms had upfield chemical shifts (excess charge densities) vs their even-numbered counterparts. More illustrative of this is the plot of the ^{13}C spectra of the linear odd-alternant α,ω -diphenylpolyenyl anions $[\text{Ph}(\text{CH})_n\text{Ph}^-]$, $n = 1, 3, 5, 7, 9, 11, 13$ shown in Figure 59. Linear least-squares treatment of the average charge density ρ_{av} vs ^{13}C chemical shift (see Figure 60), excluding DP1, gave excellent statistics and allowed a calculation of individual charge densities at each site from equation 7:

$$\rho_{\text{C}} = (\delta_{\text{C}} - 132.7) / 187.3 \quad (7)$$

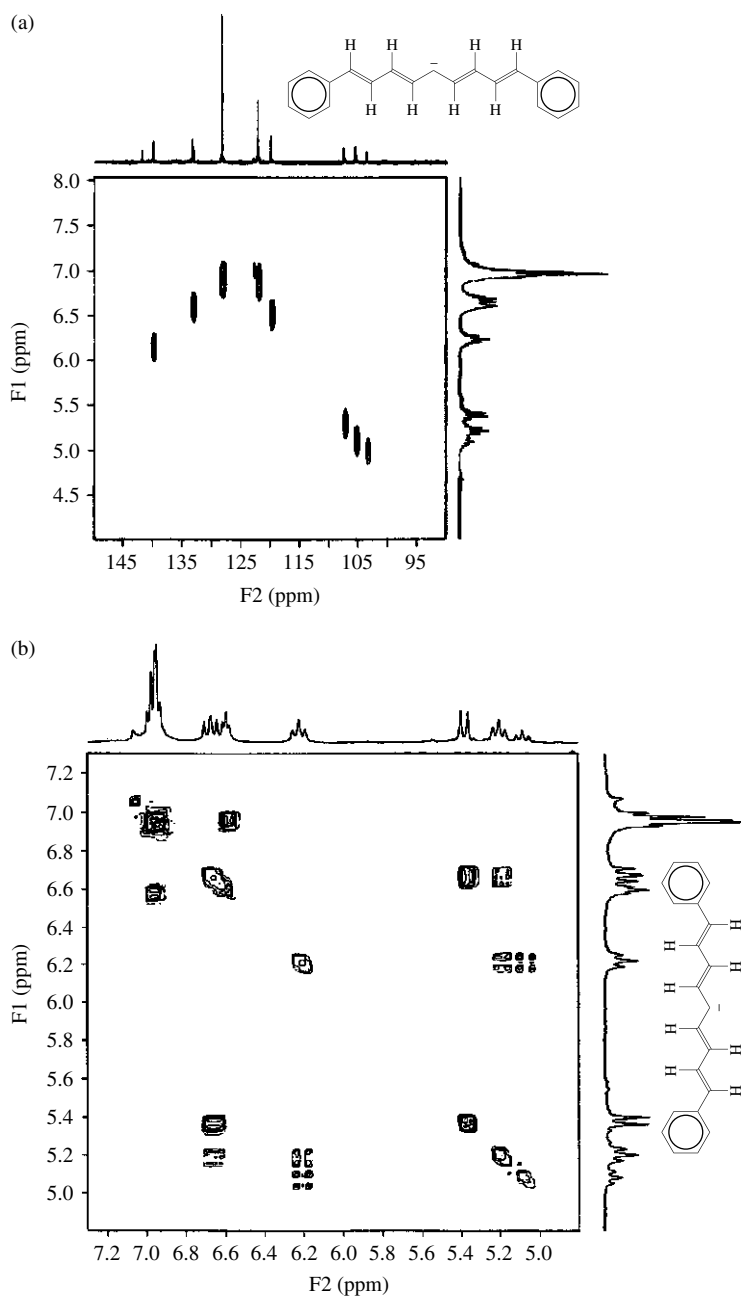


FIGURE 58. (a) HETCOR spectrum of DP9. (b) COSY spectrum of DP9. Reprinted with permission from Reference 66. Copyright (1990) American Chemical Society

TABLE 48. Chemical shift and charge densities for anions DP1 – DP13

DPN	Chemical shift δ (in ppm) and charge densities (in parentheses)										
	C1	C2	C3	C4	C5	C6	C7	<i>ipso</i>	<i>ortho</i>	<i>meta</i>	<i>para</i>
1	80.4 (-0.279)							145.2 (0.067)	116.2 (-0.091)	127.7 (-0.026)	105.9 (-0.143)
3	90.2 (-0.227)	127.9 (-0.026)						145.4 (0.068)	117.5 (-0.081)	128.1 (-0.025)	111.3 (-0.114)
5	96.5 (-0.193)	134.6 (0.010)	98.2 (-0.184)					143.9 (0.058)	119.4 (-0.071)	128.0 (-0.025)	115.0 (-0.095)
7	102.4 (-0.163)	133.7 (0.005)	101.5 (-0.167)	140.5 (0.042)				142.7 (0.053)	120.8 (-0.064)	128.1 (-0.025)	117.7 (-0.080)
9	107.4 (-0.135)	133.2 (0.003)	105.4 (-0.146)	139.8 (0.038)	103.3 (-0.157)			141.7 (0.048)	121.9 (-0.058)	128.2 (-0.024)	119.7 (-0.036)
11	111.5 (-0.113)	132.7 (0.000)	109.1 (-0.126)	139.2 (0.035)	105.9 (-0.143)	139.6 (0.037)		140.9 (0.044)	122.8 (-0.053)	128.3 (-0.023)	121.3 (-0.061)
13	114.9 (-0.095)	132.3 (-0.002)	112.5 (-0.108)	138.6 (0.032)	108.6 (-0.129)	139.0 (0.034)	107.5 (-0.135)	140.3 (0.041)	123.4 (-0.050)	128.3 (-0.023)	122.5 (-0.054)

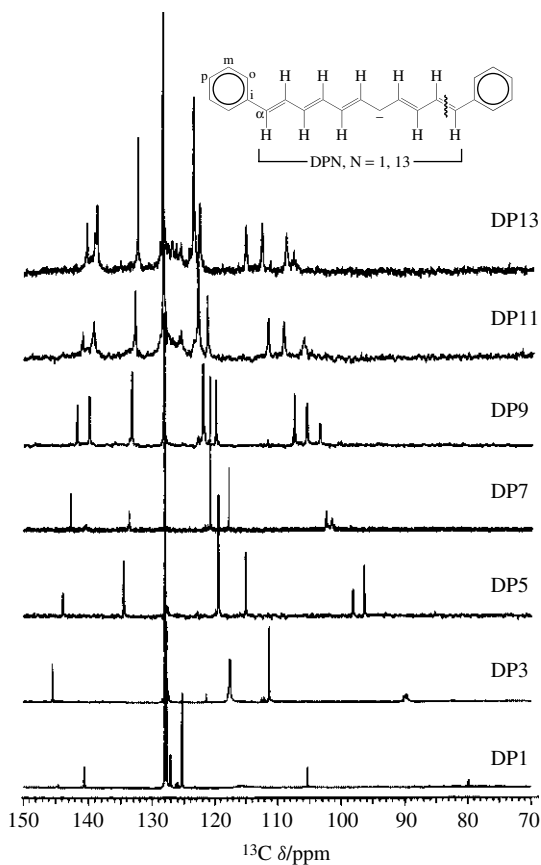


FIGURE 59. Stacked spectra of diphenylpolyenyl anions (DPN). Reprinted with permission from Reference 66. Copyright (1990) American Chemical Society

More illustrative are these results plotted in histogram form. Figure 61 indicates the results for DP13.

C. Fullerenes

The finding of fullerenes has stimulated chemists belonging to a variety of fields including those who use NMR. In this section, some examples of papers in which NMR plays an important role will be described.

Bellavia-Lund and coworkers⁶⁹ reported a nitrogen-containing fullerene carbon resonance assignment through ^{15}N - ^{13}C coupling constants and location of the sp^3 carbon atoms of $(\text{C}_{59}\text{N})_2$. While C_{60} shows a single line at 143 ppm in its ^{13}C NMR spectrum and is a magnetically deshielded moiety, a detailed assignment of all carbon resonances in a modified fullerene, which could have up to 60 resonances, is very difficult. However, for azafullerene (**112**), the carbon atoms in positions α and β to the nitrogen, as well as those linking the cage to other substituents, are potentially assignable using ^{13}C - ^{15}N coupling.

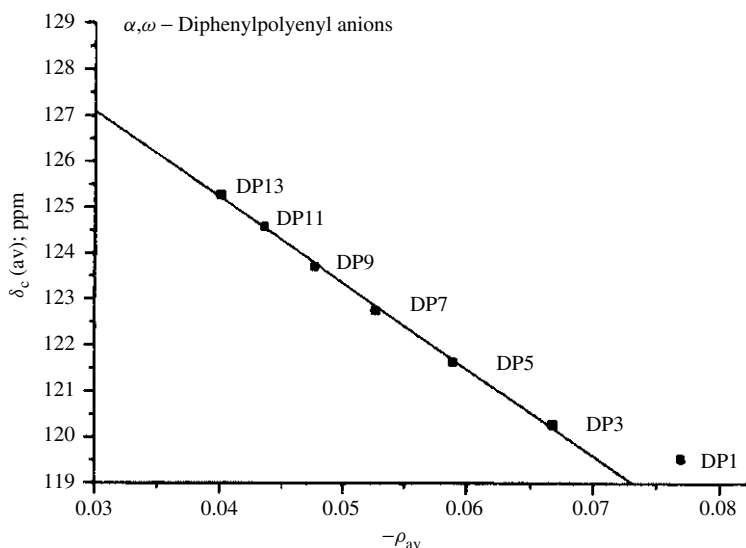


FIGURE 60. Average ^{13}C chemical shift vs average charge density (ρ_{av} for diphenylpolyenyl anions (DPN). Reprinted with permission from Reference 66. Copyright (1990) American Chemical Society

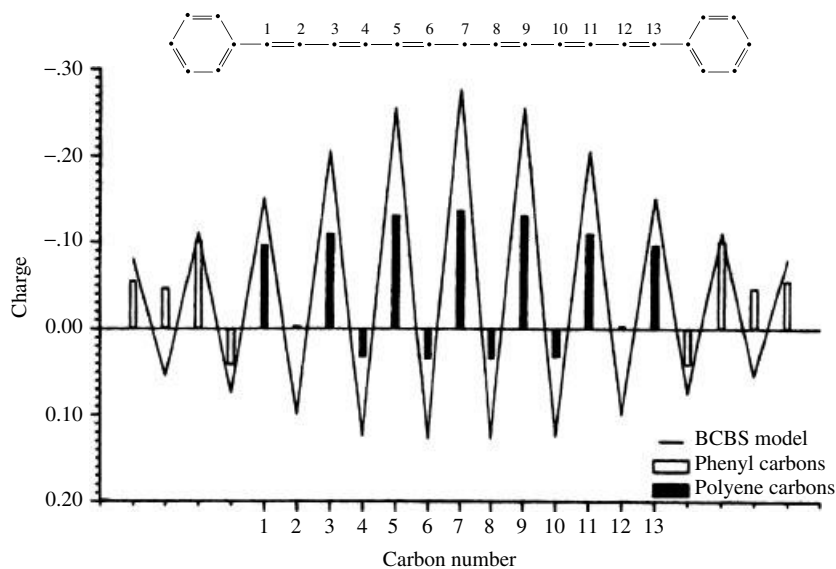


FIGURE 61. Histogram of charge density vs carbon number for DP13. Reprinted with permission from Reference 66. Copyright (1990) American Chemical Society

If such an experiment were successful, then assignment of carbons α to cage sp^3 carbons in any modified fullerene should be possible by extrapolation. The authors report that such a characterization is indeed possible for molecules $C_{59}HN$ (**113**), $(C_{59}N)_2$ (**114**) and the recently synthesized $C_{59}(CHPh_2)N$ (**115**). The nitrogen-coupled carbon NMR spectrum of the labeled ketolactam **112** revealed five carbons coupled to nitrogen at 80.8, 128.0, 139.7, 141.8 and 163.8 ppm, as shown for structure **112** (Figure 62). The labeled ketolactam was then converted to both **113** and **114**. The former heterofullerene showed five carbons coupled to nitrogen at 71.7, 124.3, 134.9, 147.1 and 155.3 ppm. Assignment of the sp^3 -hybridized α carbon at 155.3 ppm [$^1J(CN) = 12.1$ Hz] was straightforward. Low-intensity resonances at 124.3, 134.9 and 147.1 must therefore be a result of β -coupling, where the carbon resonance at 134.9 ppm is mostly modified by the ^{15}N coupling. The carbon resonating at 147.1 ppm was shown to also be β -coupled to the proton as depicted in **113** (Figure 62). This leaves the resonances at 124.3 and 134.9 ppm to be assignable to 'b' or 'c'. If resonance arguments apply to spin-spin coupling, then the unusual bond localization *sui generis* to fullerene bonding (hexagons are cyclohexatrienes and pentagones are 5-radialenes) demands that 'c' be assigned to the 134.9 ppm resonance. This would also explain why 'b' and 'd', two carbons which are not in direct conjugation with the nitrogen, show very minor coupling.

Armed with this information, the authors examined the ^{15}N -coupled ^{13}C NMR spectrum of the dimer in order to finally locate the interdimer carbon 'a'. Only one carbon resonance was found that split at 156 ppm [$^1J(CN) = 11.6$ Hz], another that broadened was found at 138 ppm, and two more carbons were found that broadened to a lesser extent at 125.1 and 148.8 ppm.

In structure **114** (Figure 67), the assignment of one out of the two possible α sites to 'e' as well as the uncertainty in assignment of the crucial α carbon 'a' are shown.

As is well known in fullerene chemistry, it is possible that when a fullerene is a substituent it has a strong deshielding effect. If $C_{59}N$ has the same magnetic properties as C_{60} , in $(C_{59}N)_2$ (**114**), each half of the molecule acts as a deshielding group on the other. Moreover, the interball bonding carbons 'a' are pressed against the opposite ball's nitrogen atom's lone pair, and this causes further deshielding. An additional complication is that the 'a' carbons are α to their own ball's nitrogen but β to the adjacent ball's nitrogen. This could cause further splitting and/or broadening of the signal corresponding to the α carbon 'a'. Quantum mechanical calculations at the LDF (local density functional) level reveal that the hybridization of 'a' is between sp^2 and sp^3 ; the C-H coupling constant in **113** also supports this theory and allows for the possible assignment of 'a' at 138 ppm. However, the magnitude of deshielding suffered by carbon 'a' was still in question.

To gain information on the chemical shift variation as a function of substituent, the labeled and unlabeled diphenylmethyl azafullerene derivative **115** was synthesized from the corresponding azafullerene dimer **114**. The ^{13}C NMR spectrum of **115** revealed the sp^3 carbon α to the nitrogen on the fullerene cage at 86.3 ppm. It seemed unreasonable that the broadened peak at 138 ppm in the spectrum of **114** could be the α carbon resonance that they had been searching for. This reasoning stems from the fact that changing the substituent from diphenylmethyl to $C_{59}N$ should not shift the ' sp^3 ' resonance downfield by 51.4 ppm, considering that in going from a proton in $C_{59}HN$ (**113**) to an alkyl substituent in $C_{59}(CHPh_2)N$ (**113**), the α carbon resonance shifted by only 14.9 ppm.

An ^{15}N -coupled ^{13}C NMR spectrum of **115** showed a pattern similar to that of its precursors: splitting at 86.3 and 155.5 correspond to the sp^3 -hybridized α carbon 'a' and the sp^2 α carbon 'e', respectively, as illustrated in **115**. Broadening was observed for β carbon resonances at 137.6 and to a lesser extent at 65.2, 124.7 and 148.9 ppm. The 1H -coupled ^{13}C NMR spectrum of **115** showed that the resonance at 148.9 ppm was also

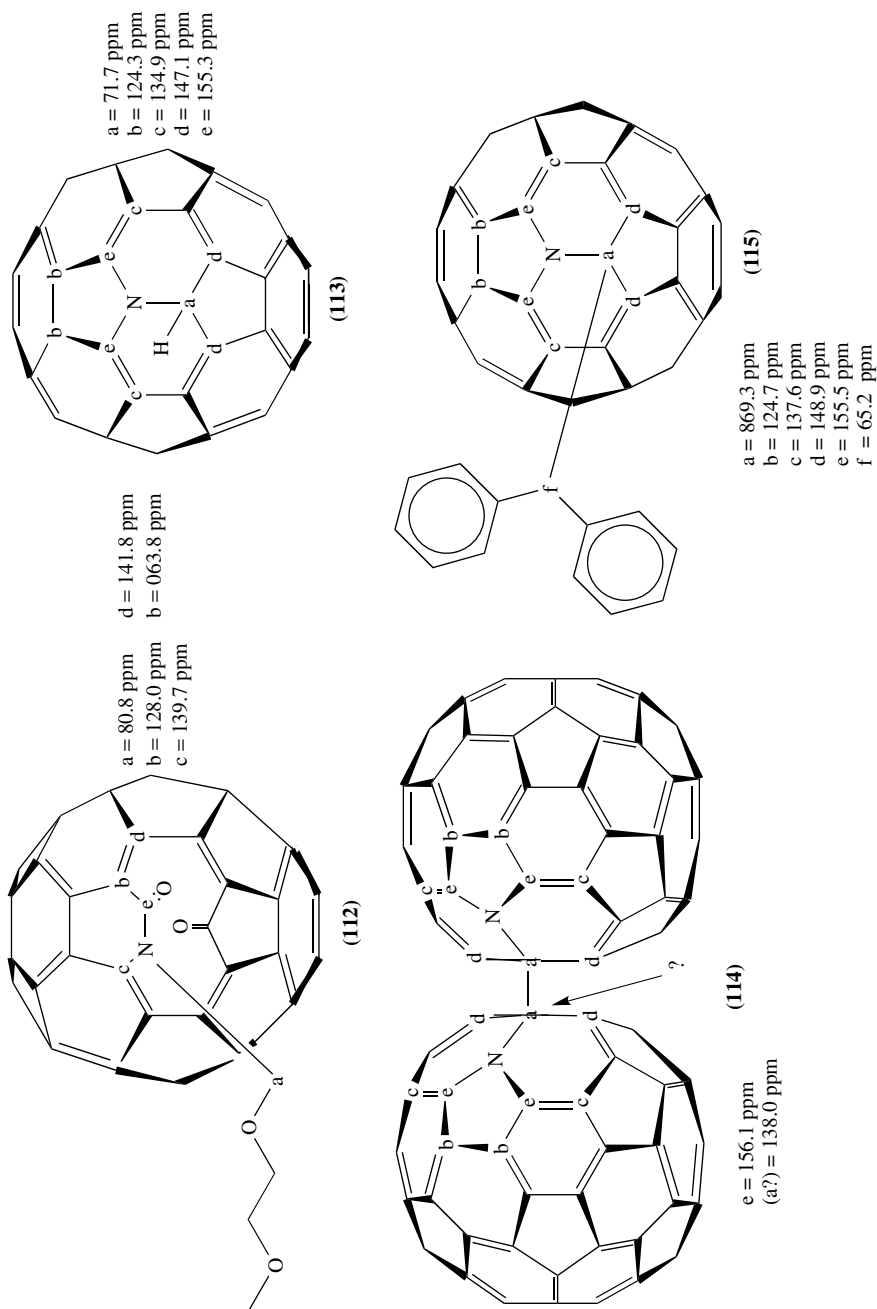


FIGURE 62. ^{13}C NMR data of azafullerenes **112**–**115**. Reprinted with permission from Reference 69. Copyright (1997) American Chemical Society

γ -coupled to the methine proton. The assignment of 'b' and 'c' in **115** is again based on the fact that 'c', unlike the other three β carbons, is in conjugation with nitrogen and should exhibit a stronger spin-spin interaction.

After comparison of the three derivatives, it is possible by extrapolation to assign the β carbons of **114** (Table 49). The assignments of the β carbons at 134.9 ppm for **113** and 137.6 ppm for **115** supported the notion that the 138 ppm resonance in the dimer was also due to β -coupling and strongly suggested that the sp^3 α carbon of **114** was still unassigned.

Re-evaluation of pulse delay times used to record fullerene ^{13}C NMR spectra revealed that a 16 s pulse delay, twice the value for a 'standard' detection, allowed the observation of a weak resonance in the sp^3 region at 90.4 ppm in the ^{13}C NMR spectrum of the 'unlabeled' heterofullerene **114**. Attempts were made to optimize the NMR experimental parameters for a long T_1 , i.e. the variation of delay times and pulse angles. Various conditions were tried on the labeled material without success. This is probably due to the mixture of the labeled and unlabeled **114** which give too low S/N for signal detection. Table 49 summarizes the NMR results obtained and illustrates a distinct pattern of the azafullerenes.

The numbers in Table 49 indicate that as the electronegativity of R increases, the chemical shifts of the sp^3 and (for the most part) the sp^2 carbon atoms α and β to the nitrogen atom also increase. In all three cases, the pattern is reproduced and similar coupling constants are observed. The only exception appears to be carbon 'd' in **115**, which has approximately the same chemical shift as that of **114**.

Brunner, Pines and coworkers⁷⁰ reported on the enhancement of ^{13}C NMR signals in solid C_{60} and C_{70} using a laser-polarized xenon. NMR signals emanating from surface nuclei of solids may be enhanced by the transfer of spin polarization from laser-polarized noble gases via SPINOE (spin polarization induced nuclear Overhauser effect). The paper describes experiments in which the spin polarization is transferred under MAS from laser-polarized ^{129}Xe to ^{13}C , a nuclear spin with a low gyromagnetic ratio in the fullerenes C_{60} and C_{70} , which are polycrystalline materials with a low surface area. In C_{70} , a different degree of enhancement of the NMR spectrum is observed for the different atomic sites in the molecule.

Spin polarization transfer via SPINOE requires effective adsorption of laser-polarized ^{129}Xe on the sample under study. Figure 63 shows the ^{129}Xe MAS NMR spectra of laser-polarized ^{129}Xe adsorbed on fullerenes at 150 K. The spectra exhibit narrow signals at *ca* 0 ppm due to gaseous xenon and broad signals centered at 100–120 ppm (50–80 ppm wide), characteristic of adsorbed xenon. The intensity of the latter signals is 4–5 times higher for C_{70} than for C_{60} , because the specific surface of the C_{70} sample was approximately twice the specific surface of C_{60} and the mass of the C_{70} sample was 2.5 times the

TABLE 49. ^{15}N -coupled carbon atoms a–f as a function of R on the fullerene cage

	a	b	c	d	e	f
R = H (113)	71.7(3.5) ^a	124.3 ^b	134.9 ^b	147.1 ^b	155.3(12.1) ^a	
R = CHPh_2 (115) ^c	86.6(4.5) ^a	124.6 ^b	137.6 ^b	149.1 ^b	155.7(11.9) ^a	65.4 ^b
R = C_{59}N (114)	90.4 ^b	125.1 ^b	138	148.8 ^a	156.1(11.6) ^a	

^a ^{15}N – ^{13}C coupling constant (Hz) in ODCB-*d*₄ (ODCB = *o*-dichlorobenzene).

^bBroad, low intensity peak.

^cChemical shifts of carbons given next to the structure of **115** differ slightly from those here because they were obtained in CS_2 .

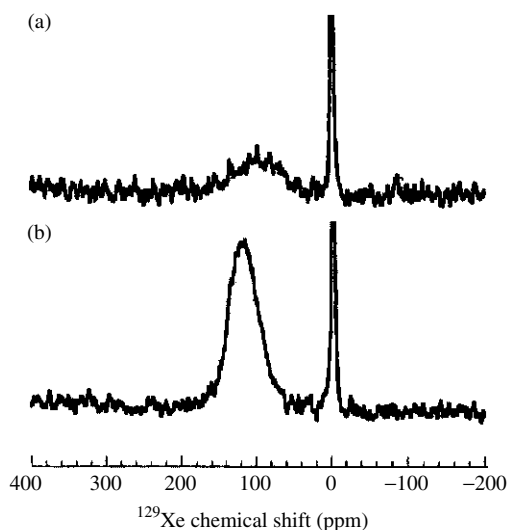


FIGURE 63. ^{129}Xe MAS NMR spectra of laser-polarized ^{129}Xe adsorbed on C_{60} (a) and C_{70} (b), measured at 150 K. Note that the sharp signals at 0 ppm due to gaseous ^{129}Xe are clipped to enlarge the scale. Reproduced by permission of Elsevier Science B. V. from Reference 70

mass of the C_{60} sample. The fractional coverage of the surface with xenon was apparently the same for both samples.

Figure 64(a) shows the ^{13}C MAS NMR spectrum of C_{60} with the characteristic single line at 144 ppm. The SPINOE spectrum shown in Figure 64(b) is obtained as the difference between the spectrum measured when the ^{129}Xe flowing into the rotor is laser-polarized and the spectrum measured when the ^{129}Xe exhibits its normal thermal equilibrium polarization. The intensity corresponds to $ca\ 15 \pm 5\%$ of the intensity of the spectrum observed when the ^{129}Xe flowing through the sample is not laser-polarized (Figure 64c).

From the mean crystalline diameter of $ca\ 4\ \mu\text{m}$ and the diameter of a C_{60} molecule ($ca\ 1\ \text{nm}$), one can estimate that only a fraction of $ca\ 0.0015$ of the C_{60} molecules is located at the surface of the particles. Assuming that effective polarization transfer only occurs for C_{60} molecules located at the surface, one concludes that the observed signal enhancement of $15 \pm 5\%$ corresponds to a polarization enhancement factor of $ca\ 100 \pm 30$. However, it should be noted that this simple estimation neglects the influence of spin diffusion which can lead to a transport of spin polarization into the bulk, resulting in a lower surface enhancement factor.

Figure 65(a) and (b) shows the ^{13}C MAS NMR spectra of C_{70} measured at room temperature and 150 K, respectively. The signal at 147 ppm arises from ^{13}C nuclei at positions C2 and C3, whereas the nuclei located at C4 and C5 give rise to the signals at 144.5 and 130 ppm, respectively. It should be noted that the signal at 150 ppm due to ^{13}C nuclei located at C1 position is clearly resolved at room temperature, but it appears only as a 'shoulder' at 150 K since the residual linewidth of the ^{13}C MAS NMR signals of C_{70} increases on decreasing the temperature. The spectrum shown in Figure 65(b) was measured in the presence of a gas stream carrying unpolarized ^{129}Xe (i.e. laser turned off). Turning the laser light on increases the signal intensity of the carbons in the C2 and C3 positions (147 ppm) by $25 \pm 5\%$, an effect that can also be seen in the difference

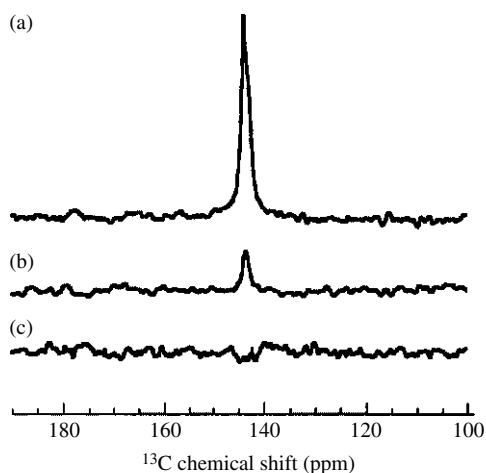


FIGURE 64. ^{13}C MAS NMR spectra of C_{60} acquired at 150 K: (a) Spectrum obtained when the gas stream is not laser-polarized (laser off). (b) Difference between the spectrum obtained when the gas stream is laser-polarized (laser on) and spectrum (A). This spectrum quantitatively represents the observed SPINOE intensity. (c) Difference between two successively recorded spectra obtained when the ^{129}Xe flowing into the rotor is not laser-polarized. This demonstrates that the difference spectrum is free of artifacts. Reproduced by permission of Elsevier Science B. V. from Reference 70

spectrum (Figure 65c and d). The intensity of the ‘shoulder’ at 150 ppm also increases, but a quantitative evaluation of this effect is difficult on the basis of the present data. The increase in the intensities of the signals at 144.5 and 130 ppm is within the experimental error and is not considered to be significant. Identical T_1 values of 5 ± 1 were measured for the ^{13}C nuclei located at positions C2, C3, C4 and C5 at 150 K. It is concluded, therefore, that the more intense SPINOE for ^{13}C nuclei located at C2 or C3, or at both positions, results from a higher cross-relaxation rate. A plausible explanation for this selective enhancement would be a better accessibility of xenon atoms to these sites and/or a higher heat of adsorption of xenon on these sites.

Pines and coworkers⁷⁰ showed the feasibility of spin polarization transfer by SPINOE from laser-polarized ^{129}Xe to surface ^{13}C nuclei in low surface area materials in high-resolution solid-state NMR experiments. This technique provides the basis for novel surface ^{13}C NMR investigations, e.g. of surface coatings, supported catalysts and electrode materials.

Under appropriate nonequilibrium growth conditions, carbon atoms form relatively stable hollow clusters of well-defined mass number, fullerenes. The mass production, purification and condensation of such clusters into a molecular solid are generally essential for a full experimental characterization. The initial discovery of C_{60} , for example, had to wait six years for a bulk synthesis method before detailed characterization of the molecule was possible. Gas-phase experiments have indicated the existence of a wide range of fullerene clusters, but beyond C_{60} only a few pure fullerene solids have been obtained, most notably C_{70} . Low-mass fullerenes are of particular interest because their high curvature and increased strain energy owing to adjacent pentagonal rings could lead to solids with unusual intermolecular bonding and electronic properties. Piskoti and coworkers⁷¹ reported C_{36} , a new carbon solid by the arc-discharge method. They

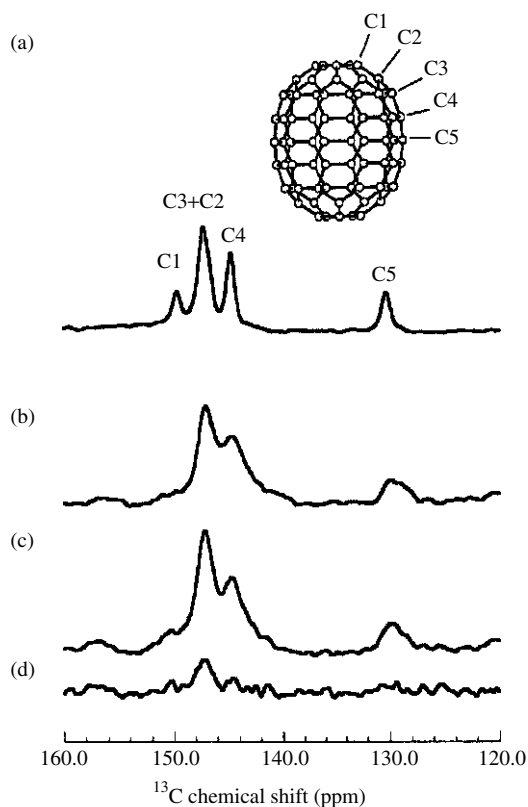


FIGURE 65. ^{13}C MAS NMR spectra of C_{70} acquired at room temperature (a) and 150 K (b–d). (b) Spectrum obtained when the ^{129}Xe flowing into the rotor is not laser-polarized. (c) Spectrum obtained when the ^{129}Xe flowing into the rotor is laser-polarized. (d) Difference between spectrum (c) and spectrum (b). Reproduced by permission of Elsevier Science B. V. from Reference 70

have developed purification methods that separate C_{36} from amorphous carbon and other fullerenes, to yield saturated solutions, thin films and polycrystalline powders of the pure solid form. Solid-state NMR measurements suggest that the molecule has D_{6h} symmetry and electron-diffraction patterns are consistent with a tightly bound molecular solid with an intermolecular spacing of 6.68\AA . Large increases in the electrical conductivity of the solid on doping with alkali metals were found.

Figure 66 shows the experimental ^{13}C NMR spectrum of C_{36} powder. The experimental spectrum contains two prominent peaks, one at 146.1 ppm and another (with approximately one-half the intensity) at 135.7 ppm . The inset to Figure 66 shows the predicted molecular NMR spectra for the isolated D_{6h} and D_{2d} isomers (along with schematic structure drawings). The experimental spectrum appears inconsistent with predictions for the D_{2d} isomer. On the other hand, taking into account experimental broadening of the peaks, one would expect for the D_{6h} isomer two peaks, one near 135 ppm and another, a ‘double intensity’ peak at higher ppm arising from the two higher, nearly degenerate resonances. This is precisely what is observed experimentally. The smaller experimentally observed

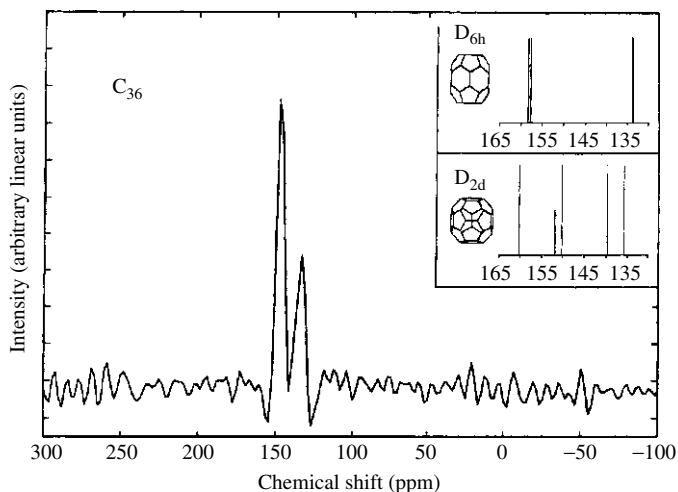


FIGURE 66. Predicted and observed NMR spectra of C_{36} . Reproduced by permission of Nature Management Offices from Reference 71

shift of the 'double intensity' peak (at 146 ppm vs the predicted 158 ppm) is accounted for by additional shielding of these reactive carbon atom sites by neighboring molecules in the solid (this shielding is not considered in the simple molecular calculations). In this way C_{36} was identified as a cage molecule having a D_{6h} symmetry.

V. REFERENCES

1. For example, J. March, *Advanced Organic Chemistry; Reactions, Mechanism and Structure*, 3rd edn., Wiley, New York, 1985, pp. 668–670.
2. For review see R. Huisgen, R. Grashey and J. Sauer, in *The Chemistry of Alkenes* (Ed. S. Patai), Chap. 11, Wiley, New York, 1964, pp. 739–953.
3. R. B. Woodward and R. Hoffmann, *The Conservation of Orbital Symmetry*, Academic Press, New York, 1970.
4. L. M. Jackman, F. Sondheimer, Y. Amiel, D. A. Ben-Efraim, Y. Gaoni, R. Wolovski and A. A. Bothner-By, *J. Am. Chem. Soc.*, **84**, 4307 (1962).
5. For example, V. S. Watts and J. H. Goldstein, 'Nuclear Magnetic Resonance Spectra of Alkenes', in *The Chemistry of Alkenes*, Vol. 2 (Ed. J. Zabicky), Chap. 1, Wiley, London, 1970, pp. 1–38.
6. (a) E. Pretsch, T. Clerc, J. Seibl and W. Simon, *Tabellen Zur Strukturaufklarung Organischer Verbindungen*, Springer-Verlag, Berlin, 1976, pp. H210–H235.
(b) L. M. Jackman and S. Sternhell, *Application of Nuclear Magnetic Resonance Spectroscopy in Organic Chemistry*, 2nd edn., Pergamon Press, Oxford, 1969, pp. 186–190.
7. H. O. Kalinowski, S. Berger and S. Braun, *Carbon-13 NMR Spectroscopy*, Wiley, New York, 1984, pp. 132–152.
8. G. C. Levy, R. L. Lichter and G. L. Nelson, *Carbon-13 Nuclear Magnetic Resonance Spectroscopy*, 2nd edn., Wiley, New York, 1980, pp. 78–91.
9. U. Fleischer and W. Kutzelnigg, *J. Chem. Phys.*, **82**, 5035 (1988).
10. K. Wokinski, J. F. Hinton and P. Pulay, *J. Am. Chem. Soc.*, **112**, 1360 (1990).
11. (a) A. E. Hansen and T. D. Bouman, *J. Chem. Phys.*, **82**, 5035 (1985).
(b) J. C. Facelli, D. M. Grant, T. D. Bouman and A. E. Hansen, *J. Comput. Chem.*, **11**, 510 (1990).

12. M. Wada, M. Sakurai, Y. Inoue, Y. Tamura and Y. Watanabe, *Magn. Reson. Chem.*, **33**, 453 (1995).
13. T. D. Bouman and A. E. Hansen, RPAC Version 9.0 (1991).
14. M. J. Frisch, M. H. Gordon, G. W. Trucks, J. B. Foresman, H. B. Schlegel, K. Raghavachari, M. A. Robb, J. S. Binkley, C. Gonzalez, D. J. Fox, R. A. Whiteside, R. Seeger, C. F. Mellius, J. Baker, R. L. Martin, L. R. Kahn, J. J. P. Stewart, S. Topio and J. A. Pople, *Gaussian 90*, Gaussian, Pittsburgh (1990).
15. W. J. Hehre, L. Radom, P. v. R. Schleyer and J. A. Pople, *Ab Initio Molecular Orbital Theory*, Wiley, New York, 1986.
16. J. M. Foster and S. F. Boys, *Rev. Mod. Phys.*, **32**, 300 (1960).
17. J. B. Stothers, ¹³C NMR Spectroscopy, Academic Press, New York, 1972.
18. A. K. Jameson and C. J. Jameson, *Chem. Phys. Lett.*, **134**, 461 (1987).
19. H. Houjou, M. Sakurai, N. Asakawa, Y. Inoue and Y. Tamura, *J. Am. Chem. Soc.*, **118**, 8904 (1996).
20. S. Tsuboi, J. Sakamoto, A. Kuroda, M. Utaka and A. Takeda, *Bull. Chem. Soc. Jpn.*, **61**, 1410 (1988).
21. D. E. Dorman, M. Jautelat and J. D. Roberts, *J. Org. Chem.*, **36**, 2757 (1971).
22. R. J. Bushby and C. Jarecki, *Tetrahedron Lett.*, **29**, 2715 (1988).
23. W. R. Roth, H. W. Lennartz, W. von E. Doering, W. R. Dolbier, Jr. and J. C. Schmidhauser, *J. Am. Chem. Soc.*, **110**, 1883 (1988).
24. P. Denis, J. F. Croizy, A. Mortreux and F. Petit, *J. Mol. Catal.*, **68**, 159 (1991).
25. A. F. Cockerill, G. L. D. Davies, R. C. Harden and D. M. Rackham, *Chem. Rev.*, **73**, 553 (1973).
26. R. Chen, L. U. Colmenares, J. R. Thiel and R. S. H. Liu, *Tetrahedron Lett.*, **35**, 7177 (1994).
27. (a) M. L. Martin, G. J. Martin and J.-J. Delpuech, *Practical NMR Spectroscopy*, Heyden, London, 1980, pp. 339–349.
(b) M. Oki, *Applications of Dynamic NMR Spectroscopy to Organic Chemistry*, VCH, Weinheim, 1985, pp. 3–11.
28. R. S. H. Liu, J. P. Zingoni, A. Kini, M. Trammell, D. Chu, A. E. Asato and T. T. Bopp, *J. Org. Chem.*, **48**, 4817 (1983).
29. E. Taskinen, *Magn. Reson. Chem.*, **33**, 256 (1995).
30. E. Taskinen and J. Hellman, *Magn. Reson. Chem.*, **32**, 353 (1994).
31. S. F. Marcel, K. J. Lie, K. P. Mohammad and S. A. Mohammad, *Lipids*, **32**, 1041 (1997).
32. A. B. Shtarev, M. M. Kremlev and Z. Chvatal, *J. Org. Chem.*, **62**, 3040 (1997).
33. F. Babudri, A. R. Cicciolessere, G. M. Farinola, V. Fiandanese, G. Marchese, R. Musio, F. Naso and O. Sciacovelli, *J. Org. Chem.*, **62**, 3291 (1997).
34. J. A. Osaheni and S. A. Jenekhe, *Macromolecules*, **28**, 1172 (1995).
35. S. H. Jin, S. W. Kang, J. G. Park, J. C. Lee and K. S. Choi, *Pure Appl. Chem.*, **A32**, 455 (1995).
36. R. Ghirlando, E. Berman, T. Baasov and M. Sheves, *Magn. Reson. Chem.*, **25**, 21 (1987).
37. K. Nakanishi, V. B. Nair, M. Arnaboldi, K. Tsujimoto and B. Honig, *J. Am. Chem. Soc.*, **102**, 7945 (1980).
38. P. E. Blatz and J. H. Mohler, *Biochemistry*, **14**, 2304 (1975).
39. Z. Li, B. J. Rawling, P. H. Harrison and J. C. Vederas, *J. Antibiot.*, **17**, 577 (1989).
40. P. Sowinski, P. Gariboldi, A. Czerwinski and E. Borowski, *J. Antibiot.*, **17**, 1631 (1989).
41. H. Hirota, A. Itoh, J. Ido, Y. Iwamoto, E. Goshima, T. Miki, K. Hasuda and Y. Ohashi, *J. Antibiot.*, **44**, 181 (1991).
42. R. Gebhard, J. T. M. van Dijk, E. van Ouwerkerk, M. V. T. J. Boza and J. Lugtenburg, *Recl. Trav. Chim. Pays-Bas*, **110**, 459 (1991).
43. E. S. Hand, K. A. Belmore and L. D. Kispert, *Helv. Chem. Acta*, **76**, 1928 (1993).
44. Y. Yamagishi, K. Shindo and H. Kawai, *J. Antibiot.*, **46**, 888 (1993).
45. S. Chatterjee, E. K. S. Vijayakumar, C. M. M. Franco, J. Blumbach, B. N. Ganguli, H. W. Fehlhaber and H. Kogler, *J. Antibiot.*, **46**, 1027 (1993).
46. K. Imai, Y. Nihei, M. Oka, T. Yamasaki, M. Konishi and T. Oki, *J. Antibiot.*, **46**, 1031 (1993).
47. M. Nakagawa, Y. Toda, K. Furihata, Y. Hayakawa and H. Seto, *J. Antibiot.*, **45**, 1133 (1992).
48. L. U. Colmenares, W. P. Niemczura, A. E. Asato and R. S. H. Liu, *J. Phys. Chem.*, **100**, 9175 (1996).

49. S. Li, S. L. Swindle, S. K. Smith, R. A. Nieman, A. L. Moore, T. A. Moore and D. Gust, *J. Phys. Chem.*, **99**, 3371 (1995).
50. P. Rochet and J. M. Lancelin, *Magn. Reson. Chem.*, **35**, 538 (1997).
51. H. Yasuda, T. Arai, T. Okamoto and A. Nakamura, *J. Organomet. Chem.*, **361**, 161 (1989).
52. J. M. Lehn, J. P. Vigneron, I. B. Waksman, J. Guihem and C. Pascard, *Helv. Chim. Acta*, **75**, 1069 (1992).
53. S. Okada, K. Hayamizu, H. Matsuda, A. Masaki, N. Minami and H. Nakanishi, *Macromolecules*, **27**, 6259 (1994).
54. O. Yamamoto, K. Hayamizu and M. Yanagisawa, *Anal. Sci.*, **4**, 461 (1988).
55. S. O. Smith, L. Paulings, M. E. Miley, J. Courtin, H. de Groot, J. Lugtenburg, R. A. Mathies and R. G. Griffin, *Biochemistry*, **29**, 8158 (1990).
56. L. C. P. J. Mollevanger, A. P. M. Kentegens, J. A. Pardoën, J. M. L. Courtin, W. S. Veeman, J. Lugtenburg and W. J. deGrip, *Eur. J. Biochem.*, **163**, 9 (1987).
57. A. S. Ulrich, A. Watts, I. Wallat and M. P. Heyn, *Biochemistry*, **33**, 5370 (1994).
58. A. S. Ulrich and A. Watts, *Solid State Nucl. Magn. Reson.*, **2**, 21 (1993).
59. A. S. Ulrich, M. P. Heyn and A. Watts, *Biochemistry*, **31**, 10390 (1992).
60. M. L. Ciavatta, M. Gavanin, R. Puliti, G. Cimino, E. Martinez, J. Ortea and C. A. Mattia, *Tetrahedron*, **53**, 17343 (1997).
61. E. L. Eliel and S. H. Wilen, *Stereochemistry of Organic Compounds*, Wiley, New York, 1994, pp. 1119–1190.
62. G. U. Barretta, F. Balzano, A. M. Caporusso, A. Iodice and P. Salvadori, *J. Org. Chem.*, **60**, 2227 (1995).
63. G. U. Barretta, F. Balzano, A. M. Caporusso and P. Salvadori, *J. Org. Chem.*, **59**, 836 (1994).
64. C. Lambert, P. v. R. Schleyer and E. U. Wurthwein, *J. Org. Chem.*, **58**, 6377 (1993).
65. E. Liepins, I. Birgele, E. Lukevics, E. T. Bogorodovsky and V. S. Zavgorodny, *J. Organomet. Chem.*, **402**, 43 (1991).
66. L. M. Tolbert and M. E. Ogle, *J. Am. Chem. Soc.*, **112**, 9519 (1990).
67. H. Kloosterziel and M. A. Werner, *Recl. Trav. Chim. Pays-Bas*, **94**, 124 (1975).
68. L. M. Tolbert and M. E. Ogle, *J. Am. Chem. Soc.*, **111**, 5958 (1989).
69. C. Bellavia-Lund, M. Keshavarz, K. T. Collins and F. Wudl, *J. Am. Chem. Soc.*, **119**, 8101 (1997).
70. E. Brunner, M. Haake, A. Pines, J. A. Reimer and R. Seydoux, *Chem. Phys. Lett.*, **290**, 112 (1998).
71. C. Piskoti, J. Yarger and A. Zettl, *Nature*, **393**, 771 (1998).